ISSN 2500-316X (Online)

RUSSIAN TECHNOLOGICAL JOURNAL

РОССИЙСКИЙ ТЕХНОЛОГИЧЕСКИЙ ЖУРНАЛ

Information systems.
Computer sciences.
Issues of information security

Multiple robots (robotic centers) and systems.
Remote sensing and nondestructive testing

Modern radio engineering and telecommunication systems

Micro- and nanoelectronics.
Condensed matter physics

Analytical instrument engineering and technology

Mathematical modeling

Economics of knowledge-intensive and high-tech enterprises and industries.
Management in organizational systems

Product quality management. Standardization

Philosophical foundations of technology and society

12+
www.rtj-mirea.ru

14(2) 2026

ISSN 2500-316X (Online)

RUSSIAN TECHNOLOGICAL JOURNAL

РОССИЙСКИЙ ТЕХНОЛОГИЧЕСКИЙ ЖУРНАЛ

- Information systems. Computer sciences. Issues of information security
- Multiple robots (robotic centers) and systems. Remote sensing and nondestructive testing
- Modern radio engineering and telecommunication systems
- Micro- and nanoelectronics. Condensed matter physics
- Analytical instrument engineering and technology
- Mathematical modeling
- Economics of knowledge-intensive and high-tech enterprises and industries. Management in organizational systems
- Product quality management. Standardization
- Philosophical foundations of technology and society

- Информационные системы. Информатика. Проблемы информационной безопасности
- Роботизированные комплексы и системы. Технологии дистанционного зондирования и неразрушающего контроля
- Современные радиотехнические и телекоммуникационные системы
- Микро- и наноэлектроника. Физика конденсированного состояния
- Аналитическое приборостроение и технологии
- Математическое моделирование
- Экономика наукоемких и высокотехнологичных предприятий и производств. Управление в организационных системах
- Управление качеством продукции. Стандартизация
- Мировоззренческие основы технологии и общества

Russian Technological Journal
2026, Vol. 14, No. 2

Russian Technological Journal
2026, том 14, № 2

https://www.rtj-mirea.ru

https://doi.org/10.32362/2500-316X

ISSN 2500-316X (Online)

Russian Technological Journal
2026, Vol. 14, No. 2

Publication date March 31, 2026.

The peer-reviewed scientific and technical journal highlights the issues of complex development of radio engineering, telecommunication and information systems, electronics and informatics, as well as the results of fundamental and applied interdisciplinary researches, technological and economical developments aimed at the development and improvement of the modern technological base.

Periodicity: six times a year.
The journal was founded in December 2013. The titles were «Herald of MSTU MIREA» until 2016 (ISSN 2313-5026) and «Rossiiskii tekhnologicheskii zhurnal» from January 2016 until July 2021 (ISSN 2500-316X).

Founder and Publisher:
Federal State Budget
Educational Institution of Higher Education
«MIREA – Russian Technological University»
78, Vernadskogo pr., Moscow, 119454 Russia.

The journal is included into the List of peer-reviewed science press of the State Commission for Academic Degrees and Titles of Russian Federation. The Journal is included in Russian Science Citation Index (RSCI), Russian State Library (RSL), Science Index, eLibrary, Directory of Open Access Journals (DOAJ), Directory of Open Access Scholarly Resources (ROAD), Google Scholar, Ulrich's International Periodicals Directory.

Editor-in-Chief:
Alexander S. Sigov, Academician at the Russian Academy of Sciences, Dr. Sci. (Phys.–Math.), Professor, President of MIREA – Russian Technological University (RTU MIREA), Moscow, Russia.
Scopus Author ID 35557510600, ResearcherID L-4103-2017, sigov@mirea.ru.

The registration number ПИ № ФС 77 - 81733 was issued in August 19, 2021 by the Federal Service for Supervision of Communications, Information Technology, and Mass Media of Russia.

The subscription index of *Pressa Rossii*: **79641**.

Russian Technological Journal
2026, том 14, № 2

Дата опубликования 31 марта 2026 г.

Научно-технический рецензируемый журнал освещает вопросы комплексного развития радиотехнических, телекоммуникационных и информационных систем, электроники и информатики, а также результаты фундаментальных и прикладных междисциплинарных исследований, технологических и организационно-экономических разработок, направленных на развитие и совершенствование современной технологической базы.

Периодичность: 6 раз в год.
Журнал основан в декабре 2013 года. До 2016 г. издавался под названием «Вестник МГТУ МИРЭА» (ISSN 2313-5026), а с января 2016 г. по июль 2021 г. под названием «Российский технологический журнал» (ISSN 2500-316X).

Учредитель и издатель:
федеральное государственное бюджетное образовательное учреждение высшего образования «МИРЭА – Российский технологический университет»
119454, РФ, г. Москва, пр-т Вернадского, д. 78.

Журнал входит в Перечень ведущих рецензируемых научных журналов ВАК РФ, в которых должны быть опубликованы основные научные результаты диссертаций на соискание ученой степени кандидата наук и доктора наук, входит в RSCI, РГБ, РИНЦ, eLibrary, Directory of Open Access Journals (DOAJ), Directory of Open Access Scholarly Resources (ROAD), Google Scholar, Ulrich's International Periodicals Directory.

Главный редактор:
Сигов Александр Сергеевич, академик РАН, доктор физ.-мат. наук, профессор, президент ФГБОУ ВО МИРЭА – Российский технологический университет (РТУ МИРЭА), Москва, Россия.
Scopus Author ID 35557510600, ResearcherID L-4103-2017, sigov@mirea.ru.

Регистрационный номер и дата принятия решения о регистрации СМИ ПИ № ФС 77 - 81733 от 19.08.2021 г. СМИ зарегистрировано Федеральной службой по надзору в сфере связи, информационных технологий и массовых коммуникаций (Роскомнадзор).

Индекс по объединенному каталогу «Пресса России» **79641**.

https://www.rtj-mirea.ru

Editorial Board

Редакционная коллегия

Contents

Information systems. Computer sciences. Issues of information security

7 *Mikhail A. Anfyorov*
Clustering of multidimensional temporal data as part of information support for management decisions

17 *Danila S. Belyakov*
Architecture of a distributed system for testing Internet of Things devices at the development stage

29 *Andrey S. Zuev, Peter N. Sovietov, Ilya E. Tarasov*
Heterogeneous computing systems with hardware acceleration of massively parallel stream processing design

42 *Evgenii A. Khalturin, Alexey A. Kytmanov, Yuliya V. Vaynshteyn, Tatiana V. Zykova*
Software methods for curriculum processing, analysis and visualization

Modern radio engineering and telecommunication systems

57 *Kirill V. Latyshev, Mihail S. Kostin, Konstantin A. Boikov*
Generation of radiovision signals by spectral saturation in transient distortion mode of integral microwave amplifiers for gesture recognition systems

Micro- and nanoelectronics. Condensed matter physics

69 *Artyom A. Egorenkov, Irina V. Danilova, Maria I. Bibinova, Sergei N. Chelyshkov, Alexei N. Vyaznikov, Konstantin S. Batalov*
Search of technological solutions aimed at reducing the number of image defects in a hybrid SWIR device

80 *Evgenii Ph. Pevtsov, Tatyana A. Demenkova, Yuri A. Korotaev, Alexander S. Sigov*
Physically unclonable functions in digital integrated circuits

103 *Natalia E. Sherstyuk, Kirill A. Brekhov, Elena D. Mishina*
Modeling of resonant excitation of ferroelectric lattice subsystem by terahertz radiation under nonequilibrium conditions

Mathematical modeling

113 *Ivan G. Lebo, Victoria A. Komarova, Maxim A. Ryzhkov*
Influence of piston nonuniformity and illumination on the formation of a hypersonic shock wave in a laser-driven shock wave

124 *Alexander S. Leontyev, Dmitry V. Zhmatov*
Performance analysis and timing characteristics in industrial networks with random and deterministic node distributions

Philosophical foundations of technology and society

134 *Stanislav A. Kudzh, Natalia B. Golovanova, Yuri G. Grafov*
Formation of a comprehensive approach to developing the scientific and educational infrastructure of a modern engineering university

Содержание

Информационные системы. Информатика. Проблемы информационной безопасности

7 *М.А. Анфёров*
Кластеризация многомерных временных данных в рамках информационной поддержки принимаемых управленческих решений

17 *Д.С. Беляков*
Архитектура распределенной системы тестирования устройств интернета вещей на этапе их разработки

29 *А.С. Зуев, П.Н. Советов, И.Е. Тарасов*
О проектировании гетерогенных вычислительных систем с аппаратным ускорением массово-параллельной потоковой обработки данных

42 *Е.А. Халтурин, А.А. Кытманов, Ю.В. Вайнштейн, Т.В. Зыкова*
Программные методы обработки, анализа и визуализации учебных планов

Современные радиотехнические и телекоммуникационные системы

57 *К.В. Латышев, М.С. Костин, К.А. Бойков*
Формирование радиовизионных сигналов спектральной сатурацией в режиме переходных искажений интегральных сверхвысокочастотных усилителей для систем распознавания жестов

Микро- и наноэлектроника. Физика конденсированного состояния

69 *А.А. Егоренков, И.В. Данилова, М.И. Бибинова, С.Н. Челышков, А.Н. Вязников, К.С. Баталов*
Поиск технологических решений, направленных на снижение количества дефектов изображения в гибридном приборе ближнего инфракрасного диапазона

80 *Е.Ф. Певцов, Т.А. Деменкова, Ю.А. Коротаев, А.С. Сигов*
Физически неклонируемые функции в цифровых интегральных схемах

103 *Н.Э. Шерстюк, К.А. Брехов, Е.Д. Мишина*
Моделирование резонансного возбуждения терагерцевым излучением решеточной подсистемы сегнетоэлектрика в условиях неравновесного состояния

Математическое моделирование

113 *И.Г. Лебо, В.А. Комарова, М.А. Рыжков*
Влияние неоднородностей поршня и облучения на формирование гиперзвуковой ударной волны в лазерной ударной трубе

124 *А.С. Леонтьев, Д.В. Жматов*
Анализ производительности и временных характеристик промышленных сетей со случайным и детерминированным эквидистантным распределением узлов

Мировоззренческие основы технологии и общества

134 *С.А. Кудж, Н.Б. Голованова, Ю.Г. Графов*
Формирование комплексного подхода к развитию научно-образовательной инфраструктуры современного инженерного университета

Information systems. Computer sciences. Issues of information security

Информационные системы. Информатика. Проблемы информационной безопасности

UDC 004.021:65.012.26
https://doi.org/10.32362/2500-316X-2026-14-2-7-16
EDN VCTFHE

RESEARCH ARTICLE

Clustering of multidimensional temporal data as part of information support for management decisions

Mikhail A. Anfyorov @

MIREA – Russian Technological University, Moscow, 119454 Russia
@ *Corresponding author, e-mail: anfyorov@inbox.ru*

• **Submitted:** 02.02.2025 • **Revised:** 20.11.2025 • **Accepted:** 09.02.2026

Abstract

Objectives. The aim of information support for management decision-making is to find the most optimal option. Cluster analysis of multivariate data characterizing socioeconomic systems is widely used. In this work, the author aims to increase the efficiency of decisions made to manage these systems based on the clustering of temporal multidimensional data.

Methods. The methods of cluster analysis were used, as well as the provisions of the theory of systems and mathematical statistics.

Results. A methodology for analyzing the functioning of socioeconomic systems was developed. The analysis is implemented in three stages. Firstly, clustering over the values of feature variances was applied. Secondly, the distance of clustering objects from the center of their cluster and their dispersion was calculated at the points of time coordinates. Thirdly, the change in belonging to a certain cluster of objects that came into view earlier was monitored. Unstable systems were then identified.

Conclusions. Two cases were considered to justify the effectiveness of the methodology developed herein. First, using the example of the tax administration, the detection of deliberate distortion of information was considered. Secondly, identifying the abnormal functioning of the regions of the Russian Federation using the example of decision-making in the framework of socioeconomic development management was considered. The analysis demonstrated good results and we can thus recommend the proposed methodology for practical use in information systems for supporting management decisions.

Keywords: information support, decision-making, cluster analysis, multivariate time data

For citation: Anfyorov M.A. Clustering of multidimensional temporal data as part of information support for management decisions. *Russian Technological Journal.* 2026;14(2):7–16. https://doi.org/10.32362/2500-316X-2026-14-2-7-16, https://www.elibrary.ru/VCTFHE

Financial disclosure: The author has no financial or proprietary interest in any material or method mentioned.

The author declares no conflicts of interest.

НАУЧНАЯ СТАТЬЯ

Кластеризация многомерных временных данных в рамках информационной поддержки принимаемых управленческих решений

М.А. Анфёров [@]

МИРЭА – Российский технологический университет, Москва, 119454 Россия
[@] *Автор для переписки, e-mail: anfyorov@inbox.ru*

• **Поступила:** 02.02.2025 • **Доработана:** 20.11.2025 • **Принята к опубликованию:** 09.02.2026

Резюме

Цели. Информационная поддержка принятия управленческих решений в различных предметных областях направлена на поиск оптимального варианта из множества альтернативных. Что касается принимаемых решений в части функционирования социально-экономических систем, то здесь широко используется кластерный анализ на многомерных данных, характеризующих эти системы, Цель работы – синтез и исследование методики анализа функционирования социально-экономических систем, построенного на кластеризации характеризующих их временных многомерных данных, с целью повышения эффективности принимаемых решений в управлении такими системами.

Методы. Использованы методы кластерного анализа, а также положения теории систем и математической статистики.

Результаты. Разработана методика анализа функционирования социально-экономических систем, использующая кластеризацию ее структурных элементов в пространстве временных многомерных данных. Анализ реализуется в три этапа. Во-первых, производится замена значений признаков на значения их дисперсий в рамках исследуемого временного интервала. Кластеризация с учетом новых значений признаков позволяет выявить объекты кластеризации с высокой неустойчивостью значений признаков во времени. Во-вторых, реализуется кластеризация во всех дискретных точках временной координаты с дальнейшим расчетом удаленностей объектов до центра своего кластера и их дисперсии. Анализ этих дисперсий также позволяет выявить объекты с высокой неустойчивостью данных. В-третьих, отслеживается изменение принадлежности определенному кластеру объектов, попавших ранее в поле зрения. Выявленные неустойчивости в данных позволяют косвенно судить о нестабильном функционировании анализируемой системы или умышленном искажении представленной информации.

Выводы. В рамках обоснования эффективности разработанной методики рассмотрено два случая: выявление умышленного искажения информации на примере налогового администрирования и случай выявления аномального функционирования регионов Российской Федерации на примере принятия решений в рамках управления их социально-экономическим развитием. Поведенный анализ показал хорошие результаты и позволяет рекомендовать предлагаемую методику к практическому использованию в информационных системах поддержки управленческих решений.

Ключевые слова: информационная поддержка, принятие решений, кластерный анализ, многомерные временные данные

Для цитирования: Анфёров М.А. Кластеризация многомерных временных данных в рамках информационной поддержки принимаемых управленческих решений. *Russian Technological Journal*. 2026;14(2):7–16. https://doi.org/10.32362/2500-316X-2026-14-2-7-16, https://www.elibrary.ru/VCTFHE

Прозрачность финансовой деятельности: Автор не имеет финансовой заинтересованности в представленных материалах или методах.

Автор заявляет об отсутствии конфликта интересов.

INTRODUCTION

Cluster analysis [1], as an effective mechanism of intelligent information technologies, is used in resolving a wide range of tasks related to decision-making in various subject areas. In the public administration, for example, it can be applied in developing socioeconomic policy at the regional level [2, 3], in tax regulation [4, 5], in the fields of education [6] and medicine [7, 8], computer science [9, 10] and information security [11], and in the field of mechanical engineering [12, 13]. A wide range of studies have addressed management processes in the economic sphere when solving decision-making problems. Examples of these are investment processes [14], assessing the financial stability of information technology (IT) companies [15], and others. In addition to management decision-making, cluster analysis is also used to support project decision-making [16, 17].

However, all of the examples given above apply static (spatial) data obtained at a specific point in time. On the other hand, analysis which takes into account the dynamics of the properties of objects reflected in the data enables the capabilities of cluster analysis to be expanded in support of management decision-making.

It is worth noting the research being implemented in this area. Firstly, there have been studies of the clustering of one-dimensional [18, 19] and multidimensional [20] time series which increases the efficiency of clustering, but not decision-making. The same goal is being pursued by the transition from the time domain of data to a two-dimensional discrete function [21] using continuous wavelet transformation [22]. The inclusion of the time parameter in the feature space during clustering [23] enables the dynamics of the state of the analyzed objects to be expressed. The clustering of objects as dynamic systems has also been studied in [24, 25].

More in-depth analytics are based on identifying patterns in the dynamics of clustered objects through the dynamics of time series data. Thus, the expansion of analytics is based on an approach which involves clustering objects based on the proximity of the dynamics of time series of a set of indicators characterizing them [26]. In this case, a range of metrics and methods for assessing such proximity are analyzed and compared, including the dynamic time warping (DTW) algorithm [27]. The study of the dynamics of cluster structures in network models of stock markets has made it possible to identify an indicator of an impending crisis in the form of an increase in the stability of these structures [28].

In this study, information support for management decisions is based on an analysis of the hidden influence of factors on the behavior (function) of the system (Fig. 1). If the explicit influence directly determines the decision being made, then the hidden influence requires identification using modern analytical tools and information technologies, as well as an adequate interpretation of the results obtained.

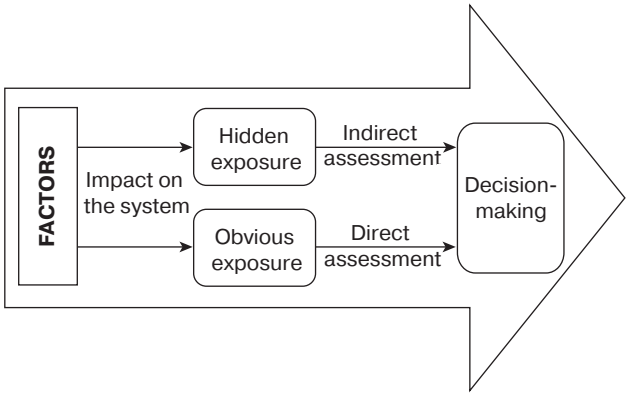

Fig. 1. Consideration of the impact of factors on the system when making decisions

At the same time, the hidden impact of factors on the system being analyzed is revealed through the variable behavior of the objects under study in relation to the clusters being formed. This variability may signal either deliberate distortion of the data provided (e.g., in tax returns) or unstable functioning of the system requiring managerial intervention.

METHODOLOGY

The temporal data analysis used is based on their clustering using the self-organizing map (SOM) method [29]. This is within the framework of the previously proposed approach and covers various levels of depth of research into system behavior [30]. Kohonen SOM enable the qualitative component of the analysis to be enhanced by visualizing the clusters formed using map data. In the proposed methodology, three data analysis tools are implemented to improve the adequacy of the decision made.

The first tool is a filter to limit the power of the analyzed set of features $\mathbf{p}_k^t = (p_{k1}^t, p_{k2}^t, \ldots, p_{kn}^t)$, which depend discretely on the time parameter t (k is the number of objects in the clustered set, m is the number of features). The values of the features are replaced with the values of their dispersions within the time interval under study (w is the number of fixed time coordinates):

$$D_{kj} = \frac{1}{w-1}\sum_{i=1}^{w}(p_{kj}^i - \overline{p}_{kj})^2, \quad \overline{p}_{kj} = \frac{1}{w}\sum_{i=1}^{w} p_{kj}^i. \qquad (1)$$

Further, clustering is performed in the space of new features with the identification of objects belonging to clusters with high dispersion values associated with high instability of the values of the

analyzed features. The objects identified are recorded for further analysis as systems with unstable time data. Objects with a high feature dispersion possibly caused by a trend in their values, characterizing a positive or negative trend, may also be noted. Additional regression analysis is required for clarification (see example below).

The second analysis tool is designed to identify instability in the images of the clustered objects within clusters and involves a series of steps.

In the first stage, clustering is implemented at all discrete points of the time coordinate (r is the number of the time coordinate). Next, the distance d_k^r of the kth object to the center of its cluster is calculated.

In the second stage, at each moment in time r, the variance of the values found in the first stage is calculated as d_k^r in the interval covering the current and previous time coordinates:

$$D_k^r = \frac{1}{r-1}\sum_{t=1}^{r}(d_k^t - \bar{d}_k^r)^2, \quad \bar{d}_k^r = \frac{1}{r}\sum_{t=1}^{r} d_k^t, \quad r = \overline{2,w}. \quad (2)$$

In the third stage, the temporal dependencies of the dispersions (2) are displayed in the form of a diagram which includes all clustered objects. The diagram enables objects with unstable temporal data to be identified at a new level.

The application of the third tool involves tracking possible changes in the affiliation of a specific cluster of objects previously in the field of view (Fig. 2). Such changes allow us to indirectly assess (Fig. 1) the unstable functioning of the system or deliberate distortion of information. They also allow us to refine previously obtained conclusions about objects which have fallen into the risk group. For this purpose, diagrams are the best way to express these objects.

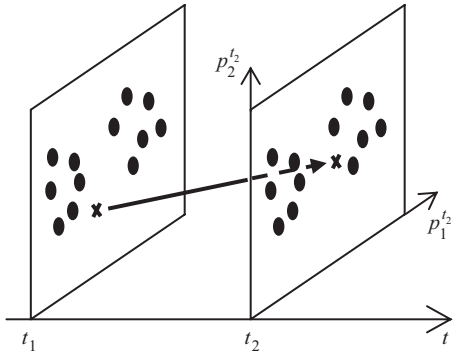

Fig. 2. Clustering results dynamics

The second and the third tools can be applied in different sequences, as well as in parallel.

The interrelationship between the stages implemented within the analysis methodology is presented in a block diagram of the corresponding algorithm (Fig. 3).

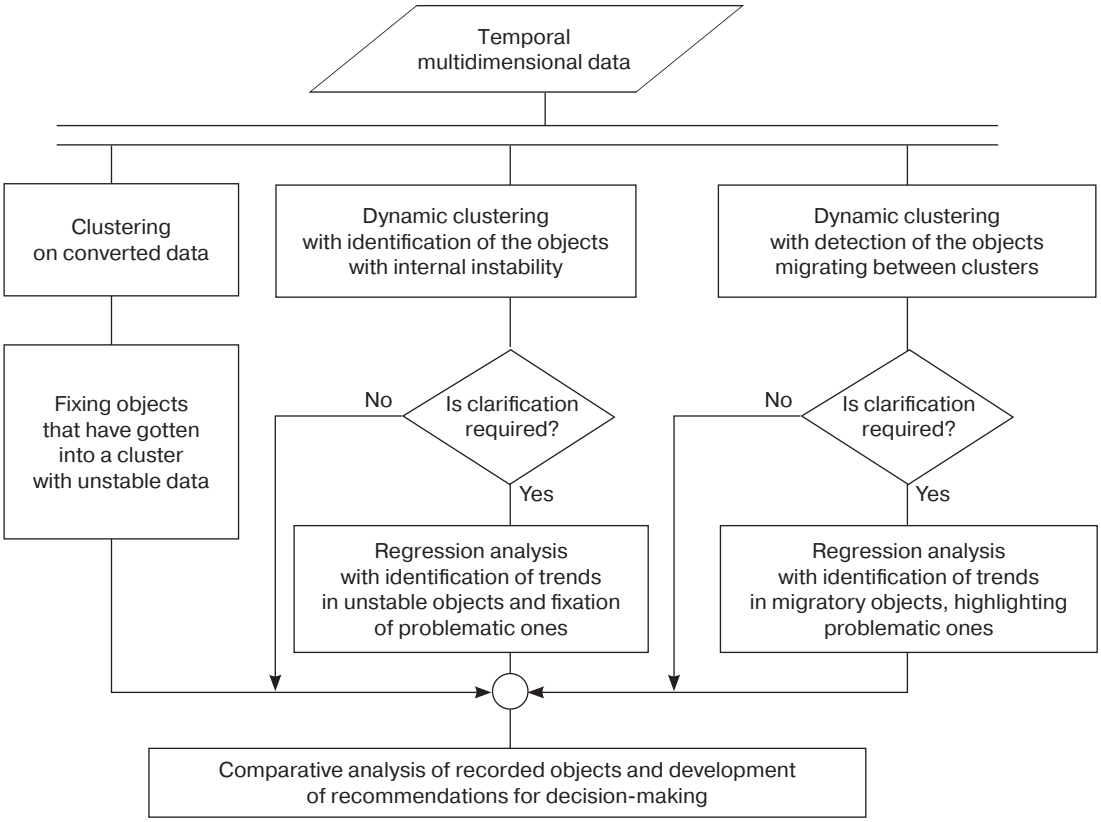

Fig. 3. Method implementation algorithm

DETECTION OF INTENTIONAL DISTORTION OF INFORMATION

The application of the proposed analysis in identifying the deliberate distortion of information is demonstrated using the example of tax administration. Here decisions need to be made about planning field tax audits at taxpayer enterprises. It is initially assumed that the aforementioned distortion allows with a certain degree of probability (Fig. 1) the dishonesty of the management of such enterprises to be assessed. The selection of parameters (features) for clustering was based on a number of preferences:

- availability of their calculation in financial statements;
- their correlation with bankruptcy risk (indicators are reflected in the relevant methodology of the Federal Insolvency Service under the State Committee of the Russian Federation for State Property Management);
- inclusion in Altman's model [31].

As a result, sixteen financial indicators were selected for the twenty companies analyzed. They enabled an assessment of their solvency to be made as well as the financial stability of their economic systems, the profitability of their production, and their business activity in terms of inventory turnover and accounts receivable and payable. The dynamics of these indicators were tracked over a period of eight quarters.

Clustering in the space of new features (1), according to the proposed methodology, allowed for enterprises with high instability of initial data values to be identified (enterprises with conditional numbers 4 and 12). According to the clustering results, they were isolated in their clusters.

The analysis of intra-cluster instability based on the value of the variances (2) resulted in the construction of a diagram (Fig. 4). The pattern of the graphs in the diagram identified critical enterprises with data instability, leading to abnormal behavior of

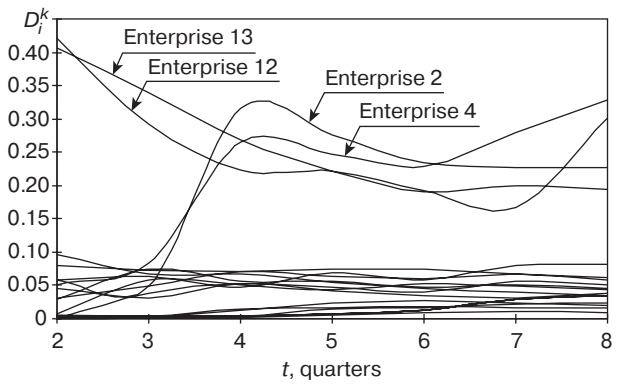

Fig. 4. Dispersion dynamics (2) in enterprise analysis

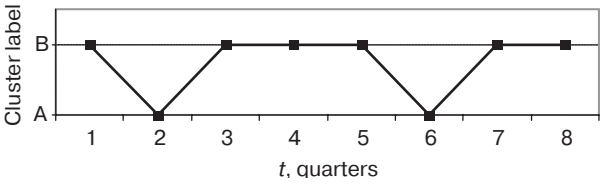

Fig. 5. Migration of enterprise 4 between clusters

the graphs corresponding to these enterprises. At this stage, the group of enterprises under review included the previously noted enterprises 4 and 12, as well as enterprises 2 and 13.

Migrations between clusters (the third tool of the analysis methodology) were found to affect enterprises 2, 4, and 12, as already been noted in previous stages of the analysis. A graphical illustration for enterprise 4 is shown in Fig. 5.

Thus, based on the results of the analysis, field tax audits were recommended for enterprises 2, 4, and 12, and, if possible, for enterprise 13.

IDENTIFYING SYSTEM FUNCTIONING INSTABILITY

The application of the proposed analysis in identifying abnormal systems functioning can be demonstrated using the example of decision-making in the context of socioeconomic development management of the regions in the Russian Federation. The analysis used key indicators characterizing the state of the regional socioeconomic system[1] for the period from 2014 to 2020 (a period of steady progressive development). The volume indicators were converted to relative values by dividing them by the number of employed people in the region. The Republic of Crimea and the city of Sevastopol were excluded from the analysis, since during this transitional period their socioeconomic systems were on the path to stabilization. Moscow, the Moscow oblast, and St. Petersburg, as well as regional structures which are part of regions (e.g., the Yamalo-Nenets Autonomous Okrug within the Tyumen oblast), were not considered.

Unlike the case discussed above, where deliberate data distortion was identified during dynamic cluster analysis of system functioning, dispersion estimates must take into account the possible trend of the relevant indicators (system characteristics) which cause high dispersion values.

In the example under consideration, when clustering in the space of feature variances (1), region 69 (Tver oblast) fell into the cluster of system

[1] *Rossiya v tsifrakh: kratkii statisticheskii sbornik* (*Russia in numbers*: *a short statistical collection*). Moscow: Rosstat; 2020, 550 p. (In Russ.). ISBN 978-5-89476-488-7

instability (high variance values). In order to identify the presence of a trend, a regression analysis was performed to identify the empirical dependence on time of the indicator $v = v(t)$, as determined by the ratio of the gross regional product (billion rubles) to the average annual number of employed population (thousand people) (Fig. 6). The high value of the coefficient of determination R^2 indicates a stable positive trend for this characteristic. This allows us to exclude this region from the cluster of unstable regions. As for other indicators, checking for trends in this region yielded positive results. Thus, for the relative volume of goods shipped from own manufacturing, a stable trend $s = s(t)$ with a coefficient of determination $R^2 = 0.77$ was confirmed.

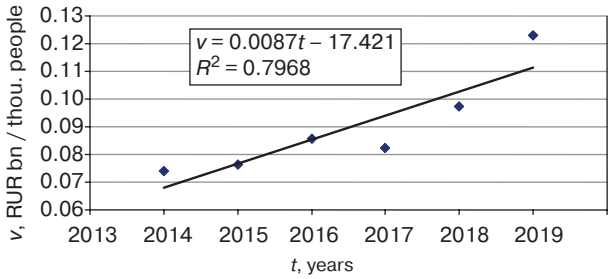

Fig. 6. Trend of indicator *v* for region 69

In the case of a specific clustering object, there may be cases where some indicators have a stable trend, while others have a stochastic spread of values. In this case, a heuristic assessment will be required to make a decision.

Other regions classified as unstable (46 in Kursk oblast, 23 in Krasnoyarsk krai, 51 in Murmansk oblast, and 76 in Yaroslavl oblast) are characterized by a high level of stochasticity, making them candidates for increased attention in terms of state socioeconomic regulation.

The diagram illustrating intracluster instability by dispersion (2) (Fig. 7) showed abnormal behavior of the graphs for the regions already mentioned above. Regions 2 (Republic of Bashkortostan) and 11 (Republic of Komi) were added.

At the stage of identifying migration between clusters (Fig. 8), regions 65 (Sakhalin oblast) and 68 (Tambov oblast) were included in the analysis.

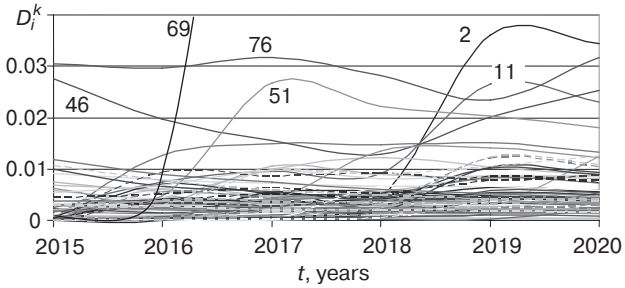

Fig. 7. Dynamics of dispersions (2) in regional analysis

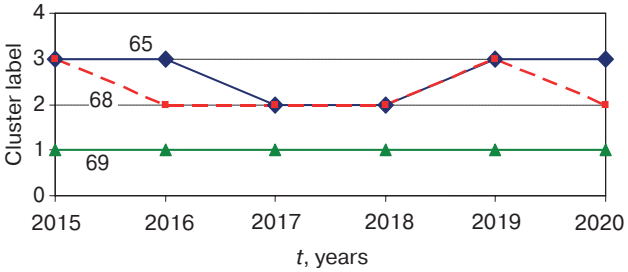

Fig. 8. Migration of regions 65, 68, and 69 between clusters

The absence of migration between clusters in region 69 once again confirmed its high level of socioeconomic development.

Regression analysis of the regions added showed that the increase in dispersion (2) for regions 2 and 11 can be largely explained by the positive dynamics of their indicators (see the example for region 2 in Fig. 9 with an acceptable R^2 value). In the case of regions 65 and 68, their migration between clusters is determined by the high level of stochasticity of economic indicators (see the example for region 65 in Fig. 9 with a low R^2 value), requiring measures to be taken within the framework of state regulation.

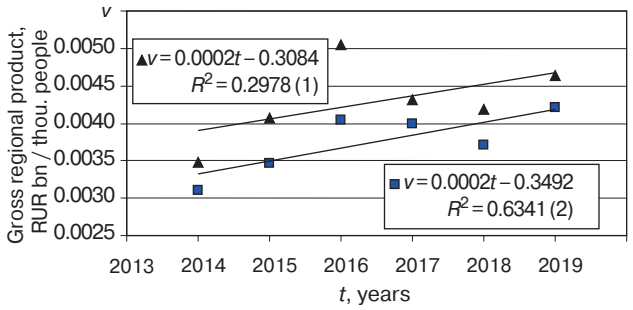

Fig. 9. Trends in relative gross regional product: (1) for region 65 (black triangles); (2) for region 2 (blue squares)

Thus, based on the results of the analysis, recommendations can be given on the development of measures within the framework of state regulation, aimed at improving and stabilizing the functioning of the socioeconomic system in regions 46, 23, 51, 76, 65, and 68.

CONCLUSIONS

The article presents an approach to information support for management decisions in conditions of uncertainty. This is achieved by means of an indirect assessment of the impact of factors on the controlled system using a method based on cluster analysis of time series data. The proposed technology is focused

on two classes of tasks: decision-making in conditions of possible deliberate data distortion; and when detecting unstable functioning of the system being analyzed.

The proposed theoretical provisions have been tested in practice using real data to resolve matters of concern to the tax administration and state regulation of the functioning of regional socioeconomic systems.

REFERENCES

1. Anfyorov M.A. Genetic clustering algorithm. *Russian Technological Journal*. 2019;7(6):134–150 (in Russ.). https://doi.org/10.32362/2500-316X-2019-7-6-134-150
2. Zamyatina E.E. Clustering of constituent entities of the Russian Federation by the level of development of creative industries. *Progressivnaya ehkonomika = Progressive Economy*. 2024;9:113–128 (in Russ.). https://doi.org/10.54861/27131211_2024_9_113
3. Protasov Yu.M., Yurov V.M. Clusterization of the Regions of the Russian Federation by their Level Socio-Economic Development. *Vestnik Moskovskogo gosudarstvennogo oblastnogo universiteta. Seriya Ehkonomika = Bulletin of Moscow Region State University. Series*: *Economicsi*. 2022;2:95–103 (in Russ.). https://doi.org/10.18384/2310-6646-2022-2-95-103
4. Anfyorov M.A., Rashitova O.B. SADT modeling of the taxation system in the Russian Federation. *Ehkonomika i upravlenie*: *nauchno-prakticheskii zhurnal = Economics and Management*: *Research and Practice Journal.* 2015;124(2):94–101 (in Russ.). https://www.elibrary.ru/tqjqfj
5. Vylkova E.S., Viktorova N.G., Naumov V.N., Pokrovskaya N.V. Tax clusterization of regions of the Russian Federation to identify territories-drivers of sustainable development. *Vestnik Tomskogo gosudarstvennogo universiteta. Ehkonomika = Tomsk State University Journal of Economics.* 2021;53:138–157 (in Russ.). https://doi.org/10.17223/19988648/53/11
6. Greenberg G.M., Nikolaeva Y.S., Hegay L.B. Cluster approach to development of electronic educational resources for students of the technical university. In: *Reshetnev Readings*: *Proceedings of the 25th International Scientific and Practical Conference.* Krasnoyarsk, November 10–12, 2021. Krasnoyarsk: Siberian State University of Science and Technology; 2021. P. 685–687 (in Russ.). https://elibrary.ru/yjchna
7. Nosova S.A., Turlapov V.E. Detection of brain cells in optical microscopy based on textural features with machine learning methods. *Program. Comput. Soft.* 2019;45(4):171–179. https://doi.org/10.1134/S0361768819040054
[Original Russian Text: Nosova S.A., Turlapov V.E. Detection of brain cells in optical microscopy based on textural features with machine learning methods. *Programmirovanie*. 2019;4:36–45 (in Russ.). https://doi.org/10.1134/S0132347419040058]
8. Hamad Y.A., Zotin A.G., Simonov K.V., Medievsky A.V., Chizhova I.G. Detection and evaluation of breast pathology based on fuzzy clustering and discrete wavelet transform. *Meditsina i vysokie tekhnologii = Medicine and High Technology*. 2023;2:5–13 (in Russ.). https://www.elibrary.ru/ujqlwd
9. Raja R., Ganeshkumar P. QOSTRP: a trusted clustering based routing protocol for mobile ad-hoc networks. *Program. Comput. Soft.* 2018;44(6):407–416. https://doi.org/10.1134/S0361768818060099
[Original Russian Text: Raja R., Ganeshkumar P. QOSTRP: a trusted clustering based routing protocol for mobile ad-hoc networks. *Programmirovanie.* 2018;6:28–41 (in Russ.). https://doi.org/10.31857/S013234740002763-4]
10. Kasimov D.R., Kuchuganov A.V., Kuchuganov V.N., Oskolkov P.P. Approximation of color images based on the clusterization of the color palette and smoothing boundaries by splines and arcs. *Program. Comput. Soft.* 2018;44(5):295–302. https://doi.org/10.1134/S0361768818050043
[Original Russian Text: Kasimov D.R., Kuchuganov A.V., Kuchuganov V.N., Oskolkov P.P. Approximation of color images based on the clusterization of the color palette and smoothing boundaries by splines and arcs. *Programmirovanie.* 2018;5:3–11 (in Russ.). https://doi.org/10.31857/S013234740001211-7]
11. Bereshpolov I.S., Kravchenko Yu.A., Sleptsov A.G. Data clustering algorithm for protecting confidential information on the internet. *Izvestiya YuFU. Tekhnicheskie nauki = Izvestiya SFedU. Engineering Sciences.* 2023;3(233):74–85 (in Russ.). https://doi.org/10.18522/2311-3103-2023-3-74-85
12. Kharakhinov V.A., Sosinskaya S.S. The visualization methods for cluster analysis results of mechanical engineering components based on neural network. *Programmnaya inzheneriya = Software Engineering*. 2017;8(4):170–176 (in Russ.). https://doi.org/10.17587/prin.8.170-176
13. Kuchuganov V.N., Kuchuganov A.V., Kasimov D.R. Clustering algorithm for a set of machine parts on the basis of engineering drawings. *Program. Comput. Soft.* 2020;46(1):25–34. https://doi.org/10.1134/S0361768820010041
[Original Russian Text: Kuchuganov V.N., Kuchuganov A.V., Kasimov D.R. Clustering algorithm for a set of machine parts on the basis of engineering drawings. *Programmirovanie*. 2020;46(1):29–38 (in Russ.). https://doi.org/10.31857/S0132347420010045
14. Matveeva I.Yu. Clustering of retail investors and portfolio structure by asset class. *Izvestiya Sankt-Peterburgskogo gosudarstvennogo ekonomicheskogo universiteta*. 2023;4(142):180–184 (in Russ.). https://www.elibrary.ru/fnmsql
15. Batrasova A.D., Konovalova T.V., Komarov P.I. Clustering as a method of studying the financial stability of IT companies. *Upravlencheskii uchet = Management Accounting.* 2022;(1-2):177–182 (in Russ.). https://www.elibrary.ru/xaufce

16. Anfyorov M.A. Formalization of the structural solutions search for CAD/CAM System. In: *Computer Science*: *Problems, Methods, Technologies*: *Proceedings of the 22nd International Scientific and Practical Conference.* Voronezh, Voronezh State University, February 10–12, 2022. Voronezh: VELBORN; 2022. P. 881–886 (in Russ.). https://elibrary.ru/dsdxhp
17. Yakovlev D.D., Petrov D.Yu. Application of exploratory data analysis for clusterization of robotic assembly complexes structures. *Avtomatizirovannoe proektirovanie v mashinostroenii.* 2024;17:71–75 (in Russ.). https://doi.org/10.26160/2309-8864-2024-17-71-75
18. Stepanov M.A. Method to identify structural transformations of time series using fuzzy clustering principles. *Vestnik Ryazanskogo gosudarstvennogo radiotekhnicheskogo universiteta = Vestnik of Ryazan state Radioengineering University*. 2019;69:149–159 (in Russ.). https://doi.org/10.21667/1995-4565-2019-69-149-159
19. Kladov D.E., Berikov V.B., Klimontov V.V. Time Series Clustering Algorithm and Its Application for Glycemic Curve Analysis. In: *KNOWLEDGE – ONTOLOGY – THEORY: Proceedings of the 9th International Conference.* Novosibirsk, October 2–6, 2023. Novosibirsk: Sobolev Institute of Mathematics, SB RAS; 2023. P. 154–161 (in Russ.). https://elibrary.ru/qqzzvw
20. Tishhenko A.K., Pliss I.P. Segmentation of Multidimensional Nonstationary Time Series Using the Fuzzy Clustering Method. *Vostochno-Evropeiskii Zhurnal Peredovykh Tekhnologii.* 2012;4(58):24–26 (in Russ.). Available from URL: https://cyberleninka.ru/article/n/segmentatsiya-mnogomernyh-nestatsionarnyh-vremennyh-ryadov-s-pomoschyu-metoda-nechetkoy-klasterizatsii. Accessed February 02, 2025.
21. Dulya I.S. Applying deep learning techniques to the time series clustering problem. *Alleya nauki*. 2021;1(5):974–978 (in Russ.). https://elibrary.ru/nokchy
22. Hurley C., Mclean J. *Wavelet Analysis and Methods.* Waltham Abbey: ED-Tech Press; 2021, 366 p.
23. Spirina P.V., Semenova A.R. Cluster analysis of the dynamics of innovation activities of the constituent entities of the Russian Federation. *Ehkonomicheskie issledovaniya i razrabotki = Economic Development Research Journal*. 2021;8:42–53 (in Russ.). https://elibrary.ru/oiqybo
24. Zhikhalkina N.F. Dynamic approach to clustering problem. *Matematicheskie struktury i modelirovanie = Mathematical Structures and Modeling.* 2000;5:133–139 (in Russ.). Available from URL: https://cyberleninka.ru/article/n/dinamicheskiy-podhod-k-zadache-klasterizatsii. Accessed February 02, 2025.
25. Ryzhkov D.V. About Dynamic Time Series Clustering Methods. In: *Science. Technologies. Innovations*: *Collection of Scientific Papers of the 17th All-Russian Scientific Conference of Young Scientists.* Novosibirsk, December 04–08, 2023. Novosibirsk: NSTU; 2024. P. 178–182 (in Russ.). https://elibrary.ru/xykvdt
26. Zaitsev R.D. Study of the Effectiveness of Multivariate Clustering of Time Series for the Analysis of the Dynamics of Scientific and Technological Development. *Perspektivy razvitiya informatsionnykh tekhnologii.* 2015;25:7–13 (in Russ.). https://www.elibrary.ru/uhrwjt
27. Ten Holt G.A., Reinders M.J.T., Hendriks E.A. Multi-dimensional dynamic time warping for gesture recognition. In: *Thirteenth Annual Conference on the Advanced School for Computing and Imaging.* Netherlands: V. 300. 2007, 8 p. Available from URL: https://www.researchgate.net/publication/228740947. Accessed February 02, 2025.
28. Kocheturov A.A., Batsyn M.V., Pardalos P.M. Dynamics of cluster structures in stock market networks. *Zhurnal novoi ehkonomicheskoi assotsiatsii = The Journal of the New Economic Association.* 2015;4(28):12–30 (in Russ.). https://www.elibrary.ru/vdzrqh
29. Kohonen T. *Self-Organizing Maps.* 3rd ed. Berlin – New York: Springer-Verlag; 2001, 521 p.
30. Anfyorov M.A. Clustering in decision-making. *Informatsionnye tekhnologii. Problemy i resheniya.* 2020;2(11):97–102 (in Russ.). https://www.elibrary.ru/rwddvo
31. Davydova G.V., Belikov A.Yu. Methodology for Quantitative Assessment of Enterprise Bankruptcy Risk. *Upravlenie riskom.* 1999;3:13–20 (in Russ.). https://www.elibrary.ru/tdgdrb

СПИСОК ЛИТЕРАТУРЫ

1. Анфёров М.А. Генетический алгоритм кластеризации. *Russian Technological Journal*. 2019;7(6):134–150. https://doi.org/10.32362/2500-316X-2019-7-6-134-150
2. Замятина Е.Э. Кластеризация субъектов Российской Федерации по уровню развития креативных индустрий. *Прогрессивная экономика*. 2024;9:113–128. https://doi.org/10.54861/27131211_2024_9_113
3. Протасов Ю.М., Юров В.М. Кластеризация регионов РФ по уровню их социально-экономического развития. *Вестник Московского государственного областного университета. Серия Экономика*. 2022;2:95–103. https://doi.org/10.18384/2310-6646-2022-2-95-103
4. Анфёров М.А., Рашитова О.Б. SADT-моделирование системы налогообложения в Российской Федерации. *Экономика и управление*: *научно-практический журнал*. 2015;124(2):94–101. https://www.elibrary.ru/tqjqfj
5. Вылкова Е.С., Викторова Н.Г., Наумов В.Н., Покровская Н.В. Кластерный анализ регионов РФ для выявления территорий – драйверов устойчивого развития: налоговая компонента. *Вестник Томского государственного университета. Экономика.* 2021;53:138–157. https://doi.org/10.17223/19988648/53/11
6. Гринберг Г.М., Николаева Ю.С., Хегай Л.Б. Кластерный подход к разработке электронных образовательных ресурсов для студентов технического университета. В сб.: *Решетневские чтения*: *Материалы XXV Международной научно-практической конференции.* Красноярск, 10–12 ноября 2021 г. Красноярск: Сибирский государственный университет науки и технологий; 2021. С. 685–687. https://elibrary.ru/yjchna

7. Носова С.А., Турлапов В.Е. Детектирование клеток мозга в оптической микроскопии на основе текстурных характеристик методами машинного обучения. *Программирование*. 2019;4:36–45. https://doi.org/10.1134/S0132347419040058
8. Хамад Ю.А., Зотин А.Г., Симонов К.В., Медиевский А.В., Чижова Т.Г. Обнаружение и оценка патологии молочной железы на основе нечеткой кластеризации и дискретного вейвлет преобразования. *Медицина и высокие технологии*. 2023;2:5–13. https://www.elibrary.ru/ujqlwd
9. Raja R., Ganeshkumar P. QoSTRP: надежный протокол маршрутизации на основе кластеризации для мобильных самоорганизующихся сетей. *Программирование*. 2018;6:28–41. https://doi.org/10.31857/S013234740002763-4
10. Кучуганов А.В., Кучуганов В.Н., Осколков П.П., Касимов Д.Р. Аппроксимация цветных изображений на основе кластеризации цветовой палитры и сглаживания границ сплайнами и дугами. *Программирование*. 2018;5:3–11. https://doi.org/10.31857/S013234740001211-7
11. Берешполов И.С., Кравченко Ю.А., Слепцов А.Г. Алгоритм кластеризации данных для защиты конфиденциальной информации в сети интернет. *Известия ЮФУ. Технические науки*. 2023;3(233):74–85. https://doi.org/10.18522/2311-3103-2023-3-74-85
12. Харахинов В.А., Сосинская С.С. Исследование способов кластеризации деталей машиностроения на основе нейронных сетей. *Программная инженерия*. 2017;8(4):170–176. https://doi.org/10.17587/prin.8.170-176
13. Кучуганов В.Н., Кучуганов А.В., Касимов Д.Р. Алгоритм кластеризации множества деталей по чертежам. *Программирование*. 2020;46(1):29–38. https://doi.org/10.31857/S0132347420010045
14. Матвеева И.Ю. Кластеризация розничных инвесторов и структура портфеля по классам активов. *Известия Санкт-Петербургского государственного экономического университета*. 2023;4(142):180–184. https://www.elibrary.ru/fnmsql
15. Батрасова А.Д., Коновалова Т.В., Комаров П.И. Кластеризация как метод исследования финансовой устойчивости IT-компаний. *Управленческий учет*. 2022;(1-2):177–182. https://www.elibrary.ru/xaufce
16. Анфёров М.А. Формализация поиска структурных решений в САПР ТП. В сб.: *Информатика*: *проблемы, методы, технологии*: *Материалы XXII Международной научно-практической конференции.* Воронеж, Воронежский государственный университет, 10–12 февраля 2022 г. Воронеж: ВЭЛБОРН. 2022. С. 881–886. https://elibrary.ru/dsdxhp
17. Яковлев Д.Д., Петров Д.Ю. Применение разведочного анализа данных для кластеризации структур робототехнических сборочных комплексов. *Автоматизированное проектирование в машиностроении.* 2024;17:71–75. https://doi.org/10.26160/2309-8864-2024-17-71-75
18. Степанов М.А. Методика выявления структурных трансформаций временных рядов с использованием принципов нечеткой кластеризации. *Вестник Рязанского государственного радиотехнического университета*. 2019;69:149–159. https://doi.org/10.21667/1995-4565-2019-69-149-159
19. Кладов Д.Е., Бериков В.Б., Климонтов В.В. Алгоритм кластеризации временных рядов и его применение для анализа гликемических кривых. В сб.: *ЗНАНИЯ – ОНТОЛОГИИ – ТЕОРИИ*: *Материалы IX Международной конференции.* Новосибирск, 02–06 октября 2023 г. Новосибирск: Институт математики им. С.Л. Соболева СО РАН; 2023. С. 154–161. https://elibrary.ru/qqzzvw
20. Тищенко А.К., Плисс И.П. Сегментация многомерных нестационарных временных рядов с помощью метода нечеткой кластеризации. *Восточно-европейский журнал передовых технологий*. 2012;4(58):24–26. URL: https://cyberleninka.ru/article/n/segmentatsiya-mnogomernyh-nestatsionarnyh-vremennyh-ryadov-s-pomoschyu-metoda-nechetkoy-klasterizatsii. Дата обращения 02.02.2025. / Accessed February 02, 2025.
21. Дуля И.С. Применение методов глубокого обучения к задаче кластеризации временных рядов. *Аллея науки.* 2021;1(5):974–978. https://elibrary.ru/nokchy
22. Hurley C., Mclean J. *Wavelet Analysis and Methods.* Waltham Abbey: ED-Tech Press; 2021, 366 p.
23. Спирина П.В., Семенова А.Р. Кластерный анализ динамики инновационной деятельности субъектов Российской Федерации. *Экономические исследования и разработки*. 2021;8:42–53. https://elibrary.ru/oiqybo
24. Жихалкина Н.Ф. Динамический подход к задаче кластеризации. *Математические структуры и моделирование.* 2000;5:133–139. URL: https://cyberleninka.ru/article/n/dinamicheskiy-podhod-k-zadache-klasterizatsii. Дата обращения 02.02.2025. / Accessed February 02, 2025.
25. Рыжков Д.В. О методах кластеризации динамических временных рядов. В сб.: *Наука. технологии. Инновации*: *Сборник научных трудов XVII Всероссийской научной конференции молодых ученых.* Новосибирск, 04–08 декабря 2023 г. Новосибирск: НГТУ; 2024. С. 178–182. https://elibrary.ru/xykvdt
26. Зайцев Р.Д. Исследование эффективности многомерной кластеризации временных рядов для анализа динамики научно-технического развития. *Перспективы развития информационных технологий*. 2015;25:7–13. https://www.elibrary.ru/uhrwjt
27. Ten Holt G.A., Reinders M.J.T., Hendriks E.A. Multi-dimensional dynamic time warping for gesture recognition. In: *Thirteenth Annual Conference on the Advanced School for Computing and Imaging.* Netherlands: V. 300. 2007, 8 p. URL: https://www.researchgate.net/publication/228740947. Дата обращения 02.02.2025. / Accessed February 02, 2025.
28. Кочетуров А.А., Бацын М.В., Пардалос П.М. Динамика кластерных структур в сетях фондовых рынков. *Журнал новой экономической ассоциации.* 2015;4(28):12–30. https://www.elibrary.ru/vdzrqh
29. Kohonen T. *Self-Organizing Maps.* 3rd ed. Berlin – New York: Springer-Verlag; 2001, 521 p.

30. Анфёров М.А. Кластеризация в принятии решений. *Информационные технологии. Проблемы и решения*. 2020;2(11): 97–102. https://www.elibrary.ru/rwddvo
31. Давыдова Г.В., Беликов А.Ю. Методика количественной оценки риска банкротства предприятий. *Управление риском*. 1999;3:13–20. https://www.elibrary.ru/tdgdrb

About the Author

Mikhail A. Anfyorov, Dr. Sci. (Eng.), Professor, Department of Domain-Specific Information Systems, Institute for Cybersecurity and Digital Technologies, MIREA – Russian Technological University (78, Vernadskogo pr., Moscow, 119454 Russia). E-mail: anfyorov@inbox.ru. RSCI SPIN-code 4829-2523, https://orcid.org/0000-0003-2853-6184

Об авторе

Анфёров Михаил Анисимович, д.т.н., профессор, кафедра «Предметно-ориентированные информационные системы», Институт кибербезопасности и цифровых технологий, ФГБОУ ВО «МИРЭА – Российский технологический университет» (119454, Россия, Москва, пр-т Вернадского, д. 78). E-mail: anfyorov@inbox.ru. SPIN-код РИНЦ 4829-2523, https://orcid.org/0000-0003-2853-6184

Translated from Russian into English by Lyudmila O. Bychkova
Edited for English language and spelling by Dr. David Mossop

Information systems. Computer sciences. Issues of information security
Информационные системы. Информатика. Проблемы информационной безопасности

UDC 004.415.53
https://doi.org/10.32362/2500-316X-2026-14-2-17-28
EDN XDBAIA

RESEARCH ARTICLE

Architecture of a distributed system for testing Internet of Things devices at the development stage

Danila S. Belyakov @

Tomsk State University of Control Systems and Radioelectronics, Tomsk, 634050 Russia
@ *Corresponding author, e-mail: cauze4concern@yandex.ru*

• **Submitted:** 11.07.2025 • **Revised:** 15.10.2025 • **Accepted:** 06.02.2026

Abstract

Objectives. The paper sets out to develop an architecture for a distributed testing system for Internet of Things (IoT) devices to ensure secure transmission and the isolated execution of test scenarios on dedicated execution modules. The study takes account of the rapid growth in the number of IoT devices operating in untrusted computing environments, in which the testing process can pose a risk of confidential data leakage or unauthorized interference with software components.

Methods. A comparative analysis of existing solutions such as *NI TestStand*, *MagicDAQ*, *PHiLIP*, and *KEOLABS ContactLAB* was conducted. Architectural components and test scenario life-cycle processes were examined and compared.

Results. The analysis identified the main stages of the test scenario life cycle, including preparation and storage of scripts, transmission and interpretation, interaction with the device under test, as well as registration and analysis of results. In addition, existing and proposed architectural solutions were compared according to the following key characteristics: application domain; type of architecture (distributed or centralized); test scenario execution environment; system scalability; level of execution isolation; availability of protection mechanisms; capability for remote management. The results of the study are presented in the form of a proposed architecture that includes a control module and autonomous execution modules with an isolated virtual MicroPython environment. To ensure security, test scenarios are transmitted over an encrypted communication channel using constrained application protocol and datagram transport layer security (protocol, while the execution of test code takes place in a restricted environment isolated from the main operating system.

Conclusions. The comparative analysis confirmed that the proposed solution eliminates the key limitations of existing solutions, namely the lack of encryption mechanisms and isolation of execution. The developed architecture enhances the security and reliability of the IoT device testing process, offering protection for intellectual property and test scenario logic in untrusted computing environments.

Keywords: Internet of Things, IoT, functional testing, testing architecture, test scenarios

For citation: Belyakov D.S. Architecture of a distributed system for testing Internet of Things devices at the development stage. *Russian Technological Journal.* 2026;14(2):17–28. https://doi.org/10.32362/2500-316X-2026-14-2-17-28, https://www.elibrary.ru/XDBAIA

Financial disclosure: The author has no financial or proprietary interest in any material or method mentioned.

The author declares no conflicts of interest.

НАУЧНАЯ СТАТЬЯ

Архитектура распределенной системы тестирования устройств интернета вещей на этапе их разработки

Д.С. Беляков @

Томский государственный университет систем управления и радиоэлектроники, Томск, 634050 Россия
@ *Автор для переписки, e-mail: cauze4concern@yandex.ru*

• **Поступила:** 11.07.2025 • **Доработана:** 15.10.2025 • **Принята к опубликованию:** 06.02.2026

Резюме

Цели. Цель работы заключается в разработке архитектуры распределенной системы тестирования устройств интернета вещей (Internet of Things, IoT), обеспечивающей защищенную передачу тестовых сценариев и их изолированное исполнение на исполнительных модулях. Актуальность исследования обусловлена стремительным ростом числа IoT-устройств, функционирующих в недоверенных вычислительных средах, где процесс тестирования может создавать риски утечки конфиденциальных данных или несанкционированного вмешательства в программное обеспечение.

Методы. Проведен сравнительный анализ существующих решений, таких как *NI TestStand*, *MagicDAQ*, *PHiLIP* и *KEOLABS ContactLAB*. Выполнено сопоставление их архитектурных компонентов и процессов жизненного цикла тестовых сценариев.

Результаты. На основании анализа выделены основные этапы жизненного цикла, на которых применяются рассмотренные инструменты: подготовка и хранение, передача и интерпретация, взаимодействие с тестируемым устройством, регистрация и анализ результатов. Кроме того, проведено сравнение существующих и предложенного архитектурных решений по ключевым характеристикам: предметная область применения, тип архитектуры (распределенная или централизованная), среда исполнения тестовых сценариев, масштабируемость системы, уровень изоляции среды исполнения, наличие механизмов защиты и возможность удаленного управления. Результаты работы представлены в виде предложенной архитектуры, включающей управляющий модуль и автономные исполнительные модули с изолированной виртуальной средой исполнения MicroPython. Для обеспечения безопасности предусмотрена передача тестовых сценариев по зашифрованному каналу связи с использованием протоколов CoAP[1] и DTLS[2] , а также выполнение кода тестовых сценариев в ограниченной среде, изолированной от основной операционной системы.

[1] Constrained application protocol – облегченный протокол интернета вещей.
[2] Datagram transport layer security – протокол передачи данных, обеспечивающий защищенность соединений для протоколов, использующих датаграммы.

Выводы. Проведенный сравнительный анализ продемонстрировал, что предлагаемое решение устраняет ключевые ограничения аналогов, связанные с отсутствием механизмов шифрования и изоляции исполнения. Разработанная архитектура повышает безопасность и надежность процесса тестирования IoT-устройств и может использоваться в недоверенных вычислительных средах для защиты интеллектуальной собственности и логики тестовых сценариев.

Ключевые слова: интернет вещей, IoT, функциональное тестирование, архитектура тестирования, тестовые сценарии

Для цитирования: Беляков Д.С. Архитектура распределенной системы тестирования устройств интернета вещей на этапе их разработки. *Russian Technological Journal*. 2026;14(2):17–28. https://doi.org/10.32362/2500-316X-2026-14-2-17-28, https://www.elibrary.ru/XDBAIA

Прозрачность финансовой деятельности: Автор не имеет финансовой заинтересованности в представленных материалах или методах.

Автор заявляет об отсутствии конфликта интересов.

INTRODUCTION

The widespread use of Internet of Things (IoT) devices requires compliance with high quality, safety, and reliability standards. In these circumstances, testing is crucial for the identification and elimination of potential malfunctions to ensure that the devices meet the specified technical requirements and can function stably in real operating conditions [1, 2].

Unlike traditional software, testing IoT devices presents a number of specific challenges. Since encompassing both hardware and software components, such testing involves the consideration of various communication protocols, limited computing resources, and the characteristics of low-level interfaces. An additional complication arises due to testing often being outsourced to third-party organizations that may not be trustworthy, which creates risks of unauthorized interference and compromised results [3].

In this regard, the paper aims to analyze existing solutions for testing IoT devices and to develop a new distributed testing system architecture that addresses the identified shortcomings.

1. THEORETICAL BASIS OF TESTING

Based on the specific characteristics of IoT devices, testing can be divided into three main levels [4–6]: device, network, and system testing.

Device testing involves checking the device itself as a separate unit. This covers both the hardware components (e.g., the microcontroller, sensors and actuators) and the embedded software. The first stage involves verifying the correct operation of the peripheral interfaces (serial peripheral interface (SPI), universal asynchronous receiver-transmitter (UART), etc.) that facilitate communication between the microcontroller and external modules. Next, the device's firmware logic, data processing algorithms, performance, and reliability under load or interference are evaluated.

Network testing focuses on the communication infrastructure. The measured parameters include the bandwidth, latency, reliability, and scalability of the communication channels used (e.g., Wi-Fi, cellular networks, low-power wide-area network, etc.). This ensures the required quality of service for IoT devices [7].

On the other hand, system testing covers the entire range of devices and infrastructure, carrying out checks into how several devices interact with each other, as well as with gateways and the cloud platform. Here it is also necessary to ascertain the correctness of end-to-end data processing and user scenarios. This comprehensive integration testing involves working through scenarios from an event on a device to the receipt of data in the cloud and the return response.

Therefore, to comprehensively assess the functioning of IoT systems, thorough testing must be conducted at each level to cover various aspects of their operation, ranging from hardware components to device interaction within a distributed environment.

2. ARCHITECTURAL ANALYSIS OF EXISTING SOLUTIONS

Testing tools are software or hardware solutions designed to automate and streamline the testing of IoT devices. They support specialists in evaluating various characteristics, including functionality, performance, stability and security. These tools are used to to simulate a wide range of operating scenarios and environmental conditions, thereby ensuring more reliable testing of device behavior in various conditions.

The majority of contemporary research and development in the realm of IoT testing revolves around system- or network-level testing. The most common solutions are those that verify the correct implementation of protocols (constrained application

protocol, MQTT[3], 6LoWPAN[4], etc.), node compatibility, performance, and network connection reliability. Platforms such as PatrIoT [8], Hector [9], F-Interop [10], MATTER [11], and Eclipse IoT-Testware [12] typically use virtualization mechanisms to facilitate scalable testing of architectural scenarios without the involvement of real physical equipment.

Checks implemented at the physical device level are usually limited to highly specialized solutions and are less formalized. Therefore, it seems appropriate to consider system architectures specifically oriented towards the device level and compare them. The basic architecture of the testing system shown in Fig. 1 includes the following components:

- The control module coordinates the launch of tests and distributes tasks among the execution modules.
- Executive modules are one or more devices that interact directly with the device under test through physical interfaces.
- The device under test is the object being tested.

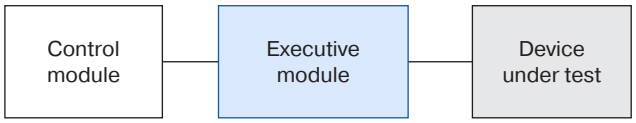

Fig. 1. Typical architecture of a testing system

Subject analysis is carried out to identify the tools used at the device testing level.

NI TestStand[5] is a commercial test management system that integrates with the *NI LabVIEW* measurement programming environment. The corresponding system architecture is depicted in Fig. 2.

The control module, which is installed on a PC, is designed for centralized control of automated execution modules. It also records test results to ensure their collection and visualization.

Executive modules are data collection systems connected to the control module that interact directly with the device under test via physical interfaces to execute test commands.

The script execution environment is located directly within the operating system (OS) on the control module. Built-in OS functions provide system security by controlling resources and test results.

The *NI TestStand* functional capabilities include creating test scenarios that can be executed for a single device or multiple devices simultaneously. Testing is coordinated through parallel interaction between several control modules via a local network. However, this interaction is currently limited to internal enterprise or laboratory networks, as the system does not initially support full remote control via an internet connection. Nevertheless, *NI TestStand* provides a command interface for initiating testing from external continuous integration (CI) systems.

Thus, *NI TestStand* is a local, centralized testing system offering a sophisticated user interface and support for continuous integration processes. However, it lacks built-in mechanisms for distributed processing or the isolated operation of test modules.

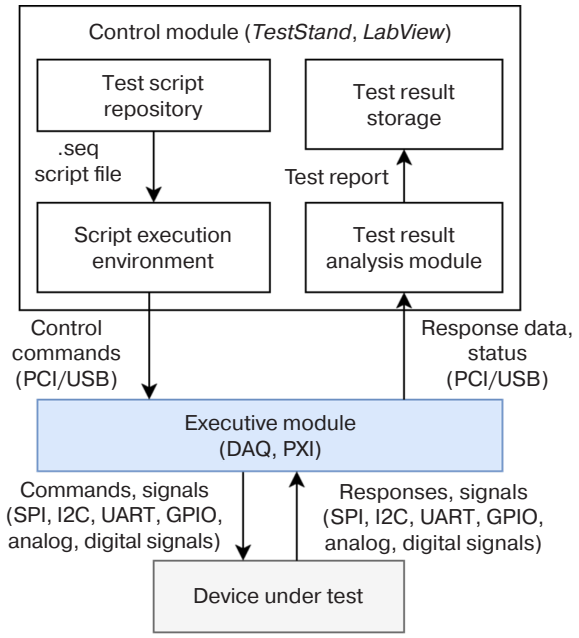

Fig. 2. *NI TestStand* testing architecture for a single device. PCI (Peripheral Component Interconnect) is an input/output bus for connecting peripheral devices to a computer motherboard; USB (Universal Serial Bus) is a universal serial bus; I2C (Inter-Integrated Circuit) is a serial asymmetric bus; GPIO (General Purpose Input/Output) is a general purpose input/output interface; DAQ (Data Acquisition) is software and hardware for collecting data; and PXI (PCI eXtensions for Instrumentation) is a PCI extension for measurement systems

MagicDAQ[6] is an executive module that connects to the control module (PC) via a USB interface (Fig. 3). All testing logic is implemented on the control module by executing test scripts in Python, which then send commands to the executive module via the USB connection. It should be noted that *MagicDAQ* is not a completely distributed system or cloud service;

[3] Message queuing telemetry transport is a lightweight, publish–subscribe, machine-to-machine network protocol for message queue/message queuing service.

[4] IPv6 over Low-Power Wireless Personal Area Networks, based on the IEEE 802.15.4 standard.

[5] TestStand Release Notes. https://www.ni.com/en/support/documentation/release-notes/product.teststand.html. Accessed July 07, 2025.

[6] *MagicDAQ* Docs. https://magicdaq.github.io/magicdaq_docs/. Accessed July 07, 2025.

rather, it is a peripheral module for a local PC, whose scalability is determined by the number of available USB ports. As test scripts are written in Python and transmitted via a local connection, security is implemented using built-in operating system tools.

Thus, *MagicDAQ* is characterized as a specialized solution for local use in measurement systems with limited scalability and no distributed data processing mechanisms.

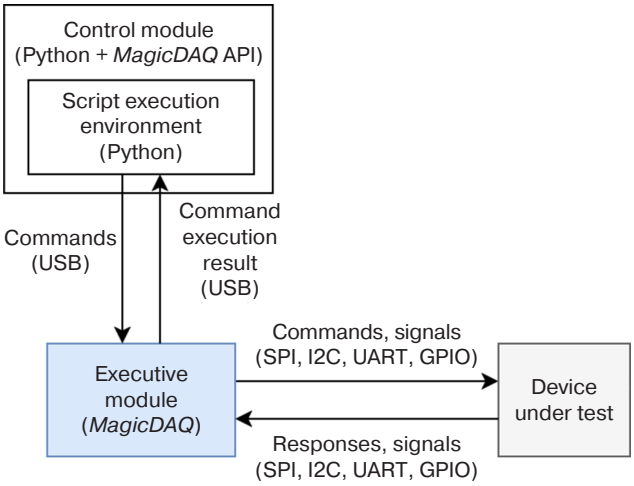

Fig. 3. *MagicDAQ* testing architecture.
API is Application Programming Interface

A software and hardware platform known as *PHiLIP* [8] has been developed for the automated testing of microcontroller peripheral interfaces in embedded systems, including IoT devices.

The *PHiLIP* testing system architecture is based on a distributed model, which provides a central control module in the form of a continuous integration server (such as Jenkins) integrated with the Git version control system for storing and updating test scripts. As illustrated in Fig. 4, the control module coordinates test runs, stores, and distributes test cases, as well as transferring firmware to the devices under test and collecting test result data for further analysis.

Each executive module, which is based on a Raspberry Pi single-board computer (manufactured by Raspberry Pi Holdings plc, United Kingdom), functions as an intermediary between the CI server and the *PHiLIP* hardware interface module. The module runs test scenarios in the Robot Framework environment[7] and uses serial wire debug or joint test action group interfaces to flash the tested devices and download new software versions. The *PHiLIP* interface module is connected to via the UART interface.

In turn, the *PHiLIP* interface module is responsible for generating and registering signals on the device under test's physical interfaces including SPI, I2C, UART, and GPIO. This module emulates the behavior of the device's external environment and records its responses, which are then returned to the execution module and subsequently to the control module for test result analysis.

As shown in Fig. 5, the system architecture allows for scaling: several executive modules can be connected to one control module, each executive module controlling its own instance of the interface module and the device under test. This structure enables parallel testing of different devices while providing centralized control and collection of results. However, [8] does not describe the mechanisms for ensuring information security, nor does it specify how test case execution is isolated, how protection against unauthorized access is ensured, or how integrity control is maintained during the transmission of test scenarios.

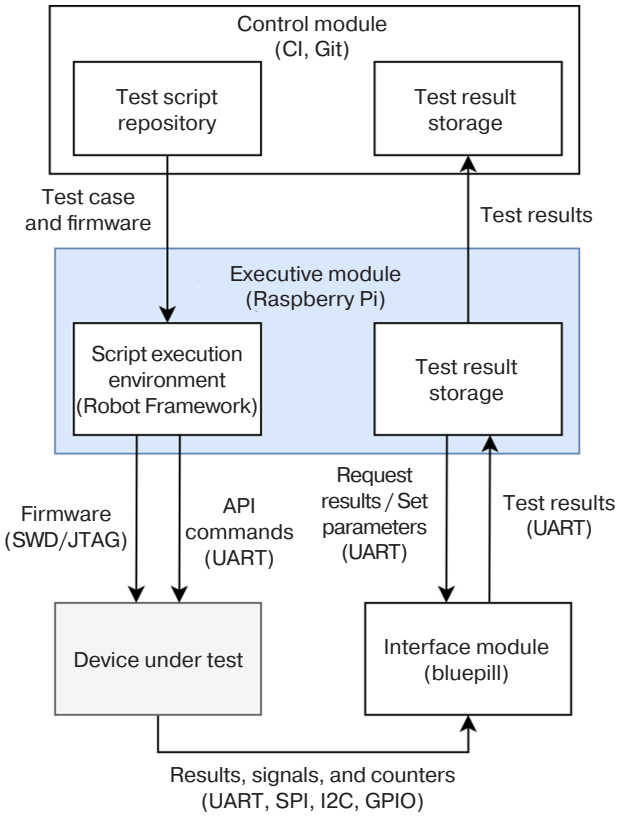

Fig. 4. *PHiLIP* testing architecture
for a single device under test

KEOLABS ContactLAB[8] is a commercial software and hardware platform designed for functional testing of smart cards, microcontrollers

[7] Robot Framework. https://robotframework.org/. Accessed July 07, 2025.

[8] Contact Tester. https://www.keolabs.com/products/platforms/contact-tester. Accessed July 07, 2025.

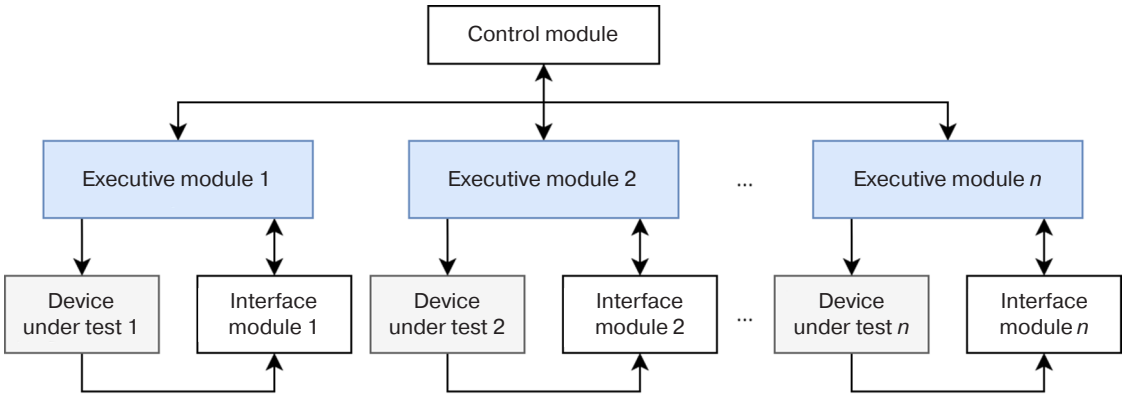

Fig. 5. *PHiLIP* test architecture for multiple devices under test

with security modules (Secure Element), as well as devices supporting NFC[9] and ISO 7816[10] contactless interfaces. It is widely used for certification testing and the development of authentication and identification tools.

The architecture of the solution (Fig. 6) is based on the use of two modules: the *SCRIPTIS*[11] software control module, which is installed on a PC, and the *ContactLAB HW* hardware execution module. The latter generates commands, measures time characteristics, and records signals from the device under test. The control and execution modules interact via a USB or Ethernet interface. Testing is performed entirely at a single workstation with no option for distributed testing or remote access. With this solution, the only way to achieve scalability is by increasing the number of stands and manually coordinating their operation. The architecture does not allow for a centralized control module or the parallel execution of scenarios on multiple devices. Security of the testing logic is ensured within the closed *SCRIPTIS* environment and its built-in access mechanisms. Test scenarios are executed in a standard user OS environment.

Therefore, *KEOLABS* is a platform for the low-level testing of secure devices in a laboratory environment. Its architecture is designed for centralized operation and lacks mechanisms for remote access or secure distributed test execution.

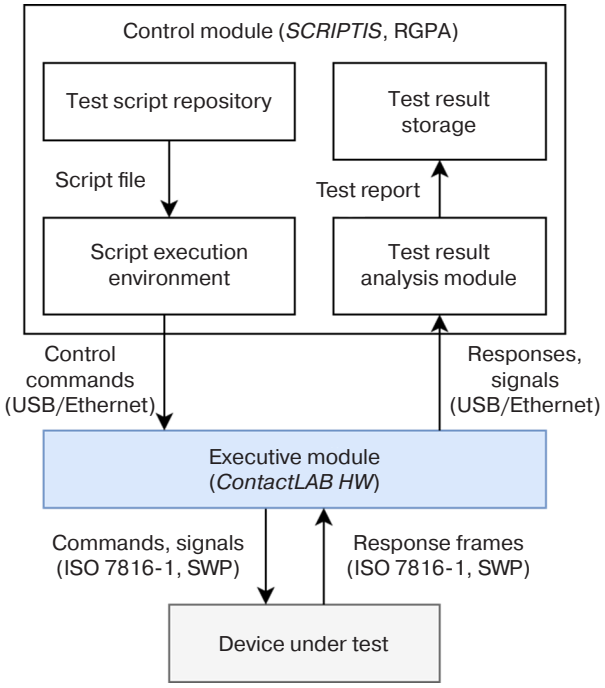

Fig. 6. *KEOLABS ContactLAB* testing architecture. RGPA (Real-Time General-Purpose Analyzer); SWP (Single Wire Protocol)

3. ANALYSIS OF TESTING PROCESSES

A number of typical processes can be identified based on the review of existing testing system architectures. As shown in Fig. 7, these processes provide a general overview of how such systems function, regardless of the specific implementation. These processes can be defined as a sequence of stages in the test scenario lifecycle:

1) preparation and storage of test scenarios;
2) planning and launching of test scenarios;
3) transfer of test scenarios to the execution module;
4) interpretation of test scenarios;
5) interaction with the object under test;
6) recording of test results;
7) analysis and generation of reports.

[9] Near Field Communication (NFC) is a technology for transmitting data wirelessly over short distances.

[10] ISO/IEC 7816-1 Identification cards—Integrated circuit cards. https://www.iso.org/standard/54089.html. Accessed July 07, 2025.

[11] *SCRIPTIS*: an intuitive testing environment. https://www.keolabs.com/products/solutions/emvco-l1-payment-testing#. Accessed July 07, 2025.

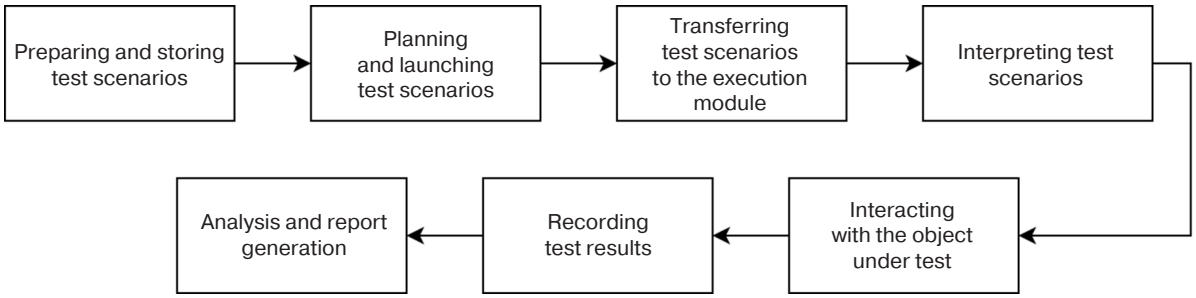

Fig. 7. Test scenario life cycle

During the preparation and storage of test scenarios, the appropriate sequence of actions, execution conditions and criteria for successful test completion are developed and described. These are created by specialists using scripting languages such as Python (e.g., in *MagicDAQ*) and Robot Framework (in *PHiLIP*), as well as other tools. Once developed, the scenarios are stored in a database or repository for subsequent use by the control module or continuous integration systems (e.g., Jenkins).

Test scenario planning and execution involves selecting the necessary tests and determining their execution sequence, as well as synchronizing and initiating the testing process. This can be performed either by an operator through the control module interface or automatically from an external continuous integration system, as with *PHiLIP* and Jenkins.

Test scripts are transferred to the execution module of the systems under review via a local network (e.g., *PHiLIP*) or physical interfaces, such as USB (e.g. *NI TestStand*, *MagicDAQ*, and *KEOLABS ContactLAB*) and Ethernet (*KEOLABS ContactLAB*). However, the analyzed solutions do not specify whether any encryption mechanisms or other measures are employed to safeguard the transmitted data.

During the test scenario interpretation stage, the scenario is processed in the execution environment, where the test logic is converted into specific commands for controlling the physical interfaces. Depending on the system, this may be the TestStand engine, a Python interpreter (*MagicDAQ*), a Robot Framework environment (*PHiLIP*), or a built-in *SCRIPTIS* environment (*KEOLABS ContactLAB*). This approach enables the test logic to be abstracted from the hardware implementation.

The test object is interacted with by an executive module that controls physical interfaces (SPI, I2C, UART, ISO 7816, etc.), ensuring the transmission of signals and commands directly to the device under test. For example, *PHiLIP* uses a separate interface module for this purpose which interacts with and depends on the Raspberry Pi as a control module.

Test result recording involves capturing data obtained during the test, such as device responses, signals, timestamps, statuses, and measured values. This data can be stored locally on the execution module or transferred immediately to the control module for further analysis.

In the final stage, the recorded data is processed and the criteria for successfully completing the test case are calculated. Reports are then generated for operators, or the results are automatically transferred to external analysis and quality management systems.

The analysis of existing IoT device testing platforms and selected typical processes revealed several limitations. All of the considered solutions have one key limitation in common: a lack of a mechanism for the secure execution of test scenarios. Test scenarios are either executed locally, delivered manually, or via a continuous integration infrastructure, with no explicit use of cryptographic protection. Additionally, many tools are local and do not support remote execution modules. In today's environment, where testing is often performed in an untrusted environment that requires the autonomous operation of execution modules, it is essential to ensure that tests can be carried out without risking interference or conflict.

Therefore, it is necessary to develop a new testing architecture for eliminating the identified shortcomings and ensuring the necessary level of security and scalability when testing IoT devices.

4. PROPOSED TESTING SYSTEM ARCHITECTURE

The proposed architecture comprises a distributed network for testing Internet of Things devices. In this network, several executive modules interact with the control module to exchange encrypted test scenarios. This architecture (Fig. 8) comprises the following key components:

- Control module. This is responsible for coordinating distributed execution modules and storing test scenarios.

- Execution modules. These are autonomous nodes that are physically connected to the devices under test. The modules execute test scenarios received from the control module, record the results, and interact with the object under test via connected interfaces. Each execution station contains a built-in, isolated execution environment in which the received test scenarios are interpreted.
- Tested devices. These are real IoT devices connected to the execution modules and tested via physical interfaces. Each test station connects to the device under test via one of the interfaces (SPI, I2C, UART, etc.). In the proposed architecture, these connections are referred to as channels, each of which comprises a logically independent unit for controlling input and output signals. Each channel corresponds to a specific interface type or interaction protocol.

The testing process begins when the operator uses the control module to initiate execution of the script. The script is then transmitted to the execution module via a secure channel and executed in an isolated environment, generating commands to interact with the device under test's interfaces. The test results are then sent back to the control module in an encrypted format for analysis.

When designing the architecture, special attention should be paid to protecting the testing logic and mitigating risks arising from operation in a potentially untrusted environment. Studies [13, 14] have shown that the various stages of the device life cycle are accompanied by threats of unauthorized access to software and leakage of test scenarios. Furthermore, the microcontrollers themselves can act as both a source and a target of attacks. In light of these threats, the system architecture incorporates a set of protective measures to be applied at various stages of the test scenario life cycle.

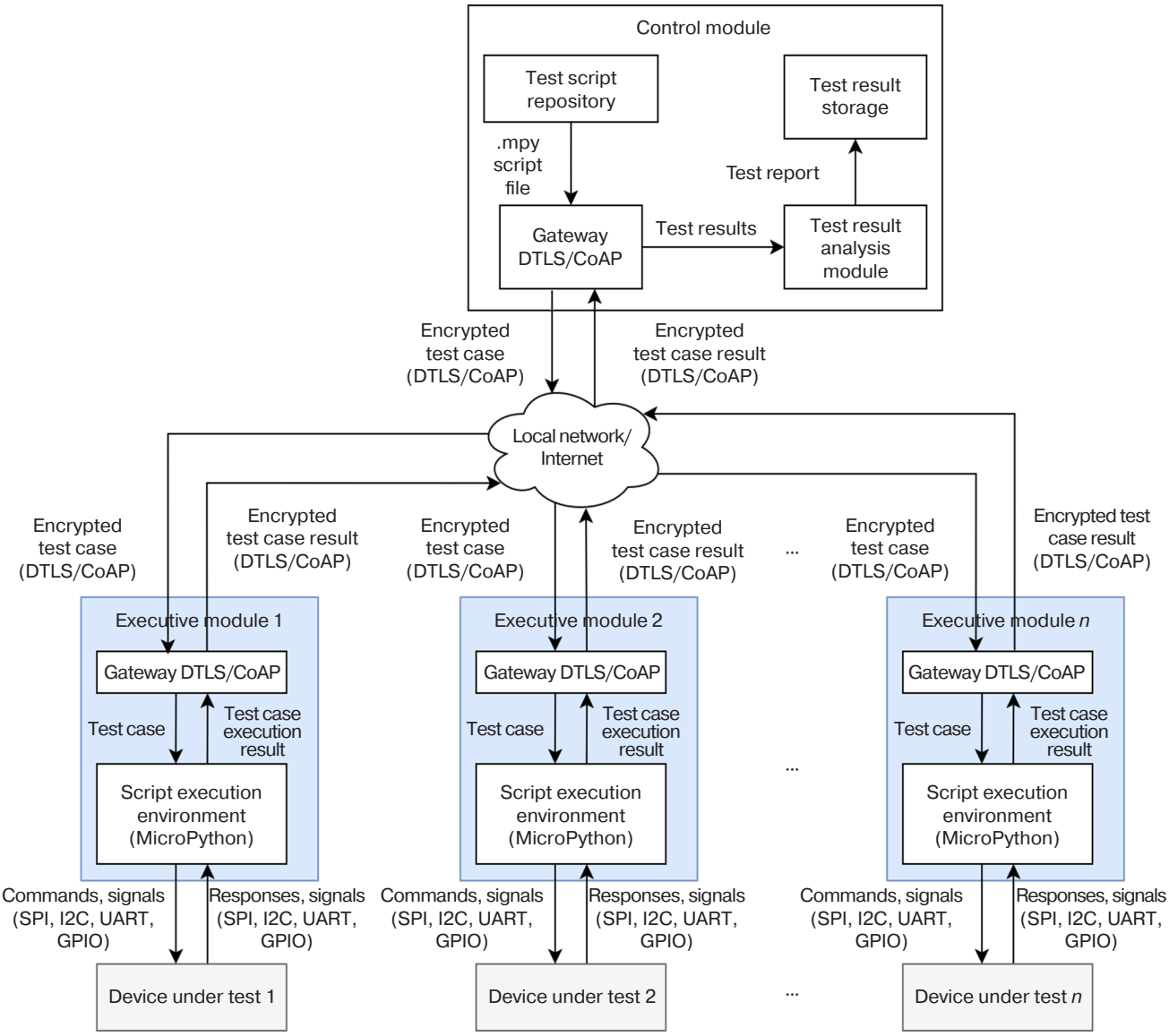

Fig. 8. Test system architecture

Table. Comparison of characteristics of existing and proposed solutions

Characteristic	*NI TestStand*	*MagicDAQ*	*PHiLIP*	*KEOLABS*	Proposed solution
Architecture type	Centralized	Centralized	Distributed	Centralized	Distributed
Execution environment	PC	PC	Executive module	PC	Executive module
Scalability	Local network (remote launch via CI)	Limited by the number of USB ports	High (adding Raspberry Pi nodes)	Limited by manual deployment	High (adding execution modules)
Execution isolation	OS	OS (Python)	Robot Framework	*SCRIPTIS*	MicroPython
Protection mechanisms	–	–	Not specified	–	DTLS
Remote control	Yes (CI)	No	Yes (CI)	No	Yes (control module)
Scope of application	General tests of electronic devices	General tests of electronic devices	Built-in OS APIs	Smart-cards, NFC	IoT devices, microcontroller interfaces

The DTLS protocol ensures the confidentiality and integrity of test scripts and results during transmission and reception. The protection of data when working in untrusted networks is particularly important for devices with limited computing resources [15].

Test scripts are executed in an isolated MicroPython[12] environment. This isolation ensures the secure execution of test scripts through compartmentalization and restricted access to resources [16].

The scalable system supports the connection of new execution modules, each of which operates autonomously. This enables parallel test execution and eliminates a single point of failure.

The table below shows the characteristics of existing and proposed architectural solutions. As can be seen, most existing systems are characterized by a centralized architecture, limited scalability, and a lack of protection mechanisms. In contrast, the proposed solution features a distributed network architecture of execution modules, an isolated execution environment, as well as encryption and authentication mechanisms. This approach ensures effective system scalability and significantly increases the protection of the test logic.

The proposed solution enhances and streamlines the processes involved in the test scenario lifecycle. Let us consider its key features and how it differs from other solutions:

- Transfer of test scenarios to the execution module. Unlike similar solutions, which transfer data via USB/Ethernet (e.g., *NI TestStand*, *MagicDAQ*, and *KEOLABS ContactLAB*) or a local network (e.g., *PHiLIP*), without using data transfer protection mechanisms, the proposed solution encrypts scenarios before transferring them from the control module to the execution module using the DTLS protocol. This ensures the confidentiality and integrity of test scenarios, even when operating in a potentially untrusted network.
- Interpretation of test scenarios. Scenarios are described as Python scripts and executed on a MicroPython virtual machine on an execution module that is isolated from the main OS. This isolation is not provided in previously discussed solutions (e.g., *NI TestStand* and *MagicDAQ*), where execution takes place in a shared user environment, creating the risk of interference with the testing logic.
- Test result recording. In many current solutions, test results either remain local (e.g., *KEOLABS ContactLAB*) or are processed manually (e.g., *MagicDAQ*), with no centralized analysis. The proposed architecture involves sending encrypted reports from modules to the control server.

The efficiency and performance of the proposed architecture are confirmed during the integration testing of the developed device. The tests are carried out on an experimental bench made up of a control module, several executive modules, and the device

[12] Micropython. https://micropython.org/. Accessed July 07, 2025.

under test. The control module is implemented on a PC, while the executive modules are implemented on SE-Discovery-GD32F427 boards (GigaDevice Semiconductor Inc., China), which have built-in software and the MicroPython environment. Interaction between the components takes place via secure network channels within a local area network. The architecture allows for remote interaction between the modules when they are connected to the internet. During testing, the following key system functions are verified: secure transmission of test scenarios and execution results and correct operation of the executive module's virtual machine. All test scenarios have been completed successfully, which confirms the operability and effectiveness of the proposed architecture.

The developed solution is used to test smart cards and hardware tokens, including verifying the correct execution of applets. During testing, power failures and unstable communication interfaces were simulated. One executive module controls the power supply to the device under test, while another ensures communication with it to reproduce real operating conditions and confirm the resistance of the system to abnormal situations.

CONCLUSIONS

The paper proposes a new architecture for a distributed testing system for IoT devices. This system was developed with consideration for the threats posed by operating in an untrusted environment. The analysis confirms that existing device testing systems are limited in terms of scalability and fail to ensure the secure transmission or execution of test scenarios. The proposed testing architecture solves these problems by implementing security measures. The use of isolated virtual execution environments and encrypted transmission channels protects test scenarios from unauthorized access or substitution.

The key advantages of the proposed architecture are therefore security (encryption and logic isolation) and scalability (the ability to add nodes without changing the architecture), making it a suitable solution for testing IoT devices in a potentially untrusted environment.

REFERENCES

1. Dyakov O.N., Belyakov D.S., Kalinin E.O. Using ePKI technology to securely update of embedded software of trusted hardware and software system. *Bezopasnost' informatsionnykh tekhnologii = IT Security* (*Russia*). 2025;32(2):152–177 (in Russ.). https://doi.org/10.26583/bit.2025.2.12
2. Venugopal M., Nanda M., Anand G., Chandana Voora H. An integrated Hardware/Software Verification and Validation methodology for Signal Processing Systems. *ITM Web Conf.* 2022;50:02001. https://doi.org/10.1051/itmconf/20225002001
3. Bures M., Cerny T., Ahmed B.S. Internet of Things: Current Challenges in the Quality Assurance and Testing Methods. *arXiv*. arXiv:1805.01241. 2018. https://doi.org/10.48550/arXiv.1805.01241
4. Mazhar T., Talpur D.B., Shloul T.A., Ghadi Y.Y., Haq I., Ullah I. Analysis of IoT Security Challenges and its Solutions Using Artificial Intelligence. *Brain Sciences*. 2023;13(4):683. https://doi.org/10.3390/brainsci13040683
5. Minani J.B., Sabir F., Moha N., Guéhéneuc Y.G. A Multimethod Study of Internet of Things Systems Testing in Industry. *IEEE Internet Things J*. 2024;11(1):1662–1684. https://doi.org/10.1109/JIOT.2023.3291233
6. Papulovskaya N.V., Izotov I.N., Blinichkin D.Y., Kataev A.Y. Core Platform Development for IoT-devices Automated Testing. *Int. J. Open Inf. Technol*. 2021;9(6):38–45 (in Russ.). https://elibrary.ru/ybxvtg
7. Castelo Branco K.D.S., Dantas V.L.L., Carvalho L.M. Interoperability Testing Guide for the Internet of Things. In: *Proceedings of the 30th Brazilian Symposium on Multimedia and the Web* (*WebMedia 2024*). (*Sociedade Brasileira de Computação*). 2024. P. 188–196. https://doi.org/10.5753/webmedia.2024.242058
8. Weiss K., Rottleuthner M., Schmidt T.C., Wählisch M. PHiLIP on the HiL: Automated Multi-Platform OS Testing with External Reference Devices. *ACM Trans. Embed. Comput. Syst*. (*TECS*). 2021;20(5s):1–26. https://doi.org/10.1145/3477040
9. Behnke I., Thamsen L., Kao O. Héctor: A Framework for Testing IoT Applications Across Heterogeneous Edge and Cloud Testbeds. In: *Proceedings of the 12th IEEE/ACM International Conference on Utility and Cloud Computing Companion.* ACM; 2019. P. 15–20. https://doi.org/10.1145/3368235.3368832
10. Ziegler S., Fdida S., Viho C., Watteyne T. F-Interop – Online Platform of Interoperability and Performance Tests for the Internet of Things. In: Mitton N., Chaouchi H., Noel T., Watteyne T., Gabillon A., Capolsini P. (Eds.). *Interoperability, Safety and Security in IoT. Lecture Notes of the Institute for Computer Sciences, Social Informatics and Telecommunications Engineering*. Springer; 2017. V. 190. P. 49–55. Available from URL: https://link.springer.com/chapter/10.1007/978-3-319-52727-7_7. Accessed July 07, 2025.
11. Olianas D., Leotta M., Ricca F. MATTER: A tool for generating end-to-end IoT test scripts. *Software Qual. J*. 2021;30(2): 389–423. Available from URL: https://link.springer.com/article/10.1007/s11219-021-09565-y. Accessed July 07, 2025.
12. Schieferdecker I., Kretzschmann S., Rennoch A., Wagner M. IoT-Testware – An Eclipse Project. In: *2017 IEEE International Conference on Software Quality, Reliability and Security* (*QRS*). IEEE; 2017. https://doi.org/10.1109/QRS.2017.59
13. Belyakov D.S., Kalinin E.O., Konev A.A., Shelupanov A.A., Mitsel A.A. Life-cycle models and security threats to the microchip during its development and exploitation. *Doklady Tomskogo gosudarstvennogo universiteta sistem upravleniya i radioehlektroniki* (*Doklady TUSUR*) = *Proceedings of TUSUR University.* 2023;26(1):76–81 (in Russ.). https://doi.org/10.21293/1818-0442-2023-26-1-76-81

14. Konev A.A. Security threat model for protected microcontroller and the information it processes. *Doklady Tomskogo gosudarstvennogo universiteta sistem upravleniya i radioehlektroniki* (*Doklady TUSUR*) = *Proceedings of TUSUR University.* 2022;25(4):80–87 (in Russ.). https://doi.org/10.21293/1818-0442-2022-25-4-80-87
15. Restuccia G., Tschofenig H., Baccelli E. Low-Power IoT Communication Security: On the Performance of DTLS and TLS 1.3. In: *Proceedings 2020 9th IFIP International Conference on Performance Evaluation and Modeling in Wireless Networks* (*PEMWN*). https://doi.org/10.23919/PEMWN50727.2020.9293085
16. Lowther D., Jacob D., Trevor J., Singer J. Secure Scripting with CHERIoT MicroPython. In: *Proceedings of the 34th ACM SIGPLAN International Conference on Compiler Construction*. ACM; 2025. P. 180–191. https://doi.org/10.1145/3708493.3712694

СПИСОК ЛИТЕРАТУРЫ

1. Дьяков О.Н., Беляков Д.С., Калинин Е.О. Использование технологии ePKI для безопасного обновления встроенного программного обеспечения доверенных программно-аппаратных комплексов. *Безопасность информационных технологий.* 2025;32(2):152–177. https://doi.org/10.26583/bit.2025.2.12
2. Venugopal M., Nanda M., Anand G., Chandana Voora H. An integrated Hardware/Software Verification and Validation methodology for Signal Processing Systems. *ITM Web Conf.* 2022;50:02001. https://doi.org/10.1051/itmconf/20225002001
3. Bures M., Cerny T., Ahmed B.S. Internet of Things: Current Challenges in the Quality Assurance and Testing Methods. *arXiv*. arXiv:1805.01241. 2018. https://doi.org/10.48550/arXiv.1805.01241
4. Mazhar T., Talpur D.B., Shloul T.A., Ghadi Y.Y., Haq I., Ullah I. Analysis of IoT Security Challenges and its Solutions Using Artificial Intelligence. *Brain Sciences*. 2023;13(4):683. https://doi.org/10.3390/brainsci13040683
5. Minani J.B., Sabir F., Moha N., Guéhéneuc Y.G. A Multimethod Study of Internet of Things Systems Testing in Industry. *IEEE Internet Things J*. 2024;11(1):1662–1684. https://doi.org/10.1109/JIOT.2023.3291233
6. Папуловская Н.В., Изотов И.Н., Блиничкин Д.Ю., Катаев А.Ю. Разработка ядра платформы автоматизированного тестирования устройств интернета вещей. *Int. J. Open Inf. Technol.* 2021;9(6):38–45. https://elibrary.ru/ybxvtg
7. Castelo Branco K.D.S., Dantas V.L.L., Carvalho L.M. Interoperability Testing Guide for the Internet of Things. In: *Proceedings of the 30th Brazilian Symposium on Multimedia and the Web* (*WebMedia 2024*). (*Sociedade Brasileira de Computação*). 2024. P. 188–196. https://doi.org/10.5753/webmedia.2024.242058
8. Weiss K., Rottleuthner M., Schmidt T.C., Wählisch M. PHiLIP on the HiL: Automated Multi-Platform OS Testing with External Reference Devices. *ACM Trans. Embed. Comput. Syst*. (*TECS*). 2021;20(5s):1–26. https://doi.org/10.1145/3477040
9. Behnke I., Thamsen L., Kao O. Héctor: A Framework for Testing IoT Applications Across Heterogeneous Edge and Cloud Testbeds. In: *Proceedings of the 12th IEEE/ACM International Conference on Utility and Cloud Computing Companion.* ACM; 2019. P. 15–20. https://doi.org/10.1145/3368235.3368832
10. Ziegler S., Fdida S., Viho C., Watteyne T. F-Interop – Online Platform of Interoperability and Performance Tests for the Internet of Things. In: Mitton N., Chaouchi H., Noel T., Watteyne T., Gabillon A., Capolsini P. (Eds.). *Interoperability, Safety and Security in IoT. Lecture Notes of the Institute for Computer Sciences, Social Informatics and Telecommunications Engineering*. Springer; 2017. V. 190. P. 49–55. URL: https://link.springer.com/chapter/10.1007/978-3-319-52727-7_7. Accessed July 07, 2025.
11. Olianas D., Leotta M., Ricca F. MATTER: A tool for generating end-to-end IoT test scripts. *Software Qual. J.* 2021;30(2): 389–423. URL: https://link.springer.com/article/10.1007/s11219-021-09565-y. Accessed July 07, 2025.
12. Schieferdecker I., Kretzschmann S., Rennoch A., Wagner M. IoT-Testware – An Eclipse Project. In: *2017 IEEE International Conference on Software Quality, Reliability and Security* (*QRS*). IEEE; 2017. https://doi.org/10.1109/QRS.2017.59
13. Беляков Д.С., Калинин Е.О., Конев А.А., Шелупанов А.А., Мицель А.А. Модели жизненного цикла и угрозы безопасности микросхемы во время ее разработки и эксплуатации. *Доклады Томского государственного университета систем управления и радиоэлектроники* (*Доклады ТУСУР*). 2023;26(1):76–81. https://doi.org/10.21293/1818-0442-2023-26-1-76-81
14. Конев А.А. Модель угроз безопасности защищенного микроконтроллера и обрабатываемой им информации. *Доклады Томского государственного университета систем управления и радиоэлектроники* (*Доклады ТУСУР*). 2022;25(4):80–87. https://doi.org/10.21293/1818-0442-2022-25-4-80-87
15. Restuccia G., Tschofenig H., Baccelli E. Low-Power IoT Communication Security: On the Performance of DTLS and TLS 1.3. In: *Proceedings 2020 9th IFIP International Conference on Performance Evaluation and Modeling in Wireless Networks* (*PEMWN*). https://doi.org/10.23919/PEMWN50727.2020.9293085
16. Lowther D., Jacob D., Trevor J., Singer J. Secure Scripting with CHERIoT MicroPython. In: *Proceedings of the 34th ACM SIGPLAN International Conference on Compiler Construction*. ACM; 2025. P. 180–191. https://doi.org/10.1145/3708493.3712694

About the Author

Danila S. Belyakov, Senior Lecturer, Department of Complex Information Security of Computer Systems, Faculty of Security, Tomsk State University of Control Systems and Radioelectronics (40, Lenina pr., Tomsk, 634050 Russia). E-mail: cauze4concern@yandex.ru. Scopus Author ID 57359476400, ResearcherID AAQ-4613-2021, RSCI SPIN-code 3368-8751, https://orcid.org/0000-0002-6111-455X

Об авторе

Беляков Данила Сергеевич, старший преподаватель, кафедра комплексной информационной безопасности электронно-вычислительных систем, факультет безопасности, ФГАОУ ВО «Томский государственный университет систем управления и радиоэлектроники» (634050, Россия, Томск, пр-т Ленина, д. 40). E-mail: cauze4concern@yandex.ru. Scopus Author ID 57359476400, ResearcherID AAQ-4613-2021, SPIN-код РИНЦ 3368-8751, https://orcid.org/0000-0002-6111-455X

Translated from Russian into English by K. Nazarov
Edited for English language and spelling by Thomas A. Beavitt

Information systems. Computer sciences. Issues of information security

Информационные системы. Информатика. Проблемы информационной безопасности

UDC 004.2
https://doi.org/10.32362/2500-316X-2026-14-2-29-41
EDN XHLRAX

RESEARCH ARTICLE

Heterogeneous computing systems with hardware acceleration of massively parallel stream processing design

Andrey S. Zuev [@], Peter N. Sovietov, Ilya E. Tarasov

MIREA – Russian Technological University, Moscow, 119454 Russia
[@] Corresponding author, e-mail: zuev_a@mirea.ru

• **Submitted:** 09.06.2025 • **Revised:** 23.09.2025 • **Accepted:** 05.02.2026

Abstract

Objectives. The growing demand for higher computational performance and energy efficiency has motivated the increasing adoption of specialized heterogeneous computing systems incorporating hardware accelerators with massive parallelism. This paper aims to develop a methodology for the analysis and evaluation of hardware accelerator implementation strategies for large-scale parallel stream data processing which systematically captures all major directions of performance improvement.

Methods. The study employs established techniques of digital system design and modeling.

Results. A comparative evaluation method is introduced to assess the efficiency of heterogeneous computing architectures based on massively parallel hardware accelerators composed of independently programmable nodes. A computational acceleration ratio is defined which consolidates three key dimensions of accelerator improvement: algorithmic support and microarchitecture; design automation tools; and fabrication technologies (lithography). Furthermore, the study proposes an optimization-based methodology for the systematic analysis and evaluation of the alternatives for hardware accelerator implementation.

Conclusions. The expressions derived herein for calculating the computational acceleration ratio and the aggregate throughput of hardware accelerators account for both multichannel and block-based massively parallel data stream processing. In contrast to conventional architectural exploration approaches, the evaluation method proposed herein enables hardware accelerator design alternatives to be assessed at the earliest stages of the design cycle. This incorporates variations in algorithmic versions and implementation strategies which influence hardware architecture optimization. The proposed methodology for analyzing and evaluating implementation options for hardware accelerators can be used to develop technical specifications for their manufacture, design them according to specified requirements, and justify configuration decisions. It can also support research and development assignments to achieve target characteristics for certain domain-specific tasks of massively parallel stream data processing and CAD capabilities.

Keywords: processor, hardware accelerator, coprocessor, special-purpose processor, architecture, compiler

For citation: Zuev A.S., Sovietov P.N., Tarasov I.E. Heterogeneous computing systems with hardware acceleration of massively parallel stream processing design. *Russian Technological Journal.* 2026;14(2):29–41. https://doi.org/10.32362/2500-316X-2026-14-2-29-41, https://www.elibrary.ru/XHLRAX

Financial disclosure: The authors have no financial or proprietary interest in any material or method mentioned.

The authors declare no conflicts of interest.

НАУЧНАЯ СТАТЬЯ

О проектировании гетерогенных вычислительных систем с аппаратным ускорением массово-параллельной потоковой обработки данных

А.С. Зуев [@], П.Н. Советов, И.Е. Тарасов

МИРЭА – Российский технологический университет, Москва, 119454 Россия
[@] Автор для переписки, e-mail: zuev_a@mirea.ru

• **Поступила:** 09.06.2025 • **Доработана:** 23.09.2025 • **Принята к опубликованию:** 05.02.2026

Резюме

Цели. Необходимость ускорения вычислений и достижения высоких показателей энергоэффективности приводит к расширению сфер использования специализированных гетерогенных вычислительных систем, имеющих в своем составе аппаратные ускорители с массовым параллелизмом вычислений. Целью настоящей работы является создание методики анализа и оценки вариантов реализации аппаратных ускорителей для задач массово-параллельной потоковой обработки данных, отражающей все направления совершенствования характеристик применяемых аппаратных ускорителей.

Методы. Использованы методы проектирования и моделирования цифровых систем.

Результаты. Предложен метод сравнительной оценки эффективности архитектуры гетерогенной вычислительной системы на основе аппаратных ускорителей с массовым параллелизмом вычислений, выполняемых независимо программируемыми узлами. Введен коэффициент ускорения вычислений, объединяющий три направления совершенствования характеристик применяемых аппаратных ускорителей – математическое обеспечение и микроархитектура, инструментарий проектирования, технологии изготовления (литография). Предложена основанная на решении оптимизационной задачи методика анализа и оценки вариантов реализации применяемых аппаратных ускорителей.

Выводы. Полученные авторами формулы расчета коэффициента ускорения вычислений и пропускной способности совокупности аппаратных ускорителей учитывают многоканальную и поблочную массово-параллельную обработку потоков данных. В отличие от известных подходов к поиску архитектурных решений, предлагаемая оценка вариантов реализации аппаратных ускорителей может быть проведена на самых ранних этапах проектирования с учетом версий алгоритма и альтернатив их реализации, влияющих на оптимизацию аппаратной архитектуры. Предложенная методика анализа и оценки вариантов реализации аппаратных ускорителей может применяться при разработке технических заданий на их изготовление, при их проектировании в соответствии с заданными требованиями, для обоснования решений относительно их конфигурации, а также при составлении заданий на научно-исследовательские и опытно-конструкторские работы с целью достижения целевых значений характеристик для конкретных задач массово-параллельной потоковой обработки данных и функциональных возможностей систем автоматизированного проектирования.

Ключевые слова: процессор, аппаратный ускоритель, сопроцессор, спецпроцессор, архитектура, компилятор

Для цитирования: Зуев А.С., Советов П.Н., Тарасов И.Е. О проектировании гетерогенных вычислительных систем с аппаратным ускорением массово-параллельной потоковой обработки данных. *Russian Technological Journal*. 2026;14(2):29–41. https://doi.org/10.32362/2500-316X-2026-14-2-29-41, https://www.elibrary.ru/XHLRAX

Прозрачность финансовой деятельности: Авторы не имеют финансовой заинтересованности в представленных материалах или методах.

Авторы заявляют об отсутствии конфликта интересов.

INTRODUCTION

The design of HPC systems is currently based on two key areas: parallel architectures and specializations of individual computing nodes. One common example is the combination of general-purpose processors and graphics accelerators. Graphics accelerators are chips comprising a large number of specialized computing nodes which perform the transformations characteristic of 3D imaging. Similar architectural solutions combining universal and specialized computing subsystems can also be applied to tasks in artificial intelligence, network security, and big data analysis.

A set of interconnected problems must be resolved when developing computing systems with a heterogeneous architecture. These include:

- developing a program model and prototypes of specialized compilers for the selected domain-specific task;
- developing the architecture and basic components of computing devices at the register transfer level;
- integrating hardware components within the chosen technological framework. This includes both programmable logic devices (PLDs) and the more recently developed very-large-scale integration (VLSI) circuits.

A key objective is complex optimization based on established criteria. This determines the quality indicators of the computing system. Depending on the purpose of the system, optimization can be carried out in absolute terms (e.g., power consumption, cost, and performance) or in terms of derived indicators (e.g., specific power consumption or cost per performance unit). Due to the wide range of characteristics determined by the technological processes in the microelectronics industry, both the program model and the architectural solutions need to be optimized. Circuit engineering approaches also need to be aligned with the technological capabilities. Therefore, the hardware and software co-design approach can be extended to encompass joint optimization at the device component design technology level.

Currently, there are a number of general provisions which describe the situation and trends in microelectronics. Moore's law indicates the techno-economic side of the process of increasing computing performance. However, the law of scaling transistor sizes formulated by Dennard [1] in the early stages of microelectronics development explained this growth as an extensive process of increasing the density of components on a chip and reducing the signal propagation delay. Between 1980 and 2000, the factors led to a significant increase in processor clock speeds. During this period the transition from 4 MHz in the early 1980s to 4 GHz in the Intel Pentium 4 was observed for mainstream desktop processors.

At the same time, as new generations of technological processes were introduced in production, the effect of saturation was observed for many technical characteristics of digital chips. Table 1 shows a comparative analysis of some technological process generation parameters.

Table 1. Comparative characteristics of some technological process parameters

Year	2013	2015	2017	2019	2021
Notation	16/14	10	7	5	3
Half pitch, nm	40	32	25	20	16
FinFET[1] transistor width, nm	7.6	7.2	6.8	6.4	6.1
Number of 4I logic valves per square mm, million	4	6.4	10.1	16.1	25.5
Transistor gate length, nm	20	17	14	12	10

As can be seen from the above, transistor size reduction has stopped. Instead, an increase in the density of components per unit area of the semiconductor chip is the main factor in improving the characteristics of the chips produced. Consequently, transistor enhancement may progress beyond the constraints of Dennard's scaling law. This may be driven by the adoption of novel materials or modifications to the gate design,

[1] A FinFET (fin field-effect transistor) is a type of MOSFET (metal–oxide–semiconductor field-effect transistor) with a three-dimensional structure.

such as FinFET [2], GAAFET[2] [3], and MBCFET[3] [4]. In this respect, the development of computing devices has undergone a number of changes which reflect the characteristics of new generations of technologies for producing integrated circuits.

The study by Patterson and Hennessy [5] provides an overview of the main historical trends in processor design. Notably, the transition to highly integrated chips occurred during the period between 1980 and 1990. Pipeline depth increased from simple processor cores to pipelined architectures such as RISC[4] and up to technological standards of 90–65 nm. The end of Dennard scaling, coupled with an increase in the number of components on a single chip, enabled the shift towards multi-core processor devices. This allowed for an increase in overall processor performance, not through an increase in clock frequency, but through the parallel operation of multiple cores.

At the same time, Amdahl's law [6] limits the increase in computing performance in parallel architecture by taking into account the dependence on data in the executed algorithm. At the present time, the constraints imposed by Amdahl's law on numerous applications (especially desktops and servers) are not of great importance. This is because the tasks performed independently are not dependent on data, meaning they can make the most of the available processor cores.

The need to speed up calculations within a single task requires the use of appropriate architectural solutions, not only to increase the number of parallel computing nodes. A key element in enhancing the performance of computing nodes is the specialization of these nodes. This can be broken down into two main aspects: the specialization of their data path and memory subsystem; and the use of a system with a heterogeneous architecture. This system comprises a combination of general-purpose processors and specialized nodes which accelerate the calculation of specific algorithms or subclasses of algorithms for common, frequently solved domain-specific tasks.

The technique outlined in the paper enables the design of specialized computing devices for use as part of software and hardware complexes for a range of purposes. A key feature of this technique is its comprehensive consideration of design levels: from the system model to the topological implementation, using feedback from lower-level designs. This allows the characteristics of the computing device to be optimized according to established criteria. This paper also introduces mathematical criteria for accelerator efficiency based on a newly defined calculation acceleration ratio compared to a general-purpose processor. The problem of optimizing the architecture of a hardware accelerator is formulated as a research task within the set of architectural options.

The formulae for calculating the acceleration factor and throughput introduced in this paper differ from the analytical models commonly used, such as Roofline [7] and LogCA [8]. This is because they take into account the massively parallel processing of multichannel and block-by-block data streams.

Unlike existing methods of searching for architectural solutions [9], the proposed evaluation of options for implementing hardware accelerators can be performed at the initial design stage. This approach considers both the specifics of massively parallel data stream processing and the ability to select various options for the accelerated algorithm and its implementations, with the optimized hardware architecture.

Heterogeneous computing systems based on specialized hardware accelerators with massively parallel computing capabilities

Figure 1 shows the authors' interpretation of the study by Patterson and Hennessy [5] in terms of trends in processor system architecture.

This illustration offers an architectural solution for the domain-specific architecture direction proposed by Patterson and Hennessy. The specialization of a computing system can formally be achieved in a variety of ways. This paper proposes and considers a solution which preserves a general-purpose processor (including a multi-core version) and adds specialized accelerators working either independently or in parallel with the system.

The diagram in Fig. 2 illustrates the roles of general-purpose processors and accelerators. The axes represent the complexity of one iteration of calculations in a cyclic algorithm and the number of iterations required to solve the problem.

As shown in Fig. 2, there are four primary zones, each involving a blend of basic and advanced iterations. These iterations are characterized by data dependencies which complicate the parallelization of calculations. The figure also provides a visual representation of the numbers involved, highlighting their small and large values. It is not difficult to implement a simple case in the form of a simple algorithm with a small number of iterations (a special case is a linear algorithm with a single iteration) on a general-purpose processor. Therefore, creating a specialized accelerator for such a case is impractical. As the algorithm becomes more complex,

[2] A GAAFET (gate-all-around field-effect transistor) is a type of transistor where the channels are surrounded by gates on all four sides.

[3] MBCFET is a multi-bridge channel field-effect transistor.

[4] RISC (reduced instruction set computer) is a computer architecture that has a reduced instruction set.

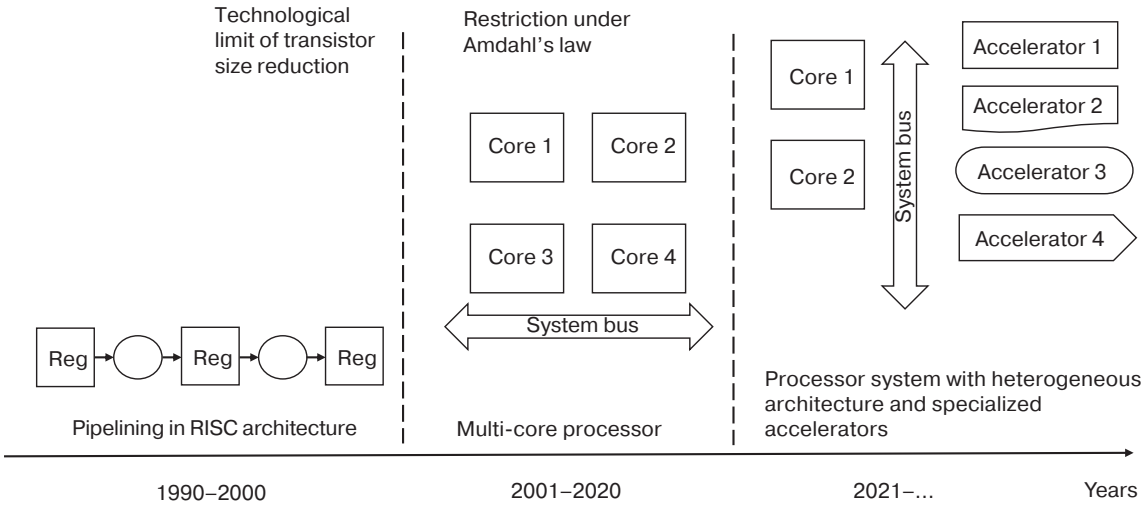

Fig. 1. Trends in processor architecture. Reg stands for register

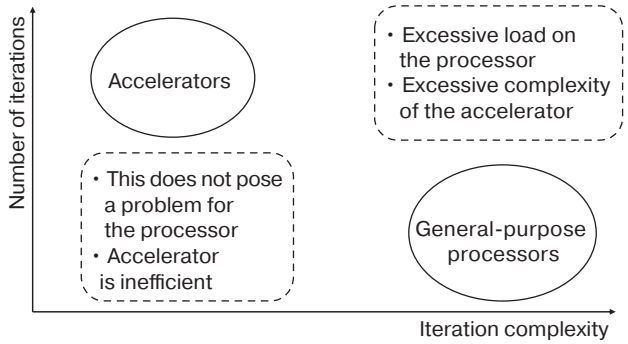

Fig. 2. Diagram showing the ratio of the complexity of iterations and their number, with the preferred computing device architectures

the device implementing it must have a well-developed set of functional nodes and enough memory to handle a long sequence of instructions. The implementation of a key computing subsystem such as an accelerator in this case can be a difficult task. Complex algorithms often require correction during system operation (e.g., updating the device's operating protocols). Conversely, a small number of iterations of such an algorithm do not create a significant computing load on the general-purpose processor.

An important issue is how to integrate the accelerator into the computing system. The increased integration of digital chips has led to the emergence of the interface wall effect [10], whereby there is an initial increase in computing performance compared to that of external interfaces (input/output (I/O) subsystems). In practice, placing in the accelerator numerous simple computing nodes which require intensive data exchange with a general-purpose processor will overload the interfaces used for data exchange. They will also reduce the accelerator's final computing performance due to an inability to provide the necessary input data stream. One example is the evolution of PLD characteristics with common architectures, such as FPGA[5], APSoC[6], and ACAP[7]. These are currently representative of highly integrated digital systems which combine subsystems for various purposes. Table 2 shows the comparative performance characteristics of the computing and interface subsystems of some PLD families manufactured by AMD/Xilinx (USA).

Table 2. Comparative performance characteristics of the computing and interface subsystems of certain AMD PLD families

PLD series	Series 7	UltraScale+	Versal
Process standard, nm	28	16	7
Logical cells, thou.	2000	8900	7350
Digital signal processing blocks	3600	12288	14352
Total computation performance, trln ops/s with int8 data	15	38.3	100
Total data transfer performance, Tb/s	2	4.1	17.6
Ratio of computation to data transfer performance	60	74	45

[5] A field-programmable gate array is a user-programmable gate array.

[6] All programmable system-on-chip is a type of programmable integrated circuit.

[7] Adaptive compute acceleration platform.

As shown in Table 2, the ratio of computation to data transfer performance generally remains between 50 and 70. This means that, for an effective computing load, at least 50–70 processing operations are performed on the data transmitted. This range of values is conditional and does not take into account the practical aspects of implementing operations. However, it should be noted that an excessively simple accelerator will reduce system efficiency, since each operation will require intensive data exchange with other system components. Figure 3 illustrates a negative use case for a compute accelerator with limited interface throughput.

Thus, in terms of architecture, it is important to ensure an appropriate level of computing performance. This guarantees the efficient use of accelerator resources at a given throughput level for its interfaces. The options for such scenarios are shown in Fig. 4.

The options provided ensure that the accelerator performs multiple operations on the transmitted data. Option 1 is used when implementing a relatively complex stand-alone algorithm which iterates calculations without the need to transmit a constant stream of data. Option 2 is used in parallel data processing where numerous operations are implemented in series-connected stages of the pipeline computer. The paper focuses on Option 2,

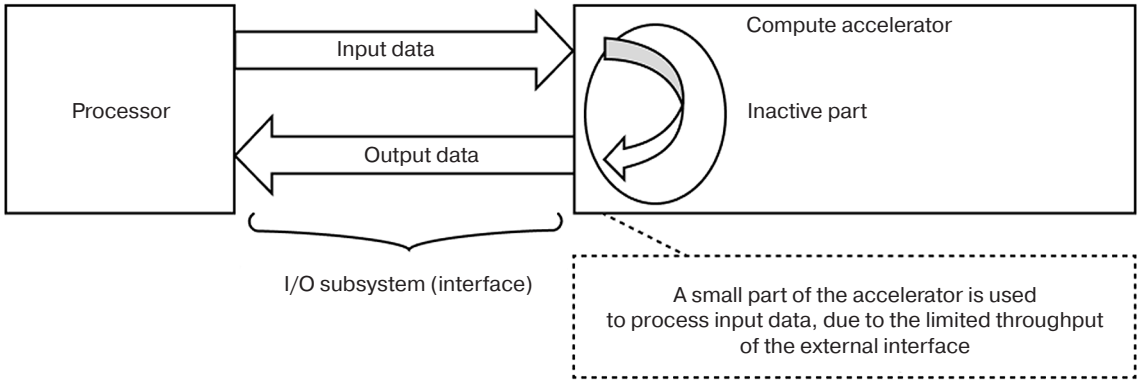

Fig. 3. Negative use case for a compute accelerator with limited I/O subsystem (interface) throughput

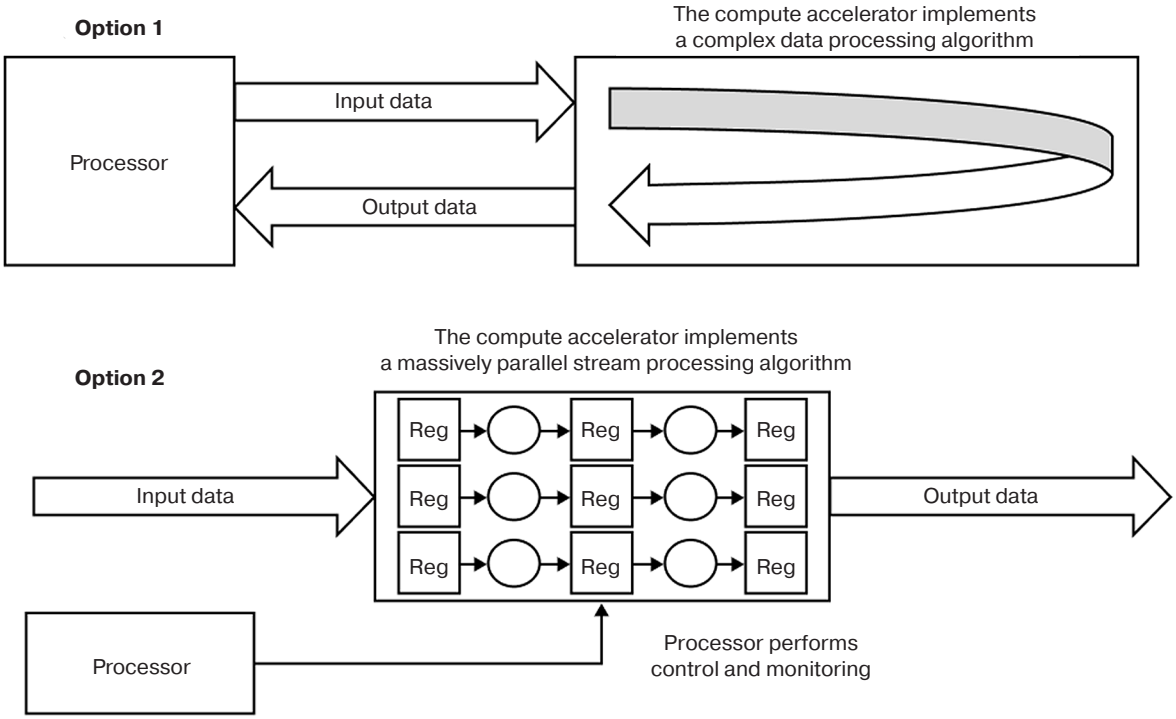

Fig. 4. Use cases (options) for a compute accelerator that uses limited interface throughput effectively (the compute pipeline is used)

shown in Fig. 4, which is a heterogeneous computing system with hardware acceleration of massively parallel data streaming.

Tasks and algorithms for massively parallel streaming data processing

Streaming tasks arise in a variety of fields, including digital signal processing, data compression, cryptography, real-time analytics, and network traffic analysis.

A streaming process involves processing each element of a potentially endless stream of data, denoted as x_1, x_2, …, x_t, …, where x_t represents the element available at time t for processing. The elements are all of the same data type and may be individual bits, bytes, or more complex structures.

Streaming algorithms are characterized by their single-pass execution. They cannot revisit elements which have already been viewed or processed. Processing takes place within a limited local memory environment with a space complexity of $O(1)$, regardless of the number of streaming elements.

Key features of streaming processing systems include a data throughput of $R = N/t_N$, where N represents the number of elements and t_N represents the total processing time. Here, $R \le R_{max}$, where R_{max} is the maximum permissible throughput which may be limited by the capabilities of the I/O subsystem. During real-time operations, the delay per element should also be limited to $L \le L_{max}$.

Hardware acceleration enables the use of parallelism at different levels in data processing. Specifically, instruction-level parallelism depends primarily on the computational intensity of an element in a stream, i.e., the dominance of computational operations over memory operations. Task parallelism, also known as channel parallelism, involves the simultaneous processing of multiple channels.

Often, the streaming algorithm must be adapted to accommodate the specific hardware architecture. For example, if the tables used by the algorithm exceed the accelerator's local memory capacity, additional calculations may be required.

The literature describes hardware accelerators for processing stream-based data in various fields and for specific tasks within domains. Specifically, accelerators have been developed which can efficiently determine whether an item belongs to a set, such as Bloom filters [11], as well as accelerators which can estimate the number of distinct items in a multiset, such as HyperLogLog [12]. Hardware accelerators have also been developed to optimize the performance of various string-processing algorithms, such as calculating the edit distance [13], searching for regular expressions [14], and JSON[8] parsing [15]. Topics of data compression acceleration and decompression processes are discussed in [16], while [17] describes a hardware accelerator that combines data decompression and JSON parsing.

A variety of database algorithms represent a significant area for the implementation of hardware accelerators. The acceleration of relational database operations through hardware is discussed in [18]. These operations include sampling, mapping, joining, collating, and various aggregate functions. The implementation of hardware acceleration for graph database pattern matching is proposed in [19]. As outlined in [20], streaming analytics is a promising area for hardware acceleration. The study describes the main algorithms in this field which can be executed on hardware. Furthermore, approaches to streaming processing have been developed for various machine learning algorithms, leading to the creation of hardware accelerators for gradient boosting [21] and clustering tasks [22].

Comparative assessment of the efficiency of data streaming processing computing systems using a general-purpose processor or hardware acceleration

The effectiveness of the accelerator can be quantitatively assessed by comparing T_{soft} (task execution time using only a general-purpose processor) and T_{hard} (task execution time using the accelerator), i.e.,

$$K = \frac{T_{soft}}{T_{hard}}.$$

When estimating program execution time, the following formula, detailed in [23], may be useful:

$$\text{time} = \frac{\text{instructions}}{\text{program}} \cdot \frac{\text{cycles}}{\text{instruction}} \cdot \frac{T_{period}}{\text{cycle}}.$$

In this equation, the terms represented as fractions correspond to the characteristics of the compiler, microarchitecture, and workflow:

1. The number of instructions executed per iteration of the program is dependent on the ability of the compiler to generate machine code that is optimized for improved performance.
2. The number of cycles required to execute an instruction is determined by the processor's microarchitecture.
3. The duration of one clock period, T_{period}, is primarily affected by the method used to manufacture the processor.

[8] JavaScript object notation is a text-based data exchange format based on JavaScript syntax.

Thus, the overall program execution time can be improved through various methods which can be combined to design specialized accelerator systems.

When designing an accelerator connected to a processor using one of several interfaces, the configuration time, T_{conf}, for sending input problem parameters and receiving solution results must also be considered.

Assuming that the same task requires b iterations, the ratio of the execution time of a general-purpose processor to that of an accelerator can be expressed as follows:

$$K = \frac{bT_{soft}}{T_{conf} + bT_{hard}}.$$

In this form, the equation does not account for several computing nodes in the accelerator working in parallel. The number of instances of the data processing algorithm performed simultaneously in the accelerator will be referred to as "stream processing nodes." For example, when processing a data stream to search for regular expressions, the number of data stream processing nodes corresponds to the number of regular expressions for which analysis of each data block is performed simultaneously and in parallel.

Let t_{hard} be the execution time of the algorithm using a single hardware accelerator node. If p denotes the number of parallel nodes involved in solving this problem, then the formula takes the following form:

$$K = \frac{bT_{soft}}{T_{conf} + bt_{hard}/p}.$$

Due to stream processing, the accelerator is configured for long periods of operation during which a large (potentially infinite) number of data blocks of the same type are processed, so the T_{conf} value can be disregarded. The calculation acceleration tends towards:

$$K = \frac{pT_{soft}}{t_{hard}} = \frac{pn_{soft}f_{hard}}{n_{hard}f_{soft}}, \quad (1)$$

wherein n_{hard} and n_{soft} are the number of clock cycles required by the accelerator and processor, respectively, to solve the problem, and f_{hard} and f_{soft} are their corresponding clock frequencies.

Equation (1) shows that the hardware acceleration of the entire computing system is based on the following two factors:

- an increase in the number of parallel nodes;
- improving the efficiency of a single node by increasing its clock frequency and reducing the number of cycles required to perform a task.

The methodology for developing specialized processor cores has been previously discussed in [24]. When developing specialized electronic component bases (ECBs), a lack of access to advanced technological processes and the need to rapidly adapt newly developed designs to existing technology can make achieving a high operating frequency for the accelerator challenging. Therefore, it may be difficult to achieve a high ratio between the operating frequency of the hardware accelerator and that of commercially available general-purpose processors (in practice, this ratio may be less than 1). It is thus essential to focus on reducing the number of clock cycles required for the hardware accelerator to process a single data block. This is equivalent to reducing the n_{hard} parameter while maintaining the operating frequency f_{hard} rather high (in general, without considering power consumption factors). This can be accomplished using specialized parallel algorithms and stages of the optimizing compiler while taking into account the hardware specifications of the accelerator.

The proposed calculation acceleration ratio (1) combines three areas for improving the characteristics of the hardware accelerators of heterogeneous, massively parallel data processing systems: mathematical software and accelerator microarchitecture (p and n_{hard}); design tools, such as computer-aided design systems (CAD); and ECB manufacturing technologies (lithography) (p and f_{hard}).

Taking into account (1), for an accelerator with p parallel stream processing nodes, the processing time $T_{hard}(n)$ of n data blocks can be defined as follows:

$$T_{hard}(n) = T_{conf} + n \cdot \max\left(T_{block}, \frac{T_{soft}}{K}\right), \quad (2)$$

wherein T_{block} is the round-trip time of the next data block and is determined by the capabilities of the I/O subsystem, so cannot be reduced. Then p is the number of algorithm instances processing the next data block in parallel.

Integrating the parallel accelerators discussed above into a single chip would enable C streams of data blocks to be processed in parallel. This combination could be considered the final version of the accelerator. In this scenario, the throughput R_{hard} of the combination of C parallel accelerators (with the $T_{hard}(n)$ characteristic of formula (2)) would be determined by the following equation:

$$R_{hard} = \frac{Cn}{T_{hard}(n)} = \frac{C}{\frac{T_{conf}}{n} + \max\left(T_{block}, \frac{T_{soft}}{K}\right)} \approx \frac{C}{\max\left(T_{block}, \frac{T_{soft}}{K}\right)}.$$

The C value is limited by the number of physically available interfaces in the implemented I/O subsystem

and the application task specification. Thus, when designing a hardware accelerator, decisions should be made not only about the technological processes of its manufacture and technical characteristics but also about the simultaneous development of tools. In particular this requires a specialized compiler to be used to optimize both the software and the hardware.

Analysis and evaluation of the implementation of hardware accelerators in heterogeneous computing systems for massively parallel stream processing

The previous section sets out a method for assessing the effectiveness of a general-purpose processor for massively parallel stream processing, compared to a specialized accelerator with the following characteristics:

- T_{block} is the time taken to receive and transmit a data block, as determined by the I/O subsystem (i.e., the implementation options for interfacing the accelerator with the computing system);
- f_{hard} is the clock frequency which depends on the purchasing or manufacturing options available for an accelerator. It is also determined by the capabilities of its design tools (CAD) and manufacturing technologies (PLD or custom chip);
- n_{hard} is the number of cycles required by the accelerator (stream processing node) to resolve a problem, depending on the composition of specialized parallel algorithms used and the phases of optimizing the compiler. This number is determined by the options available for providing a mathematical solution to a problem using an accelerator and its microarchitecture, considering the hardware features of the accelerator;
- p is the number of parallel data processing nodes within the accelerator involved in solving a problem.

The available options for f_{hard} values are determined by the characteristics of the PLDs and VLSI chips available for use when purchasing a ready-made ECB, as well as by their production options i.e., those available for the production of ECBs through technological processes and standard cell libraries.

When designing an accelerator, it is advisable to add the following parameters to the above-listed characteristics:

- T_{task} is the processing time of one data block by the accelerator, determined by the technical assignment requirements;
- C_{max} is the maximum number of available I/O subsystem channels;
- C ($C \le C_{max}$) is the number of accelerator instances placed on the chip;
- S ($S \le S_{max}$) is the area of the chip limited in its particular embodiment.

Some of the specific values of the above parameters depend on the implementation of the problem solution on the accelerator and the variant of the corresponding data processing algorithm used. Let a_i, $i = \overline{1,n}$ be a set of alternative algorithms, i.e., implementation options for resolving the problem on an accelerator. Each algorithm is characterized by the following set of parameters:

- n^i_{hard} is the number of clock cycles required by one computing node of the accelerator to resolve the problem;
- P_i is the maximum possible number of parallel instances of the algorithm running as part of the accelerator;
- local_i is the area of the chip occupied by the amount of local memory m_i required by the accelerator to execute the a_i algorithm;
- alu_i is the chip area occupied by one data streaming node;
- glob_i is the portion of the chip dedicated to storing data utilized by all instances of the a_i algorithm. This allocation may remain the same for regular expressions, for instance, or it may change depending on the throughput of the I/O subsystem, the workload requirements of the general-purpose processor and other factors.

Then $S_i = (\text{local}_i + \text{alu}_i)$ is the chip area allocated for one accelerator stream processing node, i.e., for the functioning of one instance of the a_i algorithm. For an accelerator with p_i stream processing nodes, each implementing an instance of the a_i algorithm, the required chip area can be calculated using the following equation:

$$U_i = S_i p_i = (\text{local}_i + \text{alu}_i)p_i,\ p_i \le P_i.$$

When placing accelerator instances on the C_i chip, each of which implements p_i instances of the a_i algorithm, the required chip area S_i can be determined in the following way:

$$S_i = \text{glob}_i + U_i C_i = \text{glob}_i + S_i p_i C_i = \\ = \text{glob}_i + (\text{local}_i + \text{alu}_i)p_i C_i,\ p_i \le P_i,\ S_i \le S.$$

Equation (2) allows not only the time $T_{hard}(n)$ required for processing n data blocks by an accelerator with p nodes to be defined, but also its implementation options to be analyzed and evaluated on the basis of existing (available) technological capabilities. We define a limit for the available values of the performance characteristic of the accelerator, i.e., the time T_{fix} it takes to process one data block, as follows:

$$T_{fix} = \min(T_{block}, T_{task}).$$

The T_{fix} time, determined either by the capabilities of the I/O subsystem or by the terms of reference for the accelerator development, can be considered to be

unambiguously deterministic. This imposes natural limitations on the combinations of characteristics that can be reasonably considered:

$$\frac{T_{\text{soft}}}{K} \approx T_{\text{fix}}. \quad (3)$$

Implementations of the accelerator which meet condition (3) using the '<' operator would be impractical, since their excessive efficiency would be limited by the capabilities of the I/O subsystem. Implementations which satisfy condition (3) with the '>' operator would not achieve maximum performance.

As a criterion for the optimal implementation of the accelerator, considering the specific implementation of the I/O subsystem and based on available technological capabilities, we can express the following:

$$\left| \frac{T_{\text{soft}}}{K} - T_{\text{fix}} \right| \to \min.$$

Taking into account (1) and the potential for implementing multiple alternative algorithms $a_i, i = \overline{1,n}$ on the accelerator, this expression can be written as follows:

$$\left| \frac{n^i_{\text{hard}}}{p_i f_{\text{hard}}} - T_{\text{fix}} \right| \to \min. \quad (4)$$

Given that the f_{hard} parameter can take different values (described by a vector of values), the following optimization accelerator design problem can be formulated: for each version of the problem-solving algorithm a_i, $i = \overline{1,n}$, the combinations of p_i, C_i, and f^i_{hard} values should be determined so that:

$$S_i = \text{glob}_i + (\text{local}_i + \text{alu}_i) p_i C_i,$$

$$p_i \le P_i,$$

$$S_i \le S,$$

$$\frac{n^i_{\text{hard}}}{p_i f^i_{\text{hard}}} \le T_{\text{fix}},$$

$$T_{\text{fix}} - \frac{n^i_{\text{hard}}}{p_i f^i_{\text{hard}}} \to \min. \quad (5)$$

As a result, corresponding sets $|\text{A}_i| = r_i$ of combinations of the values for the considered parameters $(p^k_i, C^k_i, f^{i,k}_{\text{hard}})$, $k = \overline{1,r_i}$, which are alternative versions of accelerator manufacture, can be determined for the algorithms a_i, $i = \overline{1,n}$. The accelerator design option(s) can then be selected based on the simulation results obtained using CAD tools, taking into account additional criteria such as power consumption, cost, and probability of failure.

It would also be advisable to automate the solution to the above problem of determining the accelerator characteristics in accordance with the implemented algorithm would be advisable. The authors will conduct further research in this area. However, a general approach to solving the problem is presented below.

Universal sets of various P, C and F values can be composed for the above parameters p_i, C_i, and f^i_{hard} of each of the a_i, $i = \overline{1,n}$ alternative algorithms. Together with the set A ($a_i \in \text{A}$, $i = \overline{1,n}$), these form a four-dimensional array W of the original data for the problem under consideration. If a specific variant of the four parameters or the value of the expression (5) is incompatible, then the elements of the corresponding array contain the "0" value. However, if their joint implementation is acceptable, the value of the expression (5) is used. The n^i_{hard}, local_i, alu_i, and glob_i parameters of the corresponding algorithm a_i, $i = \overline{1,n}$. are used to calculate it.

The P, C, and F sets are generally deterministic and there are usually only a few algorithmic variants available for solving a specific problem. Therefore, in the context of sets P, C, and F, array W is universal and, as a rule, does not have a large dimension when applied to a specific data processing task. Consequently, it does do not require a high level of computational complexity to calculate and enumerate the values of its elements, or to analyze the implementation of heterogeneous computing systems with hardware acceleration of massively parallel data streaming.

The problem statement and procedure for determining the initial data enable the development of a methodology for analyzing and evaluating the implementation of hardware accelerators in heterogeneous computer systems for massively parallel stream data processing. If further developed, the proposed methodology has the potential to become universal and could be used to develop technical specifications for hardware accelerators, when designed according to specified requirements. It can also be used to justify the decisions made regarding the configuration of a hardware accelerator. Furthermore, it can be used to set research and development goals aimed at achieving the target values of f_{hard}, n_{hard}, $C_{\max}$, and $S_{\max}$ for domain-specific massively parallel data processing tasks and CAD functionality.

In future works, the authors will describe the development of the methodology, including its application to working with the W array using online analytical processing technologies.

Considering heterogeneous systems of massively parallel data processing as a separate promising direction could advance the development of computer technology. The methodology proposed here is based on requirements for resolving popular object-oriented problems. It can be used as a tool for scientific and technical policy, enabling the determination and justification of the need to achieve target values. These include:

- characteristics of system buses and interfaces of accelerators with computing systems (T_{block});
- circuit engineering solutions and lithography technologies (f_{hard});
- integrated circuit packaging technologies (p);
- algorithms for solving problems and the mathematical support of compilers (n_{hard});
- high-level design systems and software modeling.

CONCLUSIONS

In order to improve the efficiency with which massively parallel accelerators resolve tasks and expand their range, an architecture and methodology for designing heterogeneous computing systems is proposed. These systems use specialized hardware accelerators with massive parallelism of calculations and independently programmable specialized processor cores. This solution complements general-purpose processor-based computing systems. Due to its ability to program individual nodes independently, its architecture differs from that of graphics processing unit devices. Increasing the number of parallel nodes and their specialization is shown to increase productivity. This is established by analysis of the computation graph formed by a specially developed compiler focused on a subclass of domain-specific tasks. The proposed calculation acceleration ratio demonstrates the feasibility of complex optimization during the accelerator development. This takes into account three levels of project presentation: a program model, a schematic description, and a topological representation based on the selected technology. The methodology proposed for analyzing and evaluating the implementation options for hardware accelerators of heterogeneous computing systems for massively parallel stream processing allows the technical characteristics of the required accelerator to be determined. The resulting methodology for designing computing systems of this class provides an adjustable process for optimizing performance according to the required criteria.

Authors' contributions

The research and results presented in the article were obtained jointly by the authors as an outcome of the scientific school "Specialized Heterogeneous Computing Systems" organized by the Institute of Information Technologies at the MIREA – Russian Technological University.

The main content of the section "Analysis and evaluation of implementation options for hardware accelerators in heterogeneous computing systems for massively parallel stream data processing," including the task of optimizing the hardware accelerator architecture formulation as a search problem in the space of architectural options, as well as the methodology for analyzing and evaluating implementation options of hardware accelerators, was developed by A.S. Zuev.

REFERENCES

1. Dennard R.H., Gaensslen F.H., Yu H.-N., Rideout V.L., Bassous E., LeBlanc A.R. Design of ion-implanted MOSFET's with very small physical dimensions. *IEEE Journal of Solid-State Circuits*. 1974;9(5):256–268. https://doi.org/10.1109/JSSC.1974.1050511
2. Jain P.U., Tomar V.K. FinFET Technology: As A Promising Alternatives for Conventional MOSFET Technology. In: *2020 International Conference on Emerging Smart Computing and Informatics* (*ESCI*). 2020. P. 43–47. https://doi.org/10.1109/ESCI48226.2020.9167646
3. Yakimets D., Eneman G., Schuddinck P., et al. Vertical GAAFETs for the Ultimate CMOS Scaling. *IEEE Transactions on Electron Devices*. 2015;62(5):1433–1439. https://doi.org/10.1109/TED.2015.2414924
4. Lee S.-Y., Kim S.-M., Yoon E.-J., et al. A Novel Multibridge-Channel MOSFET (MBCFET): Fabrication Technologies and Characteristics. *IEEE Transactions on Nanotechnology*. 2003;2(4):253–257. https://doi.org/10.1109/TNANO.2003.820777
5. Hennessy J.L., Patterson D.A. *Computer Architecture: A Quantitative Approach* (*The Morgan Kaufmann Series in Computer Architecture and Design*). 6th ed. 2017, 936 p.
6. Annaratone M. MPPs, Amdahl's Law, and Comparing Computers. In: *Proceedings of The Fourth Symposium on the Frontiers of Massively Parallel Computation.* 1992. P. 465–470. https://doi.org/10.1109/FMPC.1992.234879
7. Verhelst M., Benini L., Verma N. How to keep pushing ML accelerator performance? Know your rooflines! *IEEE Journal of Solid-State Circuits*. 2025;6(60):1888–1905. https://doi.org/10.1109/JSSC.2025.3553765
8. Altaf M.S.B., Wood D.A. LogCA: A high-level performance model for hardware accelerators. *ACM SIGARCH Computer Architecture News*. 2017;45(2):375–388. https://doi.org/10.1145/3079856.3080216
9. Molina R.S., Gil-Costa V., Crespo M.L., et al. High-level synthesis hardware design for FPGA-based accelerators: Models, methodologies, and frameworks. *IEEE Access*. 2022;10:90429–90455. https://doi.org/10.1109/ACCESS.2022.3201107
10. A New Golden Age for Computer Architecture: Domain-Specific Hardware/Software Co-Design, Enhanced Security, Open Instruction Sets, and Agile Chip Development. In: *2018 ACM/IEEE 45th Annual International Symposium on Computer Architecture* (*ISCA*). 2018. P. 27–29. https://doi.org/10.1109/ISCA.2018.00011
11. Liu K., Lu A., Fang Z. BitBlender: Scalable Bloom Filter Acceleration on FPGAs with Dynamic Scheduling. In: *34th International Conference on Field-Programmable Logic and Applications* (*FPL*). 2024. P. 325–331. https://doi.org/10.1109/FPL64840.2024.00052

12. Kulkarni A., Chiosa M., Preuber T.B., et al. HyperLogLog Sketch Acceleration on FPGA. In: *30th International Conference on Field-Programmable Logic and Applications* (*FPL*). 2020. P. 47–56. https://doi.org/10.1109/FPL50879.2020.00019
13. Marchisio A., Teodonio F., Rizzi A., et al. ISMatch: A Real-Time Hardware Accelerator for Inexact String Matching of DNA Sequences on FPGA. *Microprocess. Microsyst*. 2023;97:104763. https://doi.org/10.1016/j.micpro.2023.104763
14. Zhang C., Tang X., Peng Y. Enhancing Regular Expression Processing through Field-Programmable Gate Array-Based Multi-Character Non-Deterministic Finite Automata. *Electronics.* 2024;13(9):1635. https://doi.org/10.3390/electronics13091635
15. Dann J., Wagner R., Ritter D., et al. PipeJSON: Parsing JSON at Line Speed on FPGAs. In: *Proceedings of the 18th International Workshop on Data Management on New Hardware*. 2022;Article 3:1–7. https://doi.org/10.1145/3533737.3535094
16. Karandikar S., Udipi A.N., Choi J., et al. CDPU: Co-Designing Compression and Decompression Processing Units for Hyperscale Systems. In: *Proceedings of the 50th Annual International Symposium on Computer Architecture*. 2023;Article 39:1–17. https://doi.org/10.1145/3579371.3589074
17. Hahn T., Wildermann S., Teich J. JSON-CooP: A JSON Decompression/Parsing Co-Design for FPGAs. In: *34th International Conference on Field-Programmable Logic and Applications* (*FPL*). 2024. P. 11–18. https://doi.org/10.1109/FPL64840.2024.00012
18. Fang J., Mulder Y., Hidders J., et al. In-Memory Database Acceleration on FPGAs: A Survey. *The VLDB Journal.* 2020;29(10):33–59. https://doi.org/10.1007/s00778-019-00581-w
19. Dann J., Götz T., Ritter D., et al. GraphMatch: Subgraph Query Processing on FPGAs. *arXiv.* arXiv:2402.17559. 2024.
20. Kejariwal A., Kulkarni S., Ramasamy K. Real Time Analytics: Algorithms and Systems. *arXiv.* arXiv:1708.02621. 2017. https://doi.org/10.48550/arXiv.1708.02621
21. Alcolea A., Resano J. FPGA Accelerator for Gradient Boosting Decision Trees. *Electronics*. 2021;10(3):314. https://doi.org/10.3390/electronics10030314
22. Graf J.R., Perera D.G. Optimizing Density-Based Ant Colony Stream Clustering Using FPGA-Based Hardware Accelerator. In: *2023 IEEE International Symposium on Circuits and Systems* (*ISCAS*). 2023. https://doi.org/10.1109/ISCAS46773.2023.10181665
23. Shen J.P., Lipasti M.H. *Modern Processor Design: Fundamentals of Superscalar Processors.* Waveland Press; 2013, 658 p.
24. Tarasov I.E., Sovietov P.N., Lulyava D.V., Mirzoyan D.I. Method for designing specialized computing systems based on hardware and software co-optimization. *Russian Technological Journal*. 2024;12(3):37−45. https://doi.org/10.32362/2500-316X-2024-12-3-37-45

About the Authors

Andrey S. Zuev, Cand. Sci. (Eng.), Associate Professor, Head of the Department of Quantum Information Technologies, Practical and Applied Informatics, Institute of Information Technologies, MIREA – Russian Technological University (78, Vernadskogo pr., Moscow, 119454 Russia). E-mail: zuev_a@mirea.ru. Scopus Author ID 23977152300, RSCI SPIN-code 6737-5778, https://orcid.org/0000-0002-1797-7585

Peter N. Sovietov, Cand. Sci. (Eng.), Associated Professor, Department of Corporate Information Systems, Institute of Information Technologies, MIREA – Russian Technological University (78, Vernadskogo pr., Moscow, 119454 Russia). E-mail: peter.sovietov@gmail.com. Scopus Author ID 57221375427, RSCI SPIN-code 9999-1460, http://orcid.org/0000-0002-1039-2429

Ilya E. Tarasov, Dr. Sci. (Eng.), Associated Professor, Professor, Department of Corporate Information Systems, Institute of Information Technologies, MIREA – Russian Technological University (78, Vernadskogo pr., Moscow, 119454 Russia). E-mail: tarasov_i@mirea.ru. Scopus Author ID 57213354150, RSCI SPIN-code 4628-7514, http://orcid.org/0000-0001-6456-4794

Об авторах

Зуев Андрей Сергеевич, к.т.н., доцент, заведующий кафедрой квантовых информационных технологий, практической и прикладной информатики, Институт информационных технологий, ФГБОУ ВО «МИРЭА – Российский технологический университет» (119454, Россия, Москва, пр-т Вернадского, д. 78). E-mail: zuev_a@mirea.ru. Scopus Author ID 23977152300, SPIN-код РИНЦ 6737-5778, https://orcid.org/0000-0002-1797-7585

Советов Петр Николаевич, к.т.н., доцент, кафедра корпоративных информационных систем, Институт информационных технологий, ФГБОУ ВО «МИРЭА – Российский технологический университет» (119454, Россия, Москва, пр-т Вернадского, д. 78). E-mail: peter.sovietov@gmail.com. Scopus Author ID 57221375427, SPIN-код РИНЦ 9999-1460, http://orcid.org/0000-0002-1039-2429

Тарасов Илья Евгеньевич, д.т.н., доцент, профессор кафедры корпоративных информационных систем, Институт информационных технологий, ФГБОУ ВО «МИРЭА – Российский технологический университет» (119454, Россия, Москва, пр-т Вернадского, д. 78). E-mail: tarasov_i@mirea.ru. Scopus Author ID 57213354150, SPIN-код РИНЦ 4628-7514, http://orcid.org/0000-0001-6456-4794

Translated from Russian into English by Kirill V. Nazarov
Edited for English language and spelling by Dr. David Mossop

Information systems. Computer sciences. Issues of information security
Информационные системы. Информатика. Проблемы информационной безопасности

UDC 378.1
https://doi.org/10.32362/2500-316X-2026-14-2-42-56
EDN XNQJRO

RESEARCH ARTICLE

Software methods for curriculum processing, analysis and visualization

Evgenii A. Khalturin [1, @], Alexey A. Kytmanov [2], Yuliya V. Vaynshteyn [1], Tatiana V. Zykova [1]

[1] *Siberian Federal University, Krasnoyarsk, 660041 Russia*
[2] *MIREA – Russian Technological University, Moscow, 119454 Russia*
[@] *Corresponding author, e-mail: ekhalturin97@yandex.ru*

• **Submitted:** 20.02.2025 • **Revised:** 02.10.2025 • **Accepted:** 11.02.2026

Abstract

Objectives. The purpose of this study is to identify methods and approaches to developing a software package which can automate the processing, analysis, and visualization of curricula in educational programs.

Methods. We provide an overview of relevant scholarly literature and research results. The software package applies regular expressions for data processing, comparative analysis, and descriptive statistics to identify differences. It also uses a graph-based model for visualization.

Results. We designed the architecture of a software package for preprocessing, analyzing, and visualizing curricula following the SOLID[1] principles of object-oriented programming. We implemented the package in C++, in order to calculate curriculum characteristics and build a graph representation. This formed the basis of our proposed visualization method. We demonstrate the functionality of the package through a comparative analysis of curricula, identification of distinctive features, and detection of design shortcomings.

Conclusions. Our software package helps identify specific features, reveal possible weaknesses, and support the comparative analysis of different curricula. Using it improves the quality of educational process management, addresses gaps in educational data analysis, and contributes to the creation of a university digital ecosystem. The results of our study are useful for faculty members designing and developing curricula, as well as administrative and managerial staff (including those in academic affairs) and other higher education stakeholders.

Keywords: curriculum, educational program, method, software, graph model, competency-based approach, interdisciplinary links

[1] S is the single responsibility principle; O is an open-closed principle; L is the Liskov substitution principle; I is the interface segregation principle; D is the dependence inversion principle.

For citation: Khalturin E.A., Kytmanov A.A., Vaynshteyn Yu.V., Zykova T.V. Software methods for curriculum processing, analysis and visualization. *Russian Technological Journal.* 2026;14(2):42–56. https://doi.org/10.32362/2500-316X-2026-14-2-42-56, https://www.elibrary.ru/XNQJRO

Financial disclosure: The authors have no financial or proprietary interest in any material or method mentioned.

The authors declare no conflicts of interest.

НАУЧНАЯ СТАТЬЯ

Программные методы обработки, анализа и визуализации учебных планов

Е.А. Халтурин [1, @], А.А. Кытманов [2], Ю.В. Вайнштейн [1], Т.В. Зыкова [1]

[1] *Сибирский федеральный университет, Красноярск, 660041 Россия*
[2] *МИРЭА – Российский технологический университет, Москва, 119454 Россия*
[@] *Автор для переписки, e-mail: ekhalturin97@yandex.ru*

• **Поступила:** 20.02.2025 • **Доработана:** 02.10.2025 • **Принята к опубликованию:** 11.02.2026

Резюме

Цели. Цель работы – поиск методов и подходов разработки программного комплекса для обработки, анализа и визуализации данных учебных планов образовательных программ в автоматизированном режиме.

Методы. Проведен теоретический анализ научных работ и результатов в области исследования. В программном комплексе используются следующие методы: для обработки данных – регулярные выражения, для анализа посредством выявления различий – метод сравнительного анализа и методы описательной математической статистики, для визуализации результатов – графовая модель представления данных.

Результаты. Разработана архитектура программного комплекса для обработки (с предобработкой), анализа и визуализации учебных планов с использованием принципов объектно-ориентированного программирования SOLID[2]. Программная реализация на языке программирования C++ использована для подсчета характеристик учебных планов и создания графового представления, на основе которого предложен собственный способ визуализации учебных планов. Продемонстрированы возможности программного комплекса: проведен сравнительный анализ учебных планов, выявлены их особенности, обнаружены недочеты при их проектировании.

Выводы. Использование программного комплекса обработки, анализа и визуализации учебных планов может помочь выявить особенности учебного плана, указать на возможные недоработки и слабые места, провести сравнительный анализ разных учебных планов. Его применение позволит повысить качество управления образовательным процессом, заполнить пробелы в области анализа образовательных данных и будет способствовать созданию цифровой экосистемы вуза. Результаты работы могут быть полезны преподавателям, проектирующим и разрабатывающим учебные планы, представителям административно-управленческого персонала, в т.ч. работникам учебно-организационных отделов, а также другим участникам образовательного процесса вуза.

Ключевые слова: учебный план, образовательная программа, методы, программная обработка, графовая модель, компетентностный подход, междисциплинарные связи

[2] S (single responsibility principle) – принцип единственной ответственности; O (open-closed principle) – принцип открытости-закрытости; L (Liskov substitution principle) – принцип подстановки Барбары Лисков; I (interface segregation principle) – принцип разделения интерфейса; D (dependence inversion principle) – принцип инверсии зависимостей. [S is the single responsibility principle; O is an open-closed principle; L is the Liskov substitution principle; I is the interface segregation principle; D is the dependence inversion principle.]

Для цитирования: Халтурин Е.А., Кытманов А.А., Вайнштейн Ю.В., Зыкова Т.В. Программные методы обработки, анализа и визуализации учебных планов. *Russian Technological Journal*. 2026;14(2):42–56. https://doi.org/10.32362/2500-316X-2026-14-2-42-56, https://www.elibrary.ru/XNQJRO

Прозрачность финансовой деятельности: Авторы не имеют финансовой заинтересованности в представленных материалах или методах.

Авторы заявляют об отсутствии конфликта интересов.

INTRODUCTION

At the present time, the management of the educational process at universities is based on the use of a large amount of diverse data about students and their learning process, as well as information about educational programs (EPs), and teaching staff who provide their implementation, inter alia. At the same time, the available data is used only partially, as a rule, to provide administrative support for the educational process. For example, a higher education institution has data on the competencies which need to be developed as a result of completing a specific EP and statistics on the employment of graduates who have completed this program. However, the interrelationships between such data are not always analyzed in order to make changes to the EP or the educational process to ensure better results.

There are many such examples, all related to the fact that education management is currently based on the classical approach to educational analytics [1]. However, data collection, processing, and analysis technologies are rapidly evolving. This in turn is leading to the development of new approaches [2]. New software tools are needed for the successful implementation of such approaches in everyday practice. They must enable real-time access to the data on the educational process needed for analysis and adjustments. A large number of works are devoted to the creation and description of the features of information systems (IS) which use these tools and the creation of intelligent systems based on them (see, for example, [3–6]).

One of the main objects of analyzing the educational process is the EP which can be viewed as a plan for achieving the stated educational outcomes. In particular, the EP describes the features of the learning process and presents a set of competencies to be developed in the learner upon completion of the course. Therefore, the demand for the EP largely depends on how well it meets the expectations of its main consumers [7]: students; student representatives; faculty; administrative and management staff; external experts; including representatives of potential employers, etc. The quality of EPs plays a significant role in the reputation of a higher education institution.

A key component of the EP is its curriculum, describing the scheme for its implementation. The curriculum contains information about competencies, achievement indicators, and educational units (EUs). These also include disciplines, practices, state final examination, their sequence, and workload. The curriculum is a valuable source of information for managing the educational process. Analysis allows for the implementation of the EP to be assessed and its characteristic features identified.

Most research studies devoted to the processing of curriculum demonstrate a manual processing method, i.e., without the use of software tools for process automation. This work demonstrates the development and application of software methods for processing (including preprocessing), analysis, and visualization of the curriculum. Their implementation is presented in the developed software. This package enables the curriculum to be converted into a single format, their characteristics to be identified, a comparative analysis performed. It also allows them to be presented in a graph model for subsequent visualization.

The current task of the study is to assess the effectiveness of the formation of the competencies stated in the EP. This can be resolved by analyzing the interrelationships between the planned learning outcomes and a wide range of learning indicators, such as the percentage of students transferring to other programs. This article takes a step towards automating the processes of analyzing the curriculum structure and calculating their characteristics which can subsequently be linked to the quality of competence development.

1. RESEARCH METHODS

We analyzed a number of studies in order to create a software tool which identifies the optimum non-obvious features of the curriculum which corresponds to modern approaches to intelligent data analysis [8], and which can be integrated into the digital ecosystem of a university. They can be classified into five thematic areas (from general to specific):

1) Digital transformation: the impact of digital transformation in universities at different levels of data management.
2) Intelligent data-driven decision-making systems: challenges and opportunities for IS as a whole, as a modern approach to synthesizing new data and identifying patterns in existing data.

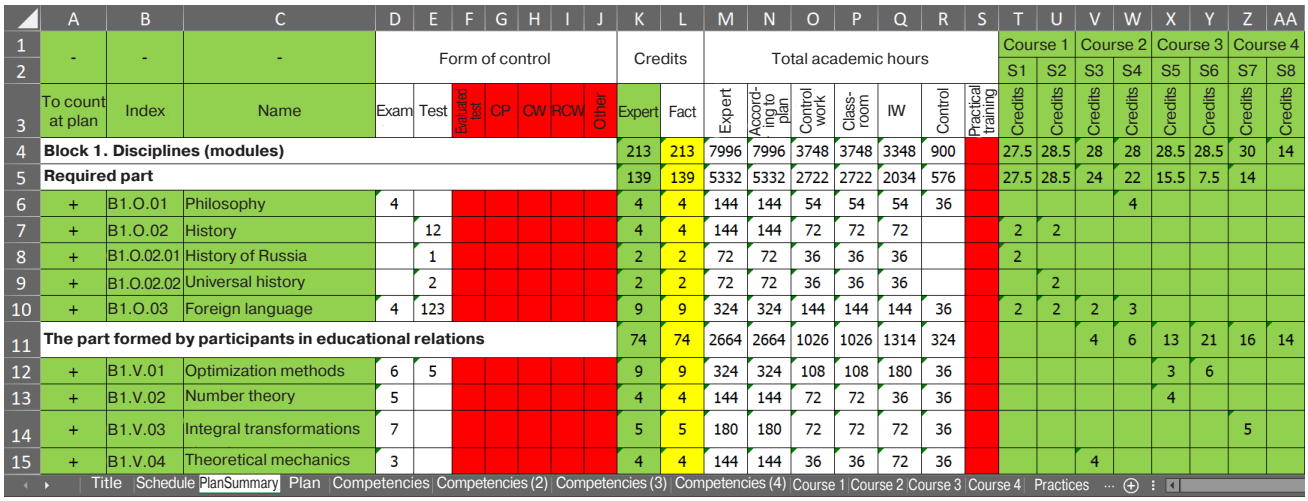

	A	B	C	D	E	F	G	H	I	J	K	L	M	N	O	P	Q	R	S	T	U	V	W	X	Y	Z	AA
1	-	-	-	Form of control							Credits		Total academic hours							Course 1		Course 2		Course 3		Course 4	
2																				S1	S2	S3	S4	S5	S6	S7	S8
3	To count at plan	Index	Name	Exam	Test	Evaluated test	CP	CW	RCW	Other	Expert	Fact	Expert	According to plan	Control work	Class-room	IW	Control	Practical training	Credits	Credits	Credits	Credits	Credits	Credits	Credits	Credits
4	Block 1. Disciplines (modules)										213	213	7996	7996	3748	3748	3348	900		27.5	28.5	28	28	28.5	28.5	30	14
5	Required part										139	139	5332	5332	2722	2722	2034	576		27.5	28.5	24	22	15.5	7.5	14	
6	+	B1.O.01	Philosophy	4							4	4	144	144	54	54	54	36					4				
7	+	B1.O.02	History		12						4	4	144	144	72	72	72			2	2						
8	+	B1.O.02.01	History of Russia		1						2	2	72	72	36	36	36			2							
9	+	B1.O.02.02	Universal history		2						2	2	72	72	36	36	36				2						
10	+	B1.O.03	Foreign language	4	123						9	9	324	324	144	144	144	36		2	2	2	3				
11	The part formed by participants in educational relations										74	74	2664	2664	1026	1026	1314	324				4	6	13	21	16	14
12	+	B1.V.01	Optimization methods	6	5						9	9	324	324	108	108	180	36						3	6		
13	+	B1.V.02	Number theory	5							4	4	144	144	72	72	36	36						4			
14	+	B1.V.03	Integral transformations	7							5	5	180	180	72	72	72	36								5	
15	+	B1.V.04	Theoretical mechanics	3							4	4	144	144	36	36	72	36				4					

Title | Schedule | PlanSummary | Plan | Competencies | Competencies (2) | Competencies (3) | Competencies (4) | Course 1 | Course 2 | Course 3 | Course 4 | Practices

Fig. 1. A fragment of a *Microsoft Excel* table exported from the Plans IS.
CP—course project, CW—course work, RCW—remote course work , IW—independent work, S1–S8—semesters 1–8

Table 1. Formats for completing curricula, differences are indicated by underlining

No.	Curricula	Data from the page “Competencies (2)” The “Competencies being developed” column
1	01.04.02.07 “Applied Computing in Science and Engineering” (reference version)	UC-1, UC-2, UC-3, UC-4, UC-6, GPC-1, GPC-3, GPC-4
2	09.04.01.06 “Microprocessor Systems” (incorrect option)	ID-1UC-6, ID-2UC-6, ID-3UC-6, ID-1GPC-1, ID-2GPC-1, ID-3GPC-1, ID-1GPC-3
3	10.03.01.31 “Computer System Security” (dual indicators)	UC-1, GPC-7, GPC-8, GPC-1.1, GPC-1.3, GPC-1.4
4	09.03.03.32 “Applied Informatics in Social Communications” (indicators are specified instead of competencies)	UC-1.1, UC-1.2, UC-1.3, GPC-1.1, GPC-1.2, GPC-1.3, GPC-4.1, GPC-4.2, GPC-4.3

Note: UC are universal competencies, GPC are general professional competencies, ID are identifiers.

3) EP assessment: assessment of their quality and potential for improvement.
4) Competency component: methods for assessing the competency component of the EP.
5) Curriculum data analysis: capabilities for analyzing the curriculum data to obtain a general understanding of the EP design.

Our research has led to the development of automated methods and approaches for creating the *SPA-SFU2*[3] software complex (from System-Plans-Analyze of Siberian Federal University). The source data for *SPA-SFU2* is the data from the Plans IS, developed by the MMIS[4] Laboratory. This IS is widely used among Russian universities for the purposes of working with the curriculum. Although it meets their needs, a level of redundancy was found (Fig. 1) when comparing the research objectives and the Plans IS database. Figure 1 shows a fragment of the input data for *SPA-SFU2*, where the colors indicate: red—empty curriculum fields; yellow—duplicate fields; green—fields with data relevant to the study. Note that column “C” lists the names of EUs—disciplines, practices, and state final examination (SFE)—to which credit units (CU) are assigned and which are the main structural elements of the curriculum.

The data formats vary significantly, since higher education institutions work with the curricula of a broad range of federal state higher education standards created over different years and by different designers. All comply with federal legislation and local regulatory documents, but their diversity complicates the development of software methods for preprocessing of the curriculum. For this reason, algorithms have been developed to bring them to a single standard in order to eliminate differences. These differences are expressed in the deviation of the format for filling in curriculum data from the most common among the curricula used in the study (Table 1, the standard data format is indicated in row 1). Examples of differences include: different data

[3] https://github.com/ekhalturin-ki15/SPA-SFU2. Accessed September 28, 2025. (In Russ.).
[4] https://www.mmis.ru. Accessed September 28, 2025. (In Russ.).

entry format; the use of different names for EUs and their corresponding competencies; a different method of indicating EU indicators (Table 1, nonstandard format is underlined); and others. When designing software methods, eliminating differences was the most labor-intensive task, since it required predicting situations which could potentially arise when working with all possible curricula.

An example of a discrepancy detected in the format of the research curricula: Table 1 shows that curriculum 09.04.01.06 "Microprocessor Systems" includes a list of indicators rather than competencies (row 2), complicating the programmatic analysis of data. In order to resolve this problem, we suggest using a backup regular expression which can extract the indicator, including from a different curriculum format. If this difference in the format of form filling is ignored, a situation will arise where a group of competencies with the name "ID-1UC" is defined instead of "UC" (universal competency). This will subsequently introduce an error in the calculations of the percentage distribution by groups of labor intensity competencies.

Another example is the discrepancy arising in the curriculum 10.03.01.31 "Computer System Security" (line 3). It contains competencies identical in appearance to the indicators of competency achievement (a situation of duplicate indicators). There are curricula which list not competencies, but a list of indicators to be formed, as presented in the curriculum 09.03.03.32 "Applied Informatics in Social Communications" (line 4). This requires additional analysis of the situation by the *SPA-SFU2* user, in order to determine what exactly is presented in the EU: competencies or indicators of their achievement.

From the point of view of software processing methods, some of the curricula data is statistical noise. For example, the list of competencies formed by the EU "Defense of the final qualification work" includes all possible curriculum competencies, negatively affecting the objectivity of the graph model obtained. The most common outliers are EUs related to practices and the state final examination, since they have a complete list of competencies formed by the entire set of EUs. They are much more labor-intensive (measured in CU) than other EUs. The presence of outliers reduces the clarity of the aggregated data obtained. For example, the metric "number of connectivity components" will be equal to one, which is not informative.

As a result, after eliminating the differences, *SPA-SFU2* operates only with the data on the curriculum necessary and sufficient for comprehensive analysis. This can be found in *Excel* tables on pages:

1) on the "Title" page, general information about the curriculum is specified;
2) the "Competencies (2)" page contains a complete EUs list;
3) on the "Competencies" page, indicators of competency achievement are compared. In addition, the nesting of EUs by modules is determined;
4) on the "PlanSummary" page shown in Fig. 1, the number of CUs allocated to the study of the course unit for each semester of study is determined, and it is also clarified whether the course unit is compulsory for completion.

The above data enables ambiguities in the data (differences in the names of identical entities and different formats for filling in the data) to be eliminated, and the final data in various categories to be determined:

1) integral characteristics for each individual semester of the curriculum, for all semesters of the curriculum, for the entire curriculum as a whole;
2) characteristics that determine the strength of interdisciplinary links;
3) data on graph models of the curriculum;
4) percentage distribution of the labor intensity of competence formation and indicators of their achievement.

The final result of *SPA-SFU2* can be used for such purposes as: pairwise comparison of the curricula, in order to identify the most successful moments (the order of EU, defined for EU formed competencies, distribution of load on EU); identifying a typical curriculum for different universities for the same EP; as well as determining specific situations which arise in the event of a large deviation from the average value of some of the curriculum characteristics. These can include, for example, situations where a large percentage of the total workload is allocated to the formation of general professional competencies. This can lead to a reduction in the workload on other competencies, since their total number is strictly regulated in the Federal State Educational Standards of Higher Education.[5]

An analysis was conducted of 49 curricula at the Institute of Space and Information Technologies of Siberian Federal University. The analysis of the curricula does not differ in terms of education levels (for bachelors, specialists, and master students), fields of study, and university affiliation, since their source is the Plans IS. This enables the study to be scaled up and replicated in any institution which uses the Plans IS to work with the curricula.

Let us note its key features of *SPA-SFU2,* in order to understand the effectiveness in resolving the task of the curriculum data analysis. The software package was developed in C++ using a minimum number of

[5] https://www.fgosvo.ru. Accessed September 28, 2025. (In Russ.).

1	Parameter name	Parameter value
2	Curricula data catalogs	plans\grad
3	Result output catalogs	result\grad
4	Divide credits by number of competencies	yes
5	Divide credits of the competence by number of competencies	yes
6	Undirected graph	yes
7	Use multi-level indicators	no
8	Max. length of discipline names	15
9	Regular expression for indicator splitting	(\w{1,}).{0,}-(.{1,})\.(.{0,})
10	Regular expression for indicator splitting (Additional)	\w{1,}.{0,}-(\d{1,})(\w{1,}).{0,}-(.{1,})
11	Regular expression for competence splitting	(\w{1,})\W{0,}-(.{1,})
12	How many semesters are there in one course	2
13	Number of quartiles	4
14	There are a lot of competencies if their number is greater than X =	6
15	Truncation of the mean for quartiles	0.05
16	Create an edge if its weight is greater than X =	0.001
17	L – Credits of the left vertex R – Credits of the right vertex A – total number of credits N – total number of disciplines K – power of intersection by competencies D – power of intersection by disciplines Supported operators +, −, *, /, ^ (degree), mod, abs, sin, cos, log	One can use any formulas, for example: 1) From SPA-SFU version No. 1: ((L + R) / (2 * A)) * K 2) Average: ((L + R) / 2) * K 3) Geometric mean: ((L * R) ^ (1 / 2)) * K
18	The weight of the graph edge where the vertex is a discipline	(5 * (L + R) / (A)) * K
19	The weight of the graph edge, where the vertex is competence	(5 * (L + R) / (A)) * D

Fig. 2. Fragment of the application configuration file

third-party libraries (only the OpenXLSX[6] library is used to work with *Excel* tables), enabling the entire data set of 10 curricula to be processed in less than a second (one curriculum has more than 2000 cells to analyze, and together with the data calculated by *SPA-SFU2* upon completion of the program, there are more than 10000 cells).

The study uses graph representations of the curriculum as a standard approach in the curriculum analysis, used in many studies [9, 10]. Graph representation allows metrics to be obtained for determining hypotheses regarding the correctness of the curriculum structure. *SPA-SFU2* calculates curriculum data about the corresponding graph model. There are many ways in which the curriculum can be represented as a graph, but in this study, four main ones were selected. In each of these methods, the edges between the vertices are calculated using the formula specified in the configuration file (Fig. 2, line 18). The formula used takes into account the number of matching competencies (the more matches, the greater the weight of the edge) and the labor intensity measured in CU.

Let us list the methods for constructing a graph model of the curriculum:

1) A standard graph model where a set of vertices corresponds to EUs. The edges between vertices indicate interdisciplinary connections at the intersection of the list of competencies being formed. The weight of a vertex corresponds to the labor intensity of the EU (how much CU is allocated for successful learning). The weight of an edge corresponds to the number of overlapping competencies (this model is described in more detail in [11]).
2) An extended graph model where a set of vertices corresponds to EUs graded by semester. One EU may belong to several vertices, if studied over several semesters. In [12], a similar graph representation is used to analyze the curricula.
3) A reverse graph model where a set of vertices corresponds to competencies. For this model, an additional formula is provided in the program configuration file (Fig. 2, line 19). A similar model is used in [13].

This study uses mathematical statistics. Measures of central tendency are determined on the basis of curriculum data, and the quartile distribution is thus calculated. Data on graph models is stored as an adjacency list which enables the best asymptotic performance of algorithms. For example, the calculation of the global clustering coefficient (the purpose of which is specified in [14]) has an asymptotic value of $O(|V| \times |E|)$, in which $|V|$ is the number of vertices and $|E|$ is the number of edges. Figure 3 presents a description of this algorithm. The use of binary search is made possible by storing vertex numbers in the adjacency list in ascending order.

[6] https://github.com/troldal/OpenXLSX. Accessed September 28, 2025.

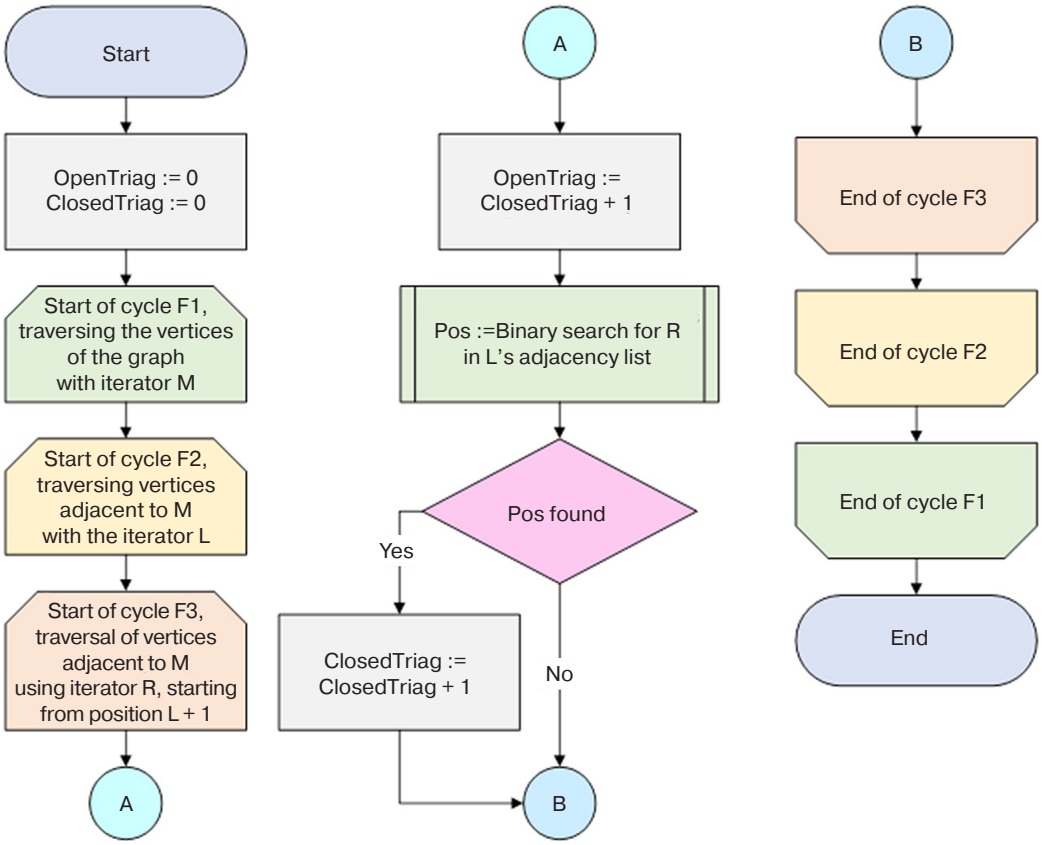

Fig. 3. Flowchart of the algorithm for calculating the global clustering coefficient of a graph

The OpenTriag variable is used to count and store the number of "open triangles," i.e., states in which only two of the three possible connections are formed for three points. The variable ClosedTriag has a similar purpose, but only for the state when all three connections are formed for three points. The clustering coefficient is equal to the ratio of ClosedTriag to OpenTriag. As you can see, its value does not exceed one.

2. RESULTS

The *SPA-SFU2* software package is presented as a console application which accepts *Excel* tables from the Plans IS as input and, upon completion, creates catalogs with *Excel* and cvs tables. The choice of the *Excel* format for the curricula is due to its clarity for the user, as well as the ease of editing and restructuring for other educational analytics tasks. For example, the user can specify EU teachers instead of competencies, in order to determine the distribution of the final workload. *SPA-SFU2* was developed using a modular architecture which enables new functionality to be added to the software complex without changing the existing one. For example, this allows for a curriculum processing module, including the xml format, to be added if necessary.

The program is controlled by configuring its parameters in the configuration file (Fig. 2, the left column lists the parameter names, and the right column lists their values). Several independent curricula samples can be specified (Fig. 2, line 2, the specified curriculum data directory contains several subdirectories with *Excel* tables). These include how to perform calculations (Fig. 2, lines 4–7), regular expressions for obtaining data from *Excel* table cells (Fig. 2, lines 9–11), threshold values (Fig. 2, lines 12–16), and formulas used for calculations (Fig. 2, lines 17–19).

Figure 4 shows an entity-relationship diagram in Martin's notation [15], corresponding to the database of the developed software (S). For convenience, the prefix before the field name indicates its data type. For example, the string data type of the sName field from the DTCurricula table stores the name of the curriculum. The colors of the tables, like their prefixes in the name, indicate their purpose: DT denotes a data storage table; R denotes a linking table; and Matrix denotes a two-dimensional data array storage table.

The architecture of the software complex is based on SOLID[7] design principles [16]. The RGlobal

[7] S is the single responsibility principle; O is the open-closed principle; L is thet Liskov substitution principle; I is the interface segregation principle; D is the dependence inversion principle.

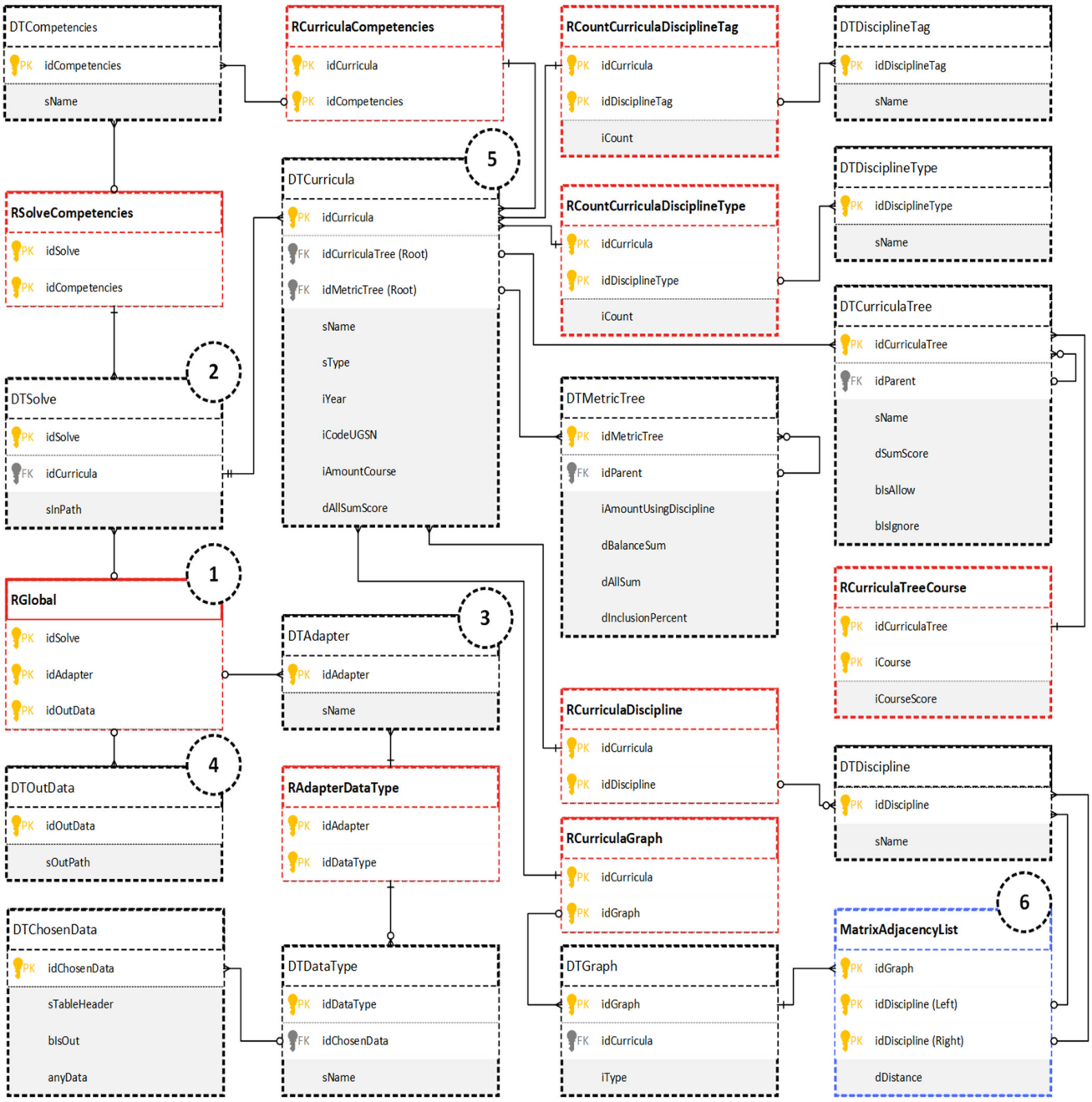

Fig. 4. Entity-relationship diagram for the application database

table (item 1 in Fig. 4) combines various methods: a) data input from DTSolve (item 2 in Fig. 4) which enables software parameters to be entered not only through the configuration file; b) aggregation from DTAdapter (item 3 in Fig. 4) which allows you to use your own methods for building a graph model of the curriculum; c) output from DTOutData (item 4 in Fig. 4) which allows you to vary the ways of displaying data, for example, to export it directly to business analytics systems, and not only to tabular files. The main table of the software is DTCurricula (item 5 in Fig. 4) which stores the input data on the curriculum. All other tables store data calculated using the software.

In order to calculate the clustering coefficient described in the research methods, an adjacency list is used, in order to improve the final asymptotics of the algorithm to the minimum possible. This is designated in the diagram as MatrixAdjacencyList (item 6 in Fig. 4). Thanks to the graph clustering coefficient, conclusions can be drawn about how strongly the EUs are interconnected.

Table 2 shows how the graph characteristics of two curricula with the maximum (curriculum 09.03.02.30) and minimum (curriclulum 09.03.03.33) clustering coefficients differ across the entire sample of bachelor's degree curricula. The characteristic is highlighted in

Table 2. Metrics of a graph model of two bachelor's curricula

Curriculum designation	09.03.02.30	09.03.03.33	Curriculum designation	09.03.02.30	09.03.03.33
Clustering coefficient	**0.92**	**0.43**	Graph density	0.14	0.12
Maximum number of CUs in EU	10 CU	15 CU	Minimum number of CUs in EU	2 CU	2 CU
Graph diameter by weight	1.01	1.36	Graph diameter by vertices	5 vertices	4 vertices
Number of linkage components	10	3	Pairs of unconnected vertices	895 pairs	89 pairs
Weight of the maximum skeleton tree	10.86	16.34	Weight of the minimum skeleton tree	7.21	8.04

bold, and this graph model is designated as "standard" in the methods section of this study. Figure 5 demonstrates a possible option for their visualization using the *Gephi*[8] software package.

Figure 5 shows the graph model of the curriculum 09.03.02.39 on the left, and curriculum 09.03.03.33 on the right. Each node represents a course unit, the name of which is given in abbreviated form. The larger the node, the greater its weight, expressed in terms of the CU allocated to the EU. The nodes are arranged from bottom to top according to the semester in which they are taught. The higher the node, the higher the semester number. For example, "Business Processes in the Media Industry," abbreviated as "BizMedia," is taught in the 8th semester of the bachelor's program. EUs taught in the same semester are highlighted in one color e.g. all red nodes are taught in semester 1. The edges between the nodes indicate interdisciplinary connections and are calculated using the formula shown in Fig. 2 in line 18. The user can change the formula to any desired one. The more teaching hours are allocated to the study of a course unit and the more competencies the education units have in common, the greater the weight of the edge between them. If there are no matching competencies, the weight is zero and there is no edge.

Table 2 shows that the calculated summary characteristics are sufficient to make preliminary conclusions. For example: in the curriculum 09.03.02.30 "Information Systems and Technologies" there are a large number of connectivity components (areas in which there is a path between any two vertices). The higher the value, the more heterogeneous the EUs are in terms of their list of competencies. Table 2 also shows other graph characteristics which can help determine the quality of a curriculum during its expert evaluation [17]. The diameter of the graph indicates the dispersion of competencies. The density of the graph and the weight of the skeleton tree indicate the total strength of interdisciplinary connections [11], while the number of unconnected disciplines indicates the dispersion of disciplines in terms of the competencies formed.

A high clustering coefficient indicates that most EUs corresponds to an identical list of competencies. This suggests that the authors of the curriculum did not pay sufficient attention to establishing the correspondence of EUs to the list of competencies they were developing. They may have copied the same data into different cells. In the curriculum 09.03.03.33 "Applied Informatics: Digital Economy," on the contrary, each EU has its own unique list of competencies.

In addition to graphical representation, *SPA-SFU2* calculates data on the number of EUs depending on their type (compulsory, elective, optional) and category (humanities, technical, and natural sciences), as well as how many CU are allocated to their study. The data obtained clearly indicates the specifics of the curriculum depending on the predominance of a certain type of discipline. For example, there may be different ratios of humanities EUs in different curricula in related fields of study, which demonstrates their specificity.

Other data calculated by *SPA-SFU2* includes the percentage distributions of CU allocated to the formation of competency groups (the Federal State Educational Standards for Higher Education[9] define three competency groups: universal, general professional, and professional). They can be used to understand which group of competencies is given priority, as well as how specialized the training program is.

Measures of central tendency are calculated, in order to identify deviations in the curriculum from their average value across the entire curriculum sample for each metric. For each curriculum parameter, *SPA-SFU2* calculates the maximum and minimum values, mode, median, and mean. This enables the most distinctive curriculum to be identified against the background of the others. Table 3 shows the metrics of the graph model of the 2021 bachelor's degree curriculum at the beginning of training, taking into account only the first year of study. As can be seen, only two curricula have elective courses in the first year of study.

[8] https://gephi.org. Accessed September 28, 2025.

[9] https://www.fgosvo.ru/news/view/5720. Accessed September 28, 2025. (In Russ.).

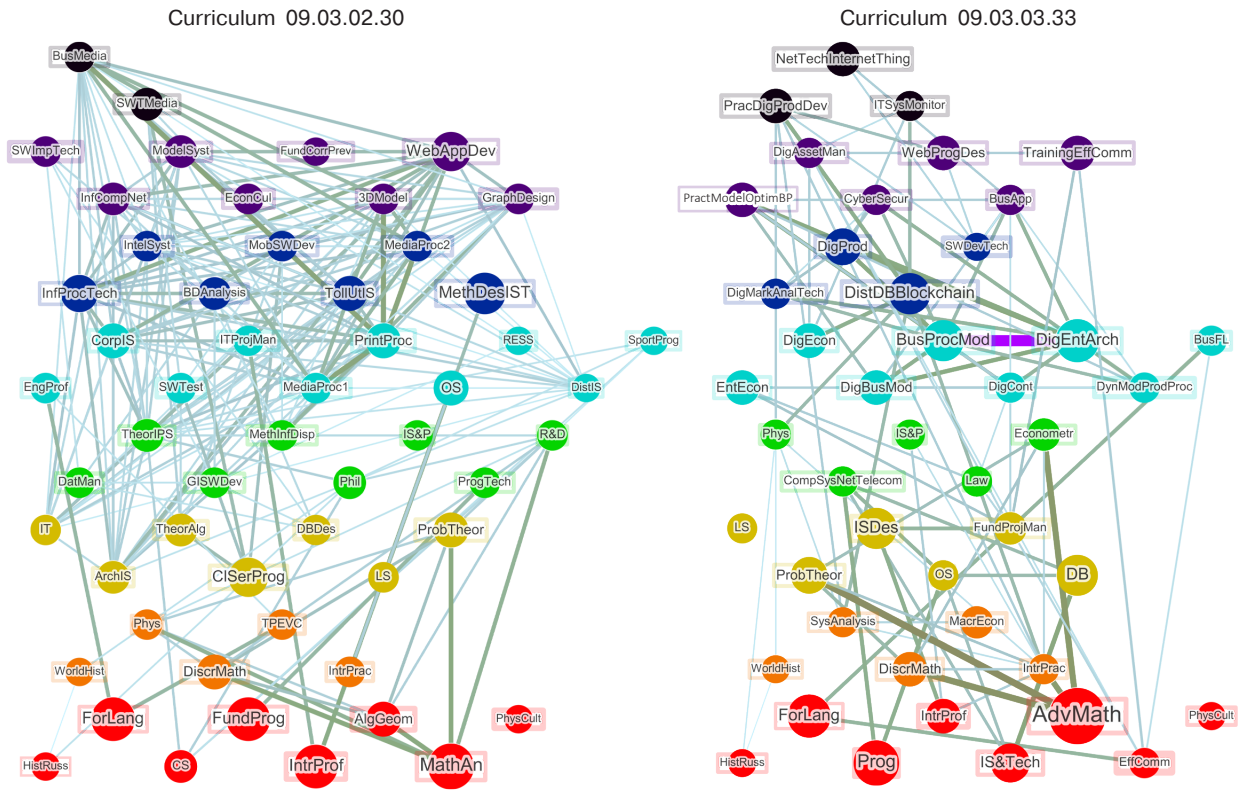

Fig. 5. Visualization of the graph model of the curriculum for all semesters of study.

IntrPrac—Introductory practice;
R&D—Research and development;
IT—Information technologies;
ArchIS—Architecture of IS;
TheorAlg—Theory of algorithms;
DatMan—Data management;
TheorIPS—Theory of information processes and systems;
ClSerProg—Client-server programming;
DBDes—Database design;
EngProf—English for professional purposes;
InfProcTech—Information processing technologies;
CorpIS—Corporate IS;
IntelSyst—Intelligent systems and technologies;
SWImpTech—Software implementation technologies;
SWTest—Software testing and quality control;
GISWDev—Geoinformation systems software development;
ITProjMan—Information technology project management;
BDAnalysis—Big data analysis;
MobSWDev—Mobile software development;
MethInfDisp—Methods and facilities of information display;
InfCompNet—Information and computing networks;
ModelSyst—Process and systems modeling;
TollUtIS—IS tools and utilities;
EconCul—Economic culture and financial competence;
FundCorrPrev—Fundamentals of corruption prevention;
3DModel—3D modeling and animation;
WebAppDev—Web application development;
BusMedia—Business processes in the media industry;
MediaProc1—Media content processing, part 1;
MediaProc2—Media content processing, part 2;
PrintProc—Printing process;
SWTMedia—Media industry software tools;
GraphDesign—Graphic design of the interface;
Phil—Philosophy;
HistRuss—History of Russia;
WorldHist—World history;
ForLang—Foreign language;
LS—Life safety;
Phys—Physics;
CS—Computer science;
FundProg—Fundamentals of programming;
IntrProf—Introduction to professional activity;
AlgGeom—Algebra and geometry;
MathAn—Mathematical analysis;
DiscrMath—Discrete mathematics;
ProbTheor—Probability theory and mathematical statistics;
TPEVC—Theory and practice of effective verbal communication;
ProgTech—Programming technologies;
MethDesIST—Methods and tools for designing ISs and technologies;
OS—Operational systems;
PhysCult—Physical culture and sport;
RESS—Remote Earth sensing systems;
DistIS—Distributed ISs;
SportProg—Sports programming;
EntEcon—Enterprise economics;
DigEcon—Digital economy;
DigBusMod—Digital business models;
BusProcMod—Business process modeling;
DigCont—Digital control;
DigMarkAnalTech—Digital market analysis technologies;
DigEntArch—Digital enterprise architecture;
DynModProdProc—Dynamic modeling of production processes;
DigProd—Digital production;
BusFL—Business foreign language;
DistDBBlockchain—Distributed databases and blockchain technologies;
PractModelOptimBP—Practicum: modeling and optimization of business processes;
DigAssetMan—Digital asset management;
CyberSecur—Cybersecurity;
WebProgDes—Web programming and computer design;
PracDigProdDev—Practicum: digital product development;
BusApp—Business applications;
NetTechInternetThing—Network technologies and the Internet of Things;
TrainingEffComm—Training course: effective communication;
ITSysMonitor—IT systems for monitoring socioeconomic development;
CompSysNetTelecom—Computing systems, networks, and telecommunications;
SysAnalysis—System analysis;
Prog—Programming;
IS&Tech—Information systems and technologies;
AdvMath—Advanced mathematics;
EffComm—Effective communication;
IS&P—Information security and protection;
Law—Law;
ISDes—IS design;
FundProjMan—Fundamentals of project management;
DB—Databases;
MacrEcon—Macroeconomics;
Econometr—Econometrics;
SWDevTech—Software development technology

Table 3. A software-generated table of aggregated data from the 1st year undergraduate curricula

Designation	Quantity of your choice	Maximum rib weight	Minimum rib weight	Graph diameter	Clustering coefficient	1st quartile	2nd quartile	3rd quartile	4th quartile	Unconnected vertices
01.03.04.30	0	0.371	*0.087*	0.371	1.000	9	9	5	1	67
09.03.01.30	0	0.341	0.091	0.614	0.805	3	6	7	7	55
09.03.02.30	0	0.338	0.090	0.338	1.000	2	3	3	0	70
09.03.03.32	0	0.461	0.092	0.461	0.000	3	2	0	2	71
09.03.03.31	0	0.459	0.092	0.459	0.000	3	2	0	2	71
09.03.03.33	0	0.446	0.089	0.692	0.333	4	2	4	7	61
09.03.03.35	0	0.439	0.088	0.439	0.000	3	2	0	2	71
09.03.04.30	0	0.369	0.099	0.591	0.800	2	4	1	5	66
10.03.01.31	0	0.376	0.111	0.376	1.000	*1*	4	2	1	70
15.03.04.32	27	0.766	0.106	0.468	0.917	10	4	13	12	*39*
27.03.03.30	11	0.670	0.089	0.580	0.882	3	3	4	8	60
27.03.04.30	*3*	*0.332*	0.088	*0.331*	1.000	2	4	4	0	68
Median	11	0.439	0.091	0.461	0.882	3	4	4	2	68
Mode	0	–	0.089	–	1.000	3	3	2	2	71
Truncated mean	13.667	0.447	0.094	0.477	0.645	3	3	3	3	64

It can also be noted that for the curriculum 09.03.03.31 "Internet technologies and mobile applications" has a global clustering coefficient of zero (Table 3, column 6 "Clustering coefficient"). This means that no three EUs form the same competence in the first year of study. Columns 8–11 show the quartile distribution of the minimum distances between all pairs of vertices. In fact, all study curricula distances (10 bachelor's curricula) are combined into a single array. They are sorted, and each value is assigned to one of the four quartiles. The first quartile includes pairs of vertices between which there is a relatively small distance in the graph model. The fourth quartile includes pairs of vertices between which there is a relatively large distance. The situation where there is no route between vertices belongs to the "Unconnected vertices" group.

As can be seen in Table 3, minimum and maximum values are determined for each calculated measure, as well as other central trend measures. The percentage of truncation of the mean value is specified in the program configuration file (Fig. 2, line 15). If a dash is indicated in a cell, it means that the value is not informative (for example, if all values are the same or all values are different, the mode value is not indicated). Unique maximum values are highlighted with underlining, minimum values are highlighted in italics. Also, the number of decimal places for all values has been reduced for greater clarity. Table 3 also shows that curriculum 15.03.04.32 "Automation of Technological Processes and Production" (gray row) stands out from the rest, as its metrics most often contain the minimum and maximum values relative to all the bachelor's degree curricula which have been analyzed. Thus, this curriculum does indeed have its own characteristics. For example, it is the only curriculum which teaches "Chemistry" and "Ecology" curricula within all areas of the institute's training in the field of information technology.

A log file is generated (Fig. 6), in order to assist *SPA-SFU2* users in identifying controversial issues in the curriculum filling format. It indicates the elements of curriculum processing and the shortcomings which may arise in the process. For example, by analyzing the errors generated by the log file, curriculum 27.03.04 "Management in Technical Systems" GPC-7 was found to have been formed only on the basis of practices (number 1). These were excluded from the analysis, since the entire set of the curriculum competencies is defined as formed for them.

3. DISCUSSION

Assessing the quality of EPs (for more details on quality, see [18]) in the context of the effectiveness of achieving educational outcomes is a complex, multifaceted task which attracts the attention of both academic researchers and developers of commercial

```
Competencies (2) [line 61]: In the curriculum
R:/grad_sfu/2703040030_op-21.plm.plx.xlsx No competencies are specified for the elective
discipline with the index B2.E.
- The R:/grad_sfu/2703040030_op-21.plm.plx.xlsx curriculum has been processed with errors.

- No course with the index GPC-7 was found in the R:/grad_sfu/2703040030_op-21.plm.
plx.xlsx curriculum ①
```

Fig. 6. Fragment of a log file generated by the application

educational platforms [19]. For example, difficulties may be associated with the ambiguity of EP assessment criteria, in particular, the high variability in the percentage distribution of the labor intensity of forming different groups of competencies at different stages of training.

As an initial stage of EP quality assessment, we propose that the task of studying the curriculum be considered from the point of view of analyzing the composition and structure of the EP. At the same time, traditional methods of curricula evaluating (expert assessments, tabular comparisons) are not as effective as software methods. This is due to the following factors: subjectivity of opinions [20]; the impossibility of analyzing a large number of curricula within a limited time frame; as well as errors in performing the analysis, inter alia. In this regard, the development of software tools to support the analysis of the curriculum, as the first step in assessing the quality of the EP, is a matter of urgency.

We recommended using the software methods presented in this work. They can be expressed in the following actions, for making decisions on curriculum modernization and applying the experience gained in creating new curricula and EPs:

1) preprocessing: converting data into a uniform format for ease of further use and expansion of processing capabilities;
2) processing: extraction from the entire set of data obtained from the *Excel* table Plans IS of the data necessary for further analysis of the characteristics of interest to the researcher;
3) analysis: calculation of aggregated data based on data obtained during processing, e.g., data that clearly indicates the characteristics of the curriculum;
4) visualization: displaying data obtained during analysis in a form that is convenient for the researcher to use for quick and accurate decision-making based on that data [21].

Let us consider the problems of implementing such software tools, related to refining the characteristics of the curricula, calibrating them based on expert opinion, and determining their relationship with other characteristics of the EP training. This includes such factors as student retention, and graduate employment rates, among others. The software methods proposed in this work are useful for solving the above-described problems and contribute to the development of automated tools for data-driven decision-making.

CONCLUSIONS

The study proposes software methods for processing, analyzing, and visualization of the curricula, implemented in the *SPA-SFU2* software package. The package helps curricula to be compared with minimal effort. It helps their characteristics to be determined based on numerical indicators, and the reasons for significant deviations of these indicators from the average value to be established. *SPA-SFU2* clearly indicates problem areas in the curriculum for decision-making on their correction. It helps to identify possible shortcomings in the curriculum, understand the resulting competence component, and determine the implicit patterns in the data contained therein.

Visualization of the curriculum using *SPA-SFU2* enables a faster and more accurate understanding of the internal structure of the curriculum and its characteristic differences. *SPA-SFU2* can be useful when demonstrating the characteristics of the curriculum to applicants, students, and teachers. For example, it can be used to demonstrate the percentage distribution into competency groups or to visualize the interrelationships of the EU through graph representation.

SPA-SFU2 can be used to create new curricula which optimize the planned educational process, the formation of which is based on a comparative analysis with the other educational curricula in related areas of training, thus ensuring their uniqueness and effectiveness.

The *SPA-SFU2* software package for curricula analyzing is a necessary link for developing a comprehensive educational analytics IS and can serve as an element of the university's digital ecosystem.

At the present time, the *SPA-SFU2* software package presented in this study is not fully automated. It requires expert opinion to make decisions based on the characteristics it obtains. This problem could be addressed by incorporating artificial intelligence modeling approaches into *SPA-SFU2*. This could be achieved by using neural networks or simulating artificial

intelligence by accumulating behavioral scenarios in predefined situations.

In the future, the following tasks in this specified order need to be addressed, in order to fully automate the processing, analysis and visualization of the curricula, as well as to better cover their useful characteristics:

1) to obtain and compare information external to the EP (for example, data on student performance, survey results, and information on graduate employment) with the characteristics of the curricula obtained and calculated by *SPA-SFU2*;
2) to introduce the complex digital solutions based on the principles of artificial intelligence and big data processing;
3) to find other ways to visualize the curriculum characteristics, in order to demonstrate their features not presented in the study.

Authors' contributions

E.A. Khalturin—methodology, original draft preparation, review and editing, presenting software methods.

A.A. Kytmanov—supervision, conceptualization writing, research problem, original draft preparation and editing.

Yu.V. Vaynshteyn—discussion, editing.

T.V. Zykova—formal analysis, practical application.

REFERENCES

1. Korolkova I.A., Zaytsev S.A. Modern factors of influence on IT education. In: *Digital Transformation of Social and Economic Systems: Proceedings of the International Scientific and Practical Conference. Moscow: Moscow Witte University.* 2023. P. 264–268 (in Russ.). https://www.elibrary.ru/qbzuya
2. Shirinkina E.V. Methods of data mining and educational analytics. *Sovremennoe obrazovanie = Modern Education.* 2022;1:51–67 (in Russ.). https://www.elibrary.ru/dinnow, https://doi.org/10.25136/2409-8736.2022.1.37582
3. Kustitskaya T.A., Esin R.V., Kytmanov A.A., Zykova T.V. Designing an Education Database in a Higher Education Institution for the Data-Driven Management of the Educational Process. *Education Sciences.* 2023;13(9):947. https://www.elibrary.ru/jnyekv, https://doi.org/10.3390/educsci13090947
4. Jarke J., Breiter A. Editorial: The datafication of education. *Learning, Media and Technology.* 2019;44(1):1–6. https://doi.org/10.1080/17439884.2019.1573833
5. Hartong S., Piattoeva N. Contextualizing the datafication of schooling – a comparative discussion of Germany and Russia. *Critical Studies in Education.* 2021;62(2):227–242. https://doi.org/10.1080/17508487.2019.1618887
6. Pangrazio L., Selwyn N., Cumbo B. Tracking technology: exploring student experiences of school datafication. *Cambridge J. Education.* 2023;53(6):847–862. https://doi.org/10.1080/0305764X.2023.2215194
7. Nouraey P., Al-Badi A., Riasati M.J., Maata R.L. Educational program and curriculum evaluation models: a mini systematic review of the recent trends. *Universal J. Educational Res.* 2020;8(9):4048–4055. https://doi.org/10.13189/ujer.2020.080930
8. McCarthy A., Maor D., McConney A., Cavanaugh C. Digital transformation in education: Critical components for leaders of system change. *Social Sciences & Humanities Open.* 2023;8(1):100479. https://doi.org/10.1016/j.ssaho.2023.100479
9. Kuzmina E.A., Nizamova G.F. Curriculum development based on the graph model. *Informatika i obrazovanie = Informatics and Education.* 2020;4(5):33–43 (in Russ.). https://www.elibrary.ru/erhqxo, https://doi.org/10.32517/0234-0453-2020-35-5-33-43
10. Ageev Yu.D., Fedoseev S.V., Kavin Yu.A., Vorona S.G., Pavlovskiy I.S. Inconsistency evaluation of the curriculum logical structure. *Statistika i ehkonomika = Statistics and Economics.* 2018;5:73–80 (in Russ.). https://www.elibrary.ru/vpnnbq, https://doi.org/10.21686/2500-3925-2018-5-73-80
11. Zykova T.V., Kytmanov A.A., Khalturin E.A., Vaynshteyn Y.V., Noskov M.V. Algorithm for analysis and evaluation of educational programs curricula. *Informatika i obrazovanie = Informatics and Education.* 2024;39(1):52–64 (in Russ.). https://www.elibrary.ru/unswxg, https://doi.org/10.32517/0234-0453-2024-39-1-52-64
12. Borzova A.S. Optimization of training components in the field of operation of air transport on the basis of expert analysis with orientation on the model-oriented approach. *Modelirovanie, optimizatsiya i informatsionnye tekhnologii = Modeling, Optimization and Information Technology.* 2017;3(18):14 (in Russ.). https://www.elibrary.ru/zrcvgd. Available from URL: https://moit.vivt.ru/wp-content/uploads/2017/08/Borzova_3_1_17.pdf. Accessed September 28, 2025.
13. Kurilova O.L. Application of genetic algorithm for curriculum optimization. *Informatsionno-upravlyayushchie sistemy = Information and Control Systems.* 2013;3(64):84–92 (in Russ.). https://www.elibrary.ru/qbpgth
14. Demina A.R., Yudin E.B. Calculation of the clustering coefficient of an incomplete network using parallel computing. *Rossiya molodaya: peredovye tekhnologii – v promyshlennost' = Young Russia: Advanced Technology – in the Industry.* 2015;3:45–48 (in Russ.). https://www.elibrary.ru/uzeonx
15. Hitchman S. The details of conceptual modelling notations are important – a comparison of relationship normative language. *Communications of the Association for Information Systems.* 2002;9(1):10. https://doi.org/10.17705/1CAIS.00910
16. Gubin A.S., Toutova N.V. Analysis of the approach to developing applications with a "clean" architecture. *Telekommunikatsii i informatsionnye tekhnologii = Telecommunications and Information Technology.* 2022;9(1):28–37 (in Russ.). https://www.elibrary.ru/nozmkg
17. Kytmanov A.A., Gorelova Yu.N., Zykova T.V., Pikhtilkova O.A., Pronina E.V. A conceptual approach to digital transformation of the educational process at a higher education institution. *Russian Technological Journal.* 2024;12(5):98–110. https://elibrary.ru/WAZLGB, https://doi.org/10.32362/2500-316X-2024-12-5-98-110

18. Korchak A.E., Khavenson T.E. Concept of “quality” in higher education: from offline to online mode. *Vysshee obrazovanie v Rossii = Higher Education in Russia*. 2024;33(1):9–27 (in Russ.). https://elibrary.ru/WAZLGB, https://doi.org/10.31992/0869-3617-2024-33-1-9-27
19. Manolev J., Sullivan A., Slee R. The datafication of discipline: ClassDojo, surveillance and a performative classroom culture. In: *The Datafication of Education.* Routledge; 2020. P. 37–52. https://doi.org/10.1080/17439884.2018.1558237
20. Williamson B., Bayne S., Shay S. The datafication of teaching in Higher Education: critical issues and perspectives. *Teaching in Higher Education.* 2020;25(4):351–365. https://doi.org/10.1080/13562517.2020.1748811
21. Zykova T.V., Kytmanov A.A., Noskov M.V., Khalturin E.A. Application of a force-directed graph drawing algorithm for the analysis of curricula of educational programs of higher education. *Sovremennye informatsionnye tekhnologii i IT-obrazovanie = Modern Information Technologies and IT-Education.* 2023;19(1):104–116 (in Russ.). https://elibrary.ru/kzhowj, https://doi.org/10.25559/SITITO.019.202301.104-116

СПИСОК ЛИТЕРАТУРЫ

1. Королькова И.А., Зайцев С.А. Современные факторы, влияющие на формирование IT компетенций у обучающихся. В сб.: *Цифровая трансформация социальных и экономических систем: материалы международной научно-практической конференции*. М.: Московский университет им. С.Ю. Витте. 2023. С. 264–268. https://www.elibrary.ru/qbzuya
2. Ширинкина Е.В. Методы интеллектуального анализа данных и образовательной аналитики. *Современное образование.* 2022;1:51–67. https://www.elibrary.ru/dinnow, https://doi.org/10.25136/2409-8736.2022.1.37582
3. Kustitskaya T.A., Esin R.V., Kytmanov A.A., Zykova T.V. Designing an Education Database in a Higher Education Institution for the Data-Driven Management of the Educational Process. *Education Sciences.* 2023;13(9):947. https://www.elibrary.ru/jnyekv, https://doi.org/10.3390/educsci13090947
4. Jarke J., Breiter A. Editorial: The datafication of education. *Learning, Media and Technology.* 2019;44(1):1–6. https://doi.org/10.1080/17439884.2019.1573833
5. Hartong S., Piattoeva N. Contextualizing the datafication of schooling – a comparative discussion of Germany and Russia. *Critical Studies in Education.* 2021;62(2):227–242. https://doi.org/10.1080/17508487.2019.1618887
6. Pangrazio L., Selwyn N., Cumbo B. Tracking technology: exploring student experiences of school datafication. *Cambridge J. Education.* 2023;53(6):847–862. https://doi.org/10.1080/0305764X.2023.2215194
7. Nouraey P., Al-Badi A., Riasati M.J., Maata R.L. Educational program and curriculum evaluation models: a mini systematic review of the recent trends. *Universal J. Educational Res.* 2020;8(9):4048–4055. https://doi.org/10.13189/ujer.2020.080930
8. McCarthy A., Maor D., McConney A., Cavanaugh C. Digital transformation in education: Critical components for leaders of system change. *Social Sciences & Humanities Open.* 2023;8(1):100479. https://doi.org/10.1016/j.ssaho.2023.100479
9. Кузьмина Е.А., Низамова Г.Ф. Формирование учебного плана на основе графовой модели. *Информатика и образование.* 2020;4(5):33–43. https://www.elibrary.ru/erhqxo, https://doi.org/10.32517/0234-0453-2020-35-5-33-43
10. Агеев Ю.Д., Федосеев С.В., Кавин Ю.А., Ворона С.Г., Павловский И.С. Оценка противоречивости логической структуры учебного плана. *Статистика и экономика.* 2018;5:73–80. https://www.elibrary.ru/vpnnbq, https://doi.org/10.21686/2500-3925-2018-5-73-80
11. Зыкова Т.В., Кытманов А.А., Халтурин Е.А., Вайнштейн Ю.В., Носков М.В. Алгоритм анализа и оценки учебных планов образовательных программ. *Информатика и образование.* 2024;39(1):52–64. https://www.elibrary.ru/unswxg, https://doi.org/10.32517/0234-0453-2024-39-1-52-64
12. Борзова А.С. Оптимизация компонентов содержания обучения в области эксплуатации воздушного транспорта на основе экспертного анализа с ориентацией на модель-ориентированный подход. *Моделирование, оптимизация и информационные технологии.* 2017;3(18):14. https://www.elibrary.ru/zrcvgd. URL: https://moit.vivt.ru/wp-content/uploads/2017/08/Borzova_3_1_17.pdf. Дата обращения 28.09.2025.
13. Курилова О.Л. Применение генетического алгоритма для оптимизации учебного плана. *Информационно-управляющие системы*. 2013;3(64):84–92. https://www.elibrary.ru/qbpgth
14. Дёмина А.Р., Юдин Е.Б. Расчет коэффициента кластеризации неполной сети с использованием параллельных вычислений. *Россия молодая: передовые технологии – в промышленность.* 2015;3:45–48. https://www.elibrary.ru/uzeonx
15. Hitchman S. The details of conceptual modelling notations are important – a comparison of relationship normative language. *Communications of the Association for Information Systems.* 2002;9(1):10. https://doi.org/10.17705/1CAIS.00910
16. Губин А.С., Тутова Н.В. Анализ подхода к разработке приложений с «чистой» архитектурой. *Телекоммуникации и информационные технологии.* 2022;9(1):28–37. https://www.elibrary.ru/nozmkg
17. Кытманов А.А., Горелова Ю.Н., Зыкова Т.В., Пихтилькова О.А., Пронина Е.В. Концептуальный подход к цифровой трансформации образовательного процесса в вузе. *Russian Technological Journal.* 2024;12(5):98–110. https://elibrary.ru/WAZLGB, https://doi.org/10.32362/2500-316X-2024-12-5-98-110
18. Корчак А.Э., Хавенсон Т.Е. Понятие «качество» в высшем образовании: от офлайн к онлайн-формату. *Высшее образование в России*. 2024;33(1):9–27. https://elibrary.ru/WAZLGB, https://doi.org/10.31992/0869-3617-2024-33-1-9-27
19. Manolev J., Sullivan A., Slee R. The datafication of discipline: ClassDojo, surveillance and a performative classroom culture. In: *The Datafication of Education.* Routledge; 2020. P. 37–52. https://doi.org/10.1080/17439884.2018.1558237
20. Williamson B., Bayne S., Shay S. The datafication of teaching in Higher Education: critical issues and perspectives. *Teaching in Higher Education.* 2020;25(4):351–365. https://doi.org/10.1080/13562517.2020.1748811

21. Зыкова Т.В., Кытманов А.А., Носков М.В., Халтурин Е.А. Применение силового алгоритма визуализации графов для анализа учебных планов образовательных программ высшего образования. *Современные информационные технологии и ИТ-образование.* 2023;19(1):104–116. https://elibrary.ru/kzhowj, https://doi.org/10.25559/SITITO.019.202301.104-116

About the Authors

Evgenii A. Khalturin, Senior Lecturer, Department of Information System, School of Space and Information Technology, Siberian Federal University (79, Svobodny pr., Krasnoyarsk, 660041 Russia). E-mail: ekhalturin97@yandex.ru. RSCI SPIN-code 5324-8252, https://orcid.org/0000-0001-9292-0370

Alexey A. Kytmanov, Dr. Sci. (Phys.-Math.), Associate Professor, Head of the Higher Mathematics Department – 3, Institute for Advanced Technologies and Industrial Programming, MIREA – Russian Technological University (78, Vernadskogo pr., Moscow, 119454 Russia). E-mail: kytmanov@mirea.ru. Scopus Author ID 6602129708, RSCI SPIN-code 6866-6079, https://orcid.org/0000-0003-3325-099X

Yuliya V. Vaynshteyn, Dr. Sci. (Education), Professor, Department of Applied Mathematics and Data Science, School of Space and Information Technology, Siberian Federal University (79, Svobodnyi pr., Krasnoyarsk, 660041 Russia). E-mail: yweinstein@sfu-kras.ru. Scopus Author ID 57205328429, RSCI SPIN-code 9765-2130, https://orcid.org/0000-0002-8370-7970

Tatiana V. Zykova, Cand. Sci. (Phys.-Math.), Associate Professor, Department of Applied Mathematics and Data Science, School of Space and Information Technology, Siberian Federal University (79, Svobodnyi pr., Krasnoyarsk, 660041 Russia). E-mail: tzykova@sfu-kras.ru. Scopus Author ID 57188699496, RSCI SPIN-code 1959-9769, https://orcid.org/0000-0002-7332-2372

Об авторах

Халтурин Евгений Александрович, старший преподаватель, кафедра информационных систем, Институт космических и информационных технологий, ФГАОУ ВО «Сибирский федеральный университет» (660041, Красноярск, пр-т Свободный, д. 79). E-mail: ekhalturin97@yandex.ru. SPIN-код РИНЦ 5324-8252, https://orcid.org/0000-0001-9292-0370

Кытманов Алексей Александрович, д.ф.-м.н., доцент, заведующий кафедрой высшей математики – 3, Институт перспективных технологий и индустриального программирования, ФГБОУ ВО «МИРЭА – Российский технологический университет» (119454, Россия, Москва, пр-т Вернадского, д. 78). E-mail: kytmanov@mirea.ru. Scopus Author ID 6602129708, SPIN-код РИНЦ 6866-6079, https://orcid.org/0000-0003-3325-099X

Вайнштейн Юлия Владимировна, д.пед.н., профессор, кафедра прикладной математики и анализа данных, Институт космических и информационных технологий, ФГАОУ ВО «Сибирский федеральный университет» (660041, Красноярск, пр-т Свободный, д. 79). E-mail: yweinstein@sfu-kras.ru. Scopus Author ID 57205328429, SPIN-код РИНЦ 9765-2130, https://orcid.org/0000-0002-8370-7970

Зыкова Татьяна Викторовна, к.ф.-м.н., доцент, кафедра прикладной математики и анализа данных, Институт космических и информационных технологий, ФГАОУ ВО «Сибирский федеральный университет» (660041, Красноярск, пр-т Свободный, д. 79). E-mail: tzykova@sfu-kras.ru. Scopus Author ID 57188699496, SPIN-код РИНЦ 1959-9769, https://orcid.org/0000-0002-7332-2372

Translated from Russian into English by Lyudmila O. Bychkova
Edited for English language and spelling by Dr. David Mossop

УДК 621.391: 621.396: 621.373
https://doi.org/10.32362/2500-316X-2026-14-2-57-68
EDN XPSWYV

RESEARCH ARTICLE

Generation of radiovision signals by spectral saturation in transient distortion mode of integral microwave amplifiers for gesture recognition systems

Kirill V. Latyshev [@], Mihail S. Kostin, Konstantin A. Boikov

MIREA – Russian Technological University, Moscow, 119454 Russia
[@] Corresponding author, e-mail: latyshev@mirea.ru

• **Submitted:** 17.06.2025 • **Revised:** 29.09.2025 • **Accepted:** 09.02.2026

Abstract

Objectives. The paper aims to investigate the mechanisms of the nonlinear formation of a wideband pulse spectrum under overload conditions in ultra-wideband (UWB) amplifier circuits in resolving problems related to radiovision gesture recognition. The relevance of the study stems from the need to enhance the accuracy and noise immunity of modern radiovision UWB systems for gestural control interfaces.

Methods. The study used statistical radiophysics, time-frequency methods of wavelet transformation of radio images, the theory of *S*-parametric vector analysis of circuits, and software-numerical modeling.

Results. The method for generating UWB signals in the microwave range based on controlled nonlinear signal distortion is presented. When the amplifier is switched to the saturation mode, a signal with sharp fronts is formed with a wide energy spectrum. A laboratory setup of a cyber-physical system for gesture recognition using radio sensing was developed, and its characteristics were investigated. The properties of the pulses generated in radiovision control systems were also studied. The effectiveness of the proposed approach for the tasks of radiovision gesture recognition was experimentally demonstrated.

Conclusions. A method of nonlinear saturation-synthesis of the spectrum of radiovision signals based on transient distortion phenomena in UWB amplifiers is proposed. It was shown that, when the initial frequency band is expanded up to 900 MHz, the interference mode can provide phase image repeatability of at least 0.94. It was also established that in the input overloaded mode of the SBB5089Z[1] type amplifier with low-mode harmonic excitation at a transition frequency of 47 MHz in a cascade amplification scheme, a signal with a modified spectrum can be obtained at the output of the radio antenna. In this case, the controlled formation of the antenna excitation spectrum for each amplifier module is determined by means of the unique impulse characteristic of the integrated UWB-amplifier. This allows for the successful application such amplifiers in resolving problems related to radiovision gesture recognition. The methodology proposed allows the use of standard UWB amplifiers to create compact sources of UWB signals without the complication of circuitry.

Keywords: radiovision signal, spectrum saturation, transient distortion, ultra-wideband amplifier, gesture recognition, cyber-physical stand

[1] High-linearity wideband, monolithic microwave integrated circuit (MMIC) amplifier was developed by Qorvo, USA.

For citation: Latyshev K.V., Kostin M.S., Boikov K.A. Generation of radiovision signals by spectral saturation in transient distortion mode of integral microwave amplifiers for gesture recognition systems. *Russian Technological Journal.* 2026;14(2):57–68. https://doi.org/10.32362/2500-316X-2026-14-2-57-68, https://www.elibrary.ru/XPSWYV

Financial disclosure: The authors have no financial or proprietary interest in any material or method mentioned.

The authors declare no conflicts of interest.

НАУЧНАЯ СТАТЬЯ

Формирование радиовизионных сигналов спектральной сатурацией в режиме переходных искажений интегральных сверхвысокочастотных усилителей для систем распознавания жестов

К.В. Латышев [@], М.С. Костин, К.А. Бойков

МИРЭА – Российский технологический университет, Москва, 119454 Россия
[@] Автор для переписки, e-mail: latyshev@mirea.ru

• **Поступила:** 17.06.2025 • **Доработана:** 29.09.2025 • **Принята к опубликованию:** 09.02.2026

Резюме

Цели. Цель работы – исследование механизмов нелинейного формирования широкополосного импульсного спектра в условиях перегрузки в сверхширокополосных (СШП) усилительных цепях для решения задач радиовизионного распознавания жестов. Актуальность исследования обусловлена необходимостью повышения точности и помехоустойчивости современных радиовизионных СШП-систем для жестикулярных интерфейсов управления.

Методы. Использованы методы статистической радиофизики, частотно-временные методы вейвлет-преобразования радиоизображений, методы теории S-параметрического векторного анализа схем, методы программно-численного моделирования.

Результаты. Представлен метод генерации СШП-сигналов в сверхвысокочастотном диапазоне, основанный на управляемых нелинейных искажениях сигнала. Показано, что при переводе усилителя в режим насыщения формируется сигнал с резкими фронтами, обладающий широким энергетическим спектром. Построен лабораторный стенд киберфизической интерференционной радиосенсорной системы распознавания жестов и исследованы его характеристики. Исследованы свойства полученных импульсов в задачах радиовизионного управления. Экспериментально показана эффективность предложенного метода для задач радиовизионного распознавания жестов.

Выводы. Предложен метод нелинейной сатурации – синтеза спектра радиовизионных сигналов, основанный на явлениях переходных искажений в СШП-усилителях. Показано, что интерференционный режим при расширении исходной полосы частот до 900 МГц способен обеспечить повторяемость фазовых изображений не менее 0.94. Установлено, что в перегруженном по входу режиме усилителя типа SBB5089Z[2] при задающем низкомодовом гармоническом возбуждении на переходной частоте 47 МГц в каскадной схеме усиления на выходе радиовизионной антенны удается получить сигнал с измененным спектром. При этом управляемое формирование спектра возбуждения антенны для каждого из усилительных модулей определяется уникальной импульсной

[2] Высоколинейный широкополосный монолитный (monolithic microwave integrated circuit – монолитная микроволновая интегральная схема) усилитель, разработанный компанией Qorvo, США. [High-linearity wideband, monolithic microwave integrated circuit (MMIC) amplifier was developed by Qorvo, USA.]

характеристикой интегрального СШП-усилителя. Это позволило успешно применить такие усилители при решении задач радиовизионного распознавания жестов. Предложенная методика позволяет использовать стандартные СШП-усилители для создания компактных источников СШП-сигналов без усложнения схемотехники.

Ключевые слова: радиовизионный сигнал, сатурация спектра, переходные искажения, сверхширокополосный усилитель, идентификация жестов, киберфизический стенд

Для цитирования: Латышев К.В., Костин М.С., Бойков К.А. Формирование радиовизионных сигналов спектральной сатурацией в режиме переходных искажений интегральных сверхвысокочастотных усилителей для систем распознавания жестов. *Russian Technological Journal*. 2026;14(2):57–68. https://doi.org/10.32362/2500-316X-2026-14-2-57-68, https://www.elibrary.ru/XPSWYV

Прозрачность финансовой деятельности: Авторы не имеют финансовой заинтересованности в представленных материалах или методах.

Авторы заявляют об отсутствии конфликта интересов.

INTRODUCTION

Radio sensor systems for close-range cyber-physical monitoring are used to dynamically identify human gestures in areas such as smart medicine, industrial automation and virtual/augmented reality. The high level of reliability and resolution requirements necessitate new methods of forming and processing radio signals [1, 2], making this research highly relevant.

The paper offers a novel approach to the spectral synthesis of such systems. Rather than using traditional high-voltage shapers, it employs an ultra-wideband (UWB) amplifier which operates in deliberate overload mode. In this mode, the amplifier acts as a nonlinear synthesizer, using transient nonlinear distortions (usually considered an undesirable effect) to expand the signal spectrum (spectral saturation). The novelty of this research lies in the deliberate use of these nonlinear effects for controlled spectrum expansion.

The saturation mechanism is due to the amplifier output transistors operating in saturation mode. In this case, the input signal is converted into an almost rectangular pulse shape with very sharp edges. This ensures the synthesis of a wideband spectrum, used in UWB systems [3, 4]. Spectrum expansion increases the resolution of the radio sensor system and improves its resistance to narrowband interference and the accuracy of temporal and spatial gesture localization.

This paper presents theoretical, modeling, and experimental studies of this method of nonlinear spectrum transformation for gesture recognition using radiovision techniques.

2. MODEL OF WIDEBAND SPECTRUM SYNTHESIS OF RADIOVISION SIGNALS BASED ON THE OCCURRENCE OF TRANSITIONAL DISTORTIONS IN UWB AMPLIFIER

The nonlinear formation of the radiovision signal spectrum occurs when UWB amplifier stages operate in overload mode due to transient distortions. These distortions are analytically described in [5] when the equivalent circuit of an UWB stage with inductive correction is analyzed (Fig. 1).

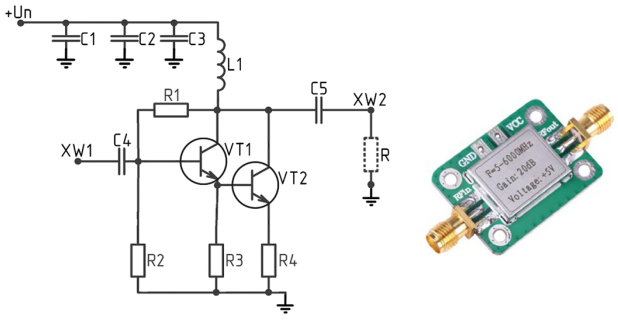

(a) (b)

Fig. 1. SBB5089Z UWB amplifier[3] with inductive correction: (a) schematic diagram; (b) external appearance. The symbols used to denote the circuit elements correspond to those used in GOST 2.710-81[4]

The paper describes the use of a monolithic SBB5089Z-type UWB amplifier, based on InGaP HBT[5] transistors. It uses a Darlington configuration with an active bias circuit.

When the input low-mode signal is formed, the UWB amplifier operates in deliberate overload mode. The L1 inductor with inductance L in the output circuit prevents a rapid increase in current through the load resistor R, equivalent to the input resistance R of the subsequent cascade. This results in a temporary accumulation of energy in the parasitic capacitances of the cascade (the equivalent capacitance C), and the capacitance of the printed circuit board. This slows down transient processes in the initial phase of the signal. As energy accumulates in the L1 inductor, the equivalent capacitance C charges to a voltage level which exceeds

[3] High-linearity wideband, monolithic microwave integrated circuit (MMIC) amplifier was developed by Qorvo, USA.

[4] GOST 2.710-81. Interstate Standard. *Unified system for design documentation. Alpha-numerical designations in electrical diagrams*. Moscow: Izd. Standartov; 1985 (in Russ.).

[5] InGaP is indium gallium phosphide and HBT is a heterojunction bipolar transistor.

the opening threshold of the VT1–VT2 composite transistor cascade. Consequently, the transistors abruptly switch to saturation mode, forming a pulse with steep fronts and a wide spectrum. This is a necessary condition for generating UWB signals.

The signal gain coefficient can be represented in operator form as follows [5]:

$$K(p) = S\frac{(pL+R)\frac{1}{pC}}{pL+R+\frac{1}{pC}} = S\frac{pL+R}{1+pRC+p^2LC},$$

wherein p is the Laplace operator and S is the steepness of the composite Darlington transistor cascade.

Let $K_0 = SR$ be the gain at low frequencies. The time constant of the equivalent circuit is $\tau_{bas} = RC$, and $m = L/CR^2 = (L/R)/CR$ is the correction parameter. Then,

$$\frac{K(p)}{K_0} = \frac{1+p\tau_{bas}m}{1+p\tau_{bas}+p^2m\tau_{bas}^2} = \\ = \frac{1}{\tau_{bas}}\cdot\frac{p+\frac{1}{m\tau_{bas}}}{p^2+\frac{1}{m\tau_{bas}}p+\frac{1}{m\tau_{bas}^2}}.$$

Therefore, the operational signal at the output of the UWB cascade with inductive correction in input overload mode can be represented as follows [5]:

$$\frac{U(p)}{K_0} = \frac{1}{\tau_{bas}}\cdot\frac{p+\frac{1}{m\tau_{bas}}}{p\left(p^2+\frac{1}{m\tau_{bas}}p+\frac{1}{m\tau_{bas}^2}\right)}.$$

The behavior of the transient process is determined by the roots of the characteristic equation of the system, which are calculated using the following formula [5]:

$$p_{1,2} = -\frac{1}{2m\tau_{bas}} \pm \frac{1}{2m\tau_{bas}}\sqrt{4m-1}.$$

When $m > 0.25$, corresponding to the condition for transient oscillations forming with discharge in the transition frequency range when the VT1–VT2 composite cascade is opened instantly, as shown in Fig. 2a, the normalized transfer function of the UWB amplifier is as follows [5]:

$$\frac{h(t)}{K_0} = 1-\frac{2m}{\sqrt{4m-1}}e^{-\frac{t}{2m\tau_{bas}}}\sin\left(\frac{\sqrt{4m-1}}{2m\tau_{bas}}t+\theta\right),$$

wherein $\theta = \pi - \arcsin\frac{\sqrt{4m-1}}{2m}$, and t is time.

In this case, the transition process represents damped oscillations with an emission the magnitude of which depends on the correction coefficient m.

When $m = 1$ (Fig. 2b), which is the condition of free oscillations at the output of the UWB amplifier, the expression for the transfer function is as follows [5]:

$$\frac{h(t)}{K_0} = 1-e^{-\frac{t}{2RC}}\left(\cos\left(\frac{\sqrt{3}t}{2RC}\right)+\frac{1}{\sqrt{3}}\sin\left(\frac{\sqrt{3}t}{2RC}\right)\right).$$

Thus, a transition process corresponding to free oscillations is formed within the transition frequency range of the UWB amplifier's transfer characteristic, which can be modeled as a second-order active bandpass filter.

During time ζ, when $f_1 > f_2$, the system completes a cycle of free oscillations (Fig. 2a), resulting in the formation of a damped radio pulse at the output of the UWB amplifier. This pulse is then amplified by an identical cascade. In this case, the radio pulse exhibits exponential attenuation and is formed in accordance with the system's impulse response. The selection of the low-mode excitation frequency f_1, which corresponds to the transition frequency range, is determined by the conditions necessary to achieve the correction parameter $m = 1$. The frequency f_2 corresponds to linear signal amplification.

It should be noted that overload of the UWB amplifier input at a certain frequency may satisfy the Barkhausen self-excitation condition [6]:

$$|A\beta| \geq 1 \text{ and } \angle A\beta = 2\pi n,\ n \in \mathbb{Z}, \quad (1)$$

wherein A is the gain coefficient, β is the feedback transfer coefficient, $\angle A\beta$ is the phase shift between the input and output through the feedback circuit, and $\mathbb{Z}$ is a set of integers.

Thus, for self-oscillation to occur, the gain must compensate for losses in the feedback circuit and the total phase shift in the circuit must be a multiple of 2π [6].

Let the UWB amplifier have a complex transfer function f, defined as

$$A(f) = \frac{A_0}{1+j\frac{f}{f_c}}, \quad (2)$$

wherein A_0 is the gain at low frequencies, ($f \ll f_c$), f_c is the amplifier cutoff bandwidth, and the following complex feedback function:

$$B(f) = \frac{1}{1+j\frac{f}{f_{band}}}, \quad (3)$$

wherein f_{band} is the feedback circuit band [7].

Taking into account (2) and (3), the loop gain is then:

$$T(f) = A(f)B(f) = \frac{A_0}{\left(1+j\frac{f}{f_c}\right)\left(1+j\frac{f}{f_{band}}\right)}. \quad (4)$$

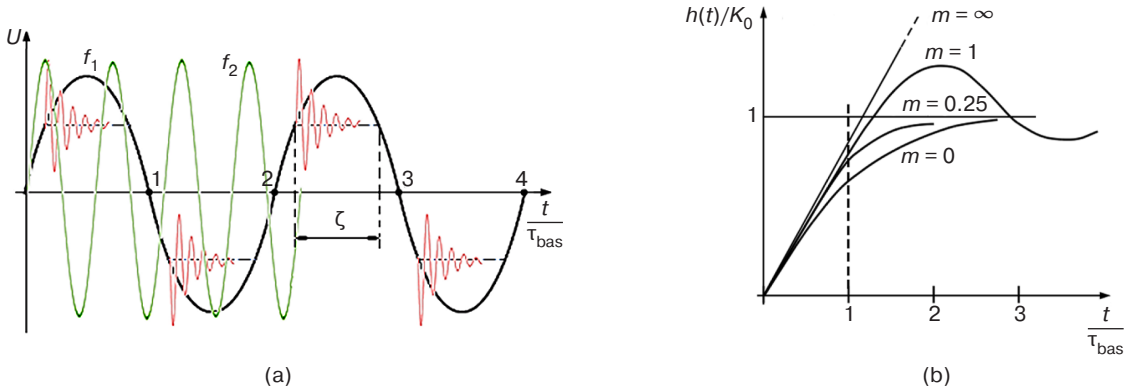

(a) (b)

Fig. 2. Transient distortions at the output of the UWB amplifier:
(a) signal distortions in overload mode within the transition frequency range (normalized values on the X and Y axes);
(b) transfer function of the UWB amplifier for various correction parameter values, *m*

In nonlinear systems, the gain of an amplifier operating in limiting mode is a function of the input signal amplitude V:

$$A(V) = \begin{cases} A_{\text{lin}}, V < V_{\text{sat}}, \\ \dfrac{V_{\text{sat}}}{V}, V \geq V_{\text{sat}}, \end{cases} \quad (5)$$

wherein A_{lin} is the linear value of the gain coefficient and V_{sat} is the amplifier's saturation voltage [8, 9].

The gain declines as $\frac{1}{V}$, when $V > V_{\text{sat}}$. If the feedback circuit transfer coefficient is frequency-dependent, then considering (1) and (3) gives us:

$$|T(f, V)| = |A(f, V)| \cdot B(f) \geq 1. \quad (6)$$

According to Barkhausen's criterion (6), the condition for amplifier self-excitation can only be fulfilled at certain frequencies where the feedback circuit transfer coefficient $B(f)$ reaches significant values. This is possible in the presence of frequency resonance, caused by the corrective (parasitic) inductances and capacitances of the circuit. The physical principle behind this phenomenon is as follows: when an UWB amplifier is operating in a nonlinear signal-limiting (saturation) mode, the output voltage waveform is significantly distorted. It is thus converted from a sinusoidal signal to a signal which is close to a rectangular pulse with sharp fronts and tails. These time variations carry a wide range of high-frequency harmonics, as follows from Fourier transform theory. If these harmonics coincide with the resonant frequencies of the corrective (parasitic) LC[6] chains, the corresponding harmonics are amplified due to an increase in the transmission coefficient $B(f)$. Consequently, the system switches to wideband signal generation mode. In the time domain, this is a damped oscillatory pulse close in shape to a Gaussian monocycle. In the frequency domain, it has a wide energy spectrum band which covers a range of up to hundreds of megahertz [8, 10–12].

Let us consider the process of exciting a radiovision antenna with a synthesized radio pulse. The electric component of the radiovision signal field ($E(t)$) at the output of the UWB antenna is known to be proportional to the derivative of the excitation signal current function:

$$E(t) \approx \frac{dI_{\text{вых}}(t)}{dt} h_A(t),$$

wherein $I_{\text{out}}(t)$ is the excitation radio pulse current formed at the output of the UWB amplifier cascades with a certain pulse characteristic, $h_A(t)$ [13].

In order to create a numerical model of the synthesis of radiovision signals based on cascades of UWB amplifiers, experimental measurements of *S*-parameters were performed on a sample of three randomly selected SBB5089Z UWB amplifiers. The *S*-parameters of the UWB amplifier line were recorded using an R&S ZNLE[7] vector network analyzer in the 0.01–5 GHz frequency band (Table 1).

Table 1. Radio technical characteristics of UWB amplifiers

Parameter	SBB5089Z	TQP7M9103[8]	WYDZ[9]
Gain, dB	20–30	30	60
Passband, MHz	50–6000	10–3000	1–2000
Noise level, dB	3.5	4	6–8
Maximum output power, dBm	23	20	15
Maximum input power, dBm	15	10	5

[6] An electrical circuit consisting of an inductor (L) and a capacitor (C) connected together.

[7] R&S ZNLE is a vector network analyzer manufactured by Rohde & Schwarz, Germany. It is designed for testing high-frequency electronic components such as filters, amplifiers, cables, and antennas.

[8] TQP7M9103 is a high-power signal amplifier manufactured by Qorvo, USA.

[9] WYDZ is a low-noise amplifier manufactured by TZT, China.

Based on the vector measurement results shown in Fig. 3, the S_{21} transfer characteristics were converted into vector arrays for the interpretation of UWB amplifiers during the software-numerical simulation of a radiovision signal generator in the *MATLAB Simulink*[10] environment (Fig. 4).

The synthesized excitation spectrum generator circuit of the UWB antenna consists of the following functional blocks: *1* is a low-mode signal generator with frequency selection corresponding to $m = 1$; *2* is a radio system input parameters block specified by a special Simscape library which determines the main characteristics of the signal transmitted to the UWB amplification path; *3* is UWB amplifier for forming transient distortions; *4* is an amplifier for further signal transmission (the S_{21} transfer characteristics are loaded from the arrays obtained from the vector measurements); *5* is a radio system output parameters block; *6* is an oscilloscope which records the UWB antenna excitation signal; and *7* is a radio system properties block which defines global simulation parameters such as frequency range, noise, impedance, etc.

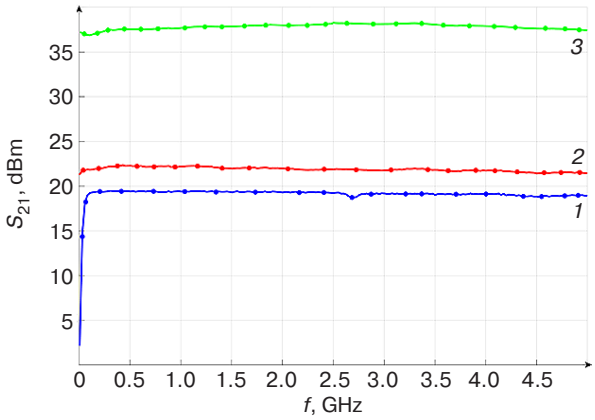

Fig. 3. Transfer characteristics of S_{21} UWB amplifiers: SBB5089Z (*1*), TQP7M9103 (*2*), and WYDZ (*3*)

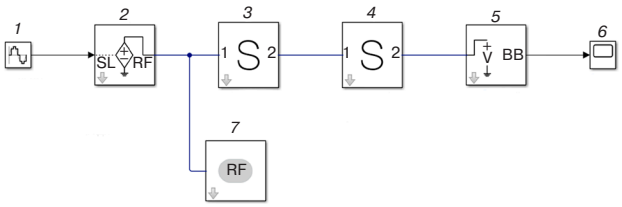

Fig. 4. A model of a nonlinear synthesizer for the radiovision excitation signal spectrum of a UWB antenna. RF stands for radio frequency, SL for *Simulink*, which receives a signal from a standard *Simulink* block, and BB for baseband

The equivalent circuit of a second-order RLC[11] filter (Fig. 5) can be used to represent an amplifying UWB cascade with inductive correction (Fig. 1). When a step input is applied to the circuit (which is equivalent to the sudden opening of a transistor in saturation mode), the transient process is governed entirely by the correction parameter *m*. Therefore, the objective is to select operating conditions for the amplifier such that $m = 1$.

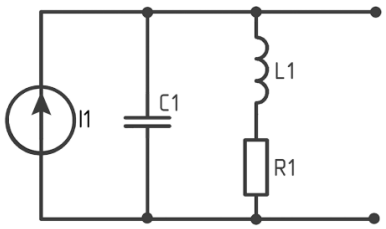

Fig. 5. Equivalent circuit of a second-order RLC filter

The parameters R1, L1, and C1 in the equivalent circuit are not constant values. Rather, they represent the effective parameters of the amplifier which depend on the frequency of the input signal. Consequently, the correction parameter *m* itself is a frequency-dependent function, $m(f)$. The objective is to determine the optimal excitation frequency, f_{opt}, at which $m(f_{opt}) = 1$ is satisfied.

Analysis of the parameters (Fig. 3) of the SBB5089Z amplifier reveals a 40–50 MHz range where the amplitude-frequency characteristic exhibits an anomaly, indicating complex interactions between internal reactive elements. This region corresponds to the zone in which the amplifier is susceptible to oscillatory transient processes. Modeling in *Simulink* (Fig. 4) has shown that excitation at a frequency of 47 MHz and input overload (amplitude 400 mV) results in a mode corresponding to $m = 1$. The simulated pulse signal of the excitation function, characterized by low-mode oscillation, is shown in Fig. 6.

After passing through the amplification path, overload at the input of the first UWB amplifier in transient mode results in a synthesized signal with an extended spectrum at the output of the second UWB amplification cascade. This exhibits nonlinear spectral saturation in the 0–900 MHz band. Considering the impulse response of the Vivaldi-type strip slot UWB antenna used in this study, the *E* radiovision signal spectrum at its output is shown in Fig. 7.

Signal spectrum conversion analysis was performed during simulation in the *MATLAB Simulink* environment. The original harmonic signal with a frequency of 47 MHz has a narrowband spectrum. The effective spectrum width of the initial signal, calculated at −10 dB from

[10] https://www.mathworks.com/products/simulink.html. Accessed February 06, 2026.

[11] An electrical circuit consisting of a resistor (R), an inductor (L) and a capacitor (C).

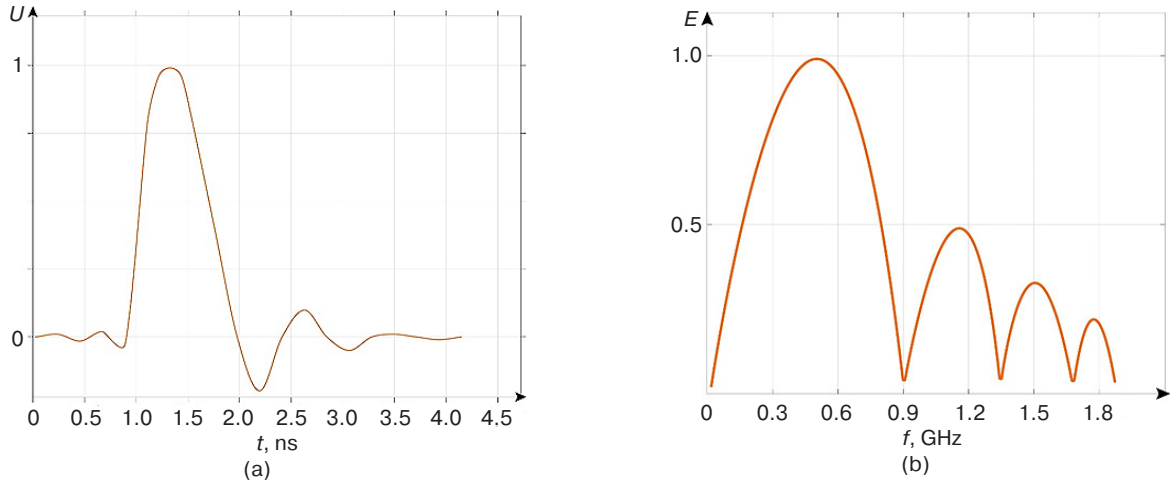

Fig. 6. Pulse excitation signal synthesized by a low-mode oscillation UWB antenna in the overloaded dynamic mode of the SBB5089Z UWB amplifier (normalized values on the vertical axes):
(a) time representation of the radio pulse *U*;
(b) spectrum *E* synthesized from the transient distortions of the radio pulse

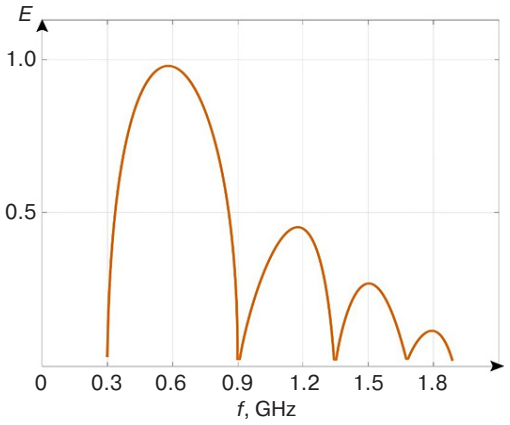

Fig. 7. Spectrum of the radiovision signal at the output of the Vivaldi UWB antenna (normalized values on the *E* axis)

peak power, is ~42.25 MHz. After passing through the proposed amplification system operating in intentional overload and controlled transient distortion mode, the signal undergoes nonlinear spectral transformation. A short radio pulse with steep fronts, characteristic of UWB signals, is formed at the system output. Analysis of the output signal shows that its effective spectral width has expanded to ~900 MHz (also at −10 dB), corresponding to a spectral expansion factor of more than 20.

2. RECOGNITION OF RADIOVISION IMAGES OF GESTURES FORMED IN RESPONSE TO A SYNTHESIZED RADIOVISION SIGNAL

The experimental part of the study aimed to verify the effectiveness of nonlinear formation of the radiovision signal spectrum and to confirm the results of numerical modeling. The effectiveness of identification systems is largely determined by the characteristics of the probing signal, so this approach was chosen. The width of the spectrum and the pulse shape directly affect the resolution, noise immunity, and reliability of feature extraction. The aim of the experiment was to identify four different hand gestures and evaluate the accuracy, stability, and reliability of the recognition system.

In order to conduct experiments based on the model of a nonlinear synthesizer of the radiovision signal excitation spectrum of an SSP antenna (Fig. 4), a cyber-physical stand for identifying hand gestures (Fig. 8) was created. This stand consists of the following blocks:

- R&S SMBV100B[12] vector pulse generator designed to generate the initial harmonic signal. Using the data obtained in the first part of the article, the signal is generated at a frequency of 47 MHz;
- an UWB signal generation block consisting of two low-noise SBB5089Z UWB amplifiers operating in a deliberately overloaded mode (Fig. 3);
- an antenna system comprising a pair of Deepace R101C[13] Vivaldi-type UWB transceiver antennas which emit a probing signal (Fig. 7) and receive the reflected response from the object (hand);
- a received signal amplification unit consisting of two UWB signal amplifiers;

[12] SMBV100B is a high-performance vector signal generator manufactured by Rehde & Schwarz, Germany. It is designed to generate complex and modulated radio frequency (RF) signals for testing and measuring purposes.

[13] Deepace R101C is an ultra-wideband, directional antenna manufactured by Deepace, China. It is used for the reception and transmission of high-frequency signals over a wide range of frequencies.

- data acquisition system consisting of an R&S RTO2032[14] digital oscilloscope to digitize and record the received signals;
- a processing unit consisting of a personal computer with specialized software for processing, analyzing, and visualizing the data received.

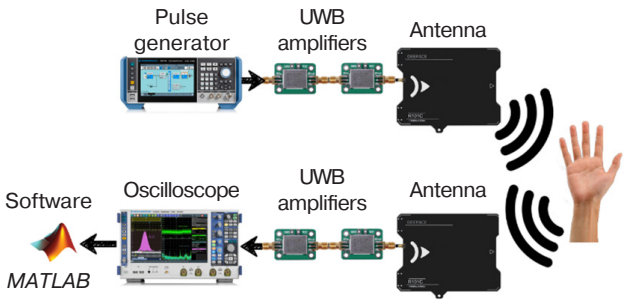

Fig. 8. Cyber-physical stand for identifying hand gestures

The experiment involves the following gestures: rotating the wrist (rotation), pushing the wrist away from the chest (pushing), swiping from right to left (swiping), and clenching the fist (clenching), as shown in Fig. 9. These movements cover a wide range of characteristics of gesture kinematics, providing variety in terms of direction and type of movement [14–16]. They are simple and easy for humans to understand, and are widely used in everyday life for controlling digital devices [17]. The choice of gestures is also dictated by their functional significance in interfaces (Table 2).

Each gesture is represented by a set of ten control frames, combined into a single final radio image or "reference radio portrait" which uniquely identifies the gesture in question (Fig. 10). During the experiment, correlation coefficients are calculated to analyze the linear relationship between the selected gestures. The results of the experiment demonstrate the high level of accuracy of the identification system in recognizing repeated gestures, as indicated by intra-group correlation values close to 1. The coefficients are 0.95 for hand rotation, 0.99 for repulsion, 0.96 for fist clenching, and 0.97 for swiping (Table 3). These results confirm the stability of the system in recognizing the same movements.

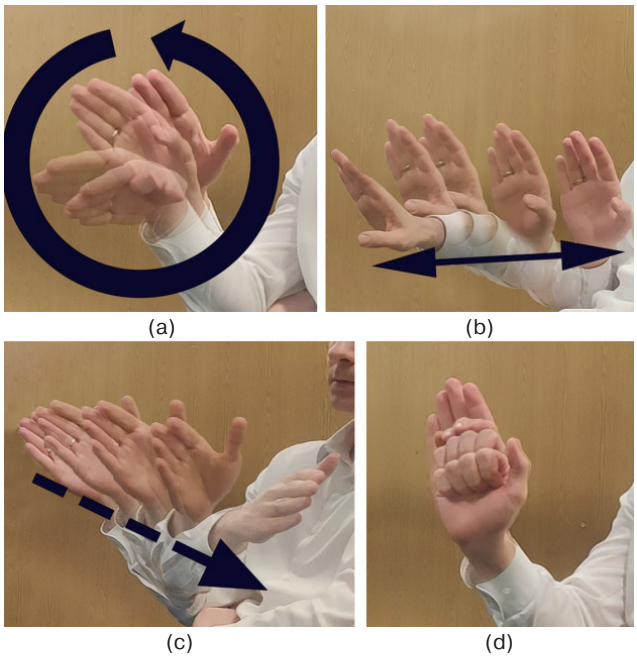

Fig. 9. Gestures used in the experiment: (a) rotation; (b) pushing; (c) swiping; (d) clenching

Table 2. Gesture characteristics

Characteristics / Gesture	Type of movement	Amplitude, cm	Gesture duration, s	Kinematic characteristics	Functionality in the interface
Rotation	Continuous and periodic	<15	0.4	Changing the angle of the hand in relation to the signal direction	Managing settings, scrolling settings
Pushing	Forward	>30	0.8	Movement from the center of the body	Cancel/Dismiss
Swiping	Horizontal	15–30	0.6	Clearly defined direction	Navigating the interface
Clenching	Static	<5	0.3	Altering the hand shape without significantly moving it	Confirming or activating commands

[14] R&S RTO2032 is a digital oscilloscope designed for analyzing complex signals in a variety of fields. It is manufactured by Rehde & Schwarz, Germany.

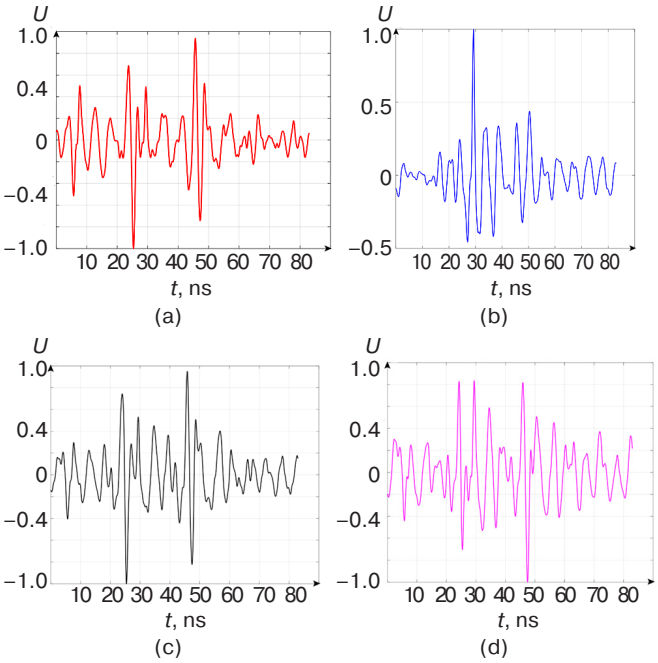

Fig. 10. Representation of reference radio gesture images (normalized values along the vertical axis): (a) rotation, (b) pushing, (c) clenching, and (d) swiping

Certain pairs of gestures exhibit a strong correlation, for instance, clenching a fist and swiping, with a value of 0.84. This suggests a similarity in the signs utilized by the system for their recognition. Conversely, rotation and swiping exhibit an average correlation of 0.62 which could be attributed to the shared elements of hand movement. Furthermore, a moderate relationship exists between pushing and swiping, with a score of 0.65. This can be explained by the directional aspect inherent to both motions.

A low correlation is observed between rotation and pushing (0.30), as well as between pushing and clenching (0.48). These motions have significantly different kinetic characteristics, indicating that they can be easily distinguished by the system.

Based on the findings, it can be inferred that the system successfully recognizes the selected gestures with a high level of accuracy and reliability. This is attributed to the consistent and reproducible UWB pulse waveform obtained when the SBB5089Z amplifier is activated.

The experiment also studied the response of the gesture recognition system to erroneous or missing control frames of a gesture. In order to evaluate the system's tolerance for error, the number of distorted or skipped frames was consistently increased from one to nine. The findings indicate that different gestures exhibit varying degrees of resilience to incorrect (missing) frames (Fig. 11). Specifically, the push-off gesture demonstrated the greatest stability, whereas the swipe gesture exhibited the least. These results suggest that successful gesture recognition necessitates a different number of control frames for each gesture.

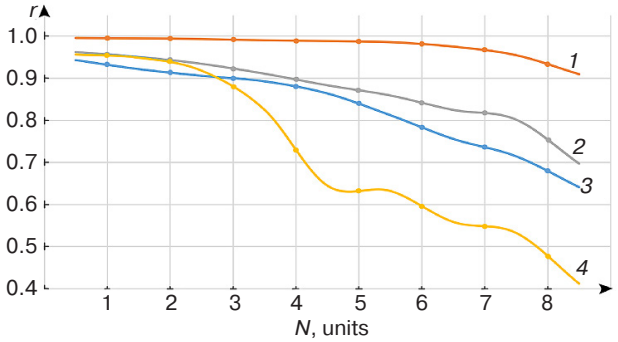

Fig. 11. Impact of the number *N* of incorrect gesture frames on the correlation coefficient *r* with the reference image: *1* is pushing; *2* is clenching, *3* is rotation; and *4* is swiping

The experiment demonstrates that the recognition system achieves a correlation coefficient of over 0.95 for gesture recognition. However, its resistance to false negatives (missed frames) varies depending on the specific gesture. Repulsion and compression gestures

Table 3. Average correlation coefficient between reference radio portraits and performed gestures

Gesture \ Reference radio portrait	Rotation	Pushing	Clenching	Swiping
Rotation	**0.95**	0.30	0.82	0.62
Pushing	0.30	**0.99**	0.48	0.65
Clenching	0.82	0.48	**0.96**	0.84
Swiping	0.62	0.65	0.84	**0.97**

Table 4. Evaluation of experiment repeatability

Gesture	Number of gestures performed	Number of correctly recognized gestures	Repeatability
Rotation	100	95	0.95
Pushing		98	0.98
Swiping		96	0.96
Clenching		94	0.94

are more robust, achieving a correlation coefficient of over 0.90 with up to four missed frames. These gestures are therefore suitable for use in challenging conditions where data may be incomplete or distorted due to interference or reduced recording quality. In contrast, swiping with a brush requires more stringent quality control, since it relies on the accuracy of the entire image sequence.

The results highlight the need to analyze each gesture in detail when developing recognition systems. Gestures which are highly sensitive to distortion, such as swiping, may require additional optimization of data processing algorithms or the incorporation of error compensation mechanisms. This would improve the reliability of the system in real-world environments, where data loss or partial corruption is inevitable.

An experiment was also conducted to assess the repeatability of gesture identification. Each gesture was repeated 100 times and the identification results were analyzed (Table 4).

Based on the results, it can be inferred that the recognition accuracy has consistently exceeded 0.94. Considering this level, the experiment can be regarded as reliable. The impact of random factors is negligible and the findings can be confidently applied in practice.

CONCLUSIONS

1. The S-parameters of three UWB radio-frequency amplifiers were determined and analyzed. As a result, it was found that the SBB5089Z UWB has the ability to control signal distortion within the range of 40–50 MHz, in order to expand the output spectrum. The correction parameter was determined to be 1 at 47 MHz.
2. A method for the nonlinear synthesis of a radio imaging signal spectrum was proposed, enabling a spectrum expansion coefficient value of over 20 to be achieved.
3. The proposed gesture recognition system based on the proposed method demonstrated a high level of accuracy. The correlation coefficients between the recognized gestures and their corresponding fiducial gestures are 0.99 for the repulsive gesture, 0.95 for the rotation gesture, 0.96 for the scrolling gesture, and 0.96 for the compression gesture.
4. Particular attention was paid to system resilience to erroneous or missing frames influencing the gesture recognition process. System response to partial data loss within each gesture was also investigated. The findings show that all gestures can be recognized with a correlation coefficient of over 0.9.
5. The repeatability of gesture recognition is at least 0.94.

Authors' contributions

K.V. Latyshev—developing the software-numerical model and laboratory stand of a cyber-physical monitoring system for radio-frequency identification of human gestures.

M.S. Kostin, K.A. Boikov—developing the nonlinear synthesized spectrum of a radiovision signal under overloaded ultra-wideband amplification mode.

REFERENCES

1. Khan I., Kwon Y. Radar-based Hand Gesture Recognition with Feature Fusion using Robust CNN-LSTM and Attention Architecture. *IEEE Access*. 2025;13:69281–69291. https://doi.org/10.1109/ACCESS.2025.3558293
2. Kostin M.S., Boikov K.A. Digital technologies for signal radio vision and radio monitoring. *Russian Technological Journal*. 2024;12(4):59–69. https://doi.org/10.32362/2500-316X-2024-12-4-59-69
3. Wu M. Gesture Recognition Based on Deep Learning: A Review. *EAI Endorsed Transactions on e-Learning*. 2024;10. https://doi.org/10.4108/eetel.5191
4. Qu C., Zhang Y., Jin L., et al. Exploring hand gesture recognition using micro-Doppler radar data based on vision transformers. *J. Phys.: Conf Ser*. 2023;2504:012046. https://doi.org/10.1088/1742-6596/2504/1/012046

5. Sedra A., Smith K., Carusone T., Gaudet V. *Microelectronic Circuits* (*The Oxford Series in Electrical and Computer Engineering*). 8th ed. Oxford University Press; 2020. P. 58–134, 174–246, 508–696.
6. He F., Ribas R., Lahuec C., Jézéquel M. Discussion on the general oscillation startup condition and the Barkhausen criterion. *Analog Integr. Circ. Signal Process*. 2009;59:215–221. https://doi.org/10.1007/S10470-008-9250-1
7. Razavi B. *RF Microelectronics* (*Prentice Hall Communications Engineering and Emerging Technologies Series*). 2nd ed. Prentice Hall Press; 2011. P. 255–333, 751–831.
8. Wang Y., Lang L., Lee C.H., Zhang B., Chong Y. Topologically enhanced harmonic generation in a nonlinear transmission line metamaterial. *Nat. Commun*. 2019;10:Article number:1102. https://doi.org/10.1038/s41467-019-08966-9
9. Guarcello C., Ahrens F., Avallone G., et al. Nonlinear Behavior of Josephson Traveling Wave Parametric Amplifiers. *IEEE Transactions on Applied Superconductivity*. 2024;34(3):1–5. https://doi.org/10.1109/TASC.2024.3367615
10. Hong M., Chang Y.H., Dienes A., Delfyett P., Dijaili S., Patterson F. Femtosecond self- and cross-phase modulation in semiconductor laser amplifiers. *IEEE Journal of Selected Topics in Quantum Electronics*. 1996;2(3):523–539. https://doi.org/10.1109/2944.571753
11. Hussain S., Siddiqui H., Saleem A., et al. Therapeutic Exercise Recognition Using a Single UWB Radar with AI-Driven Feature Fusion and ML Techniques in a Real Environment. *Sensors*. 2024;24(17):5533. https://doi.org/10.3390/s24175533
12. Oppermann I., Hämäläinen M., Iinatti J. *UWB Theory and Applications*. John Wiley & Sons; 2004, 248 p.
13. Taylor J.D. (Ed.). *Advanced Ultrawideband Radar. Signals, Targets, and Applications.* CRC Press; 2016, 494 p.
14. Bulygin D.A., Mamonova T.E. Recognition of hand gestures in real time. *Sistemy analiza i obrabotki dannykh = Analysis and Data Processing Systems.* 2020;78(1):25–40 (in Russ.). https://doi.org/10.17212/1814-1196-2020-1-25-40
15. Shadinov S.S. Spatial ultra-wideband visualization of probed near-field surveillance objects. *Zhurnal Radioelektroniki = J. Radio Electronics*. 2020;7 (in Russ.). https://doi.org/10.30898/1684-1719.2020.7.8. Available from URL: http://jre.cplire.ru/jre/jul20/8/text.pdf. Accessed May 02, 2026.
16. Wang X., Dinh A., Teng D. Radar Sensing Using Ultra Wideband – Design and Implementation. In: Matin M.A. (Ed.). *Ultra Wideband – Current Status and Future Trends*. 2013;11:41–63. https://doi.org/10.5772/48587
17. Latyshev K.V. Cyberphysical radio-gestural FPV control drones. In: *Actual Problems and Prospects of Development of Radio Engineering and Information Communication systems* (*Radioinfocom – 2024*): *Proceedings of the 8th International Scientific and Practical Conference*. Moscow: RTU MIREA; 2024. P. 441–445 (in Russ.). https://www.elibrary.ru/dukcnp

СПИСОК ЛИТЕРАТУРЫ

1. Khan I., Kwon Y. Radar-based Hand Gesture Recognition with Feature Fusion using Robust CNN-LSTM and Attention Architecture. *IEEE Access*. 2025;13:69281–69291. https://doi.org/10.1109/ACCESS.2025.3558293
2. Костин М.С., Бойков К.А. Цифровые технологии сигнального радиовидения и радиомониторинга. *Russian Technological Journal*. 2024;12(4):59–69. https://doi.org/10.32362/2500-316X-2024-12-4-59-69
3. Wu M. Gesture Recognition Based on Deep Learning: A Review. *EAI Endorsed Transactions on e-Learning*. 2024;10. https://doi.org/10.4108/eetel.5191
4. Qu C., Zhang Y., Jin L., et al. Exploring hand gesture recognition using micro-Doppler radar data based on vision transformers. *J. Phys.: Conf Ser*. 2023;2504:012046. https://doi.org/10.1088/1742-6596/2504/1/012046
5. Sedra A., Smith K., Carusone T., Gaudet V. *Microelectronic Circuits* (*The Oxford Series in Electrical and Computer Engineering*). 8th ed. Oxford University Press; 2020. P. 58–134, 174–246, 508–696.
6. He F., Ribas R., Lahuec C., Jézéquel M. Discussion on the general oscillation startup condition and the Barkhausen criterion. *Analog Integr. Circ. Signal Process*. 2009;59:215–221. https://doi.org/10.1007/S10470-008-9250-1
7. Razavi B. *RF Microelectronics* (*Prentice Hall Communications Engineering and Emerging Technologies Series*). 2nd ed. Prentice Hall Press; 2011. P. 255–333, 751–831.
8. Wang Y., Lang L., Lee C.H., Zhang B., Chong Y. Topologically enhanced harmonic generation in a nonlinear transmission line metamaterial. *Nat. Commun*. 2019;10:Article number:1102. https://doi.org/10.1038/s41467-019-08966-9
9. Guarcello C., Ahrens F., Avallone G., et al. Nonlinear Behavior of Josephson Traveling Wave Parametric Amplifiers. *IEEE Transactions on Applied Superconductivity*. 2024;34(3):1–5. https://doi.org/10.1109/TASC.2024.3367615
10. Hong M., Chang Y.H., Dienes A., Delfyett P., Dijaili S., Patterson F. Femtosecond self- and cross-phase modulation in semiconductor laser amplifiers. *IEEE Journal of Selected Topics in Quantum Electronics*. 1996;2(3):523–539. https://doi.org/10.1109/2944.571753
11. Hussain S., Siddiqui H., Saleem A., et al. Therapeutic Exercise Recognition Using a Single UWB Radar with AI-Driven Feature Fusion and ML Techniques in a Real Environment. *Sensors*. 2024;24(17):5533. https://doi.org/10.3390/s24175533
12. Oppermann I., Hämäläinen M., Iinatti J. *UWB Theory and Applications*. John Wiley & Sons; 2004, 248 p.
13. Taylor J.D. (Ed.). *Advanced Ultrawideband Radar. Signals, Targets, and Applications.* CRC Press; 2016, 494 p.
14. Булыгин Д.А., Мамонова Т.Е. Распознавание жестов рук в режиме реального времени. *Системы анализа и обработки данных.* 2020;78(1):25–40. https://doi.org/10.17212/1814-1196-2020-1-25-40
15. Шадинов С.С. Пространственная сверхширокополосная визуализация зондируемых объектов ближнего радионаблюдения. *Журнал радиоэлектроники*. 2020;7. https://doi.org/10.30898/1684-1719.2020.7.8. URL: http://jre.cplire.ru/jre/jul20/8/text.pdf. Дата обращения 05.02.2026.
16. Wang X., Dinh A., Teng D. Radar Sensing Using Ultra Wideband – Design and Implementation. In: Matin M.A. (Ed.). *Ultra Wideband – Current Status and Future Trends*. 2013;11:41–63. https://doi.org/10.5772/48587

17. Латышев К.В. Киберфизическое радиожестикуляционное FPV-управление дронами. В сб.: *Актуальные проблемы и перспективы развития радиотехнических и инфокоммуникационных систем* («*Радиоинфоком – 2024*»): *Сборник научных статей по материалам VIII Международной научно-практической конференции.* М.: РТУ МИРЭА; 2024. С. 441–445. https://www.elibrary.ru/dukcnp

About the Authors

Kirill V. Latyshev, Senior Lecturer, Department of Radio Wave Processes and Technologies, Institute of Radio Electronics and Informatics, MIREA – Russian Technological University (78, Vernadskogo pr., Moscow, 119454 Russia). E-mail: latyshev@mirea.ru. RSCI SPIN-code 7415-5362, https://orcid.org/0009-0007-4393-6887

Mihail S. Kostin, Dr. Sci. (Eng.), Associate Professor, Head of the Department of Radio Wave Processes and Technologies, Deputy Director, Institute of Radio Electronics and Informatics, MIREA – Russian Technological University (78, Vernadskogo pr., Moscow, 119454 Russia). E-mail: kostin_m@mirea.ru. Scopus Author ID 57208434671, RSCI SPIN-code 5819-2178, http://orcid.org/0000-0002-5232-5478

Konstantin A. Boikov, Dr. Sci. (Eng.), Professor, Department of Radio Wave Processes and Technologies, Institute of Radio Electronics and Informatics, MIREA – Russian Technological University (78, Vernadskogo pr., Moscow, 119454 Russia). E-mail: boykov@mirea.ru. Scopus Author ID 57208926258, RSCI SPIN-code 2014-6951, http://orcid.org/0000-0003-0213-7337

Об авторах

Латышев Кирилл Валерьевич, старший преподаватель, кафедра радиоволновых процессов и технологий, Институт радиоэлектроники и информатики, ФГБОУ ВО «МИРЭА – Российский технологический университет» (119454, Россия, Москва, пр-т Вернадского, д. 78). E-mail: latyshev@mirea.ru. SPIN-код РИНЦ 7415-5362, https://orcid.org/0009-0007-4393-6887

Костин Михаил Сергеевич, д.т.н., доцент, заведующий кафедрой радиоволновых процессов и технологий, заместитель директора Института радиоэлектроники и информатики, ФГБОУ ВО «МИРЭА – Российский технологический университет» (119454, Россия, Москва, пр-т Вернадского, д. 78). E-mail: kostin_m@mirea.ru. Scopus Author ID 57208434671, SPIN-код РИНЦ 5819-2178, http://orcid.org/0000-0002-5232-5478

Бойков Константин Анатольевич, д.т.н., профессор, кафедра радиоволновых процессов и технологий, Институт радиоэлектроники и информатики ФГБОУ ВО «МИРЭА – Российский технологический университет» (119454, Россия, Москва, пр-т Вернадского, д. 78). E-mail: boykov@mirea.ru. Scopus Author ID 57208926258, SPIN-код РИНЦ 2014-6951, http://orcid.org/0000-0003-0213-7337

Translated from Russian into English by Kirill V. Nazarov
Edited for English language and spelling by Dr. David Mossop

Micro- and nanoelectronics. Condensed matter physics

Микро- и наноэлектроника. Физика конденсированного состояния

UDC 67.02
https://doi.org/10.32362/2500-316X-2026-14-2-69-79
EDN HEGGBA

RESEARCH ARTICLE

Search of technological solutions aimed at reducing the number of image defects in a hybrid SWIR device

Artyom A. Egorenkov [@], Irina V. Danilova, Maria I. Bibinova, Sergei N. Chelyshkov, Alexei N. Vyaznikov, Konstantin S. Batalov

NRI Electron, Saint Petersburg, 194223 Russia
[@] Corresponding author, e-mail: a.egorenkov@niielectron.ru

• **Submitted:** 11.08.2025 • **Revised:** 24.10.2025 • **Accepted:** 04.02.2026

Abstract

Objectives. The primary aim of this study is to minimize image defects in a hybrid photodetector with a sensitivity range of 0.95–1.65 μm, based on an InP/InGaAs photocathode. In order to achieve this, the surface quality of the photocathode must be improved prior to lift-off photolithography. In addition, the photolithographic process must be made highly reproducible.

Methods. In order to achieve this goal, a series of experiments on surface cleaning and improvement of the lift-off photolithography process were conducted. The following surface preparation methods were tested: chemical etching of the InGaAs surface; coating the photocathode surface with a protective photoresist layer before cutting the plate; using various photoresist removal methods (in dimethylformamide and plasma); and mechanical surface cleaning. In order to improve photolithography, experiments were conducted on drying times and photoresist methods, exposure and development modes were varied, and photoresist was replaced.

Results. Samples manufactured using the improved technology demonstrate a more than ninefold reduction in the average percentage of defects on the photocathode surface from 0.317% to 0.035%. Thanks to the improved quality of the photocathode surface, the image in the finished device is more uniform and the number of image defects significantly decreased. The process is highly reproducible.

Conclusions. Improvements in surface preparation technology, coupled with a reduction in the thickness of the photoresist used in lift-off photolithography lead to greater uniformity of images in hybrid devices and fewer defects. The proposed approach can be used for the mass production of high-sensitivity near-infrared hybrid photodetectors, making them competitive with those produced elsewhere.

Keywords: SWIR photodetectors, InP/InGaAs photocathode, surface cleaning of InGaAs, lift-off photolithography

For citation: Egorenkov A.A., Danilova I.V., Bibinova M.I., Chelyshkov S.N., Vyaznikov A.N., Batalov K.S. Search of technological solutions aimed at reducing the number of image defects in a hybrid SWIR device. *Russian Technological Journal.* 2026;14(2):69–79. https://doi.org/10.32362/2500-316X-2026-14-2-69-79, https://www.elibrary.ru/HEGGBA

Financial disclosure: The authors have no financial or proprietary interest in any material or method mentioned.

The authors declare no conflicts of interest.

НАУЧНАЯ СТАТЬЯ

Поиск технологических решений, направленных на снижение количества дефектов изображения в гибридном приборе ближнего инфракрасного диапазона

А.А. Егоренков [@], И.В. Данилова, М.И. Бибинова, С.Н. Челышков, А.Н. Вязников, К.С. Баталов

АО «ЦНИИ «Электрон», Санкт-Петербург, 194223 Россия
[@] Автор для переписки, e-mail: a.egorenkov@niielectron.ru

• **Поступила:** 11.08.2025 • **Доработана:** 24.10.2025 • **Принята к опубликованию:** 04.02.2026

Резюме

Цели. Основная цель работы – уменьшение дефектов изображения, получаемого в гибридном фотоприемнике с диапазоном чувствительности 0.95–1.65 мкм на основе фотокатода из фосфида индия/арсенида галлия-индия (InP/InGaAs). Для этого необходимо улучшить качество поверхности фотокатода перед взрывной фотолитографией, а также обеспечить высокую воспроизводимость фотолитографического процесса.

Методы. Для достижения поставленной цели проведена серия экспериментов по очистке поверхности и по усовершенствованию технологического процесса взрывной фотолитографии. Для подготовки поверхности опробованы следующие методы: химическое травление поверхности InGaAs, покрытие поверхности фотокатода защитным слоем фоторезиста перед резкой пластины, использование различных способов удаления фоторезиста (в диметилформамиде и плазме), внедрение механической очистки поверхности. Для усовершенствования фотолитографии проведены эксперименты со временем и способами сушки фоторезиста, проведено варьирование режимов экспонирования и проявления, заменен фоторезист.

Результаты. Изготовленные по усовершенствованной технологии образцы демонстрируют более чем девятикратное снижение среднего процента дефектов от общей площади поверхности фотокатода по сравнению со старыми образцами: с 0.317% до 0.035%. Благодаря улучшению качества поверхности фотокатода изображение в готовом приборе стало более однородным, количество дефектов изображения значительно уменьшилось. Обеспечена высокая воспроизводимость процесса.

Выводы. Усовершенствованная технология подготовки поверхности, а также уменьшение толщины фоторезиста, используемого во взрывной фотолитографии, привело к увеличению однородности изображения в гибридном приборе, а также к уменьшению дефектов. Предлагаемый подход может быть применен при серийном производстве гибридных высокочувствительных фотоприемников ближнего инфракрасного (ИК) диапазона и позволяет им быть конкурентоспособными с мировыми аналогами.

Ключевые слова: фотоприемники ближнего ИК-диапазона, InP/InGaAs-фотокатод, очистка поверхности InGaAs, взрывная фотолитография

Для цитирования: Егоренков А.А., Данилова И.В., Бибинова М.И., Челышков С.Н., Вязников А.Н., Баталов К.С. Поиск технологических решений, направленных на снижение количества дефектов изображения в гибридном приборе ближнего инфракрасного диапазона. *Russian Technological Journal*. 2026;14(2):69–79. https://doi.org/10.32362/2500-316X-2026-14-2-69-79, https://www.elibrary.ru/HEGGBA

Прозрачность финансовой деятельности: Авторы не имеют финансовой заинтересованности в представленных материалах или методах.

Авторы заявляют об отсутствии конфликта интересов.

INTRODUCTION

One of the popular imaging ranges is the short-wave infrared (SWIR) spectral diapason. Its radiation has properties similar to the radiation of visible range. SWIR is also promising in a variety of applications due to its unique features:

- transparency of some materials in the SWIR diapason[1];
- use of invisible radiation as illumination (nightglow, laser radiation with a wavelength of 1.55 μm, which is safe for human eye) [1];
- ability to distinguish objects with the same color in the visible range [2];
- compared to the visible range, the ability to observe at longer distances and in poor visibility (smog, rain, fog) [3].

Cameras operating in the near-infrared diapason have a wide range of applications both in scientific research, as well as in the civil and military-defense industries. For example, in the electronics industry, they are used for defect identification in printed circuit boards and solar panels[2]. In the food industry, they are used to inspect the quality of products [4]. In the military-defense industry, they are used for reconnaissance and tactical operations to detect camouflaged objects and track them [5]. In medicine, they are used for non-invasive tissue analysis and visualization of subcutaneous tissues [6].

Hybrid photodetectors operating in the SWIR are promising photosensitive devices. They consist of a photocathode and a solid-state electron-sensitive element (anode) in a single vacuum volume (Fig. 1). The photocathode operating in the pass-through mode absorbs photons. Thus electron-hole pairs are generated inside its volume. The electrons then move to the surface, then emit into the vacuum where they are accelerated by the electric field. The electron sensitive anode registers the electron flux, the intensity of which is directly proportional to the intensity of radiation absorbed by the photocathode.

This type of a device operates on the basis of an external photoelectric effect, so there is a need to locate such a system in vacuum conditions. Signal amplification is an advantage over solid-state analogs due to the generation of a large number of electron-hole pairs in the anode volume by accelerated electrons. It is also worth noting that the hybrid devices have a high level of

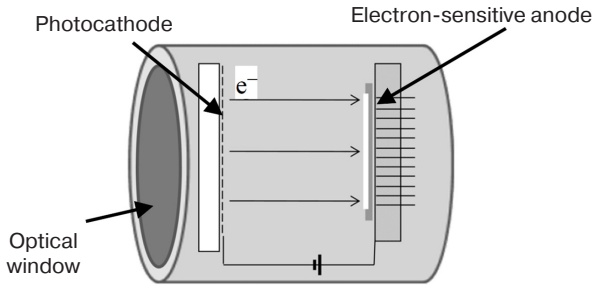

Fig. 1. Diagram of the hybrid photodetector device [7]

variability in the types of possible photocathodes [8–10] and anodes within a single structure.

In this work, InP/InGaAs heterostructure (wavelength range of 0.95–1.65 μm) is used as a photocathode. Aa metal layer (electrode) is deposited on its surface to form a Schottky barrier, in order to transfer the photocharge from the active layer of the photocathode to the emitter layer with a larger band gap. When an external voltage is applied, the barrier between the active and emitter layers decreases, and photoelectrons are able to travel into the emitter and then into vacuum [11, 12]. The surface is activated with a Cs/O layer [13, 14], in order to reduce the work function of electron from the photocathode surface into the vacuum gap.

Lift-off photolithography is used to create a metal electrode. However, the contamination of the surface of the photocathode with small and large particles causes complications during the photolithography process. Large and small particles prevent the creation of a uniform electrode during photolithography. This can lead to image defects in the hybrid photodetector device. These particles are also visible in the final image from the device (Fig. 2).

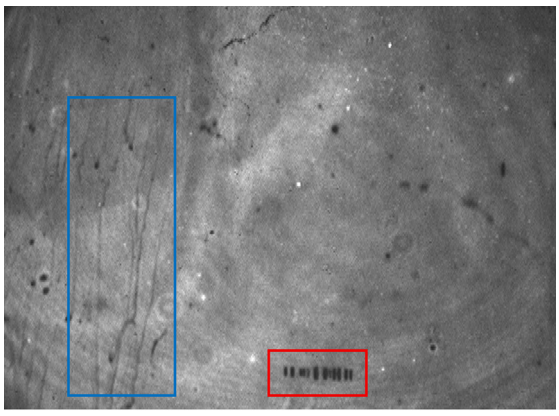

Fig. 2. Image defects caused by surface contamination and inhomogeneity of the electrode

Defects can be observed in the area marked with a red rectangle (Fig. 2) showing the non-uniformity of the electrode. The black rectangular areas are metal residues not removed during lift-off photolithography.

[1] Edmund Optics. What is SWIR? https://www.edmundoptics.com/knowledge-center/application-notes/imaging/what-is-swir/?srsltid=AfmBOopNG8OgK_q1N35-W5tpY9aS7jqGYNeYN3mLq96-xOienoMu9u2T. Accessed June 04, 2025.

[2] HWYL En-Vision Technology. SWIR Cameras: What Are They? [Imaging & Application Guide] https://hwyl.in/swir-cameras/. Accessed June 10, 2025.

Dark lines are visible in the area bounded by the blue rectangle. These are assumed to be traces of a brush used to remove metal residues after photolithography. In [15], the presence of dark dots and lines in images from image intensifier tubes in visible and infrared ranges is associated with the photocathode surface contamination.

NRI "Electron"[3] uses substrates with an InP/InGaAs heterostructure in the production technology of a hybrid SWIR-range photodetector. A single wafer can be used to create photosensitive areas for up to four devices. Due to the fragility of the wafer, it must be cut before the photolithography process. Various small and large particles are adsorbed on the surface during cutting. These particles must be removed because they prevent contact during exposure and therefore increase the percentage of image defects. In addition, for the best operability of photocathodes with negative electron affinity, an atomically clean surface is required [16]. This will ensure the uniformity of Cs/O layer deposition for surface activation [17]. Moreover, the atomically clean surface increases the lifetime of the photocathodes [18].

A suitable cleaning technique must be found to remove contaminations from the surface of the photocathodes, in order to improve the image quality from the hybrid photodetector device. Several cleaning methods are available: chemical cleaning, plasma cleaning, and ion cleaning. Chemical cleaning is the most attractive method due to the low cost and ease of the process. Acidic solutions are widely used for etching of III–V group semiconductors. Among acidic etchants, the hydrochloric acid (HCl) and hydrogen peroxide (H_2O_2) solution (HCl/H_2O_2) is considered one of the most suitable, since it provides the lowest degree of anisotropy during etching [19, 20]. An increase in the H_2O_2 concentration in etchant solutions leads to a significant growth in the etching rate [21]. This is not desirable for our applications, since it can change the thickness of the outer epitaxial layer of the heterostructure. Therefore, low concentrations of H_2O_2 must be used, in order to ensure low etching rates. In [20] a solution of HCl + H_2O_2 + ADS (ammonium dodecyl sulfate) was proposed for the purposes of the more efficient purification of nanoparticles from the InGaAs surface. The addition of ADS reduces the zeta potential of the surface, leading to a decrease in the particle's adsorption [20].

In addition to surface contamination, lift-off lithography was not successful in every experiment (it is not always possible to remove the excess metal layer completely to form the desired pattern). Possible reasons for this may be the use of a positive photoresist which creates an overcut border profile (Fig. 3a). The metal layer deposited on the walls of the photoresist prevents the penetration of the solvent used to remove the photoresist and the metal film. This makes the process of lift-off difficult or impossible. In general, negative photoresists are used in lift-off photolithography which create an undercut border profile (Fig. 3b). They help remove excessive metallization.[4]

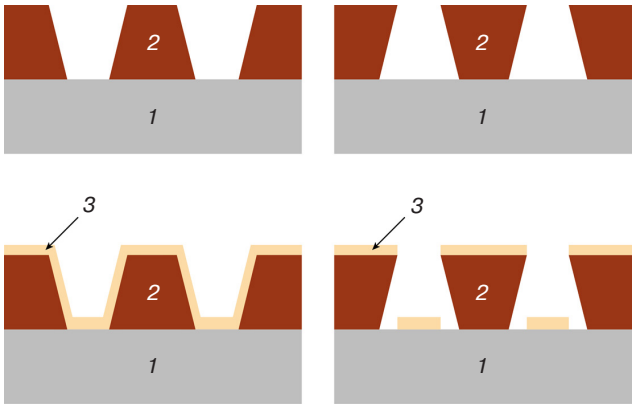

Fig. 3. Schematic diagram of the photoresist walls: (a) overcut border profile, (b) undercut border profile, where *1* is the substrate, *2* is the photoresist, and *3* is the metal

In order to use negative photoresists, the photomask must be modified and the solvents replaced. This requires additional technological development. The study of such technological changes is the subject of future research.

This article presents the results of experiments on surface cleaning after cutting, and selection of the optimal sequence of actions for getting the best cleaning of the photocathode surface. The results of experiments aimed at improving the reproducibility of lift-off photolithography process are also presented. A new photoresist was selected and by means of its use, lift-off occurs on each sample.

1. MATERIALS AND METHODS

Previously, the photocathode surface preparation and subsequent photolithography were performed as follows:

- manual cutting of a two-inch InP/InGaAs photocathode plate into 20 × 22-mm samples;
- cleaning plates in deionized water in the ultrasonic unit UZU-0.25 (Ulyanovsk Instrument Manufacturing Association, USSR) for 5 min;
- during the photolithography process, a positive photoresist FP-9120-1.0 (NIOPIK, Russia) with 1.1–1.3 μm thickness was used;

[3] https://www.niielectron.ru/ (in Russ.). Accessed September 25, 2025.

[4] Image reversal (lift-off) photoresist FPN-20-ISO. https://www.frast.ru/obrashchennaya-vzryvnaya (in Russ.). Accessed September 25, 2025. (In Russ.).

- photolithographic operations (exposure and development) and deposition of the metal layer with subsequent lift-off were carried out on different days.

1.1. Surface preparation before photolithography

Surface cleaning experiments were performed on InP/InGaAs photocathodes, as well as on silicon wafers with a diameter of 3 inches.

A number of experiments were carried out in the technological process of surface preparation, in order to reduce contamination on the photocathode surface:

1) etching of InGaAs surface with H_2O_2 + HCl + ADS solution with 0.001 M hydrogen peroxide, 0.05 M hydrochloric acid and 0.05 mM ADS;
2) automated cutting of photocathode into samples of 20 × 22 mm;
3) coating the photocathode with protective layer of photoresist before cutting;
4) removal of photoresist in dimethylformamide followed by plasma treatment to remove photoresist residues;
5) surface cleaning process: mechanical washing of the surface in deionized water, then cleaning in an ultrasonic bath for 5 min, mechanical washing in deionized water.

1.2. Photolithography process

The following experiments were performed, in order to improve the lift-off photolithography process:

1. Change of the photoresist drying modes: Infrared drying, drying on hot plate at T = 105°C for 1 min, drying in the air forced convection oven at T = 115°C and different exposure times: 3, 5, 10, and 20 s. For certain photocathodes, a method of creation of an undercut border profile was tested. After exposure, the plate was additionally dried: for 1 min on the hot plate for one and for 5 min in the air forced convection oven for another.
2. Change of exposure modes (different exposure duration, different power) and, accordingly, of the development (different developer concentration and development time).
3. Reduction of the time, spent by the sample between the processes of exposure, development, metal deposition and lift-off.
4. Usage of the different positive photoresist with a smaller film thickness: FP-9120-0.4 (NIOPIK, Russia) with thickness of 0.4 μm instead of FP-9120-1.0 with thickness of 1 μm.

1.3. Visualization of experiments

Images of the samples were obtained with MBS-1 (Lytkarinsky Optical Glass Factory, USSR) and NORGAU NVM-2010 (NORGAU, Russia) optical microscopes.

A test bench was used to obtain the image from the device at uniform illumination. The block diagram is shown in Fig. 4.

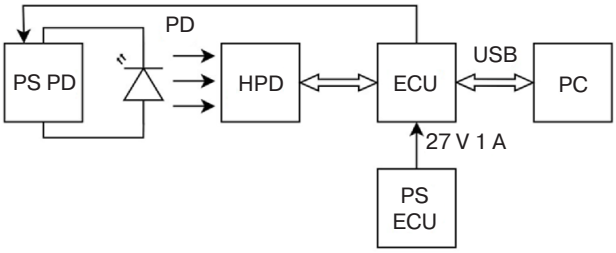

Fig. 4. Block diagram of the test bench for getting an image from the hybrid photodetector, where: PS—Power Supply, PD—Photodiode with a center wavelength sensitivity at 1.55 μm, HPD—Hybrid Photodetector, ECU—Electronic Control Unit, USB—Universal Serial Bus, PC—Personal Computer for image display and control

2. RESULTS

Etching of the InP/InGaAs photocathode (manually cut) surface in the solution of H_2O_2 + HCl + ADS in an ultrasonic unit for 5 min did not show any particular result. The surface was not successfully cleaned from small and large particles. As can be seen in Fig. 5, only certain large particles were removed. It is possible that some may have changed their position on the surface.

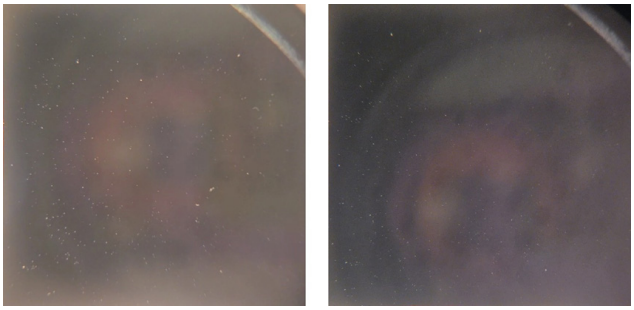

(a) (b)

Fig. 5. InP/InGaAs photocathode surface: (a) before etching in H_2O_2 + HCl + ADS solution, (b) after etching. Field of view area 20 × 22 mm^2

A positive result was obtained when manual cutting was replaced by automated cutting. Automated cutting resulted in a significant reduction in the number of large particles adsorbed on the sample surface. Automated cutting led to a significant reduction in the number of large particles adsorbed on the sample surface (Fig. 6).

However, the surface still contains a large number of small particles of approximately 10 ± 5 μm in size (Fig. 7a). The number of such particles can be reduced by coating the sample surface with a photoresist

before the cutting process (Fig. 7b). The number of small particles adsorbed on the surface during cutting is reduced. However, an oval shaped pattern appeared on the surface of the sample after coating with the photoresist and after its removal in dimethyl formamide. This pattern consists of small particles with a size of 10 ± 3 μm. These particles were not removed after the cleaning. These particles may not completely be removed with dimethylformamide.

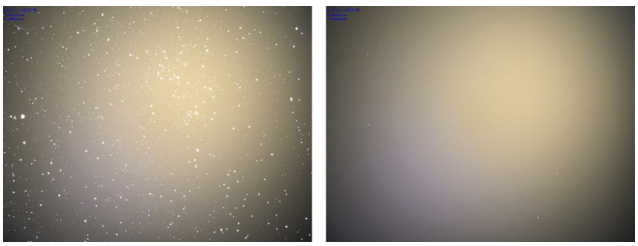

(a) (b)

Fig. 6. Si surface after (a) manual cutting, (b) automated cutting. Image taken at 0.7 magnification, field of view area 6.311 × 6.312 μm^2

(a) (b)

Fig. 7. Si surface after automated cutting: (a) without photoresist, (b) with photoresist. Image at magnification 2.0, field of view area 2.21 × 2.21 μm^2

These patterns do not appear when oxygen plasma is used to remove the photoresist [22]. However, as a result, the surface is insufficiently clean (Fig. 8).

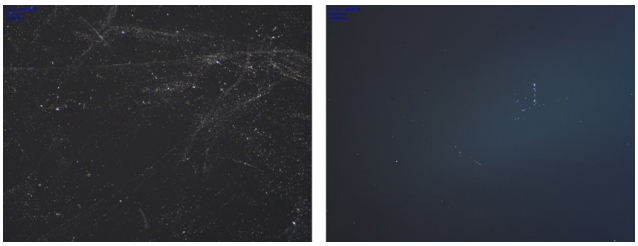

(a) (b)

Fig. 8. Si surface after plasma-chemical etching: (a) not cleaned, (b) after cleaning. Image at magnification 2.0, field of view area 2.21 × 2.21 μm^2

Therefore, the following surface preparation method is used:

1) the initial two-inch wafer is covered with a layer of photoresist FP-9120-1.0;
2) then it is automatically cut into samples of the required size;
3) the protective layer of the photoresist FP-9120-1.0 is removed in dimethylformamide, then the photoresist residues are additionally removed in the oxygen plasma;
4) final cleaning of samples mechanically under the flow of deionized water after 5 min of the ultrasonic cleaning.

Changes in the photolithographic process (drying, exposure, development) did not affect the lift-off process. Excessive metallization was not removed. However, change in the photoresist thickness led to positive results.

Repeatability of the photolithography process can be achieved with the use of the new photoresist FP-9120-0.4 with a reduced level of thickness, and by means of the lift-off photolithography process (exposure and developing the pattern, metal deposition, removing excess metal) during one day. This could not have been achieved earlier. When using the previous thicker photoresist FP-9120-1.0, it was not always possible to remove metal completely, and thus create the necessary pattern on the photocathode surface.

The reduction in photoresist thickness is assumed to make its walls steeper. Therefore, the removal of metal (lift-off) occurs more successfully. It is reproduced at the moment of creating of a photosensitive region on each photocathode. This trend can also be observed in [23], where the photoresist walls became flatter as its thickness increased.

The photolithographic pattern obtained with use of the new technological approach is more uniform. It has fewer defects, compared to samples obtained with the use of the old technology.

Data analysis on the area and percentage of defects was carried out (Table), in order to quantify the effectiveness of the new technological approach. A sample of 12 photocathodes based on the new technological approach shows a low percentage of the number of defects from the area of the working area. N1–N12 are samples made with the use of the new technology, O1–O3 are samples made with the use of the old technology.

The average defect percentage using the modified technology for samples from the N1–N8 group was 0.086%, and for the N9–N12 group was 0.035%. This is 9 times lower compared to the indicator for the old technology group O1–O3 (0.317%). The standard deviation for the new technology is also significantly lower (0.039% and 0.019% *vs* 0.127%), which indicates a high reproducibility of the process.

Figure 9 shows that the working area of samples N9–N12 has the lowest percentage of defects. When preparing for photolithography, these samples were additionally mechanically cleaned after 5 min in an ultrasonic bath.

Table. Area and percentage of defects in the working area on the photocathode

Sample number	Total defect area, mm^2	Percentage of defects from the working area 130 mm^2, %
N1	0.059	0.05
N2	0.107	0.01
N3	0.073	0.06
N4	0.102	0.08
N5	0.080	0.06
N6	0.102	0.08
N7	0.031	0.02
N8	0.395	0.04
N9	0.020	0.02
N10	0.076	0.06
N11	0.020	0.02
N12	0.076	0.06
O1	0.349	0.27
O2	0.600	0.46
O3	0.288	0.22

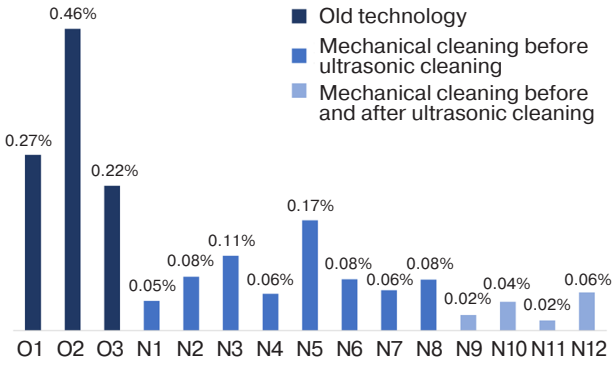

Fig. 9. Distribution of the defect fraction from the total area of the samples

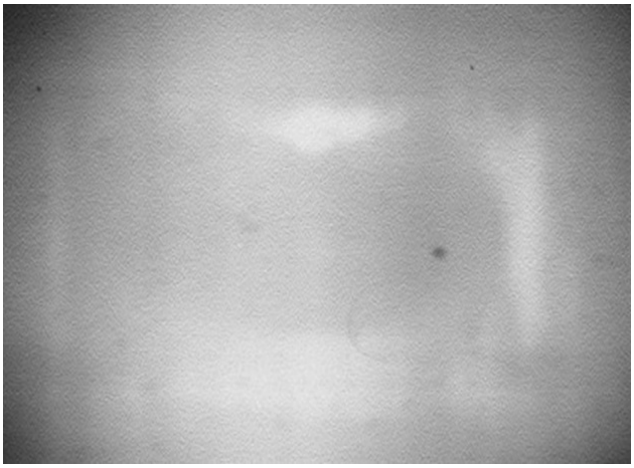

Fig. 10. Image of the device with a photocathode obtained using advanced technology

Thus, the improved technological process not only reduces defects, but also provides more stable results in mass production.

Compared to Fig. 2, the quality of the image from the new device (Fig. 10) is significantly improved. The image has become more uniform, black dots from dirt are almost absent, and dark rectangles are completely absent.

The results show that the reduction of the photoresist thickness and elimination of long-term interoperative sample storage significantly reduces the number of defects. The greatest contribution to quality improvement is made by a complex of measures: protection of

the surface with a photoresist before cutting, the use of plasma cleaning; sequential execution of the stages of exposure; deposition and removal of the excess metal; as well as reduction of the used photoresist thickness.

The achieved level of the defect rate according to the photocathode measurements corresponds to the best world samples of the solid-state SWIR photodetectors IMX991 from SONY[5].

CONCLUSIONS

An improved technology of the surface preparation and photolithography processes for the hybrid SWIR photodetectors has been developed.

The average defect percentage was reduced by more than 9 times, from 0.317% to 0.035%. This corresponds to the best currently available world samples of solid-state SWIR photodetectors.

The image quality from the hybrid photodetector device is improved as a result, The image is more uniform, with fewer defects such as black dots, lines, and streaks.

A high level of reproducibility of the process is provided (reduction of the standard deviation by more than 6 times), enabling the proposed technology for mass production of the hybrid SWIR photodetectors to be scaled.

ACKNOWLEDGMENTS

The authors thank the staff of NRI "Electron" for their help in conducting the research.

Authors' contributions

A.A. Egorenkov—formulating the aims and objectives of the research, scientific guidance and coordinating the research.

I.V. Danilova—interpretating the results, selecting technological routes for surface cleaning, practical testing and optimizing the modes on experimental samples, editing the article.

M.I. Bibinova—selecting technological routes of photolithography, practical testing and optimizing the modes on experimental samples.

S.N. Chelyshkov—conducting experimental measurements of sample parameters and deposition processes.

A.N. Vyaznikov—collecting, processing and statistical analysis of experimental data, preparing tables and samples.

K.S. Batalov—developing the experimental methods and verifying the obtained results.

REFERENCES

1. Kriksunov L.Z. *Spravochnik po osnovam infrakrasnoi tekhniki* (*Handbook of the Fundamentals of Infrared Technology*). Moscow: Sovetskoe Radio; 1978, 400 p. (In Russ.).
2. Hansen M.P., Douglas S.M. Overview of SWIR detectors, cameras, and applications. In: *Proceedings of SPIE 6939 Defense and Security Symposium* (*Thermosense XXX*). 2008. P. 69390I-1–69390I-11. https://doi.org/10.1117/12.777776
3. Ainbund M.R., Egorenkov A.A., Pashuk A.V. Features of images of water, ice, snow, objects and a human formed by a hybrid television camera in the near-infrared range. *Nauchno-tekhnicheskii vestnik informatsionnykh tekhnologii, mekhaniki i optiki = Scientific and technical journal of information technologies, mechanics and optics*. 2021;21(5):619–625 (in Russ.). https://doi.org/10.17586/2226-1494-2021-21-5-619-625
4. Song H., Yeo S., Jin Y., Park I., Ju H., Nalcakan Y., Kim S. Short-Wave Infrared (SWIR) Imaging for Robust Material Classification: Overcoming Limitations of Visible Spectrum Data. *Appl. Sci*. 2024;14(23):11049. https://doi.org/10.3390/app142311049
5. Pavlovic M.S., Milanovic P.D., Stankovic M.S., Peric D.B., Popadic I.V., Peric M.V. Deep Learning Based SWIR Object Detection in Long-Range Surveillance Systems: An Automated Cross-Spectral Approach. *Sensors*. 2022;22(7):2562. https://doi.org/10.3390/s22072562
6. Wilson R.H., Nadeau K.P., Jaworski F.B., Tromberg B.J., Durkina A.J. Review of short-wave infrared spectroscopy and imaging methods for biological tissue characterization. *J. Biomed. Opt.* 2015;20(3):030901. http://doi.org/10.1117/1.JBO.20.3.030901
7. Egorenkov A.A., Zubkov V.I., Solomonov A.V., Mironov D.E, Pashuk A.V., Ainbund M.R. Hybrid matrix photodetector for infrared spectral range. *Izvestiya SPbGETU "LETI" = Proceedings of Saint Petersburg Electrotechnical University*. 2021;4:15–22 (in Russ.). https://www.elibrary.ru/wvtgwi
8. Enloe W., Sheldon R., Reed L., Amith A. Electron-bombarded CCD image intensifier with a GaAs photocathode. In: *Proceedings of Symposium on Electronic Imaging*: *Science and Technology*. 1992. P. 41–49. https://doi.org/10.1117/12.60337
9. Zhang Y., Chen J., Yang J., Fu M., Cao Y., Dong M., Yu J., Dong S., Yang X., Shao L., Hu Z., Cai H., Liu C., Huang F. Sensitive SWIR Organic Photodetectors with Spectral Response Reaching 1.5 μm. *Adv. Mater.* 2024;36(41):2406950. https://doi.org/10.1002/adma.202406950
10. Costello K.A., Davis G.A., Weiss R.E., Aebi V.W. Transferred electron photocathode with greater than 5% quantum efficiency beyond 1 micron, In: *Proceedings SPIE 1449* (*Electron Image Tubes and Image Intensifiers II*). 1991. P. 40–50. https://doi.org/10.1117/12.44264

[5] NPK Photonica. IMX991-AABA-C. https://www.npk-photonica.ru/product/21366/. Accessed August 09, 2025. (In Russ.).

11. Musatov A.L., Izraelyants K.R., Korotkikh V.L., Filippov S.L., Russu E.V., Dyakonu I.I. Emission characteristics of semiconductor heterostructures with a Schottky barrier InGaAs-InP-Ag. *Phizika i technika polyprovodnikov = Physics and Techniks of Semiconductors*. 1990;24(9):1523–1530 (in Russ.).
12. Aebi V., Costello K., Davis G., LaRue R., Weiss R. Near IR Photocathode Development. In: *Proceedings of 1997 Meeting of the IRIS Specialty Group on Active System*. 1997. Tucson. US.
13. Wang X., Shi M., Su L., Yang L., Deng X., Zhang Y., Tan H. NEA GaAs photocathode for electron source: From growth, cleaning, activation to performance. *Mater. Today Phys.* 2025;52:101680. https://doi.org/10.1016/j.mtphys.2025.101680
14. Sun Y., Liu Z., Pianetta P. Surface dipole formation and lowering of the work function by Cs adsorption on InP(100) surface. *Vac. Sci. Technol. A*. 2007;25(5):1351–1356. https://doi.org/10.1116/1.2753845
15. Dolgikh A.V., Leonov I.A. High resolution scanning ellipsometry as test method of NEA-photocathode surface cleanliness in image intensifier tubes manufacture. *Prikladnaya Fizika = Applied Physics*. 2007;4:121–123 (in Russ.). https://www.elibrary.ru/iadlst
16. Tereshchenko O.E., Shaibler G.É., Yaroshevich A.S., et al. Low-temperature method of cleaning *p*-GaN(0001) surfaces for photoemitters with effective negative electron affinity. *Phys. Solid State.* 2004;46(10):1949–1953. https://doi.org/10.1134/1.1809437
[Original Russian Text: Tereshchenko O.E., Shaibler G.É., Yaroshevich A.S., Shevelev S.V., Terekhov A.S., Lundin V.V., Zavarin E.E., Besyulkin A.I. Low-temperature method of cleaning *p*-GaN(0001) surfaces for photoemitters with effective negative electron affinity. *Fizika Tverdogo Tela.* 2004;46(10):1881–1885 (in Russ.). https://www.elibrary.ru/rczyer]
17. Machucaa F., Liu Z., Sun Y., Pianetta P., Spicer W.E., Pease R.F.W. Simple method for cleaning gallium nitride (0001). *Am. Vac. Soc. A*. 2002;20(5):1784–1786. https://doi.org/10.1116/1.1503782
18. Pastuszka S., Terekhov A.S., Wolf A. 'Stable to unstable' transition in the (Cs, O) activation layer on GaAs (100) surfaces with negative electron affinity in extremely high vacuum. *Appl. Surf. Sci.* 1996;99(4):361–365. https://doi.org/10.1016/0169-4332(96)00106-7
19. Jin M., Zhang Y., Chen X., Hao G., Chang B., Shi F. Effect of surface cleaning on spectral response for InGaAs photocathodes. *Appl. Opt.* 2015:54(36):10630–10635. https://doi.org/10.1364/AO.54.010630
20. Choi I-C., Kim H-T., Yerriboina N.P., Lee J.H., Teugels L., Kim T-G., Park J-G. Post-CMP Cleaning of InGaAs Surface for the Removal of Nanoparticle Contaminants for Sub-10nm Device Applications. *ECS J. Solid State Sci. Technol.* 2019;8(5): 3028–3034. https://doi.org/10.1149/2.0051905jss
21. Na J., Lim S. Elemental behaviors of InGaAs surface after treatment in aqueous solutions. *Microelectron. Eng.* 2019;212: 27–36. https://doi.org/10.1016/j.mee.2019.04.002
22. Brussaard G.J.H., Letourneur K.G.Y., Schaepkens M., van de Sanden M.C.M., Schram D.C. Stripping of photoresist using a remote thermal Ar/O_2 and $Ar/N_2/O_2$ plasma. *J. Vac. Sci. Technol. B.* 2003;21(1):61–66. https://doi.org/10.1116/1.1532021
23. Kim J.H., Choi N., Kim Y.-H., Kim T.-S. Thickness dependence of the lithographic performance in 193nm photoresists. In: *Proceedings of SPIE 6153, Advances in Resist Technology and Processing XXIII.* 2006. V. 615337. https://doi.org/10.1117/12.655777

СПИСОК ЛИТЕРАТУРЫ

1. Криксунов Л.З. *Справочник по основам инфракрасной техники*. М.: Сов. Радио; 1978, 400 с.
2. Hansen M.P., Douglas S.M. Overview of SWIR detectors, cameras, and applications. In: *Proceedings of SPIE 6939 Defense and Security Symposium* (*Thermosense XXX*). 2008. P. 69390I-1–69390I-11. https://doi.org/10.1117/12.777776
3. Айнбунд М.Р., Егоренков А.А., Пашук А.В. Особенности изображений воды, льда, снега, предметов и человека, формируемых гибридной телевизионной камерой в ближнем инфракрасном диапазоне. *Научно-технический вестник информационных технологий, механики и оптики*. 2021;21(5):619–625. https://doi.org/10.17586/2226-1494-2021-21-5-619-625
4. Song H., Yeo S., Jin Y., Park I., Ju H., Nalcakan Y., Kim S. Short-Wave Infrared (SWIR) Imaging for Robust Material Classification: Overcoming Limitations of Visible Spectrum Data. *Appl. Sci.* 2024;14(23):11049. https://doi.org/10.3390/app142311049
5. Pavlovic M.S., Milanovic P.D., Stankovic M.S., Peric D.B., Popadic I.V., Peric M.V. Deep Learning Based SWIR Object Detection in Long-Range Surveillance Systems: An Automated Cross-Spectral Approach. *Sensors*. 2022;22(7):2562. https://doi.org/10.3390/s22072562
6. Wilson R.H., Nadeau K.P., Jaworski F.B., Tromberg B.J., Durkina A.J. Review of short-wave infrared spectroscopy and imaging methods for biological tissue characterization. *J. Biomed. Opt.* 2015;20(3):030901. http://doi.org/10.1117/1.JBO.20.3.030901
7. Егоренков А.А., Зубков В.И., Соломонов А.В., Миронов Д.Е., Пашук А.В., Айнбург М.Р. Гибридный матричный фотоприемник для ИК-области спектра. *Известия СПбГЭТУ «ЛЭТИ»*. 2021;4:15–22. https://www.elibrary.ru/wvtgwi
8. Enloe W., Sheldon R., Reed L., Amith A. Electron-bombarded CCD image intensifier with a GaAs photocathode. In: *Proceedings of Symposium on Electronic Imaging*: *Science and Technology*. 1992. P. 41–49. https://doi.org/10.1117/12.60337
9. Zhang Y., Chen J., Yang J., Fu M., Cao Y., Dong M., Yu J., Dong S., Yang X., Shao L., Hu Z., Cai H., Liu C., Huang F. Sensitive SWIR Organic Photodetectors with Spectral Response Reaching 1.5 μm. *Adv. Mater.* 2024;36(41):2406950. https://doi.org/10.1002/adma.202406950
10. Costello K.A., Davis G.A., Weiss R.E., Aebi V.W. Transferred electron photocathode with greater than 5% quantum efficiency beyond 1 micron, In: *Proceedings SPIE 1449* (*Electron Image Tubes and Image Intensifiers II*). 1991. P. 40–50. https://doi.org/10.1117/12.44264

11. Мусатов А.Л., Израэльянц К.Р., Коротких В.Л., Филиппов С.Л., Руссу Е.В., Дякону И.И. Эмисионные характеристики полупроводниковых гетероструктур с барьером Шоттки InGaAs-InP-Ag. *Физика и техника полупроводников*, 1990;24(9):1523–1530.
12. Aebi V., Costello K., Davis G., LaRue R., Weiss R. Near IR Photocathode Development. In: *Proceedings of 1997 Meeting of the IRIS Specialty Group on Active System*. 1997. Tucson. US.
13. Wang X., Shi M., Su L., Yang L., Deng X., Zhang Y., Tan H. NEA GaAs photocathode for electron source: From growth, cleaning, activation to performance. *Mater. Today Phys.* 2025;52:101680. https://doi.org/10.1016/j.mtphys.2025.101680
14. Sun Y., Liu Z., Pianetta P. Surface dipole formation and lowering of the work function by Cs adsorption on InP(100) surface. *Vac. Sci. Technol. A*. 2007;25(5):1351–1356. https://doi.org/10.1116/1.2753845
15. Долгих А.В., Леонов И.А. Сканирующая эллипсометрия высокого разрешения как метод контроля чистоты поверхности ОЭС-фотокатодов при производстве электронно-оптических преобразователей. *Прикладная физика.* 2007;4:121–123. https://www.elibrary.ru/iadlst
16. Терещенко О.Е., Шайблер Г.Э., Ярошевич А.С., Шевелев С.В., Терехов А.С., Лундин В.В., Заварин Е.Е., Бесюлькин А.И. Низкотемпературная методика очистки поверхности *p*-GaN(0001) для фотоэмиттеров с эффективным отрицательным электронным сродством. *Физика твердого тела.* 2004;46(10):1881–1885. https://www.elibrary.ru/rczyer
17. Machucaa F., Liu Z., Sun Y., Pianetta P., Spicer W.E., Pease R.F.W. Simple method for cleaning gallium nitride (0001). *Am. Vac. Soc. A*. 2002;20(5):1784–1786. https://doi.org/10.1116/1.1503782
18. Pastuszka S., Terekhov A.S., Wolf A. 'Stable to unstable' transition in the (Cs, O) activation layer on GaAs (100) surfaces with negative electron affinity in extremely high vacuum. *Appl. Surf. Sci.* 1996;99(4):361–365. https://doi.org/10.1016/0169-4332(96)00106-7
19. Jin M., Zhang Y., Chen X., Hao G., Chang B., Shi F. Effect of surface cleaning on spectral response for InGaAs photocathodes. *Appl. Opt.* 2015:54(36):10630–10635. https://doi.org/10.1364/AO.54.010630
20. Choi I-C., Kim H-T., Yerriboina N.P., Lee J.H., Teugels L., Kim T-G., Park J-G. Post-CMP Cleaning of InGaAs Surface for the Removal of Nanoparticle Contaminants for Sub-10nm Device Applications. *ECS J. Solid State Sci. Technol.* 2019;8(5):3028–3034. https://doi.org/10.1149/2.0051905jss
21. Na J., Lim S. Elemental behaviors of InGaAs surface after treatment in aqueous solutions. *Microelectron. Eng.* 2019;212: 27–36. https://doi.org/10.1016/j.mee.2019.04.002
22. Brussaard G.J.H., Letourneur K.G.Y., Schaepkens M., van de Sanden M.C.M., Schram D.C. Stripping of photoresist using a remote thermal Ar/O_2 and $Ar/N_2/O_2$ plasma. *J. Vac. Sci. Technol. B.* 2003;21(1):61–66. https://doi.org/10.1116/1.1532021
23. Kim J.H., Choi N., Kim Y.-H., Kim T.-S. Thickness dependence of the lithographic performance in 193nm photoresists. In: *Proceedings of SPIE 6153, Advances in Resist Technology and Processing XXIII.* 2006. V. 615337. https://doi.org/10.1117/12.655777

About the Authors

Artyom A. Egorenkov, Head of Scientific Research Department, JSC "NRI Electron" (68, Toreza pr., Saint Petersburg, 194223 Russia). E-mail: a.egorenkov@niielectron.ru. https://orcid.org/0000-0002-0084-564X

Irina V. Danilova, Engineer, JSC "NRI Electron" (68, Toreza pr., Saint Petersburg, 194223 Russia). E-mail: i.danilova@niielectron.ru. https://orcid.org/0009-0009-7160-8308

Maria I. Bibinova, Engineer, JSC "NRI Electron" (68, Toreza pr., Saint Petersburg, 194223 Russia). E-mail: m.bibinova@niielectron.ru. https://orcid.org/0009-0007-0006-867X

Sergei N. Chelyshkov, Engineer, JSC "NRI Electron" (68, Toreza pr., Saint Petersburg, 194223 Russia). E-mail: s.chelyshkov@niielectron.ru. https://orcid.org/0000-0002-0664-1808

Alexei N. Vyaznikov, CEO, JSC "NRI Electron" (68, Toreza pr., Saint Petersburg, 194223 Russia). E-mail: a.vyaznikov@niielectron.ru. https://orcid.org/0009-0003-7248-5852

Konstantin S. Batalov, Deputy Head of the Research Department, JSC "NRI Electron" (68, Toreza pr., Saint Petersburg, 194223 Russia). E-mail: k.batalov@niielectron.ru. https://orcid.org/0009-0009-4140-8794

Об авторах

Егоренков Артём Александрович, начальник научно-исследовательского отдела, АО «ЦНИИ «Электрон» (194223, Россия, Санкт-Петербург, пр-т Тореза, д. 68, лит. Р). E-mail: a.egorenkov@niielectron.ru. https://orcid.org/0000-0002-0084-564X

Данилова Ирина Владимировна, инженер, АО «ЦНИИ «Электрон» (194223, Россия, Санкт-Петербург, пр-т Тореза, д. 68, лит. Р). E-mail: i.danilova@niielectron.ru. https://orcid.org/0009-0009-7160-8308

Бибинова Мария Ивановна, инженер-технолог, АО «ЦНИИ «Электрон» (194223, Россия, Санкт-Петербург, пр-т Тореза, д. 68, лит. Р). E-mail: m.bibinova@niielectron.ru. https://orcid.org/0009-0007-0006-867X

Челышков Сергей Николаевич, инженер, АО «ЦНИИ «Электрон» (194223, Россия, Санкт-Петербург, пр-т Тореза, д. 68, лит. Р). E-mail: s.chelyshkov@niielectron.ru. https://orcid.org/0000-0002-0664-1808

Вязников Алексей Николаевич, генеральный директор, АО «ЦНИИ «Электрон» (194223, Россия, Санкт-Петербург, пр-т Тореза, д. 68, лит. Р). E-mail: a.vyaznikov@niielectron.ru. https://orcid.org/0009-0003-7248-5852

Баталов Константин Сергеевич, заместитель начальника научно-исследовательского отдела, АО «ЦНИИ «Электрон» (194223, Россия, Санкт-Петербург, пр-т Тореза, д. 68, лит. Р). E-mail: k.batalov@niielectron.ru. https://orcid.org/0009-0009-4140-8794

Translated from Russian into English by the Authors
Edited for English language and spelling by Dr. David Mossop

Micro- and nanoelectronics. Condensed matter physics

Микро- и наноэлектроника. Физика конденсированного состояния

UDC 004.832.32
https://doi.org/10.32362/2500-316X-2026-14-2-80-102
EDN LLZOKJ

REVIEW ARTICLE

Physically unclonable functions in digital integrated circuits

Evgenii Ph. Pevtsov [@], Tatyana A. Demenkova, Yuri A. Korotaev [@], Alexander S. Sigov

MIREA – Russian Technological University, Moscow, 119454 Russia
[@] Corresponding authors, e-mail: pevtsov@mirea.ru, korotaevya@yandex.ru

• **Submitted:** 16.09.2025 • **Revised:** 23.09.2025 • **Accepted:** 12.02.2026

Abstract

Objectives. Modules that implement physically unclonable functions (PUFs) within a digital chip facilitate the direct use of challenge–response pairs by device applications that can query and read the PUF without external tools or exposing data outside the chip. A PUF can be implemented using technological processes and components already applied in device fabrication. The first of two reviews on PUFs as elements of hardware security infrastructure, the present paper focuses on the formal description of PUFs and designs based on memory modules and timing analysis.

Methods. The following quantitative indicators were applied to formally describe PUFs: computability, uniqueness, feasibility, cloning resistance, and protection against unauthorized access.

Results. PUFs are considered as physical devices with unique signatures. A classification into three PUF groups is proposed: delay-based, memory-based, and analog. Typical examples of the first two groups are outlined. While delay-based solutions provide a large challenge–response space, they require symmetry and/or calibration. In contrast, memory-based PUFs are easier to implement in integrated circuits. With suitable post-processing, they can achieve high reproducibility, making them practical for many applications. Approaches to mitigating voltage and temperature variations are described along with examples of strong memory-oriented PUFs and circuit techniques that enhance resistance to attacks.

Conclusions. PUF-based security technologies demonstrate significant potential, particularly for the Internet of Things. When combined with post-processing and compensation methods, PUFs constitute a mature and effective tool for hardware security.

Keywords: physically unclonable function, PUF, integrated circuits, hardware security, arbiter PUF, memory-based PUF, SRAM, DRAM, Internet of Things

For citation: Pevtsov E.Ph., Demenkova T.A., Korotaev Yu.A., Sigov A.S. Physically unclonable functions in digital integrated circuits. *Russian Technological Journal.* 2026;14(2):80–102. https://doi.org/10.32362/2500-316X-2026-14-2-80-102, https://www.elibrary.ru/LLZOKJ

Financial disclosure: The authors have no financial or proprietary interest in any material or method mentioned.

The authors declare no conflicts of interest.

ОБЗОРНАЯ СТАТЬЯ

Физически неклонируемые функции в цифровых интегральных схемах

Е.Ф. Певцов [@], Т.А. Деменкова, Ю.А. Коротаев [@], А.С. Сигов

MIREA – Russian Technological University, Moscow, 119454 Russia
[@] *Авторы для переписки, e-mail: pevtsov@mirea.ru, korotaevya@yandex.ru*

• **Поступила:** 16.09.2025 • **Доработана:** 23.09.2025 • **Принята к опубликованию:** 12.02.2026

Резюме

Цели. Преимуществом модулей, реализующих физически неклонируемые функции (ФНФ) и встроенных в цифровой чип, является то, что отклики на запросы могут быть напрямую использованы другими приложениями устройства. Устройство способно запрашивать и считывать ФНФ без привлечения внешних инструментов и вывода запроса и ответа за пределы чипа. ФНФ может быть реализована с использованием технологических операций и компонентов, применяемых при изготовлении самого устройства. Статья является первой из двух обзорных публикаций, посвященных ФНФ как компонентам инфраструктуры аппаратной безопасности. Данная статья фокусируется на формальном описании ФНФ и их конструкциях, основанных на модулях памяти и анализе временных характеристик сигналов.

Методы. Использованы методы определения количественных показателей и признаков для формального описания ФНФ: вычислимость, уникальность, возможность реализации, сложность клонирования, защита от несанкционированного доступа.

Результаты. Рассмотрены реализации ФНФ как физических устройств, обладающих уникальной сигнатурой. Предложена их классификация: ФНФ на основе временных характеристик сигналов, ФНФ на основе схем памяти и аналоговые ФНФ. Приведены наиболее типичные примеры реализаций первых двух типов. Показано, что решения на основе задержек сигналов обеспечивают широкое пространство пар «запрос – ответ», но требуют симметрии и/или калибровки, тогда как ФНФ на базе памяти проще реализуются в интегральных схемах и при корректной постобработке достигают высокой воспроизводимости, что делает их практичным выбором для многих приложений. Описаны подходы к компенсации влияния вариаций напряжения и температуры. Приведены примеры «сильных» память-ориентированных ФНФ и схемотехнические приемы повышения их стойкости к атакам.

Выводы. Технология обеспечения безопасности на основе ФНФ обладает значительным потенциалом, особенно для применения в устройствах интернета вещей. Проведенный анализ показывает, что в сочетании с методами постобработки и компенсации эксплуатационных факторов ФНФ является зрелым инструментом обеспечения аппаратной безопасности.

Ключевые слова: физически неклонируемая функция, ФНФ, интегральные схемы, аппаратная безопасность, ФНФ типа «арбитр», ФНФ на основе памяти, SRAM, DRAM, интернет вещей

Для цитирования: Певцов Е.Ф., Деменкова Т.А., Коротаев Ю.А., Сигов А.С. Физически неклонируемые функции в цифровых интегральных схемах. *Russian Technological Journal*. 2026;14(2):80–102. https://doi.org/10.32362/2500-316X-2026-14-2-80-102, https://www.elibrary.ru/LLZOKJ

Прозрачность финансовой деятельности: Авторы не имеют финансовой заинтересованности в представленных материалах или методах.

Авторы заявляют об отсутствии конфликта интересов.

INTRODUCTION

The presence of sensitive intellectual data in hardware devices designed to carry out specialized artificial intelligence (AI) tasks makes them an attractive target for cyberattacks. As well as intercepting data for financial gain by compromising the security of these devices, attackers can steal intellectual property in order to reverse engineer them and produce counterfeit versions. In addition to producing counterfeit copies, refurbished or re-manufactured devices may also be sold as new products, resulting in lost revenue for original manufacturers and security concerns due to reduced product lifespan and reliability.

Equipment security can be ensured through the physical implementation of secure circuits. Such circuits are used along with other increasingly complex methods of protection against counterfeiting for device authentication and random-access key generation. Security circuits have a unique signature resembling that of human retinal, fingerprint, and DNA patterns. Due to the random nature of such signatures, they are difficult to predict and clone, thus preventing unauthorized access to data. In this context, the implementation of reliable hardware platforms for secure communication, device authentication, and protection against various software and hardware risks and hacker attacks becomes a priority research direction.

A physically unclonable function (PUF) is a physical object whose functionality cannot be duplicated (cloned) through physical means (e.g., by creating another system based on the same technology). Given set of input data and operating conditions (i.e., challenge), a PUF provides a unique output signal (i.e., response) that acts as a digital fingerprint or unique identifier for a specific instance of the device. This property makes PUFs useful in applications that require high levels of security, such as in cryptographic systems, Internet of Things (IoT) devices, and other applications that prioritize privacy protection.

By definition, a PUF performs a specific operation when provided with certain input data to produce an output that can be evaluated or measured. In the engineering sense, a PUF should be considered a function, i.e., a procedure performed by or affecting a specific (physical) system. Typically, the input data for a PUF is referred to as a challenge, to which a specific response is generated at the output. The combination of the challenge and response is commonly referred to as a challenge-response pair (CRP). The CRP generation process is defined by the relationship between challenges and responses established using a specific PUF implementation.

PUFs have been widely studied in the scientific literature, particularly due to the importance of ensuring the security of IoT devices [1]. The paper summarizes the findings presented in recent publications regarding modern PUFs and their implementations [2-4].

QUANTITATIVE PUF INDICATORS

A comprehensive explanation of the features that can be utilized to evaluate various PUF implementations is provided in [5–7]. Classification and identification theories are applied within a single PUF type as well as for comparing different types of PUFs.

The effects of a particular PUF design are measured using two types of quantitative indicators:

- Inter-distance. This metric measures the difference in responses obtained from a single challenge for two instances of the same PUF. The corresponding designation for this indicator is proposed in [7] and represents a random variable that describes the distance between the responses of two PUF instances from the same call.
- Intra-distance. A quantitative measure that describes the difference between two estimates of a single PUF instance. It represents the difference in response values when the same challenge is applied twice to the same physical implementation of the PUF. Such an intra-distance metric is a random variable that describes the distance between response values from the same PUF instance using the same challenge.

These indicators, which determine the reproducibility and uniqueness of a PUF, use the same challenge for both metrics. However, the specific value of the quantitative characteristics of one or more instances of a PUF may vary depending on the complexity and number of tests. In other words, the quantitative estimates used to measure these characteristics may vary depending on the nature of the response. In cases where the response is a bit string, the inter-Hamming distance (inter-HD) is used as the criterion.

In order to summarize the inter- and intra-distance characteristics of a specific type of PUF, histograms are often used. Such histograms show the results of running a number of challenges on one PUF device and the results of running a series of different challenges on several PUF devices of the same type. As stated in [6], both histograms can be approximated by a Gaussian distribution in many cases, with respective mean values μ_{inter} and μ_{intra} and, if available, respective standard deviations σ_{inter} and σ_{intra}.

From the definition it follows that μ_{intra} represents the average noise level of the responses to characterize the reproducibility of the measured response compared to other observations of the same response. Clearly,

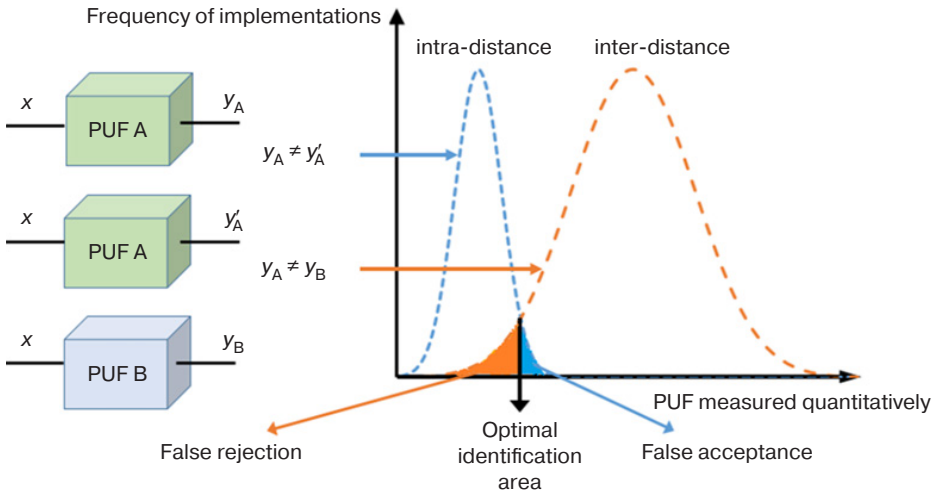

Fig. 1. Quantitative characteristics of a PUF [6].
Here, x is the challenge; y_A and y'_A are the responses of a specific PUF instance to the challenge; y_B is the response of a different PUF instance to the same challenge

the smaller the μ_{intra} value, the more reliable the responses implemented by a given PUF. Conversely, μ_{inter} expresses uniqueness; it measures the average uniqueness of two systems based on their PUF responses. If the responses are bit strings, the best uniqueness is achieved when half of the bits differ on average. In particular, if μ_{inter} is expressed as a relative value of the Hamming distance, the optimal result is a value close to 50%. In practice, implementing the minimum μ_{intra} alongside 50% μ_{inter} strikes a balance between the methods used to implement PUF. Figure 1 depicts the practical application of these concepts on an example of using a PUF for identification purposes [6].

Since an obtained PUF response is usually associated with physical measurement, there are a number of undesirable side effects that can affect the result. These include random noise and measurement errors. Consequently, the same challenge does not necessarily elicit the same response, resulting in what is known as intra-distance (see definition) between PUF responses. External factors, such as temperature or supply voltage when the PUF is implemented in an integrated circuit (IC), also systematically influence the response measurement. Therefore, in order to correctly compare different results from the literature, it is necessary to consider the conditions under which the μ_{intra} values have been obtained. An example of the influence of temperature on the reproducibility of a PUF response is given in [8]. If the environmental impact is systematic, methods can be employed to minimize its effect on the PUF response. Other options include the introduction of compensation coefficients [9] and special PUF implementation strategies that minimize dependence on the environment [7, 10].

In terms of effectiveness, PUFs can be classified as weak or strong. A PUF is considered weak if there are only a few combinations of CRP with reactions that are generally insensitive to changes in the environment. Although weak PUFs have relatively low resistance to hacker attacks, they can be used to create secret keys due to their high stability. If a PUF is strong, the number of CRPs in the device is sufficiently large that an attacker cannot destroy the identification system in real time. Therefore, when physically implementing a PUF, special attention should be paid to protection against attacks aimed at cracking the PUF, particularly those using machine learning methods.

The standard procedure for characterizing a PUF involves running statistical tests to determine the degree of randomness of binary sequences generated by hardware or software random number generators. These tests, which are developed by the Information Technology Laboratory at the National Institute of Standards and Technology (NIST)[1], are based on statistical properties that are unique to random sequences.

FORMAL PUF DESCRIPTION

An attempt to formally describe the PUF based on a description of the physical procedure for responding to challenges was carried out in [7]. Rather than being regarded as a purely abstract concept, the creation of any PUF instance is always associated with a specific physical object. PUF is defined as a procedure Π represented by some input-output functionality,

[1] https://www.nist.gov/. Accessed July 19, 2025.

which can be formally expressed as the c-response transformation of the PUF Π: X → Y: Π(x). A challenge-response procedure can be formally classified as a PUF if it exhibits the following properties:

1. Computability. Given procedures Π and arguments x from set X, it is possible to compute Y = Π(x) in polynomial algorithmic time. When it is integrated into a chip, it is therefore necessary for a PUF to be created with minimal effort, for example, under conditions of limited time, space, power, and energy consumption. Clearly, if a PUF is computable, it can be constructed. It is also clear that all versions of PUF that provide experimental results can be constructed and, at least in theory, evaluated.
2. Uniqueness. Π(x) contains certain information about the identity of the physical object implementing Π. If a set of PUF instances is clearly defined, identification can be made from this set based on the PUF Π(x) response. Sequential responses enable identification uncertainties to be reduced until a single PUF instance is optimal for identification. In this case, the challenge-response set under consideration will uniquely identify the PUF in the set of objects. Depending on the size of the set and the characteristics of the PUF responses, such an unique identification may or may not be possible. One possible indicator of uniqueness is the histogram of intermediate inter-distance metrics, summed by their μ_{inter} mean value, as shown in most experimental results.
3. Reproducibility. y = Π(x) can be reproduced with sufficient error for PUF identification. Responses to different challenges x within the same PUF Π should be similar in terms of the response difference metric under consideration. When interpreting experimental results, these are primarily measured using an intra-distance histogram and summed by their mean value, μ_{intra}. Reproducibility is a property that differentiates PUFs from true random number generators (TRNGs).
4. Unclonability. For a given procedure Π, there is no other procedure Γ that is not equivalent to Π and such that $\forall x \in X\ \Gamma(x) \approx \Pi(x)$ with an accuracy of implementation error. It should be noted that the cloning procedure Γ is not necessarily physically implementable; physical and mathematical unclonability differ. If it is difficult to find a physical object containing another PUF $\Pi_\Gamma \neq \Pi$, so that $\forall x \in X\ \Pi_\Gamma(x) \neq \Pi(x)$, then it is claimed that implementing the PUF is physically impossible. Even the manufacturer of the original PUF would find it difficult to create a physical clone. This is referred to as "manufacturer resistance." If an abstract mathematical procedure f_Γ cannot be devised such that $\forall x \in X\ f_\Gamma(x) \approx \Pi(x)$, then it may be claimed that Π is mathematically undecidable. Physical and mathematical unclonability are fundamentally different properties; i.e., a structure may be able to be easily cloned physically but not mathematically, or *vice versa*. For a PUF to be truly unclonable, its implementation procedure Π must be both physically and mathematically unclonable. It should be noted that physical cloning can be very difficult or even impossible, whereas proving unclonability in theory is also very challenging. In principle, systems based on quantum physics are impossible to clone in practice.
5. Unpredictability. For a set of procedures Q = $\{f(x_i, y_i) = \Pi(x_i)\}$ having an error margin, it is impossible to determine $y_c \approx \Pi(x_c)$ for a random challenge x_c such that $(x_c) \notin$ Q. If the PUF response to a random challenge could be accurately predicted simply by observing the CRP set, it would be easy to create a mathematical clone with access to the full catalogue of PUF response options.
6. One-wayness. For any argument y and procedure Π within an acceptable error margin, it is impossible to find an x such that Π(x) = y. In some papers, PUFs are simplistically described as physical versions of one-way cryptographic functions [11].
7. Obvious interference. Modification of the physical object described by procedure Π during the implementation of transforming Π → Π′, such that $\forall x \in X\ \Pi(x) \neq \Pi'(x)$ is true with high probability even when considering the Π implementation error. A distinction should be made between systems that protect against unauthorized access (i.e., systems where interference does not actually result in the acquisition of any useful information) and systems in which interference is obvious and harmful (i.e., systems in which interference with a physical object containing a PUF changes the CRP behavior).

PUF IMPLEMENTATIONS BASED ON ANALYSIS OF SIGNAL TIME CHARACTERISTICS

A major advantage of embedding a PUF in a digital chip consists in the possibility for responses to challenges to be used directly by other applications running on the same device. Notably, the device can query and read its own PUF without requiring external tools such that the challenge and response never leave the device. Furthermore, the PUF can be implemented using only the technological operations and components used to manufacture the device in which the PUF node is located. This requires virtually no additional cost.

Several options for classifying PUFs are provided in review publications [2, 3, 12–18]. These include the time of the first developments, physical

design properties (hybrid or fully electronic) and implementation technologies (electronic, optical, radio frequency, or magnetic), CRP pair sizes, and areas of application. In summary, there are three main types of PUF implementation in ICs: (1) based on signal timing characteristics; (2) based on memory circuits; (3) analog and passive.

Ring oscillator (RO) PUFs

These devices exploit the frequency mismatch effect of ring oscillators based on inverters to create the PUF [19]. Due to manufacturing variations, even two nominally identical ring oscillators implemented on a single chip will have a detectable frequency difference. As shown in Fig. 2, an array of *N* oscillators is embedded in RO-PUF.

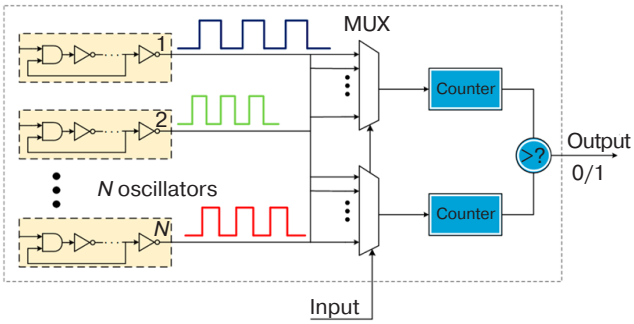

Fig. 2. Example of RO-PUF implementation [3]. MUX is a multiplexer

By comparing the frequencies of two ring oscillators, a response bit is produced. Since the challenge consists of the number or location of ring oscillators, the response is the result of the difference in their oscillation frequencies. To reliably compare frequencies, counters are used to count the number of pulses from each oscillator over a specified time interval. An alternative approach is to connect the outputs of the two oscillators to the inputs of a SR-latch.

RO-PUF implementations demonstrate moderate complexity involving a circuit that consists of repeating blocks of oscillators and simple digital counters/comparators. Since each bit requires a unique RO pair, at least 2*N* oscillators are required to obtain *N* bits. More economical circuits are often used; for example, frequencies can be sorted within a set of ROs and a set of bits can be generated by comparing different pairs in an ordered list. Although this approach allows several bits to be obtained from *N* oscillators, it can complicate analysis. According to [3], the uniqueness of a well-designed RO-PUF is close to 50% due to random frequency spreads giving equal probability of one oscillator being superior to another. Repeatability can also be high; if the frequency difference between the selected pairs is large enough, the order of their comparison is preserved even when temperature and voltage change. Under experimental conditions, 95–99% reliability is achieved. However, under unfavorable conditions (for example, when frequencies converge due to temperature drift), some response bits may be inverted. Therefore, a frequency margin should be introduced—or response encoding should be used—to increase reliability.

In modern technical processes, the scaling of RO-PUF to higher frequencies requires consideration of increased period fluctuations due to errors comparable to the frequency difference between ring oscillators arising as a result of noise at the nanometer scale.

Studies have demonstrated successful RO-PUF implementation in field-programmable gate arrays (FPGAs) [20, 21]. Several proposed developments for improving RO-PUF characteristics are aimed at bringing them into the category of strong PUF [22]. Other works have described the architecture of a configurable RO-PUF (CRO-PUF) which uses frequency and phase shift changes [23, 24]. Each delay block, S_0, …, S_n, is made of logic elements formed by pairs of the *n*- and *p*-MOS (metal–oxide–semiconductor) transistors such that the total delay time increases in accordance with the tightening of technological tolerances for their manufacture. Figure 3a depicts an example in which each delay block S is configured to form a 4-bit challenge. Figure 3b shows *N* delay cascades connected in series where the output data from each cascade is used to switch the counter start signals. The values of these signals are then compared by a comparator to generate a response signal.

As well as eliminating the duplication of ring oscillators, the proposed design reduces switching activity and introduces inter-stage delay as an additional source of randomness. The PUF is implemented in 22 nm mode using fully depleted silicon-on-insulator technology and Synopsys[2] tools. Tests carried out on eight chips successfully passed NIST tests, achieving intra-HD and inter-HD values of 9.95% and 45.5%, respectively.

The CRO-PUF proposed in [25] is implemented as a modification of the basic circuit, which consists of XOR2 elements acting as controlled delay elements. A complete set of challenges can be applied to this circuit. It is shown that the delay depends not only on the challenge value but also on the configuration of the interconnections of the circuit structural elements with the configurable ring oscillator. A proposed temporal model of the modified CRO PUF allows the influence of interconnections on the frequency

[2] Synopsis Electronic Design Automation Solutions. https://www.synopsys.com/silicon-design.html. Accessed July 19, 2025.

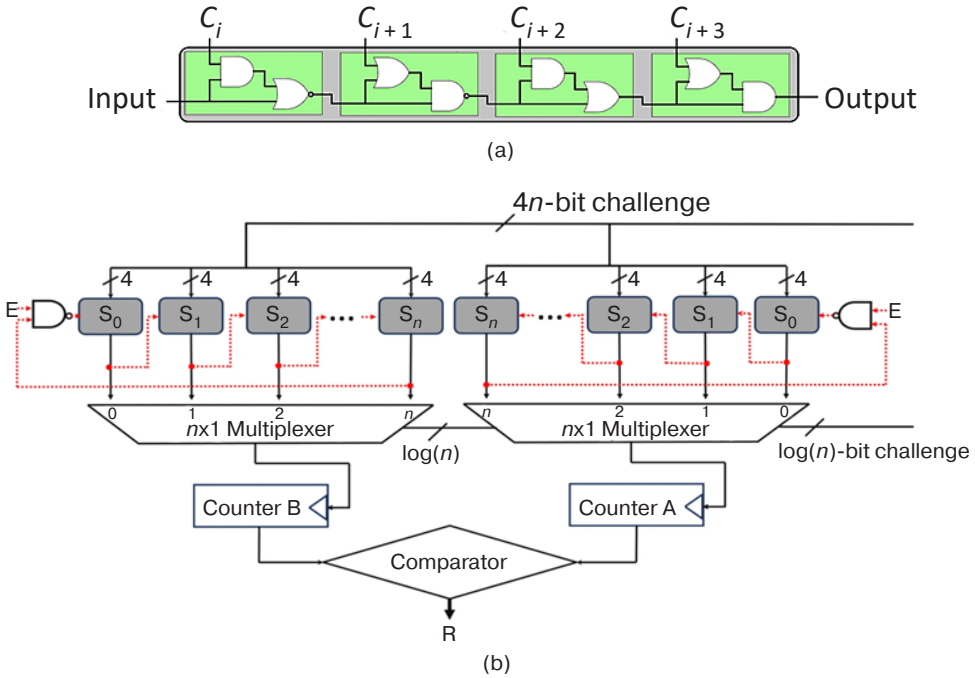

Fig. 3. RO-PUF microarchitecture:
(a) delay generation module; (b) response bit generation device for a configurable 4-bit challenge [24]. Here, C_i, ..., C_{i+3} are the challenges; E is the enable signal; *n*x1 is the multiplexer with *n* inputs and 1 output; and R is the response

of the generated signal to be proven analytically as confirmed by experiment using the Xilinx Zynq-7000 series FPGA (Xilinx, USA).

The problem of compensating for the influence of temperature on PUF is discussed in [26, 27]. The authors analyze the impact of metal-oxide-semiconductor field-effect transistor temperature characteristics on RO-PUF properties without altering the original circuit structure. Simulations of the 55-nm process performed using Cadence Virtuoso[3] tools and the Monte Carlo method show that temperature changes having the least effect on generation frequency occur when using an *N*-type high voltage *n*MOS transistor in the generation block. In this case, the frequency of the ring oscillator changes by 7.83% over an operating temperature range of 50 to 200°C, which is less than the 14.35% change observed in a classic RO-PUF. When several ring oscillators are implemented in parallel and the frequency is measured by counting the rising edges, the measurement remains the same. However, when a challenge is applied to the PUF, an arbitrary pair of oscillators is selected to form a response as a logical function of the comparison of the two obtained counter values (Fig. 3).

The successful implementation of RO-PUF in FPGA is demonstrated in [28, 29] through experiments conducted on 15 programmable logic ICs (FPGAs) comprising 1024 circuits that yield values of $\mu_{inter} = 46.15\%$ and $\mu_{intra} = 0.48\%$. The authors apply a method for eliminating metastable states that takes into account only the most stable response bit from eight pairs of oscillator cycles. The source of variation is a random difference in signal propagation delay along nominally identical paths. In [29], the authors propose a pseudo linear feedback shift register (LFSR) PUF architecture in which the LFSR structure is implemented as a closed chain of inverters and XOR elements. This forms a single circuit that allows the reliable extraction of signal propagation delay variations that are unique to each chip.

In a transient effect ring oscillator (TERO) PUF, changes in the frequency and duration of signals in signal lines and logic elements are analyzed depending on the type of their manufacture [30]. As shown in Fig. 4, a transient effect ring oscillator consists of two series-connected bistable ring oscillator circuits.

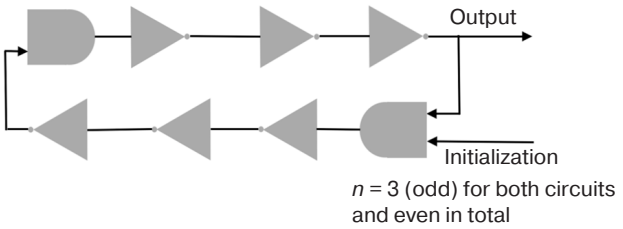

Fig. 4. Transient effect ring oscillator [30]

[3] https://cadence-ds.ru/virtuoso/. Accessed July 19, 2025.

The ring oscillator formed with an even number of inverters results in a transient effect. This causes the output signal of the cell to transition to a stable state, which is similar to the behavior of a bistable ring or a bus keeper memory cell. However, prior to this transition, certain temporary oscillations of the circuit must stabilize. After counting the number of oscillations that occur in each TERO cell before it transitions to a stable state, the values for several cells are combined to form a characteristic response for the TERO-PUF. In this case, the challenge is the number or location of the TERO cell (if there is more than one), while the response is the transient oscillations that occur when the system stops.

TERO cells should be designed with a symmetrical structure, requiring the careful selection of control elements and connection delays. Since the FPGA structure prevents developers from automatically selecting connections between elements, implementing such components in FPGAs is a specific task. However, the required symmetry can be achieved by setting constraints manually and using specific features of the target FPGA family. Study [30] describes the TERO-PUF design for two different FPGA technologies: 45 nm Xilinx Spartan 6[4] and 28 nm Altera Cyclone V[5]. Statistical processing of the TERO-PUF using these two target FPGAs produced uniqueness results of 48.46% and 47.62%, and stability results of 2.63% and 1.8%, respectively. These results are close to those obtained in several studies using the RO-PUF ring oscillator, which is considered the best candidate for implementing a PUF on FPGA. It should be noted that TERO-PUF is less susceptible to side-channel attacks than RO-PUF. Additionally, unlike RO-PUF, TERO-PUF can generate multiple bits (from one to three) for each challenge. The authors demonstrate that TERO-PUF provides between 0.85 and 1 bit of entropy per response bit. This study shows that TERO-PUF is a promising alternative to RO-PUF for implementing a PUF on FPGA.

Although the design of a bistable ring (BR) PUF [22] is similar to that of a ring PUF, it can maintain a stable state for a certain period of time. Like a ring oscillator-based PUF, it consists of a chain of NOT gates (or inverters); however, in this case an even number of gates form a bistable system instead of an oscillatory one (see Fig. 5).

When restarted, such a system transitions to one of several stable states. This occurs after a period of time determined by the unique technological variations in ring manufacture. There are many possible configurations of the ring, each of which strives independently for a preferred state. The preferred state is the response; the configuration—particularly that of the bistable ring—is determined by the PUF challenge (in this case, the reset signal).

As first demonstrated in the original work [22], in which the BR-PUF architecture is proposed, the number of topologically distinct rings is 2^n. This enables this primitive to be categorized as a strong PUF, while the natural variation in technological parameters ensures good inter-chip uniqueness and a broadly distributed spectrum of ring convergence times. In FPGA experiments, the BR-PUF demonstrates near-ideal uniqueness (around 50%) and a reliability of approximately 97%. The long “tails” of the stabilization time distribution form a basis for the rejection of slow or unstable CRPs, thereby increasing repeatability. Conversely, it has been found that a single ring can be modelled using a machine learning algorithm trained on a million challenge-response pairs, which can predict the responses of 64-, 128-, and 256-stage instances with an error rate of less than 5%. Resilience can be increased by simply XOR-combining more than four independent rings in parallel [31].

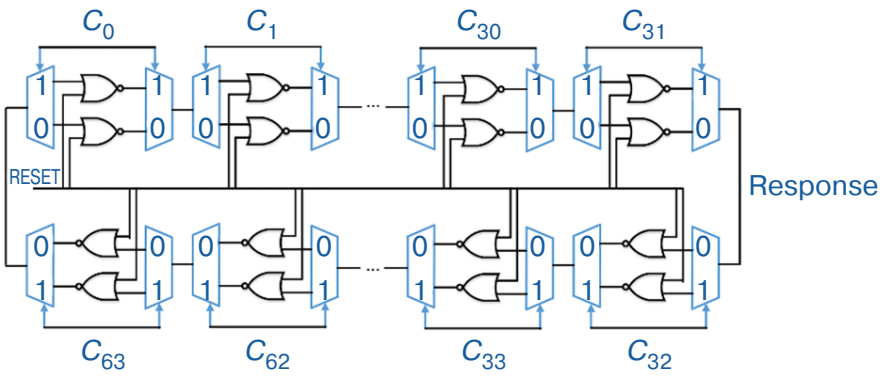

Fig. 5. Bistable ring PUF. C_0, C_1, C_{30}, C_{31}, C_{63}, C_{62}, C_{33}, C_{32} are challenges

[4] Spartan 6 FPGAs. https://www.amd.com/en/products/adaptive-socs-and-fpgas/fpga/spartan-6.html. Accessed July 19, 2025.
[5] Cyclone V FPGA and SoC FPGA. https://www.altera.com/products/fpga/cyclone/v. Accessed July 19, 2025.

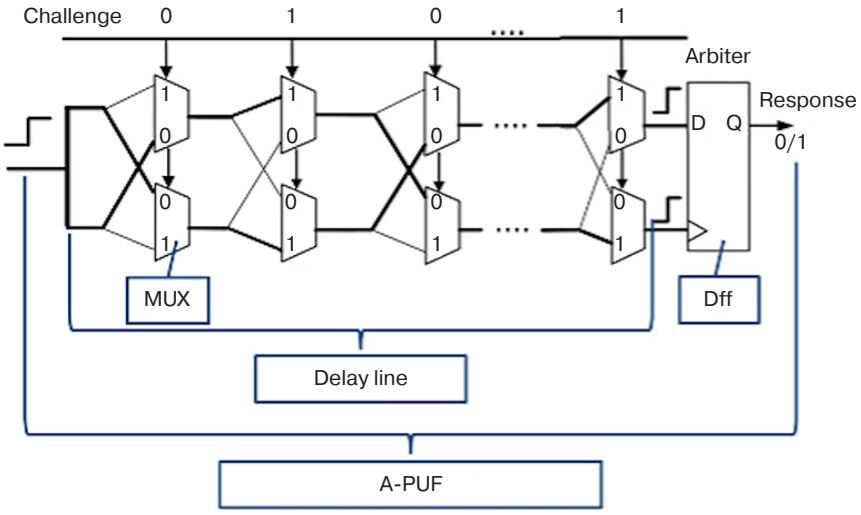

Fig. 6. Example of an arbiter PUF implementation. D is input; Q is output; Dff is a D flip-flop

The chaotic-BR-PUF hybrid scheme further strengthens this architecture by obfuscating the output of the basic BR ring through a nonlinear logistic mapping. This reduces the effectiveness of attacks to the level of random guessing (50–60%), while using comparable FPGA resources [32].

As evidenced by the use of ternary BR-PUF on carbon nanotube field-effect transistors (CNTFETs), which generates ternary responses, the current trend is towards multi-valued logic. This expands the CRP space to increase entropy without significantly raising hardware costs. Modeling on a 32-nm library of standard elements shows that it is more unpredictable and resistant to machine learning-based attacks than the binary prototype. Furthermore, the high-temperature stability of CNTFET transistors makes this approach particularly promising for IoT devices [33].

Arbiter PUFs (A-PUFs)

This type of PUF operates by comparing the transit times of two signals propagating along theoretically symmetrical paths. As shown in Fig. 6, the A-PUF module consists of several cells that connect the signal source to the arbiter component.

Each cell contains a switch that can route signals through other signal lines. The arbiter component outputs a binary signal whose value depends on which of the two input signals, which are separated from the signal source, reaches the component first. Due to random variations in the conductors and switching elements through which the signals pass, their speeds will vary relative to each other. Therefore, the challenge is based on the on/off switching nature of the routing switches (and the multiplicity of the number/position of the arbiter in these systems), while the response depends on the faster path after switching.

If the setup/hold time is violated, the arbitrator may enter a metastable state, which can affect its operation. This state is not determined by the comparison of signal propagation times, but rather by random noise in the responses (see [8] for more details).

This type of PUF has the advantage of being simple to implement and having a small footprint, with one n-stage A-PUF consisting of $2n$ multiplexers and one arbiter implemented as a D flip-flop. With $n = 64$, the circuit occupies only a few hundred gates. Since the spread of delays sufficient to generate random differences is preserved as process technology norms decrease, the corresponding device can be easily scaled up on silicon. Practical implementations of A-PUFs, particularly in more complex design modifications, demonstrate a level of uniqueness close to the theoretically optimal value of 50%. An analysis of publications on A-PUFs reveals a variety of implementation methods. In addition to the basic A-PUF structure, the review [3] provides brief descriptions of modifications to this architecture, including two-channel and multi-channel variants with XOR elements, multiplexer-based circuits and combinations with RO-PUF. However, the vulnerability of conventional A-PUF functions to machine learning-based attacks significantly limits their applicability in secure environments with limited resources.

The architecture of the arbiter-type improved PUF is presented in [34–37]. Figure 7 [28] shows an example of an implementation where several independent modules

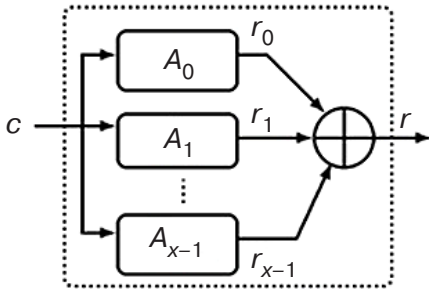

Fig. 7. A-PUF modification with response combination using the XOR function.
Here, c is challenge, A_0, ..., A_{x-1} represent A-PUF instances; r_0, ..., r_{x-1} are responses from A-PUF instances; and r is the XOR response from the A-PUF

are combined by the XOR function to form a single response.

Another architecture[6] involves a feed-forward memory-based arbiter (FF-MB-A) PUF module which combines weak PUF modules based on volatile memory with nonlinear feedback logic in order to increase entropy and enhance resistance to simulation attacks. A comprehensive experimental system was developed to evaluate the proposed solution, using up to 50 mln call-response pairs (CRPs). The results showed that the number and exact location of feedback cycles critically affect simulation resistance. To enable comparison with similar implementations, this work implemented and tuned the most advanced modeling strategies, including deep neural networks and the covariance matrix adaptation evolution strategy. The optimized FF-MB-A-PUF configuration, which incorporated 63 feedback cycles, exhibited robust resistance to simulation-based attacks, enhanced randomness (49.23%), and improved uniqueness between devices (49.20%), leading to balanced output distribution and high entropy. These results suggest that the FF-MB-A-PUF is a scalable, hardware-efficient, and secure primitive ideally suited to next-generation embedded systems and low-power IoT systems.

Typical methods for stabilizing A-PUF against noise, aging, and voltage and temperature fluctuations are described in [37], in particular averaging and masking unstable bits.

PUFs based on clock signal delays (clock PUF)

In synchronous circuits, clock PUF [38] analyzes changes in the speed of signal propagation from the clock generator to various parts of the circuit itself on the basis of differences in manufacturing during its physical implementation. While modern IC designs aim to eliminate these parasitic phase shift effects, variations and distortions still occur. In this PUF variant, the delays of paired signals in presumably similar circuits are compared to uniquely characterize the circuit in a manner similar to an A-PUF. In this case, the challenge is the clock signal lines, and the response is the delay in each corresponding line.

In [39], a lightweight, symmetric version of the PUF based on a three-phase D flip-flop with increased uniqueness is proposed and implemented in an IC using standard 40-nm complementary MOS (CMOS) technology. Following the chip layout, simulation results predict the device's uniqueness to be 0.4994, the highest among all the considered architectures. Compared to an A-PUF, this device consumes 73.3% less power, occupies 93.6% less area, and uses 95.7% less energy per bit. The corresponding figures for RO-PUF are 98.3%, 96.9%, and 99.9%, respectively. Additionally, unlike other flip-flop-based PUFs, the proposed variant does not require a post-processing block to eliminate bias voltage, thus contributing to savings in the overall implementation area and system power. To demonstrate the concept, the device was implemented on a FPGA. As a means of comparing the performance of the considered architectures, a proposed figure of merit (FOM) considers power, reliability, delay, silicon area, and uniqueness. It should be noted that the proposed architecture provides the highest FOM of all the considered PUF architectures.

In [38], new PUF technologies are presented that extract bits from pairwise distortions between IC clock network domains. An algorithm was implemented to select equidistant receivers, route the reverse network and

[6] Mishra A. *Enhancing the security scalability of Arbiter PUFs using memory-based weak PUFs*. Thesis. West Lafayette (IN): Purdue University; 2025. https://hammer.purdue.edu/articles/thesis/enhancing_the_security_scalability_of_arbiter_pufs_using_memory-based_weak_pufs/28899152. Accessed July 19, 2025.

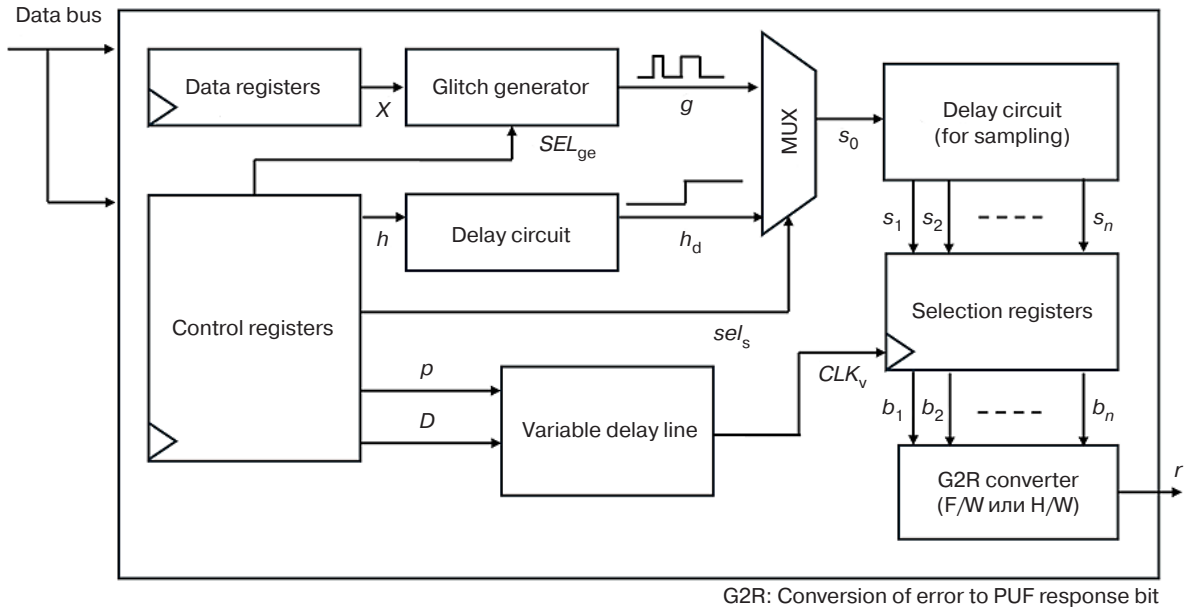

Fig. 8. Example of a device with glitch PUF [41].
Here, X is input data fed to the glitch generator; SEL_{ge} is the glitch generator output selection signal; g is the selected glitch generator output bit; s_0 is the initial Glitch-signal; $s_1, ..., s_n$ are signals after the delay circuit (sampling points); h is the calibration pulse; h_d is the calibration pulse after the delay circuit; sel_s is the input selection signal; p is the trigger signal; D is the time delay control code; CLK_v is the clock signal after variable delay; $b_1, ..., b_n$ are values read by the selection registers and representing the form of glitches; G2R is Glitch-to-Response (glitch-to-response conversion device); F/W is firmware; H/W is hardware; and r is response

then extract random bits for a specific chip. Evaluation of clock pulses based on a SPICE[7] simulation of 45 nm CMOS technology confirms the feasibility, stability, uniqueness, randomness, and low overhead of this implementation.

The analysis of clock signal phase shifting is also considered as an option in [40]. The proposed software-based PUF (S-PUF) option causes the video encoding circuit to malfunction using a clock signal. The response key with circuit characteristics is generated using the dependence of the response on the synchronization path. The video encoding circuit, which forms part of the IP core[8] of an open-source video encoding microcircuit, serves as the carrier circuit for the PUF. Based on an analysis of the timing path of the encoding circuit, a trigger signal is selected to place the circuit into abnormal operation mode. Random data is generated and subjected to video encoding and compression operations, which are then masked using Gray code and false bit exclusion operations. Test results show that this implementation of the proposed S-PUF variant passes the NIST test with 48.87% uniqueness and an autocorrelation coefficient of 0.0204 at 95% confidence.

PUFs based on transient processes (glitch PUFs)

These PUFs are more complex than RO-PUF and A-PUF schemes due to their analyzing the transient characteristics of signals that cause device malfunctions. In this PUF concept, the circuit itself is the challenge, while the response is the specific implementation of the glitches that occur and how they evolve over time (see the example in Fig. 8 [41, 42]).

In the glitch PUF architecture described in [41], glitches arising from changes in the delay between transistor gates in the circuit, which affect the pulse propagation characteristics from each gate, are used to form the PUF. The paper describes a procedure for simulating a simple implementation of such a circuit at the design stage. The results coincide well with the data obtained during the hardware implementation of such a PUF in real microcircuits.

As noted in [43], susceptibility to noise is an inherent issue in the hardware implementation of glitch PUF. To address this, the paper proposes a fault control module with a multi-level, parallel architecture

[7] Simulation program with IC emphasis is an open-source simulator of general-purpose electronic circuits.

[8] IP cores (intellectual property) are ready-made blocks for designing microchips.

for generating multi-bit stable information entropy. A noise reduction circuit has also been developed which uses a hysteresis effect, a feedback mechanism with Schmitt triggers and a pulse width detection circuit to filter out noise and extract output data from glitch signals during transient processes. A 128-bit glitch PUF circuit has been implemented using the TSMC[9] 65 nm CMOS technology. Experimental results demonstrate that the randomness (intra-distance = = 0.01) is 99.9%, while the uniqueness (inter-distance) is 50.03%. These results suggest that the proposed design could be widely adopted to enhance the security of IoT devices.

As stated in [44], the performance of such PUFs varies slightly due to environmental changes, necessitating error correction methods to eliminate these variations. One option for such a method is proposed. To demonstrate the effectiveness of this method quantitatively, evaluation experiments are conducted using an FPGA.

IMPLEMENTATION OF PUF BASED ON STATIC RANDOM-ACCESS MEMORY (SRAM)

SRAM-based PUFs

The implementation of PUFs based on static SRAM memory [45, 46] is rooted in the random distribution of the 6T memory cell states (Fig. 9), which determine their behavior when activated. This distribution is directly related to the manufacturing conditions and tolerances of the technological processes involved in forming the cells. The random initial state of the SRAM cells, which acts as a "fingerprint" of the chip, can be used either directly as a key or as a basis for generating responses to challenges. Therefore, compared to a standard SRAM array, only a controlled reset or power-up of the memory is required, and no additional energy is consumed in idle mode.

Studies have demonstrated that SRAM-PUFs have the capacity to provide near-perfect uniqueness. However, their reliability, which is limited by noise and environmental influences, is approximately 88–90% without correction [16]. To enhance the reliability of the output, averaging circuits (multiple reads at power-up) and error correction algorithms (e.g., Reed–Solomon code or fuzzy extractor) are employed [17].

Scaling of SRAM-PUF can be achieved as demonstrated by implementations in processes down to 7 nm, which show continued operability [18, 47]. However, reducing the size of transistor leads to a decrease in the absolute values of mismatches. This may necessitate more sophisticated bit processing (e.g., discarding unstable cells) to ensure reliability. Data from SRAM-based PUF experiments involving the inclusion of 8190 bytes of SRAM from various memory blocks on different FPGAs show that the average difference between two different blocks under fixed environmental conditions is μ_{inter} = 49.97%, while the average difference between multiple measurements in a single block is μ_{intra} = 3.57%. However, μ_{intra} increases to 12% for large temperature variations. The authors estimate the entropy content of SRAM turn-on states is to be 0.76 bits per SRAM cell.

Similar results are presented in [46, 48], which examine the behavior of SRAM when enabled on two different platforms. For 5120 blocks of 64 SRAM cells

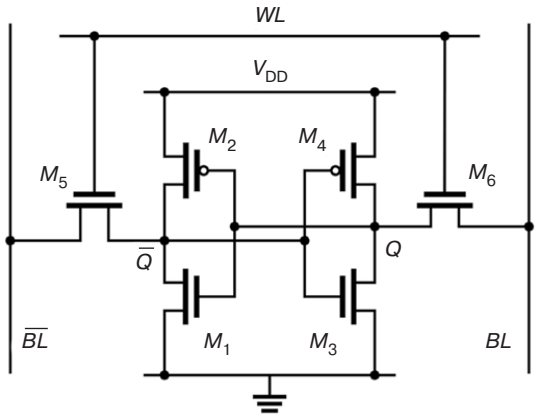

Fig. 9. 6T SRAM cell.
Here, *WL* is the word line, which controls two access transistors; V_{DD} is the power supply; M_1, ..., M_6 are MOS transistors; Q, $\overline{Q}$ are complementary data storage nodes; and $BL, \overline{BL}$ are complementary bit lines, which are used for writing and reading data

[9] The Taiwan Semiconductor Manufacturing Company (TSMC) is a manufacturer of ICs and semiconductor wafers.

measured on eight commercial SRAM chips, μ_{inter} and μ_{intra} values of 43.16% and 3.8%, respectively, are obtained. For 15 blocks of 64 SRAM cells from the built-in memory of three microcontroller chips, μ_{inter} and μ_{intra} values of 49.34% and 6.5%, respectively, are obtained.

One disadvantage of implementing a PUF on a FPGA in this way is due to the fact that, in the most common type of FPGA, all SRAM cells are reset to zero immediately after powering up, resulting in a loss of randomness. To address this issue, butterfly-type circuits and latch circuits have been proposed for use with PUFs. The butterfly circuit proposed in [49] consists of two cross-linked latches with a clock signal set to one, thereby simulating a combinational bistable element (Fig. 10).

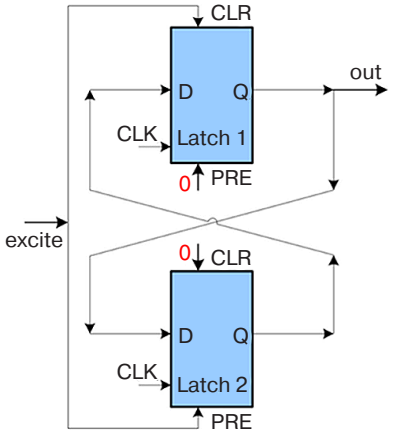

Fig. 10. Butterfly-type PUF [49].
Here, Latch 1/2 is a latch; excite is an initialization signal; CLR (clear) is an asynchronous latch reset input; PRE (preset) is an asynchronous latch preset input; CLK (clock) is a clock signal input; D is a latch data input; Q is a latch output; and out is a circuit output

The excite signal produces different levels (0/1) at the outputs of both elements, placing the cell in a metastable state. When the signal is removed, the circuit transitions to a random stable state. The specific value of this state is determined by the physical implementation of the latches and cross-connections forming the response bit. The measurement results presented in [50] are obtained using 64 circuits with a butterfly-type PUF on 36 PLDs. The values μ_{inter} = 50% and μ_{intra} < 5% are obtained at significant temperature fluctuations. As with other PUFs, error correction methods are employed in this type of PUF.

Another option for identifying the IC is proposed in [51]. Here, rather than cross-connecting two inverters or two latches, two NOR gates are cross-connected to form a NOR latch. When a reset signal is applied, the latch enters an unstable state and returns to one of two stable states depending on the mismatch between the internal electronic components. Tests involving 128 NOR latches are carried out on 19 ultra-large ICs produced using CMOS technology with 0.130 μm technology, resulting in values of μ_{inter} = 50.55% and μ_{intra} = 3.04%.

PUFs based on dynamic random-access memory (DRAM)

DRAM-PUF, another type of PUF based on volatile memory, is present in almost all modern computing devices, including resource-constrained embedded systems and IoT platforms. This makes it an attractive basis for embedded hardware security primitives. The large number of cells provides a significant pool of entropy and a potentially wide range of challenge-response pairs; moreover, DRAM can be accessed both during boot-up and while the system is running. These properties are particularly important in cases where classic discrete security modules are impossible or expensive to use. Additionally, DRAM typically consumes less power than SRAM for comparable capacity.

A typical 1T1C[10] DRAM cell comprises a transistor and a capacitor (see Fig. 11), and requires periodic refreshing due to charge leakage.[11]

The unique signature of a cell is created by differences that occur during manufacturing due to variations in capacitance, leakage currents, and threshold voltages. Leakage can occur within a row and between adjacent rows/lines. Active interaction between neighboring rows enhances charge flow, leading to bit inversions that increase entropy. The phenomenon of variable retention time is also observed, whereby the same cell switching unpredictably between states with high and low retention capacity. Finally, shortened read/write delays (e.g., tRCD[12] and tRP[13]) can cause cells to fail to settle correctly, forming a characteristic error pattern. These mechanisms of varying stability enable the creation of both reproducible PUFs (where unstable bits are discarded and/or errors are corrected) and high-entropy random number generators (TRNGs), which operate in modes where the result is as unstable as possible.

The DRAM-PUF studies are traditionally grouped according to the physical effect used, with start-up values when power is turned on, retention/decay when refresh is stopped or power is turned off (start-up DRAM-PUF,

[10] One-transistor, one-capacitor is a RAM cell consisting of one field-effect transistor and one capacitor.

[11] DRAM Scaling Challenges Grow. https://semiengineering.com/dram-scaling-challenges-grow/. Accessed July 19, 2025.

[12] Time row address to column address delay is row activation delay.

[13] Row precharge time is row refresh time.

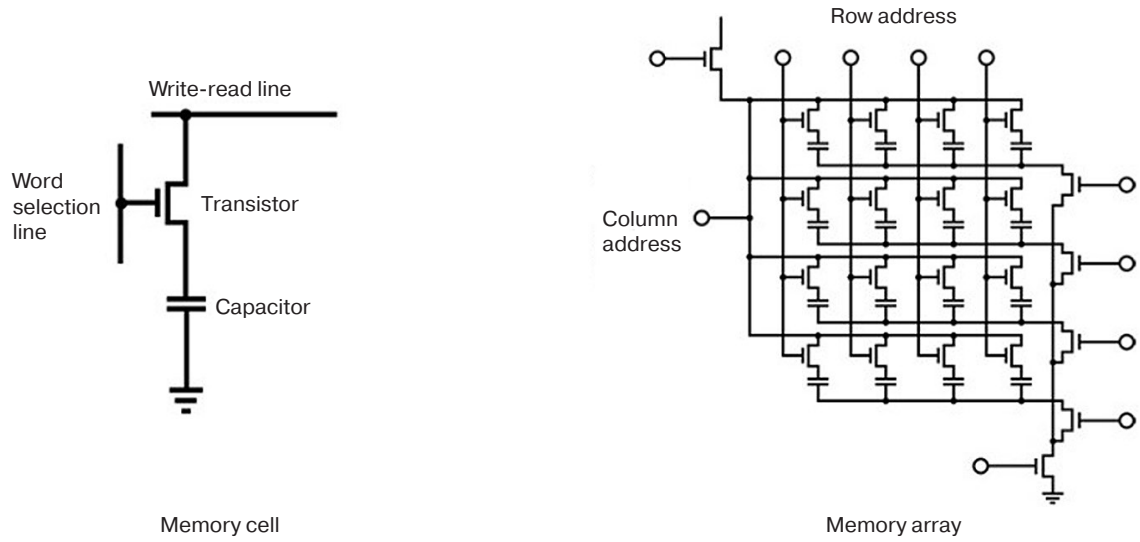

Fig. 11. DRAM memory and 1T1C cell

retention-based DRAM-PUF), and timing violations (latency-based DRAM-PUF). Solutions involving more specific effects are also being studied, including Rowhammer PUF and combined solutions.

The operation of the start-up DRAM-PUF is based on the initial distribution of cell charges after power is applied. In [52], the PUF's stability is examined in terms of temperature (0–80°C), power supply (4.5–5.5 V), and accelerated aging. The PUF, which is shown to be capable of forming 2048-bit responses (16 × 128-bit keys), features increased reliability through an algorithm for selecting cells with stable neighbors. Subsequent analysis shows that reducing the temperature and the supply voltage has a greater impact on stability than increasing them; the aging effect (negative bias temperature instability, NBTI) is moderate

Similar works have utilized the entire DRAM array as an "image" (converted to grayscale), with subsequent feature extraction by an artificial neural network for identification. A classification accuracy of ~98.8% was achieved, albeit in the absence of a detailed evaluation of classical PUF stability metrics [53]. The paper also discusses an attempt to improve randomness by post-processing LFSR.

Retention-based DRAM-PUF uses variations in charge retention time when auto-refresh (or power) is disabled and the array is read at specified intervals. The resulting pattern of bit inversions is unique to the memory segment. In [54], the possibility of reducing PUF waiting time to 20–60 s is demonstrated if the response is formed as a map of bit inversion locations. Uniqueness is demonstrated not only at the microcircuit level, but also between memory blocks within a single DRAM module. Reliability is maintained when the temperature changes within the range of 20–40°C ± 10°C; the effect of aging at 85°C for 48 h is additionally studied.

In latency-based DRAM-PUF, entropy is extracted from differences in cell access speeds. Implementing a PUF involves the controller deliberately underestimating the timings (tRCD, tRP, etc.), causing individual cells to produce read/write errors in characteristic positions. This architecture greatly speeds up the operation of the PUF, with a reported time of ~0.875 ms, which is more than 10000 times faster than typical retention DRAM-PUFs (approximately 10 s). The implementation example [54] uses tRP/tRCD variation to write a known pattern, reading with disrupted timings, and constructing entropy maps. Subsequently, XNOR filtering is employed to eliminate unstable bits.

The Rowhammer effect involves repeatedly accessing specific DRAM rows over a short period of time, causing accelerated charge leakage in neighboring rows and deterministic bit inversions. In [28], this phenomenon was first used to implement a PUF. The Rowhammer PUF method involves selecting two PUF memory rows from the DRAM array that are pre-filled with opposite patterns: 0x55 and 0xAA. At a certain point, the refresh of these rows is disabled, and they begin to discharge rapidly under the influence of two actively working (activation + precharge) neighboring Rowhammer rows to form a unique pattern.

Combined solutions, such as the combination of SRAM-PUF and DRAM-PUF, allow the advantages of different memory types to be combined and the disadvantages of each to be partially compensated. Implementations with high entropy, numerous CRPs,

and stable authentication over a wide temperature range (20–60°C) have been demonstrated.

A comparison of DRAM-PUF types reveals that, while most studies achieve an inter-HD value close to the ideal 50%, reliability varies depending on the class. Retention-based DRAM-PUFs are more sensitive to temperature and voltage, while latency-based DRAM-PUFs are usually more reproducible when the timing thresholds are selected correctly, and start-up DRAM-PUFs occupy an intermediate position, requiring algorithms to select stable cells [55].

Although a wide CRP space can be provided in principle by a large amount of DRAM, the number of stable bits suitable for use is sharply reduced in practice after reliability and randomness filtering. In application systems, most DRAM PUFs are therefore classified as weak PUFs (with a limited number of stable CRPs), which are primarily suitable for key generation and episodic authentication.

NVM-PUFs

NVM-PUFs use random variations in memory cell characteristics to create unique fingerprints of microcircuits. The key physical effects determining the uniqueness and stability of such PUFs are variations in materials and leakage currents, as well as stochastic switching processes.

In resistive random-access memory (ReRAM) PUF [56], the randomness comes from the stochastic process of formation of conductive sections in a dielectric; the switching thresholds and resistance of the high/low state vary slightly from cell to cell due to technological tolerances. In other ReRAM-PUF designs, the resistance spread in a pre-formed array is measured without overwriting it [57].

Similarly, the unique differences in magnetoresistive random-access memory (MRAM) are due to variations in the resistance of magnetic tunnel junctions (MTJs) that occur during production [58]. In MRAM, variability is influenced by the thickness of the barrier and the magnetic anisotropy of the MTJ; small variations result in differences in cell resistance within the same state. The reproducibility of the response is improved due to the significant stability of these technological variations over time.

In phase-change memory (PCM), in which each cell has a slightly different level of conductivity due to fluctuations in the structure during manufacturing or after switching to an amorphous state, the basis is taken from the differences in the material's states. This makes it possible to read the memory state as a random pattern [59]. To ensure reproducibility, the resistance drift of the amorphous state over time must be considered. Studies have shown that selection of the appropriate reading mode (e.g., differential) and calibration can minimize the impact of drift and generate stable bits [60].

The physical processes that generate randomness, such as the random formation of conducting channels, variations in tunnel resistance, and the dispersion of phase states, generate high entropy. Engineering solutions aim to minimize the instability of these effects to ensure reproducibility. Thus, ReRAM-, MRAM-, and PCM-PUF form the response bit either by directly reading the uncontrolled initial state of the cells or by using a special read/write mode that highlights the spread of cell characteristics. Recently, many PUF architectures based on these types of NVM have been proposed to improve their characteristics. The basic scheme is a weak PUF based on a memory array, where the response is formed from the state of numerous cells (for example, an *N*-bit starting vector is read from uninitialized memory). Although this approach is simple and economical, it provides a limited number of challenge-response pairs (a fixed fingerprint) [61].

The challenge-response space is expanded by using modified architectures to transfer them to the strong PUF class. ReRAM, for example, uses 2T2R and 1T4R cells to enable different methods of reading and comparing resistances. This results in a vast number of possible responses [59]. The paper proposes an approach in which the ReRAM array operates in the in-memory calculation mode. This is achieved by combining several cells *via* XOR or by reading using a special template to create an output that is insensitive to modeling and resistant to machine learning attacks.

In terms of circuit design, emphasis is also placed on the suppression of side channels. In particular, symmetrical structures (such as mirror-switched differential pairs of cells) eliminate systematic bias to increase the difficulty for an attacker to predict the outcome [57]. Modern implementations also include a self-destruct mode, whereby an increased voltage is provided to the ReRAM-PUF, irreversibly destroying part of the cells if an attacker attempts to access them, thus destroying the key [56].

NVM-PUFs can be found in a range of architectures, from compact embedded memory cells that produce a single hardcoded key to large-scale tunable arrays capable of generating multiple responses and resisting simulation attacks. NVM-PUFs are capable of providing near-ideal performance. In experiments with ReRAM, MRAM and PCM, uniqueness is usually around 50%, while the difference between repeated reads is less than 1–2%. Several papers report bit error rates of 0.01–0.1% without correction. For example, values of ~49.96% and ~0.98%, respectively, are obtained

for inter-HD and intra-HD in an MRAM-PUF based on an MTJ array. The entropy of the generated responses approaches the maximum value; the 0/1 distribution is typically around 50% (uniformity ~50%), as confirmed by NIST statistical randomness tests for PUF bit sequences. It is noted in reviews that, after unstable bits have been rejected, information saturation of approximately 1 bit of entropy per cell is provided by modern ReRAM-PUFs.

The reliability of NVM-PUFs is characterized by their ability to maintain a stable response to various disturbances, such as temperature changes, supply voltage, and component aging. Since the state of NVM is physically fixed (e.g., conducting regions in ReRAM, magnetic vectors in MRAM, and phase structures in PCM), such PUFs are less sensitive to external influences. For example, an MRAM-PUF demonstrates stability from −40 to 150°C [59]. ReRAM-PUF shows only a slight increase in resistance spread during temperature cycling (for example, from 25 to 125°C). It has been experimentally confirmed that >91% of bits remain error-free at 125°C [56]. The issue of aging has also been investigated. While slow degradation of the oxide conductive sections or tunnel barriers during the device's service life can increase bit errors, built-in threshold margins and correction algorithms can ensure long-term stability.

Although post-processing in memory-based schemes can reduce bias and improve statistical performance, it adds overhead and introduces potential vulnerabilities if applied incorrectly [55].

SUMMARY RESULTS FOR THE REVIEWED PUFs

The following table summarizes the characteristics of some of the key PUF options discussed in this series of reviewed papers. It reflects studies that produced original results following the implementation of one or more PUFs, where inter-distance and intra-distance were selected as key metrics. In a number of publications, these are referred to as uniqueness and reliability, respectively.

Sensitivity to external conditions indicates the voltage/temperature variations at which the characteristics are measured and how much they change. If such data is provided, the intra-distance changes are indicated in parentheses.

The "Estimated implementation complexity" column (high, medium, or low) is intended to demonstrate the relative hardware costs of implementing a particular type of a PUF, as well as the technical complexity involved, such as balancing paths, selecting element parameters, and changing technical processes.

Table. Summary results for the reviewed PUFs

PUF type/operation	Publication year	PUF characteristics					
		Inter-distance	Intra-distance	Platform	Inter-distance		Estimated implementation complexity
					Temperature	Voltage	
RO [7]	2007	46.15%	0.48%	15 × Xilinx Virtex-4 LX25 FPGA	−20–120°C	1.2 V ± 10%	medium
Arbiter [7]	2007	23%	0.7%	ASIC TSMC 180-nm	20–70°C (+4.8%), 20–120°C (+9%)	±2% (+3.7%), ±33% (+9%)	medium
RO [10]	2009	47.8%	~0%	SPICE model 90-nm CMOS	−15–65°C	0.2–1.0 V (+7% at 0.5 V)	medium
SRAM PUF (FinFET[14] 16-nm) [17]	2022	–	14%	NVIDIA Jetson, 16-nm LP FinFET	0–85°C	–	low
SRAM PUF (FinFET 14-nm) [17]	2022	–	10%	NXP LPC, 14-nm LP FinFET	0–85°C	–	low
SRAM PUF (FinFET 7-nm) [17]	2022	–	11%	Xilinx Versal, 7-nm HP FinFET	0–85°C	–	low

[14] Fin field-effect transistor is a 3D-structured transistor.

Table. Continued

PUF type/operation	Publication year	PUF characteristics					
		Inter-distance	Intra-distance	Platform	Inter-distance		Estimated implementation complexity
					Temperature	Voltage	
TERO [19]	2014	48.07%	1.73%	FPGA (Altera Cyclone II)	–	–	medium
BR [22]	2011	49.8%	0.7%	FPGA (Xilinx Virtex-II Pro)	5–45°C (+2.7%)	±10% (+2.2%)	medium
CRO[23]	2024	45.5%	9.95%	ASIC 22-nm FDSOI	−40–70°C	0.72–0.88 V	medium
RO [26]	2025	–	0.38%	SPICE-model 55-nm CMOS	−50–200°C (+9.38%)	–	medium
Rowhammer [27]	2017	–	<5%	DDR3/4 DRAM	−40–60°C	–	low
XOR Arbiter [28]	2022	48.69%	0.59%	FPGA (Xilinx Artix 7)	0–85°C	0.95–1.05 V	medium
Pseudo-LFSR [29]	2011	65.6%	1.8%	FPGA (Xilinx Virtex 5)	–	1 V	medium
TERO [30]	2016	47.22%	2.36%	FPGA (Xilinx Spartan 6)	−15–65°C	1.1–1.3 V	medium
TERO [30]	2016	48.58%	2.66%	FPGA (Altera Cyclone V)	−15–65°C	1.05–1.15 V	medium
XOR BR [31]	2015	14.8%	0.8%	FPGA (Xilinx Spartan 6)	27–75°C	–	medium
BR [32]	2021	48.0%	–	FPGA (Xilinx Artix 7)	–	–	medium
BR [33]	2024	66.26%	1.58%	SPICE-model CNTFET 32-nm CMOS	0–100°C	0.8–1.0 V	medium
Eye-Opening Arbiter[15] [37]	2025	44.99%	3.49%	FPGA (Xilinx Zynq-7010)	−40–125°C	0.81–0.99 V	medium
Clock [38]	2013	50.11%	1.19%	SPICE-model 45-nm CMOS	–	–	medium
Tri-state Flip-Flop[16] [39]	2020	~49%	~2%	FPGA (Altera Cyclone)	–	–	low
Overclocking clock software[17] [40]	2025	48.87%	–	SPICE model TSMC 65-nm CMOS	−25–125°C	1.0–1.4 V	low
Glitch [41]	2010	~32%	1.3%	FPGA Xilinx XC3S400A–4FTG256C (16 boards)	100°C (+5.3%)	–	medium
Glitch PUF with a Schmitt Trigger [43]	2021	50.03%	–	ASIC TSMC 65-nm CMOS	−25–125°C	0.8–1.4 V	medium
SRAM [45]	2007	49.97%	3.57%	FPGA	−20–80°C	–	low

[15] Arbiter PUF with a phase window.
[16] PUF based on high-impedance flip-flops.
[17] S-PUF based on overclocking.

Table. Continued

PUF type/operation	Publication year	PUF characteristics					
		Inter-distance	Intra-distance	Platform	Inter-distance		Estimated implementation complexity
					Temperature	Voltage	
Butterfly [49]	2007	~50%	~10%	FPGA (Xilinx Virtex-5)	−20–80°C	–	medium
MRAM [58]	2024	49.96%	0.98%	MRAM (STT[18]-MRAM array)	−25–100°C	0.65–0.85 V	medium
3D ReRAM [60]	2022	49.4%	0.014%	ReRAM (8-layer 3D array)	0–80°C (+1.93%)	1.65–2.2 V (+1.93%)	high
Dual-Mode[19] ReRAM [61]	2025	~50%	~1%	ReRAM (1T1R cells + logic)	–	–	high

CONCLUSIONS

A class of devices known as PUFs is based on the time characteristics of signals. These devices use frequency, phase, and transient analysis to generate responses due to manufacturing variations. Such solutions typically necessitate a carefully balanced combination of layout, calibration, and post-processing modules to ensure a consistent response. The advantage of these functions is that they offer virtually unlimited space for challenge-response pairs, making them ideal for authentication protocols. However, they are vulnerable to simulation-based attacks.

Memory-based PUFs create a "fingerprint" of the initial states and/or characteristics of SRAM/DRAM/NVM arrays. These functions can be easily integrated into existing on-chip blocks and are highly reproducible at moderate overhead costs. However, the space of the challenge-response pairs is typically limited, restricting their use to tasks such as key generation and device identification.

Stabilization measures for operating conditions (temperature, supply voltage, and aging) and the use of auxiliary data, error correction, and/or analysis modules are important for both classes. The selection of a particular PUF should be predicated on the requirements of the application and the target platform.

ACKNOWLEDGMENTS

This work was supported by the Ministry of Science and Higher Education of the Russian Federation (State task for universities No. FSFZ-2026-0003) and using the equipment of the Center for Collective Use of RTU MIREA (agreement dated September 01, 2021, No. 075-15-2021-689, unique identification number 2296.61321X0010).

Authors' contributions

E.Ph. Pevtsov—study conceptualization, review outline and structure, manuscript writing.

T.A. Demenkova—study conceptualization, review outline and structure, synthesis of the results.

Yu.A. Korotaev—literature analysis and systematization, manuscript writing, synthesis of the results.

A.S. Sigov—scientific consulting, scientific editing, final approval of the manuscript.

All authors have read and approved the published version of the manuscript.

[18] Spin-torque-transfer.
[19] Dual-channel RAM mode.

REFERENCES

1. Khalil K., Idris H., Idriss T., Bayoumi M. *Lightweight Hardware Security and Physically Unclonable Functions: Improving Security of Constrained IoT Devices*. Cham: Springer Nature Switzerland; 2025, 152 p.
2. McGrath T., Bagci I.E., Wang Z.M., Roedig U., Young R.J. A PUF taxonomy. *Appl. Phys. Rev.* 2019;6(1):011303. https://doi.org/10.1063/1.5079407
3. Zerrouki F., Ouchani S., Bouarfa H. A survey on silicon PUFs. *J. Syst. Archit.* 2022;127:102514. https://doi.org/10.1016/j.sysarc.2022.102514
4. Alhamarneh R.A., Mahinderjit Singh M. Strengthening Internet of Things Security: Surveying Physical Unclonable Functions for Authentication, Communication Protocols, Challenges, and Applications. *Appl. Sci.* 2024;14(5):1700. https://doi.org/10.3390/app14051700
5. Tehranipoor M., Pundir N., Vashistha N., Farahmandi F. *Hardware Security Primitives*. Cham: Springer; 2023, 350 p.
6. Maes R., Verbauwhede I. Physically Unclonable Functions: A Study on the State of the Art and Future Research Directions. In: Sadeghi A.-R., Naccache D. (Eds.). *Towards Hardware-Intrinsic Security: Foundations and Practice*. Berlin: Springer; 2010. P. 3–37. https://doi.org/10.1007/978-3-642-14452-3_1
7. Suh G.E., Devadas S. Physical Unclonable Functions for Device Authentication and Secret Key Generation. In: *Proceedings of the 44th ACM/IEEE Design Automation Conference* (*DAC 2007*), San Diego, CA, USA, June 4–8, 2007. New York: ACM; 2007. P. 9–14. https://doi.org/10.1145/1278480.1278484
8. Lebedev V.R., Pevtsov E.F., Demenkova T.A., Maleto M.I., Filimonov V.V. Method for studying the implementation of Physical Unclonable Function in information systems. *Int. J. Open Inf. Technol.* 2024;12(1):28–36 (in Russ.). Available from URL: http://injoit.org/index.php/j1/article/view/1712. Accessed July 10, 2025.
9. Gassend B., Clarke D., van Dijk M., Devadas S. Silicon physical random functions. In: *Proceedings of the 9th ACM Conference on Computer and Communications Security* (*CCS 2002*), Washington, DC, USA, November 18–22, 2002. New York: ACM; 2002. P. 148–160. https://doi.org/10.1145/586110.586132
10. Vivekraja V., Nazhandali L. Circuit-level techniques for reliable physically unclonable functions. In: *Proceedings of the 2009 IEEE International Workshop on Hardware-Oriented Security and Trust* (*HOST 2009*), San Francisco, CA, USA, July 27, 2009. Piscataway, NJ: IEEE; 2009. P. 30–35. https://doi.org/10.1109/HST.2009.5225054
11. Pappu R., Recht B., Taylor J., Gershenfeld N. Physical one-way functions. *Science*. 2002;297(5589):2026–2030. https://doi.org/10.1126/science.1074376
12. Anandakumar N.N., Hashmi M.S., Tehranipoor M. FPGA-based Physical Unclonable Functions: A comprehensive overview of theory and architectures. *Integration*. 2021;81:175–194. https://doi.org/10.1016/j.vlsi.2021.06.001
13. Cao Y., Xu J., Wu J., Wu S., Huang Z., Zhang K. Advances in Physical Unclonable Functions Based on New Technologies: A Comprehensive Review. *Mathematics* (*Basel*). 2024;12(1):77. https://doi.org/10.3390/math12010077
14. Vatalaro M., De Rose R., Lanuzza M., Crupi F. Weak physically unclonable functions in CMOS technology: A review. *Chips*. 2025;4(1):3. https://doi.org/10.3390/chips4010003
15. Sklavos N., Chaves R., Di Natale G., Regazzoni F. *Hardware Security and Trust: Design and Deployment of Integrated Circuits in a Threatened Environment*. Cham: Springer; 2017, 254 p. https://doi.org/10.1007/978-3-319-44318-8
16. Lata K., Cenkeramaddi L.R. FPGA-Based PUF Designs: A comprehensive review and comparative analysis. *Cryptography*. 2023;7(4):55. https://doi.org/10.3390/cryptography7040055
17. Masoumian S., Selimis G., Wang R., Schrijen G-J., Hamdioui S., Taouil M. Reliability analysis of FinFET-based SRAM PUFs for 16 nm, 14 nm and 7 nm technology nodes. In: *Proceedings of the 2022 Design, Automation & Test in Europe Conference & Exhibition* (*DATE 2022*), Antwerp, Belgium, March 14–23, 2022. Piscataway, NJ: IEEE; 2022. P. 1189–1192. https://doi.org/10.23919/DATE54114.2022.9774735
18. Eiroa S., Baturone I., Acosta A.J., Dávila J. Using physical unclonable functions for hardware authentication: A survey. In: *Proceedings of the 25th Conference on Design of Circuits and Integrated Systems* (*DCIS 2010*), Lanzarote, Canary Islands, Spain, November 17–19, 2010. Lanzarote; 2010. Available from URL: https://digital.csic.es/bitstream/10261/96029/1/Using%20Physical.pdf
19. Bossuet L., Ngo X.T., Cherif Z., Fischer V. A PUF based on a transient effect ring oscillator and insensitive to locking phenomenon. *IEEE Trans. Emerg. Top. Comput.* 2014;2(1):30–36. https://doi.org/10.1109/TETC.2013.2287182
20. Brzuska C., Fischlin M., Schröder H., Katzenbeisser S. Physically uncloneable functions in the universal composition framework. In: Rogaway P. (Ed.). *Advances in Cryptology – CRYPTO 2011*, Santa Barbara, CA, USA, August 14–18, 2011. Book Series: Lecture Notes in Computer Science. Berlin: Springer; 2011. V. 6841. P. 51–70. https://doi.org/10.1007/978-3-642-22792-9_4

21. Tuyls P., Schrijen G-J., Škorić B., van Geloven J., Verhaegh N., Wolters R. Read-proof hardware from protective coatings. In: Goubin L., Matsui M. (Eds.). *Cryptographic Hardware and Embedded Systems. CHES 2006*, Yokohama, Japan, October 10–13, 2006. Book Series: Lecture Notes in Computer Science. Berlin: Springer; 2006. V. 4249. P. 369–383. https://doi.org/10.1007/11894063_29
22. Chen Q., Csaba G., Lugli P., Schlichtmann U., Rührmair U. The bistable ring PUF: a new architecture for strong physical unclonable functions. In: *Proceedings of the 2011 IEEE International Symposium on Hardware-Oriented Security and Trust* (*HOST 2011*), San Diego, CA, USA, June 5–6, 2011. Piscataway, NJ: IEEE; 2011. P. 134–141. https://doi.org/10.1109/HST.2011.5955011
23. Abulibdeh E., Saleh H., Mohammad B., Al-Qutayri M., Veeran A. Area and power efficient implementation of configurable ring oscillator PUF. *TechRxiv Preprint*; April 2, 2024. https://doi.org/10.36227/techrxiv.171207533.30573247/v1
24. Abulibdeh E., Saleh H., Mohammad B., Al-Qutayri M., Hussain A. Kernel-based response extraction approach for efficient configurable ring oscillator PUF. *Sci. Rep.* 2025;15:5938. https://doi.org/10.1038/s41598-025-89769-5
25. Ivaniuk A.A., Yarmolik V.N. Configurable ring oscillator with controlled interconnections. *Bezopasnost' informatsionnykh tekhnologii = IT Security* (*Russia*). 2024;31(2):121–133 (in Russ.). https://doi.org/10.26583/bit.2024.2.08
26. Du H., Guo C., Cui S. Optimization design of the RO PUF temperature reliability based on MOSFET temperature characteristics. In: *The International Conference Optoelectronic Information and Optical Engineering* (*OIOE 2024*), Wuhan, China, October 18–20, 2024. Proc. SPIE 13513; 2025. Art. 1351324. https://doi.org/10.1117/12.3045630
27. Schaller A., Xiong W., Anagnostopoulos N.A., Saleem M.U., Gabmeyer S., Katzenbeisser S., Szefer J. Intrinsic Rowhammer PUFs: Leveraging the Rowhammer effect for improved security. In: *Proceedings of the 2017 IEEE International Symposium on Hardware-Oriented Security and Trust* (*HOST 2017*), McLean, VA, USA, May 1–5, 2017. Piscataway, NJ: IEEE; 2017. P. 1–7. https://doi.org/10.1109/HST.2017.7951729
28. Anandakumar N.N., Hashmi M.S., Chaudhary M.A. Implementation of efficient XOR arbiter PUF on FPGA with enhanced uniqueness and security. *IEEE Access*. 2022;10:129832–129842. https://doi.org/10.1109/ACCESS.2022.3228635
29. Hori Y., Kang H., Katashita T., Satoh A. Pseudo-LFSR PUF: A compact, efficient and reliable physical unclonable function. In: *Proceedings of the 2011 International Conference on Reconfigurable Computing and FPGAs* (*ReConFig'11*), Cancun, Mexico, November 30 – December 2, 2011. Cancun: IEEE; 2011. P. 223–228. https://doi.org/10.1109/ReConFig.2011.72
30. Marchand C., Bossuet L., Cherkaoui A. Enhanced TERO-PUF implementations and characterization on FPGAs. In: *Proceedings of the 2016 ACM/SIGDA International Symposium on Field-Programmable Gate Arrays* (*FPGA 2016*), Monterey, CA, USA, February 21–23, 2016. New York: ACM; 2016. P. 282. https://doi.org/10.1145/2847263.2847298
31. Xu X., Rührmair U., Holcomb D.E., Burleson W.P. Security evaluation and enhancement of bistable ring PUFs. In: Mangard S., Schaumont P. (Eds.). *Radio Frequency Identification. RFIDSec 2015*. Book Series: Lecture Notes in Computer Science. Cham: Springer; 2015. V. 9440. P. 3–16. https://doi.org/10.1007/978-3-319-24837-0_1
32. Thirumoorthi M., Jovanovic M., Mirhassani M., Khalid M.A.S. Design and evaluation of a hybrid chaotic-bistable ring PUF. *IEEE Trans. Very Large Scale Integr.* (*VLSI*) *Syst.* 2021;29(11):1912–1921. https://doi.org/10.1109/TVLSI.2021.3111588
33. Sharifi F., Momeni H., Hosseini A. Ternary bistable ring PUF for high-secure applications. *J. Supercomput.* 2024;80: 12663–12685. https://doi.org/10.1007/s11227-024-05935-y
34. Rührmair U., van Dijk M. On the practical use of physical unclonable functions in oblivious transfer and bit commitment protocols. *J. Cryptogr. Eng.* 2013;3(1):17–28. https://doi.org/10.1007/s13389-013-0052-8
35. Rührmair U. Oblivious transfer based on physical unclonable functions. In: Acquisti A., Smith S.W., Sadeghi A.-R. (Eds.). *Trust and Trustworthy Computing. TRUST 2010*. Berlin: Springer; 2010. V. 6101. P. 430–440. https://doi.org/10.1007/978-3-642-13869-0_31
36. Roy A., Roy D., Stănică P. On combining Arbiter based PUFs. *Cryptogr. Commun.* 2025;17(2):493–510. https://doi.org/10.1007/s12095-024-00769-0
37. Driemeyer B., Mandry H., Wiens D.-P., Becker J., Kauffman J.G., Ortmanns M. An eye-opening Arbiter PUF for fingerprint generation using auto-error detection for PVT-robust masking and bit stabilization achieving a BER of 2e-8 in 28 nm CMOS. In: *Proceedings of the 2025 IEEE International Solid-State Circuits Conference* (*ISSCC 2025*), San Francisco, CA, USA, February 16–20, 2025. Piscataway, NJ: IEEE; 2025. P. 300–302. https://doi.org/10.1109/ISSCC49661.2025.10904785
38. Yao Y., Kim M., Li J., Markov I., Koushanfar F. ClockPUF: physical unclonable functions based on clock networks. In: *Proceedings of the Design, Automation & Test in Europe Conference & Exhibition* (*DATE 2013*), Grenoble, France, March 18–22, 2013. Piscataway, NJ: IEEE; 2013. P. 422–427. https://doi.org/10.7873/DATE.2013.095
39. Khan S., Shah A.P., Chouhan S.S., Roy A., Roy D., Stănică P. Utilizing manufacturing variations to design a tri-state flip-flop PUF for IoT security applications. *Analog Integr. Circ. Sig. Process.* 2020;103:477–492. https://doi.org/10.1007/s10470-020-01642-9

40. Yuan T., Wang P., Zhang Y., Zhou Z. An overclocking clock software PUF circuit with no additional hardware resource overhead based on video coding circuit. *Integration*. 2025;101:102319. https://doi.org/10.1016/j.vlsi.2024.102319
41. Suzuki D., Shimizu K. The Glitch PUF: a new Delay-PUF architecture exploiting glitch shapes. In: Mangard S., Standaert F.-X. (Eds.). *Cryptographic Hardware and Embedded Systems. CHES 2010*, August 17–20, 2010. Santa Barbara, CA, USA. Book Series: Lecture Notes in Computer Science. Berlin: Springer; 2010. V. 6225. P. 366–382. https://doi.org/10.1007/978-3-642-15031-9_25
42. Anderson J. A PUF design for secure FPGA-based embedded systems. In: *Proceedings of the 15th Asia South Pacific Design Automation Conference* (*ASP-DAC 2010*), Taipei, Taiwan, January 18–21, 2010. Piscataway, NJ: IEEE; 2010. P. 1–6. https://doi.org/10.1109/ASPDAC.2010.5419927
43. Ni L., Wang P., Zhang Y., Chen J., Li L., Zhang H. A reliable multi-information entropy glitch PUF using Schmitt trigger sampling method for IoT security. In: *2021 IEEE 14th International Conference on ASIC* (*ASICON 2021*), Kunming, China, October 26–29, 2021. Piscataway, NJ: IEEE; 2021. P. 1–4. https://doi.org/10.1109/ASICON52560.2021.9620406
44. Nozaki Y., Takemoto S., Yoshikawa M. Error correction method for lightweight cipher PRINCE-based physically unclonable function. In: *Proceedings of the 6th International Conference on Information Technology and Computer Communications* (*ITCC 2024*), Xi'an, China, July 5–7, 2024. New York: ACM; 2024. P. 38–42. https://doi.org/10.1145/3704391.3704397
45. Guajardo J., Kumar S.S., Schrijen G-J., Tuyls P. FPGA intrinsic PUFs and their use for IP protection. In: Paillier P., Verbauwhede I. (Eds.). *Cryptographic Hardware and Embedded Systems – CHES 2007*, Vienna, Austria, September 10–13, 2007. Lecture Notes in Computer Science. Berlin: Springer; 2007. V. 4727. P. 63–80. https://doi.org/10.1007/978-3-540-74735-2_5
46. Holcomb D.E., Burleson W.P., Fu K. Initial SRAM state as a fingerprint and source of true random numbers for RFID tags. *Proceedings of the Conference on RFID Security*. 2007;7(2):01–012.
47. Gebali F., Mamun M. Review of physically unclonable functions (PUFs): Structures, models, and algorithms. *Front. Sens.* 2022;2:751748. https://doi.org/10.3389/fsens.2021.751748
48. Holcomb D.E., Burleson W.P., Fu K. Power-up SRAM state as an identifying fingerprint and source of true random numbers. *IEEE Trans. Comput.* 2009;58(9):1198–1210. https://doi.org/10.1109/TC.2008.212
49. Kumar S., Guajardo J., Maes R., Schrijen G-J., Tuyls P. The butterfly PUF: protecting IP on every FPGA. In: *Proceedings of the IEEE International Workshop on Hardware-Oriented Security and Trust* (*HOST 2008*), Anaheim, CA, USA, June 3–4, 2008. Piscataway, NJ: IEEE; 2008. P. 67–70. https://doi.org/10.1109/HST.2008.4559053
50. Farha F., Ning H., Ali K., Chen L., Nugent C. SRAM-PUF-based entities authentication scheme for resource-constrained IoT devices. *IEEE Internet Things J.* 2021;8(7):5904–5913. https://doi.org/10.1109/JIOT.2020.3032518
51. Su Y., Holleman J., Otis B. A 1.6 μJ/bit stable chip-ID generating circuit using process variations. In: *Proceedings of the IEEE International Solid-State Circuits Conference* (*ISSCC 2007*), San Francisco, CA, USA, February 11–15, 2007. Piscataway, NJ: IEEE; 2007. P. 606–611. https://doi.org/10.1109/ISSCC.2007.373466
52. Tehranipoor F., Karimian N., Yan W., Chandy J.A. Investigation of DRAM PUFs reliability under device accelerated aging effects. In: *Proceedings of the 2017 IEEE International Symposium on Circuits and Systems* (*ISCAS 2017*), Baltimore, MD, USA, May 28–31, 2017. Piscataway, NJ: IEEE; 2017. P. 1–4. https://doi.org/10.1109/ISCAS.2017.8050629
53. Yue M., Karimian N., Yan W., Anagnostopoulos N.A., Tehranipoor F. DRAM-based authentication using deep convolutional neural networks. *IEEE Consum. Electron. Mag.* 2021;10(4):8–17. https://doi.org/10.1109/MCE.2020.3002528
54. Sutar S., Raha A., Raghunathan V. D-PUF: an intrinsically reconfigurable DRAM PUF for device authentication in embedded systems. In: *Proceedings of the 2016 International Conference on Compilers, Architectures and Synthesis of Embedded Systems* (*CASES 2016*), Pittsburgh, PA, USA, October 2–7, 2016. New York: ACM; 2016. P. 1–10. https://doi.org/10.1145/2968455.2968519
55. Chew Y.Y., Lim W.L., Tan J.L., Ooi C.Y. In-depth review and comparative analysis of DRAM-based PUFs. *IEEE Access*. 2025;13:79367–79384. https://doi.org/10.1109/ACCESS.2025.3566068
56. Wilson T., Cambou B. Tamper-sensitive pre-formed ReRAM-based PUFs: Methods and experimental validation. *Front. Nanotechnol.* 2022;4:1055545. https://doi.org/10.3389/fnano.2022.1055545
57. Napolean A., Sivamangai N.M., Sharon N., Naveen Kuma R. Review on resistive random access memory based physical unclonable function circuits for high security. *Procedia Environ. Sci. Eng. Manag.* 2023;10(1):41–52. Available from URL: http://www.procedia-esem.eu/pdf/issues/2023/no1/5_Napolean_22.pdf
58. Adel M.J., Rezayati M.H., Moaiyeri M.H., et al. A robust deep learning attack immune MRAM-based physical unclonable function. *Sci. Rep.* 2024;14:20649. https://doi.org/10.1038/s41598-024-71730-7
59. Go S.X., Wang Q., Lim K.G., Lee T.H., Bajalovic N., Loke D.K. Ultrafast near-ideal phase-change memristive physical unclonable functions driven by amorphous state variations. *Adv. Sci.* (*Weinh.*) 2022;9(36):e2204453. https://doi.org/10.1002/advs.202204453

60. Yang J., Lei D., Chen D., Li J., Jiang H., Luo Q., et al. Machine-learning-resistant 3D PUF with 8-layer stacking vertical RRAM and 0.014% bit error rate using in-cell stabilization scheme for IoT security applications. In: *2020 IEEE International Electron Devices Meeting* (*IEDM*), San Francisco, CA, USA, December 12–18, 2020. Piscataway, NJ: IEEE; 2020. P. 28.6.1–28.6.4. https://doi.org/10.1109/IEDM13553.2020.9372107
61. Li J., Cui Y., Gu C., Wang C., Liu W., Kvatinsky S. A highly reliable dual-mode RRAM PUF with key concealment scheme. *IEEE Trans. Comput.-Aided Des. Integr. Circuits Syst.* 2025. https://doi.org/10.1109/TCAD.2025.3536376

About the Authors

Evgenii Ph. Pevtsov, Cand. Sci. (Eng.), Director of Center for the Design of Integrated Circuits, Nanoelectronics Devices and Microsystems, MIREA – Russian Technological University (78, Vernadskogo pr., Moscow, 119454 Russia). E-mail: pevtsov@mirea.ru. Scopus Author ID 6602652601, ResearcherID M-2709-2016, RSCI SPIN-code 1410-2483, http://orcid.org/0000-0001-6264-1231

Tatyana A. Demenkova, Cand. Sci. (Eng.), Associated Professor, Computer Technology Department, Institute of Information Technologies, MIREA – Russian Technological University (78, Vernadskogo pr., Moscow, 119454 Russia). E-mail: demenkova@mirea.ru. Scopus Author ID 57192958412, ResearcherID AAB-3937-2020, RSCI SPIN-code 3424-7489, http://orcid.org/0000-0003-3519-6683

Yuri A. Korotaev, Postgraduate Student, Department of Nanoelectronics, Institute for Advanced Technologies and Industrial Programming, MIREA – Russian Technological University (78, Vernadskogo pr., Moscow, 119454 Russia). E-mail: korotaevyua@yandex.ru. RSCI SPIN-code 7428-683, https://orcid.org/0009-0000-3976-7872

Alexander S. Sigov, Academician at the Russian Academy of Sciences, Dr. Sci. (Phys.–Math.), Professor, President, MIREA – Russian Technological University (78, Vernadskogo pr., Moscow, 119454 Russia). E-mail: sigov@mirea.ru. Scopus Author ID 35557510600, ResearcherID L-4103-2017, RSCI SPIN-code 2869-5663, https://www.researchgate.net/profile/A_Sigov

Об авторах

Певцов Евгений Филиппович, к.т.н., директор структурного подразделения «Центр проектирования интегральных схем, устройств наноэлектроники и микросистем», ФГБОУ ВО «МИРЭА – Российский технологический университет» (119454, Россия, Москва, пр-т Вернадского, д. 78). E-mail: pevtsov@mirea.ru. Scopus Author ID 6602652601, ResearcherID M-2709-2016, SPIN-код РИНЦ 1410-2483, https://orcid.org/0000-0001-6264-1231

Деменкова Татьяна Александровна, к.т.н., доцент, кафедра вычислительной техники, Институт информационных технологий, ФГБОУ ВО «МИРЭА – Российский технологический университет» (119454, Россия, Москва, пр-т Вернадского, д. 78). E-mail: demenkova@mirea.ru. Scopus Author ID 57192958412, ResearcherID AAB-3937-2020, SPIN-код РИНЦ 3424-7489, https://orcid.org/0000-0003-3519-6683

Коротаев Юрий Александрович, аспирант, кафедра наноэлектроники, Институт перспективных технологий и индустриального программирования, ФГБОУ ВО «МИРЭА – Российский технологический университет» (119454, Россия, Москва, пр-т Вернадского, д. 78). E-mail: korotaevyua@yandex.ru. SPIN-код РИНЦ 7428-6831, https://orcid.org/0009-0000-3976-7872

Сигов Александр Сергеевич, академик Российской академии наук, д.ф.-м.н., профессор, президент ФГБОУ ВО «МИРЭА – Российский технологический университет» (119454, Россия, Москва, пр-т Вернадского, д. 78). E-mail: sigov@mirea.ru. Scopus Author ID 35557510600, ResearcherID L-4103-2017, SPIN-код РИНЦ 2869-5663, https://www.researchgate.net/profile/A_Sigov

Translated from Russian into English by K. Nazarov
Edited for English language and spelling by Thomas A. Beavitt

Russian Technological Journal. 2026;14(2):103–112 ISSN 2500-316X (Online)

UDC 537.226.8
https://doi.org/10.32362/2500-316X-2026-14-2-103-112
EDN OEWULY

RESEARCH ARTICLE

Modeling of resonant excitation of ferroelectric lattice subsystem by terahertz radiation under nonequilibrium conditions

Natalia E. Sherstyuk [@], Kirill A. Brekhov, Elena D. Mishina

MIREA – Russian Technological University, Moscow, 119454 Russia
[@] Corresponding author, e-mail: nesherstuk@mail.ru

• **Submitted:** 28.03.2025 • **Revised:** 21.10.2025 • **Accepted:** 16.02.2026

Abstract

Objectives. The search for a fundamentally new, fast, and least dissipative method for controlling the ferroic order parameter is a pressing and ambitious task of basic and applied research on the development of low-dissipation and high-speed functional elements of information systems operating at terahertz (THz) frequencies for 6G[1] network technologies. The aim of the work is to study the conditions for modulating ferroelectric polarization using a short THz pulse. This will also include the influence of additional factors on the efficiency of the THz-induced dynamics of the ferroic order parameter, such as stationary heating and the application of an additional electric field to the ferroelectric.

Methods. The numerical simulation of resonant excitation of the lattice subsystem by THz radiation was performed for a $Ba_{0.8}Sr_{0.2}TiO_3$ ferroelectric film using the Landau–Khalatnikov equation system, and the equation of phonon mode oscillations with the phonon–phonon interaction as a driving force. The novelty of the proposed approach lies in the interaction of the THz pulse with a previously coherently excited phonon mode with a significant amplitude.

Results. The time dependencies were presented for the polarization and the effective amplitude of infrared-active mode oscillations with varying THz field parameters. The results also included constants of expansion of the thermodynamic potential of the nonequilibrium state in powers of order parameter in various exposure modes, including temperature changes and the application of an additional external electric field.

Conclusions. The approach proposed herein describes polarization switching under the action of a THz pulse with preliminary excitation of a coherent phonon by a femtosecond optical pulse. The most important parameter when determining the threshold effect of a THz pulse on phonon excitation is pulse energy (amplitude). In the region of small amplitudes, an increase in temperature does not exacerbate switching conditions.

Keywords: terahertz radiation, ferroelectrics, polarization, resonant excitation, phonon modes

[1] Sixth generation of mobile communications technology.

For citation: Sherstyuk N.E., Brekhov K.A., Mishina E.D. Modeling of resonant excitation of ferroelectric lattice subsystem by terahertz radiation under nonequilibrium conditions. *Russian Technological Journal.* 2026;14(2):103–112. https://doi.org/10.32362/2500-316X-2026-14-2-103-112, https://www.elibrary.ru/OEWULY

Financial disclosure: The authors have no financial or proprietary interest in any material or method mentioned.

The authors declare no conflicts of interest.

НАУЧНАЯ СТАТЬЯ

Моделирование резонансного возбуждения терагерцевым излучением решеточной подсистемы сегнетоэлектрика в условиях неравновесного состояния

Н.Э. Шерстюк [@], К.А. Брехов, Е.Д. Мишина

МИРЭА – Российский технологический университет, Москва, 119454 Россия
[@] Автор для переписки, e-mail: nesherstuk@mail.ru

• **Поступила:** 28.03.2025 • **Доработана:** 21.10.2025 • **Принята к опубликованию:** 16.02.2026

Резюме

Цели. Поиск принципиально нового наиболее быстрого и наименее диссипативного способа управления ферроидным параметром порядка является актуальной и весьма амбициозной задачей фундаментальных и прикладных исследований в области разработки малодиссипативных и быстродействующих функциональных элементов информационных систем, оперирующих на терагерцевых (ТГц) частотах, для сетевых технологий 6G[2]. Целью работы является исследование условий модуляции поляризации сегнетоэлектрика при помощи короткого ТГц-импульса, в т.ч. изучение влияния дополнительных факторов на эффективность ТГц-индуцированной динамики ферроидного параметра порядка.

Методы. Численное моделирование резонансного возбуждения ТГц-излучением решеточной подсистемы проводилось для сегнетоэлектрической пленки титаната бария-стронция $Ba_{0.8}Sr_{0.2}TiO_3$ на основе системы уравнений, состоящей из уравнения Ландау – Халатникова и уравнения колебаний фононной моды, где в качестве вынуждающей силы выступает фонон-фононное взаимодействие. Новизна подхода заключается во взаимодействии ТГц-импульса с ранее когерентно возбужденной фононной модой, имеющей значительную амплитуду.

Результаты. Представлены временные зависимости поляризации, а также эффективной амплитуды колебаний инфракрасно-активной моды при варьировании параметров ТГц-поля и констант разложения термодинамического потенциала неравновесного состояния в виде ряда по степеням параметра порядка в разных режимах воздействия, включая изменение температуры и дополнительное воздействие внешнего электрического поля.

Выводы. Предложенный подход описывает переключение поляризации под действием ТГц-импульса при предварительном возбуждении когерентного фонона фемтосекундным оптическим импульсом. Наиболее важным параметром, определяющим пороговое воздействие ТГц-импульса на возбуждение фонона, является энергия (амплитуда) импульса. В области малых амплитуд увеличение температуры не приводит к ухудшению условий переключения.

Ключевые слова: терагерцевое излучение, сегнетоэлектрики, поляризация, резонансное возбуждение, фононные моды

[2] Sixth generation – шестое поколение мобильной связи. [Sixth generation of mobile communications technology].

Для цитирования: Шерстюк Н.Э., Брехов К.А., Мишина Е.Д. Моделирование резонансного возбуждения терагерцевым излучением решеточной подсистемы сегнетоэлектрика в условиях неравновесного состояния. *Russian Technological Journal*. 2026;14(2):103–112. https://doi.org/10.32362/2500-316X-2026-14-2-103-112, https://www.elibrary.ru/OEWULY

Прозрачность финансовой деятельности: Авторы не имеют финансовой заинтересованности в представленных материалах или методах.

Авторы заявляют об отсутствии конфликта интересов.

INTRODUCTION

The development of terahertz (THz) devices is one of the most pressing areas in modern micro- and nanoelectronics and photonics. In addition to the methods of THz spectroscopy and visualization for diagnostics of materials already widely used, THz-range systems and functional devices designed to monitor and control THz signals are currently attracting increasing attention [1, 2]. The use of the THz range (0.1–10 THz) for data transmission has been shown to provide high throughput and data density, and is considered to be the most promising approach for 6G[3] network technologies [3, 4].

One of the key challenges in this area is the search for new materials to ensure efficient optical and/or electrical control of the generation, detection, and propagation of THz radiation. Ferroelectric materials play an important role in the study of functional devices operating in the THz range. This is due to their response time, low dielectric loss, and tunability. As demonstrated in a number of studies, the ability to manipulate optically the permittivity of thin ferroelectric films allows for significant modulation depth in the THz range. This is of great importance for the development of all-optical and hybrid chips.

It is important therefore to excite the soft mode of a ferroelectric and use this excitation to switch the polarization of the ferroelectric by a short THz pulse. The first works on THz excitation by relatively low fields (to 100 kV/cm) reported on coherent excitation of small-amplitude polar modes in strontium titanate ($SrTiO_3$) crystals [5], relaxor ferroelectrics [6], and an organic ferroelectric [7]. The progress achieved in recent years in the development of THz sources capable of generating pulses (including single ones) of high power has made it possible to observe not only the excitation of coherent phonons, but also ultrafast (subpicosecond) polarization switching. Such switching was recorded either directly by X-ray diffraction methods [8–11] or by optical methods [12–14]. Recent studies have also discussed the effect of an ultrashort electromagnetic pulse leading to two types of polarization switching: permanent switching, such that the switching to the opposite polarization state under an external action persists after the end of the action; and dynamic switching, such that, after exposure to a THz pulse, the polarization state can switch to the opposite state and back several times. Then eventually the system relaxes to the initial state.

While the problem of the direct influence on the soft mode has been resolved in a certain sense, the influence of phonon–phonon interaction on the processes is still actively debated. A number of studies have proposed an approach based on the Landau–Khalatnikov equation [15]. In such studies the influence on the soft mode is considered within the framework of a model for coupling between the Raman and infrared-active (IR-active) modes [16, 17]. Mankowsky et al. [13] and Subedi [18] proposed describing ultrafast polarization switching processes using an approach based on a nonlinear coupling between the low-frequency, fully symmetric phonon mode A_1. This involves the motion of cations and anions of the material in such a way the electric polarization is changed, as well as the highest-frequency, and IR-active phonon mode. In this case, the switching processes are characterized in terms of the displacements of ions in the crystal lattice, described by the generalized coordinates Q_{P} and Q_{IR}. The coupling between the modes is proportional to the product of the generalized coordinate of the polar mode and the square of the generalized coordinate of the IR-active mode. This allows different switching conditions to be assumed for polarization vectors directed in opposite directions before the start of the action. However, Mertelj and Kabanov [19] indicated that such a representation is erroneousness due to the symmetry of the transformation. They proposed to consider the product of the squares of the generalized coordinates of the polar and IR-active modes as the main term. It was also noted that the products of the first powers of the generalized coordinates of the polar and IR-active modes also satisfy the symmetry conditions. However, when considered without the quadratic term, they do not explain the experimental dependencies presented by Mankowsky et al. [13].

The aforementioned models describing the modulation of polarization and its permanent switching yield unstable solutions. Small changes in any parameter cause an abrupt change in the properties of the system, as

[3] Sixth generation of mobile communications technology.

described by the Landau–Khalatnikov equation, taking into account the strong nonlinearity of polarization near resonance [20]. Therefore, it is important to consider possible additional influences on the ferroelectric such as: heating, electric field, and optical illumination. A comprehensive solution to this problem will only be possible with the identification of physical mechanisms capable of achieving practical polarization switching using an electromagnetic pulse.

In this paper, we considered the processes of modulation of the polarization of a ferroelectric by a short THz pulse using barium strontium titanate $Ba_{0.8}Sr_{0.2}TiO_3$ (BST) as an example. An extension of the theoretical model [19] was presented using two terms in the expansion of the phonon–phonon interaction energy: the sum of the linear and quadratic terms over the product of the generalized coordinates of the polar and IR-active modes. The simulation took into account the conditions of experimental observation of the THz-induced modulation of the ferroelectric polarization in the optical pumping–THz probing geometry.

CALCULATION METHOD

Polarization switching under the action of a THz pulse with preliminary excitation of a coherent phonon by a femtosecond optical pulse

Let us consider a system consisting of unexcited ferroelectric cells with a two-minimum potential and an optically excited phonon in the field of a THz pulse. In this case, excitation of the soft mode via phonon–phonon interaction is energetically more favorable. Since the polarization of a ferroelectric is determined by the asymmetric displacement of cations and anions in the crystal structure, excitation of a coherent optical phonon increases the effective vibration amplitude of the corresponding group of atoms. This amplitude, which increases with increasing optical pulse intensity, will serve as the initial condition in the problem under consideration.

Let us also assume that a THz pulse, resonant with the ferroelectric's soft mode, is incident on the ferroelectric after some delay. Thus, the soft mode will be excited both directly by the THz pulse and through phonon–phonon interaction by an optical phonon. This in turn, was excited by femtosecond optical pumping. The question to be addressed is as follows: will this interaction be more effective than direct interaction with a single THz pulse, and will it lead to a higher probability of polarization switching in the ferroelectric?

Since BST is a multiaxial ferroelectric, its order parameter is multicomponent. In accordance with the ap proach published [13, 18, 19], we will restrict ourselves to considering the change in the polarization state under the action of the selective excitation of lattice vibrations by the electric field of a short THz pulse along the direction specified by the polarization plane of the THz radiation. In the initial state, we assume that the polarization caused by the total dipole moment of the set of cells considered in the region of action of the THz pulse is zero.

Taking into account Mertelj and Kabanov's comment [19], we can write the interaction energy of the polar and IR-active modes per unit volume in the following form:

$$W(\xi_P, \xi_{IR}) = j\xi_P\xi_{IR} + h\xi_P^2\xi_{IR}^2,$$

wherein ξ_P and ξ_{IR} are the effective coordinates of the polar and high-frequency phonon (IR-active) modes, respectively; and j and h are the expansion coefficients of $W(\xi_P, \xi_{IR})$ in powers of coordinates.

In accordance with Mertelj and Kabanov [19], since the coupling coefficient between the polar and IR-active modes depends significantly on the effective coordinate of the polar mode, the potential energy describing the phonon–phonon interaction must be physically significant, if the displacement of the polar ion relative to the equilibrium position is small. Within the framework of this model, the modulation of the effective coordinates does not exceed 5% of the lattice parameter. However, for the case of dynamic polarization switching, i.e., the hopping of a polar ion from one well to another, this restriction is imposed on the modulation of the effective coordinate ξ_P after such a hop.

Considering the definition of dielectric polarization $P = \frac{q_P\xi_P}{V}$ (where q_P is the effective charge, the displacement of which determines the excitation of the polar mode, and V is the cell volume), expressing the polar coordinate ξ_P through polarization, and introducing the notations $C_1 = j\frac{V}{q_P}$ and $C_2 = h\left(\frac{V}{q_P}\right)^2$, we can write the interaction energy in the following form:

$$W(P, \xi_{IR}) = C_1P\xi_{IR} + C_2P^2\xi_{IR}^2. \quad (1)$$

The equation of oscillations of the effective coordinate of the IR-active phonon mode is the equation of an anharmonic oscillator:

$$\ddot{\xi}_{IR} = 2\gamma_{IR}\dot{\xi}_{IR} + \omega_{IR}^2\xi_{IR} = -\frac{V}{m_{IR}}F_{IR}, \quad (2)$$

where γ_{IR} is the attenuation coefficient, and the right-hand side is determined by the derivative of free energy (1) with respect to the corresponding coordinate:

$$F_{IR} = -\frac{\partial W(\xi_P, \xi_{IR})}{\partial \xi_{IR}}.$$

In accordance with the Landau–Khalatnikov equation, the equation describing the dynamics of the order parameter under damping conditions takes the following form [20]:

$$\ddot{P} + \gamma\dot{P} + \frac{1}{\mu}(a_1 P + a_{11}P^3 + a_{111}P^5 + a_{1111}P^7) = \\ = \frac{1}{\mu}F_P + \frac{1}{\mu}E(t). \quad (3)$$

Here, $F_P = -\frac{\partial W(\xi_P, \xi_{IR})}{\partial \xi_P}$, $\mu = \frac{m_P V}{q_P^2}$, and $E(t) = E_{ext}(t) + E_1(t)$ is the electric field acting on the ferroelectric, equal to the sum of the external field $E_{ext}(t)$ and the depolarizing field $E_1(t)$.

The external field is a time-dependent electrical component of a picosecond THz pulse: $E_{ext}(t) = E_{THz} e^{-\frac{4t^2}{\tau^2}} \frac{\sin z}{z}$, where $z = \omega_{THz} t$; and ω_{THz} and τ are the central frequency and the inverse attenuation of the THz field, respectively. These parameters were chosen to match the temporal shape of the calculated pulse with the experimental pulse, and are equal to $\omega_{THz} = 2\pi \cdot 1.5 \frac{\text{rad}}{\text{s}}$ and τ = 0.5 ps. The depolarizing field is directly proportional to the polarization: $E_1(t) = E_{0,dep}\frac{P(t)}{P_S}$, wherein P_S is the spontaneous polarization corresponding to the position in one of the minima [21], and depolarizing field $E_{0,dep} = \frac{P_S}{\varepsilon\varepsilon_0}$.

Finally, using the introduced notations, we obtain a system of equations

$$\ddot{P} + \gamma_P\dot{P} + \frac{1}{\mu}(2a_1 P + 4a_{11}P^3 + 6a_{111}P^5 + 8a_{1111}P^7) = \\ = -\frac{1}{\mu}(C_1\xi_{IR} + C_2 P\xi_{IR}^2) + \frac{1}{\mu}E(t), \quad (4)$$

$$\ddot{\xi}_{IR} = 2\gamma_{IR}\dot{\xi}_{IR} + \omega_{IR}^2\xi_{IR} = -\frac{V}{m_{IR}}(C_1 P + C_2 P^2\xi_{IR}). \quad (5)$$

The experiment for which the simulation was performed can be carried out by means of the THz pumping–probing method in transmission geometry. Under THz pumping, several scenarios are possible (Fig. 1): (1) the THz field amplitude is insufficient for the effective charge to overcome the potential barrier, and the system oscillates around the initial minimum and returns to its initial state; (2) the effective charge overcomes the potential barrier but then returns to the initial minimum; and (3) the effective charge overcomes the potential barrier and remains at the opposite minimum of the double-well potential for a long time. The first two scenarios describe dynamic polarization switching, while the last describes a permanent one.

In the simulation using the system of equations (4)–(5), the time dependencies were calculated for the polarization and the effective amplitude of the IR-active mode oscillations parallel to the crystallographic axis *c*. The following parameters were varied: the THz field amplitude E_{THz}; the values of the phonon–phonon interaction constants C_1 and C_2; and the attenuation coefficient γ_{IR} of the IR-active mode.

The most important varying parameter was also the initial condition. This was determined by the intensity of optical radiation for the IR-active mode amplitude. The simulation used the parameters of the expansion of the thermodynamic potential in a series in powers of the order parameter (hereinafter referred to as the Landau expansion) for a $Ba_{0.8}Sr_{0.2}TiO_3$ film [22]: $a_1 = -0.13 \cdot 10^8$ J·m/C^2, $a_{11} = -1.33 \cdot 10^8$ J·m^5/C^4, $a_{111} = 1.03 \cdot 10^9$ J·m^9/C^6, and $a_{1111} = 3.09 \cdot 10^{10}$ J·m^{13}/C^8.

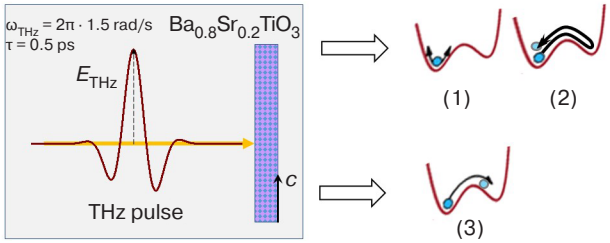

Fig. 1. Schematic diagram of the experiment for which the simulation is performed and a schematic representation of the THz-induced processes of the polarization switching scenarios under consideration

The frequency $\omega_{IR}/2\pi$ = 7.55 THz was chosen as the resonant frequency of the IR-active phonon. This corresponds to the frequency of the A_1 (transverse optical) mode [23]. Figure 2 presents the simulation results.

The first calculation was made with varying initial conditions for the IR-active mode (A_{IR} = 0.1–0.23 Å), while the amplitude of the THz field was insignificant (incapable of causing polarization switching, see the lowermost curve in Fig. 2b). In the calculations, it was assumed that at the initial moment, the total polarization of the cell array under consideration is zero. The other parameters were chosen as follows: $\gamma_{IR} = 0.5$ ps^{-1}, $\gamma_P = 2$ ps^{-1}, $C_1 = 5 \cdot 10^{17}$ J/(C·m^2), and $C_2 = 5 \cdot 10^{29}$ J/(C^2·m).

The corresponding time dependencies of the amplitude of the IR-active mode itself and the ferroelectric polarization are shown in Figs. 2a and 2b, respectively. The bottom graph in Fig. 2b presents the time dependence of the THz field (thin maroon line). The insets of Figs. 2b and 2c show the polarization

spectra at A_{IR} = 0.23 Å and E_{THz} = 0.8 MV/cm, respectively. The graphs are shifted along the vertical axis for clarity. Dynamic polarization switching occurs already at the initial IR-active mode oscillation amplitude A_{IR} = 0.13 Å. With increasing A_{IR}, dynamic polarization switching is observed in all curves. However, due to the stochastic nature of the solution to the Landau–Khalatnikov equation, given small changes in the variable parameters, permanent switching (i.e., a transition from one of the minima of the potential well to another without a reverse transition at large times) is not possible at all values of the parameters. For example, in Fig. 2, there is no permanent transition at A_{IR} = 0.17 Å.

The polarization spectrum (Fig. 2b, inset) exhibits frequencies of both modes: the polar mode in the 1–2 THz range; and the IR-active mode in the 7.55 THz range. Since no features are observed in the time dependencies of polarization at the time delay corresponding to the THz pulse (2 ps), the conclusion can be drawn that the effects observed are associated solely with the action of a coherent optical phonon.

Let us now consider the case of a weak initial IR oscillation (A_{IR} = 0.125 Å), incapable of causing dynamic polarization switching, but with an increase in the THz field. Switching appears at $E_{THz} \geq 0.8$ MV/cm. The IR-active mode is weakly manifested in the polarization spectra (Fig. 2c, inset). By increasing the THz field amplitude, stable polarization switching is achieved.

Overall, the system of equations considered here does indeed describe polarization switching under the influence of a THz pulse with preliminary excitation of a coherent phonon by a femtosecond optical pulse. The critical effect of the THz pulse, leading to phonon excitation, occurs when the THz pulse has an energy slightly lower (in our calculations, by a maximum of 20%) than the energy required for switching without optical stimulation. Then, the combined effect of these two excitations leads to polarization switching.

Influence of an additional external electric field

Let us consider the influence of an additional applied electric field E_0 directed parallel to the field E_{THz} of the THz pulse in the plane of the surface of the material. In both cases, the field strengths are chosen in such a way that one field in the absence of the other does not cause polarization switching. In the first case, this condition corresponds to E_{THz} = 0.7 MV/cm (E_0 = 0), while in the second, it corresponds to E_0 = 0.5 MV/cm (E_{THz} = 0). Figure 3 shows the simulation results. The graphs are shifted along the vertical axis for clarity.

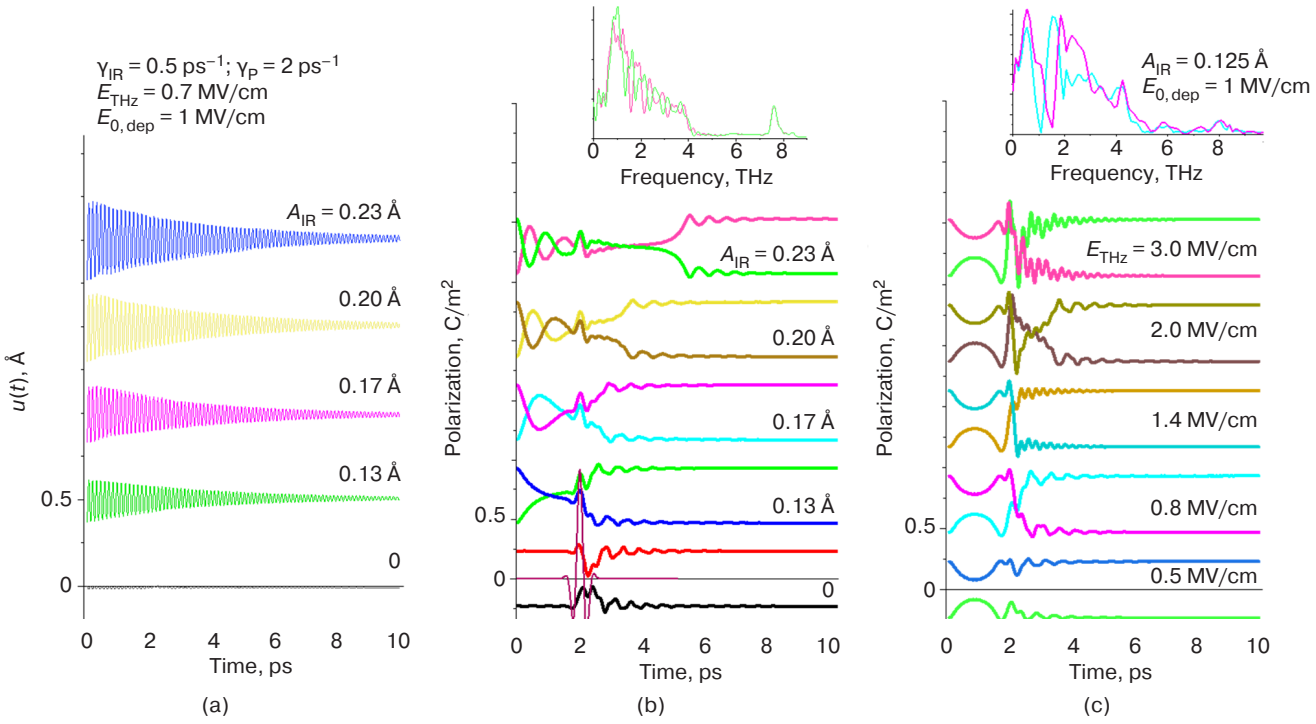

Fig. 2. (a) Time dependencies of the effective coordinate $u(t)$ of the IR-active mode, calculated with varying initial effective amplitude A_{IR} of the IR-active mode at a low field of the THz pulse (the values of the phonon–phonon interaction constants are taken to be equal to $C_1 = 5 \cdot 10^{17}$ J/(C·m^2) and $C_2 = 5 \cdot 10^{29}$ J/(C^2·m)). Time dependencies of the polarization in cells with the opposite initial positions of the effective charge, calculated within the framework of the considered model with varying (b) A_{IR} and (c) the THz pulse field at a small initial amplitude of the IR-active mode

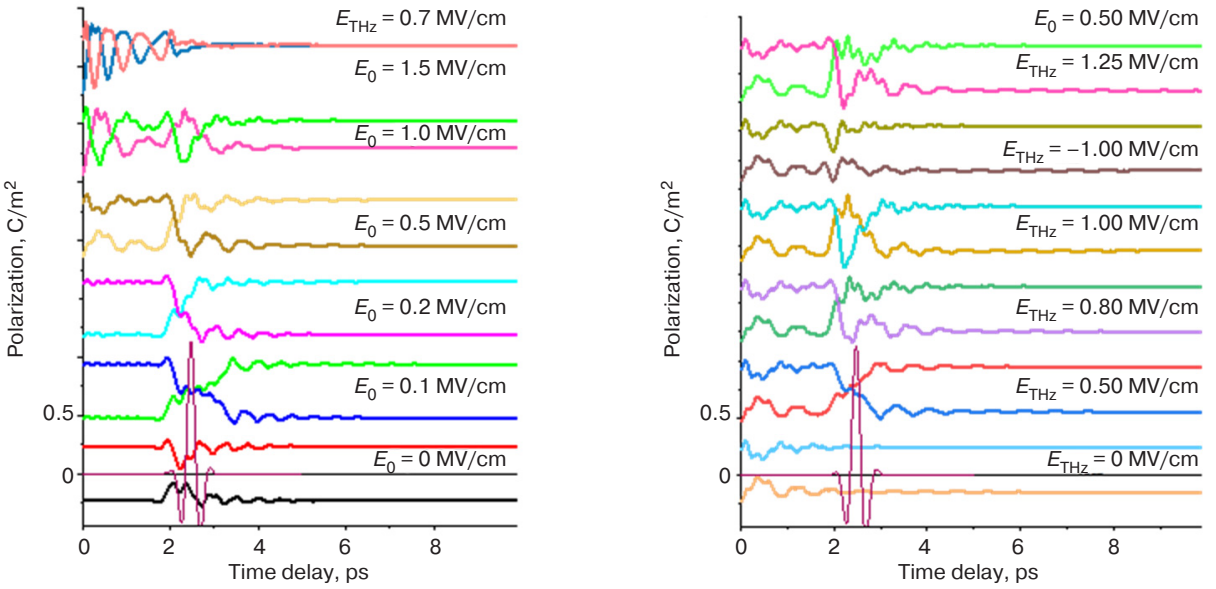

Fig. 3. Time dependencies of polarization upon application of an additional constant electric field (a) with increasing strength of the constant field while maintaining the THz pulse amplitude and (b) with increasing THz pulse amplitude while maintaining the strength of the constant field

At the same THz pulse field (Fig. 3a), the constant field with $E_0 \geq 0.1$ MV/cm ($E_0/E_{THz} = 0.14$) leads to switching of polarization. In this case, also at certain strengths of the constant field ($E_0 = 1$ MV/cm), both ions return to their original state. At fields $E_0 \geq 0.1$ MV/cm, oscillations caused by the constant field alone are observed during the time preceding the THz pulse. The combined action of the constant and THz fields leads to dynamic polarization switching in both cells up to $E_0 = 1.5$ MV/cm ($E_0/E_{THz} = 2.14$). Further, the THz pulse has practically no effect, and the entire system switches under the influence of a constant field, leading to uniform polarization in the direction of the constant field.

With an increase in the amplitude of the THz field and maintaining the strength of the constant field (Fig. 3b), dynamic switching is observed from $E_{THz} = 0.5$ mV/cm ($E_0/E_{THz} = 1$). At some THz field strengths, permanent switching is absent in both branches (0.9 MV/cm < E_{THz} < 1.2 MV/cm), while the behavior of the system at positive values of the constant field (codirectional with the THz pulse field at the point of its maximum amplitude) and its negative values is different. Figure 3b shows the dependencies at $E_0 = -1$ MV/cm, in which even dynamic switching is absent (polarization does not intersect the coordinate axis). A further increase in the THz pulse field leads to the predominance of the response to this pulse, although the constant field has a slight effect on the time dependence of polarization.

All the dependencies presented here are illustrative. The temporal behavior of polarization depends on many parameters (Landau expansion constants and the associated frequency, as well as the soft-mode coefficient).

Nevertheless, an important result of these calculations is the establishment of the fact that even a weak constant field can effectively facilitate polarization switching. This result is extremely important for the experimental observation of polarization switching. Strong THz fields, firstly, are not always achievable and, secondly, can lead to irreversible changes in the physical properties of ferroelectrics [24]. We also noted that the enhancement of the effect of a THz field was previously observed in magnetic materials during studies of magnetization switching in a constant magnetic field.

CONCLUSIONS

This paper proposes a new approach to describing a system with polarization as an order parameter pre-exposed to a femtosecond optical pulse. A phonon mode was excited which subsequently interacted with a high-power THz pulse. The approach is based on a system of the Landau–Khalatnikov equation (where the electric field of the THz pulse and the phonon–phonon interaction act as the driving force) and the phonon mode oscillation equation (where the phonon–phonon interaction acts as the driving force). The novelty of this approach lies in the interaction of the THz pulse with a previously coherently excited phonon mode of significant amplitude.

It was shown that switching occurs at the moment of arrival of a THz pulse, within the time interval of

high-amplitude phonon oscillations (determined by the damping constant of this mode). Phonon excitation exerts a critical effect when the THz pulse has an energy slightly lower (in our calculations, by a maximum of 20%) than the energy required for switching without optical stimulation. Then, the combined effect of these two excitations leads to polarization switching. If the field is strong (when polarization can be switched solely by a THz pulse), an increase in the phonon oscillation amplitude does not affect the switching process. Thus, preliminary optical stimulation can induce polarization switching at THz fields lower than the switching threshold. This is crucial for applications, since it allows the use of lower-power THz sources.

The same model considered an additional driving force in the Landau–Khalatnikov equation. It was shown that only low, far-from-saturating, constant fields can effectively promote switching. This result is important for its use in experiments. A negative experimental result had previously been obtained in which the application of a significant field had no effect on polarization switching. The model presented here may explain this result.

ACKNOWLEDGMENTS

The work was partially supported by the Russian Science Foundation, grant No. 25-19-00575 (modeling) and the Ministry of Science and Higher Education of the Russian Federation, State Assignment for Universities No. FSFZ-2023-0005 (code development, initial stages of modeling, experimental section).

Authors' contribution

All authors contributed equally to the research work.

REFERENCES

1. Leitenstorfer A., Moskalenko A.S., Kampfrath T., Kono J., Castro-Camus E., Peng K., Qureshi N., Turchinovich D., Tanaka K., Markelz A.G., Havenith M., Hough C., Joyce H.J., Padilla W.J., Zhou B., Kim K-Y., Zhang X.-C., Uhd Jepsen P., Dhillon S., Vitiello M., Linfield E., Davies A.G., Hoffmann M.C., Lewis R., Tonouchi M., Klarskov P., Seifert T.S., Gerasimenko Y.A., Mihailovic D., Huber R., Boland J.L., Mitrofanov O., Dean P., Ellison B.N., Huggard P.G., Rea S.P., Walker C., Leisawitz D.T., Gao J.R., Li C., Chen Q., Valûsis G., Wallace V.P., Pickwell-MacPherson E., Shang X., Hesler J., Ridler N., Renaud C.C., Kallfass I., Nagatsuma T., Zeitler J.A., Arnone D., Johnston M.B., Cunningham J. The 2023 terahertz science and technology roadmap. *J. Phys. D: Appl. Phys*. 2023;56:223001(67 p.). https://doi.org/10.1088/1361-6463/acbe4c
2. Brekhov K., Bilyk V., Ovchinnikov A., Chefonov O., Mukhortov V., Mishina E. Resonant Excitation of the Ferroelectric Soft Mode by a Narrow-Band THz Pulse. *Nanomaterials*. 2023;13(13):1961. https://doi.org/10.3390/nano13131961
3. Monnai Y., Lu X., Sengupta K. Terahertz Beam Steering: from Fundamentals to Applications. *J. Infrared, Milli. Terahz Waves.* 2023;44(3):169–211. https://doi.org/10.1007/s10762-022-00902-1
4. Quy V.K., Chehri A., Quy N.M., Han N.D., Ban N.T. Innovative Trends in the 6G Era: A Comprehensive Survey of Architecture, Applications, Technologies, and Challenges. *IEEE Access*. 2023;11:39824–39844. https://doi.org/10.1109/ACCESS.2023.3269297
5. Katayama I., Aoki H., Takeda J., Shimosato H., Ashida M., Kinjo R., Kawayama I., Tonouchi M., Nagai M., Tanaka K. Ferroelectric Soft Mode in a $SrTiO_3$ Thin Film Impulsively Driven to the Anharmonic Regime Using Intense Picosecond Terahertz Pulses. *Phys. Rev. Lett*. 2012;108(9):097401(5 p.). https://doi.org/10.1103/PhysRevLett.108.097401
6. Hoffmann M.C., Hwang H.Y., Brandt N.C., et al. Terahertz-induced Kerr-effect in Relaxor Ferroelectrics. *MRS Online Proceedings Library*. 2009;1230:408. https://doi.org/10.1557/PROC-1230-MM04-08
7. Yamakawa H., Miyamoto T., Morimoto T., Takamura N., Liang S., Yoshimochi H., Terashige T., Kida N., Suda M., Yamamoto H.M., Mori H., Miyagawa K., Kanoda K., Okamoto H. Terahertz-field-induced polar charge order in electronic-type dielectrics. *Nat. Commun*. 2021;12:953(11 p.). https://doi.org/10.1038/s41467-021-20925-x
8. Hamm P., Meuwly M., Johnson S.L., Beaud P., Staub U. Perspective: THz-driven nuclear dynamics from solids to molecules. *Struct. Dyn*. 2017;4(6):061601(19 p.). https://doi.org/10.1063/1.4992050
9. Chen F., Zhu Y., Liu S., Qi Y., Hwang H.Y., Brandt N.C., Lu J., Quirin F., Enquist H., Zalden P., Hu T., Goodfellow J., Sher M.-J., Hoffmann M.C., Zhu D., Lemke H., Glownia J., Chollet M., Damodaran, Park J., Cai Z., Jung I.W., Highland M.J., Walko D.A., Freeland J.W., Evans P.G., Vailionis A., Larsson J., Nelson K.A., Rappe A.M., Sokolowski-Tinten K., Martin L.W., Wen H., Lindenberg A.M. Ultrafast terahertz-field-driven ionic response in ferroelectric $BaTiO_3$. *Phys. Rev. B.* 2016;94(18):180104(6 p.). https://doi.org/10.1103/PhysRevB.94.180104
10. Kozina M., Pancaldi M., Bernhard C., van Driel T., Glownia J.M., Marsik P., Radovic M., Vaz C.A.F., Zhu D., Bonetti S., Staub U., Hoffmann M.C. Local terahertz field enhancement for time-resolved x-ray diffraction. *Appl. Phys. Lett*. 2017;110(8):081106. https://doi.org/10.1063/1.4977088
11. Kozina M., van Driel T., Chollet M., Sato T., Glownia J.M., Wandel S., Radovic M., Staub U., Hoffmann M.C. Ultrafast X-ray diffraction probe of terahertz field-driven soft mode dynamics in $SrTiO_3$. *Struct. Dyn*. 2017;4(5):054301(7 p.). https://doi.org/10.1063/1.4983153
12. Grishunin K.A., Ilyin N.A., Sherstyuk N.E., Mishina E.D., Kimel A., Mukhortov V.M., Ovchinnikov A.V., Chefonov O.V., Agranat M.B. THz Electric Field-Induced Second Harmonic Generation in Inorganic Ferroelectric. *Sci. Rep*. 2017;7(1):687. https://doi.org/10.1038/s41598-017-00704-9

13. Mankowsky R., von Hoegen A., Först M., Cavalleri A. Ultrafast Reversal of the Ferroelectric Polarization. *Phys. Rev. Lett*. 2017;118:197601(5 p.). https://doi.org/10.1103/PhysRevLett.118.197601
14. Bilyk V., Mishina E., Sherstyuk N., Bush A., Ovchinnikov A., Agranat M. Transient polarization reversal using intense THz pulse in silicon-doped lead germinate. *Physica Status Solidi* (*RRL*). *Rapid Research Letters*. 2021;15(1):2000460(5 p.). https://doi.org/10.1002/pssr.202000460
15. Landau L.D., Khalatnikov I.M. On anomalous absorption of sound near a second order phase transition point. *Doklady Akademii Nauk SSSR*. 1954;96:469–472 (in Russ.).
16. Juraschek D.M., Fechner M., Spaldin N.A. Ultrafast Structure Switching through Nonlinear Phononics. *Phys. Rev. Lett.* 2017;118:054101(5 p.). https://doi.org/10.1103/PhysRevLett.118.054101
17. Radaelli P.G. Breaking symmetry with light: Ultrafast ferroelectricity and magnetism from three-phonon coupling. *Phys. Rev. B*. 2018;97:085145(9 p.). https://doi.org/10.1103/PhysRevB.97.085145
18. Subedi A. Proposal for ultrafast switching of ferroelectrics using midinfrared pulses. *Phys. Rev. B.* 2015;92:214303(6 p.). https://doi.org/10.1103/PhysRevB.92.214303
19. Mertelj T., Kabanov V.V. Comment on "Ultrafast Reversal of the Ferroelectric Polarization". *Phys. Rev. Lett*. 2019;123:129701. https://doi.org/10.1103/physrevlett.123.129701
20. Blinc R., Žekš B. *Soft Modes in Ferroelectrics and Antiferroelectrics*: transl. from Engl. Moscow: Nauka; 1975, 398 p. (In Russ.).
[Blinc R., Žekš B. *Soft Modes in Ferroelectrics and Antiferroelectrics*. Amsterdam: North–Holland Publishing Company; 1974, 317 p.]
21. Abalmasov V.A. Ultrafast reversal of the ferroelectric polarization by a midinfrared pulse. *Phys. Rev. B*. 2020;101:014102(8 p.). https://doi.org/10.1103/PhysRevB.101.014102
22. Original Russian Text: Shirokov V.B., Yuzyuk Yu.I., Kalinchuk V.V., Lemanov V.V. Material constants of (Ba,Sr)TiO_3 solid solutions. *Fizika tverdogo tela*. 2013;55(4):709–714 (in Russ.). https://elibrary.ru/rcsvjh
[Shirokov V.B., Yuzyuk Yu.I., Kalinchuk V.V., Lemanov V.V. Material constants of (Ba,Sr)TiO_3 solid solutions. *Phys. Solid State*. 2013;55:773–779. https://doi.org/10.1134/S1063783413040276]
23. Anokhin A.S., Yuzyuk Yu.I., Lyanguzov N.V., Razumnaya A.G., Stryukov D.V., Bunina O.A., Golovko Yu.I., Shirokov V.B., Mukhortov V.M., El Marssi M. Direct transition from the rhombohedral ferroelectric to the paraelectric phase in a (Ba,Sr)TiO_3 thin film on a (111)MgO substrate. *Europhysics Letters*. 2015;112(4):47001(6 p). https://doi.org/10.1209/0295-5075/112/47001
24. Kwaaitaal M., Lourens D.G., Davies C.S., Kirilyuk A. Disentangling thermal birefringence and strain in the all-optical switching of ferroelectric polarization. *Sci. Rep.* 2024;14:24956(9 p.). https://doi.org/10.1038/s41598-024-75670-0

About the Authors

Natalia E. Sherstyuk, Dr. Sci. (Phys.–Math.), Professor, Department of Nanoelectronics, Institute for Advanced Technologies and Industrial Programming, MIREA – Russian Technological University (78, Vernadskogo pr., Moscow, 119454 Russia). E-mail: nesherstuk@mail.ru. Scopus Author ID 6602267129, ResearcherID A-3460-2014, RSCI SPIN-code 9016-8296, https://orcid.org/0000-0002-7068-4028

Kirill A. Brekhov, Cand. Sci. (Phys.–Math.), Senior Researcher, Laboratory of Physics for Neuromorphic Computing Systems, Institute for Advanced Technologies and Industrial Programming, MIREA – Russian Technological University (78, Vernadskogo pr., Moscow, 119454 Russia). E-mail: brekhov_ka@mail.ru. Scopus Author ID 55452447100, ResearcherID: Q-1014-2017, RSCI SPIN-code 9957-7662, https://orcid.org/0000-0001-9091-2609

Elena D. Mishina, Dr. Sci. (Phys.-Math.), Professor, Head of the Laboratory of Femtosecond Optics for Nanotechnology, Department of Nanoelectronics, Institute for Advanced Technologies and Industrial Programming, MIREA – Russian Technological University (78, Vernadskogo pr., Moscow, 119454 Russia). E-mail: mishina_elena57@mail.ru. Scopus Author ID 7005350309, ResearcherID D-6402-2014, RSCI SPIN-code 9352-8339, https://orcid.org/0000-0003-0387-5016

Об авторах

Шерстюк Наталия Эдуардовна, д.ф.-м.н., доцент, профессор кафедры наноэлектроники, Институт перспективных технологий и индустриального программирования, ФГБОУ ВО «МИРЭА – Российский технологический университет» (119454, Россия, Москва, пр-т Вернадского, д. 78). E-mail: nesherstuk@mail.ru. Scopus Author ID 6602267129, ResearcherID A-3460-2014, SPIN-код РИНЦ 9016-8296, https://orcid.org/0000-0002-7068-4028

Брехов Кирилл Алексеевич, к.ф-м.н., старший научный сотрудник, лаборатория физики нейроморфных вычислительных систем, Институт перспективных технологий и индустриального программирования, ФГБОУ ВО «МИРЭА – Российский технологический университет» (119454, Россия, Москва, пр-т Вернадского, д. 78). E-mail: brekhov_ka@mail.ru. Scopus Author ID 55452447100, ResearcherID: Q-1014-2017, SPIN-код РИНЦ 9957-7662, https://orcid.org/0000-0001-9091-2609

Мишина Елена Дмитриевна, д.ф.-м.н., профессор, заведующий лабораторией фемтосекундной оптики для нанотехнологий, кафедра наноэлектроники, Институт перспективных технологий и индустриального программирования, ФГБОУ ВО «МИРЭА – Российский технологический университет» (119454, Россия, Москва, пр-т Вернадского, д. 78). E-mail: mishina_elena57@mail.ru. Scopus Author ID 7005350309, ResearcherID D-6402-2014, SPIN-код РИНЦ 9352-8339, https://orcid.org/0000-0003-0387-5016

Translated from Russian into English by V. Glyanchenko
Edited for English language and spelling by Dr. David Mossop

Mathematical modeling

Математическое моделирование

UDC 004.9:539.17
https://doi.org/10.32362/2500-316X-2026-14-2-113-123
EDN CZALAC

RESEARCH ARTICLE

Influence of piston nonuniformity and illumination on the formation of a hypersonic shock wave in a laser-driven shock wave

Ivan G. Lebo [@], Victoria A. Komarova, Maxim A. Ryzhkov

MIREA – Russian Technological University, Moscow, 119454 Russia
[@] Corresponding author, e-mail: lebo@mirea.ru

• **Submitted:** 12.09.2025 • **Revised:** 24.11.2025 • **Accepted:** 05.02.2026

Abstract

Objectives. The study investigates the influence of inhomogeneities of laser flux intensity and piston (mylar film) thickness in a laser shock tube by comparing the conditions for the formation and dynamics of shock wave propagation in a laser shock tube in the case of an open and closed plasma corona.

Methods. Along with mathematical modeling methods, analysis of the results of computational experiments was carried out using the two-dimensional Lagrangian program *Atlant_C* in cylindrical coordinates were used.

Results. The results of four series of calculations of the dynamics of hypersonic shock waves in a laser shock tube are presented: (1) formation and propagation of a shock wave in a profiled target; (2) formation and propagation of a shock wave with strong inhomogeneity of the incident laser flux; (3) comparison of the dynamics of shock waves for different values of the absorbed laser pulse energy and target (piston) thicknesses; (4) comparison of shock wave dynamics in the cases of open and closed plasma coronas.

Conclusions. Based on the results of the computational experiments, the following conclusions can be drawn: (1) as a strong shock wave propagates in the profiled piston, the pressure and density equalize in the transverse direction. If the duration of the laser pulse is noticeably longer than the transit time of the transverse shock waves in the target (piston), the shock wave front flattens out in the gas inside the LUT cell; (2) in cases when the incident laser pulse contains significant emission intensities or speckles (more than 10% of the pulse energy), jets are formed in the accelerated piston, which can overtake the shock wave front in the gas; (3) during laser heating of the target in the closed corona mode, the propagation velocity of the shock wave front increases by ~40%; (4) when the piston is destroyed due to strong nonuniformity of irradiation or development of hydrodynamic instability and fragmentation of the polymer CH film, a dense turbulent layer can form, which will also create a shock wave in the gas. This case requires separate consideration.

Keywords: mathematical modeling, computational experiment, laser shock tube, two-dimensional Lagrangian code Atlant_C

For citation: Lebo I.G., Komarova V.A., Ryzhkov M.A. Influence of piston nonuniformity and illumination on the formation of a hypersonic shock wave in a laser-driven shock wave. *Russian Technological Journal.* 2026;14(2):113–123. https://doi.org/10.32362/2500-316X-2026-14-2-113-123, https://www.elibrary.ru/CZALAC

Financial disclosure: The authors have no financial or proprietary interest in any material or method mentioned.

The authors declare no conflicts of interest.

НАУЧНАЯ СТАТЬЯ

Влияние неоднородностей поршня и облучения на формирование гиперзвуковой ударной волны в лазерной ударной трубе

И.Г. Лебо [@], В.А. Комарова, М.А. Рыжков

МИРЭА – Российский технологический университет, Москва, 119454 Россия
[@] Автор для переписки, e-mail: lebo@mirea.ru

• **Поступила:** 12.09.2025 • **Доработана:** 24.11.2025 • **Принята к опубликованию:** 05.02.2026

Резюме

Цели. Цель исследования – изучение влияния неоднородностей интенсивности лазерного излучения и толщины поршня (лавсановой пленки) на формирование гиперзвуковых потоков в лазерной ударной трубе (ЛУТ), сравнение условий формирования и динамики распространения ударных волн (УВ) в ЛУТ в случаях «открытой» и «закрытой» плазменной короны.

Методы. Методы математического моделирования, анализ результатов вычислительных экспериментов, выполненных с помощью двумерной лагранжевой программы *Atlant_C* в цилиндрических координатах.

Результаты. Представлены результаты четырех серий расчетов динамики гиперзвуковых УВ в ЛУТ: 1) формирование и распространение УВ в профилированной мишени; 2) формирование и распространение УВ при сильной неоднородности падающего лазерного потока; 3) сравнение динамики УВ при различных значениях поглощенной энергии лазерного импульса и толщинах мишени (поршня); 4) сравнение динамики гиперзвуковых УВ с данными экспериментов в случаях «открытой» и «закрытой» плазменной короны.

Выводы. На основании данных вычислительных экспериментов можно сделать следующие выводы: 1) по мере распространения сильной УВ в профилированном поршне происходит выравнивание давления и плотности в поперечном направлении. Если длительность лазерного импульса заметно больше, чем время прохождения поперечных УВ в мишени (поршне), то в газе внутри ячейки ЛУТ происходит выполаживание фронта УВ; 2) в том случае, когда в падающем лазерном импульсе имеются значительные выбросы интенсивностей излучения – спеклы (~10% от энергии импульса), в ускоренном поршне формируются струи, которые в газе могут обгонять фронт УВ; 3) при лазерном нагреве мишени в режиме «закрытой» короны скорость поршня в ЛУТ возрастает примерно на 40%; 4) при разрушении поршня из-за сильной неоднородности облучения или развития гидродинамической неустойчивости и фрагментации полимерной CH-пленки, может формироваться плотный турбулентный слой, который будет также создавать УВ в газе.

Ключевые слова: математическое моделирование, вычислительный эксперимент, лазерная ударная труба, двумерная лагранжевая программа Atlant_C

Для цитирования: Лебо И.Г., Комарова В.А., Рыжков М.А. Влияние неоднородностей поршня и облучения на формирование гиперзвуковой ударной волны в лазерной ударной трубе. *Russian Technological Journal*. 2026;14(2):113–123. https://doi.org/10.32362/2500-316X-2026-14-2-113-123, https://www.elibrary.ru/CZALAC

Прозрачность финансовой деятельности: Авторы не имеют финансовой заинтересованности в представленных материалах или методах.

Авторы заявляют об отсутствии конфликта интересов.

INTRODUCTION

One of the most important and yet unsolved problems in laser thermonuclear fusion is associated with the development of hydrodynamic instability during the acceleration and compression of thermonuclear targets. Similar problems arise in astrophysics and in a number of applied problems involving high-energy concentrations [1, 2]. In modern theoretical physics, the construction of a physical and mathematical model of the transition from the evolutionary stage of hydrodynamic instability to a turbulent state is of fundamental importance.

Gas dynamics involving the development of hydrodynamic instability are described by equations of nonlinear partial differential equations (PDEs) in two-dimensional and three-dimensional geometries. Since such equations generally do not have analytical solutions, the use of mathematical modeling methods is required for analyzing the development of the associated processes. Complex software packages developed for these purposes must be tested on simplified problems (in particular, on car model solutions [3] and linearized equations describing the behavior of small perturbations of gas-dynamic quantities [4]), comparison with data from full-scale experiments [2, 5–8].

In order to achieve a numerical solution of the PDE system, various algorithms and mathematical codes are being developed [2, 5]. As a rule, the finite difference method is used [9–12]. Since the objects under study have a complex configuration that requires the use of difference grids having a large number of nodes along with corresponding random-access memory and high computer performance requirements, it is often necessary to resort to the development of parallel algorithms and calculations carried out on multiprocessor complexes to simulate physical processes [13].[1]

In the present work, mathematical modeling methods are used to investigate the acceleration of thin films in a laser shock tube (LST) [14]. The advantages of such a device are:

1) the formation of hypersonic shock waves (SW) with Mach numbers $M_x = V_{sw}/V_s \geq 10$ (where V_{sw} is the propagation velocity of the SW front, V_s is the speed of sound in the gas in front of the SW front) and gas flow velocities behind the SW front of the order of the first cosmic velocity;
2) miniaturization of the LST cell and the possibility of its quick replacement;
3) the ability to create complex configurations of obstacles for gas flow;
4) relatively low consumption of materials (e.g., inert gases or expensive mixtures).

1. PHYSICAL AND MATHEMATICAL FORMULATION OF THE PROBLEM

The calculations were performed using the two-dimensional Lagrangian program *Atlant_C* in cylindrical geometry (*r*—radius; *z*—coordinate along the axis; *t*—time) [5]. This program was developed by a team of authors to enable the solving nonlinear equations of plasma dynamics in Lagrangian coordinates in two-dimensional geometry numerically [5]. The advantage of Lagrangian coordinates is that they are "frozen" in matter. Therefore, during sublimation and compression of this substance (i.e., when the volume changes by several orders of magnitude), it is possible to maintain satisfactory approximation accuracy[2]. Below are the basic equations of plasma dynamics in a two-temperature approximation, which are solved in the *Atlant_C*.

$$\frac{d\rho}{dt} = -\rho\nabla\vec{v},$$

$$\rho\frac{d\vec{v}}{dt} = -\nabla(Z_i P_e + P_i),$$

$$Z_i\rho\frac{dE_e}{dt} = -Z_i P_e\nabla\vec{v} + \nabla(\kappa_e\nabla T_e) - Q_{ei} - R_{rad}(\rho, T_e) + \nabla\vec{q},$$

$$\rho\frac{dE_i}{dt} = -P_i\nabla\vec{v} + \nabla(\kappa_i\nabla T_i) + Q_{ei},$$

$$\left(\frac{\vec{q}}{|\vec{q}|}, \nabla\right)\vec{q} = \kappa(\rho, T_e)\vec{q},$$

$$P_e = P_e(\rho, T_e),\ P_i = P_i(\rho, T_i),$$

$$E_e = E_e(\rho, T_e),\ E_i = E_i(\rho, T_i),$$

$$Q_{ei} = Q_0(\rho, T_e)\frac{T_e - T_i}{T_e^{1.5}}\rho^2.$$

[1] In [13], there is a typo in formula (2) on p. 10: the operator div should be preceded by a "+" sign.

[2] Lebo I.G., Lebo A.I. *Contemporary Issues in Mathematical Modeling*. M.: RTU MIREA; 2025, 208 p. (In Russ.).

Here, ρ, P_e, P_i, T_e, T_i, E_e, E_i are the density, pressure, temperature, and specific internal energy of the electron (index e) and ion (index i) components, respectively; Q_{ei} is the heat power exchange between the components; κ_e and κ_e are the electron and ion thermal conductivity coefficients, respectively; $\vec{q}$ is the intensity of laser radiation; $\vec{v}$ is the velocity vector; Z_i is the average charge of plasma ions per Lagrangian cell; $R_{rad}(\rho, T_e)$ is the power of re-radiation from plasma; Q_0 is the scale factor.

The laser beam hits the outside of the film, at which boundary the following conditions are set: the pressure is equal to the pressure in the extreme Lagrangian cell at the moment $t = 0$, while the heat conduction flows are zero. The normal velocity component and heat flows are also set to zero on the axis of symmetry and on the side surface, as well as on the opposite side of the cylindrical region.

Studies of the formation and propagation of SW in the LST cell were based on the analysis of computational experiment data [15]. The size of the cylindrical region is defined as follows: $0 < z < (1 + d_0)$ cm; $0 < r < R_{max} = 0.282$ cm; d_0 is the film thickness. The presented calculations assumed 100% energy absorption at a laser pulse having a trapezoidal time profile at energy E_{las} with vertices: $t_1 = 0$ ns; $t_2 = 30$ ns; $t_3 = 60$ ns; $t_4 = 100$ ns. The parameters of the KrF laser pulse (wavelength in the ultraviolet range $\lambda = 0.248$ μm) correspond to the GARPUN installation (Lebedev Physical Institute of the Russian Academy of Sciences (LPI RAS)[3], Moscow, Russia [16]). The LST cell was filled with an initial density of $\rho = 1.29 \cdot 10^{-3}$ g/cm^3 and a pressure $P = 1$ atm.

2. TWO-DIMENSIONAL NUMERICAL MODELING OF LASER ACCELERATION OF A NONUNIFORMITY PISTON AND FORMATION OF SW IN GAS

Calculations were performed for the formation and propagation of SW radiation in the air inside the LST. The target (piston) consisted of a polymer film (CH) located at the upper end of a cylindrical LST cell filled with air. The dimensions of the LST cell corresponded to the dimensions of the calculation area. The shape of the film varied in terms of its thickness d_0, the energy of the laser pulse E_{las}, and the distribution of radiation intensity along the radius r.

In the first series of calculations, the formation of SW in the air was modeled in the case where the piston had a stepped or profiled shape (Fig. 1a). Two calculations were made: (1) sole $d_1 = 1.5$ μm, step $d = 1.5$ μm, $d_0 = d_1 + d = 3.0$ μm (variant Zvor6); (2) sole $d_1 = 2.0$ μm, step $d = 3.0$ μm, $d_0 = d_1 + d = 5.0$ μm (variant Zvor8).

With laser radiation falling on the upper surface of the CH layer, the sublimated corona part of the film scatters towards the laser beam, while SW radiation propagates along the unevaporated substance to reach the rear surface of the sole, where the substance is discharged and scattered in the direction of the laser beam (Fig. 1a). At the same time, transverse waves

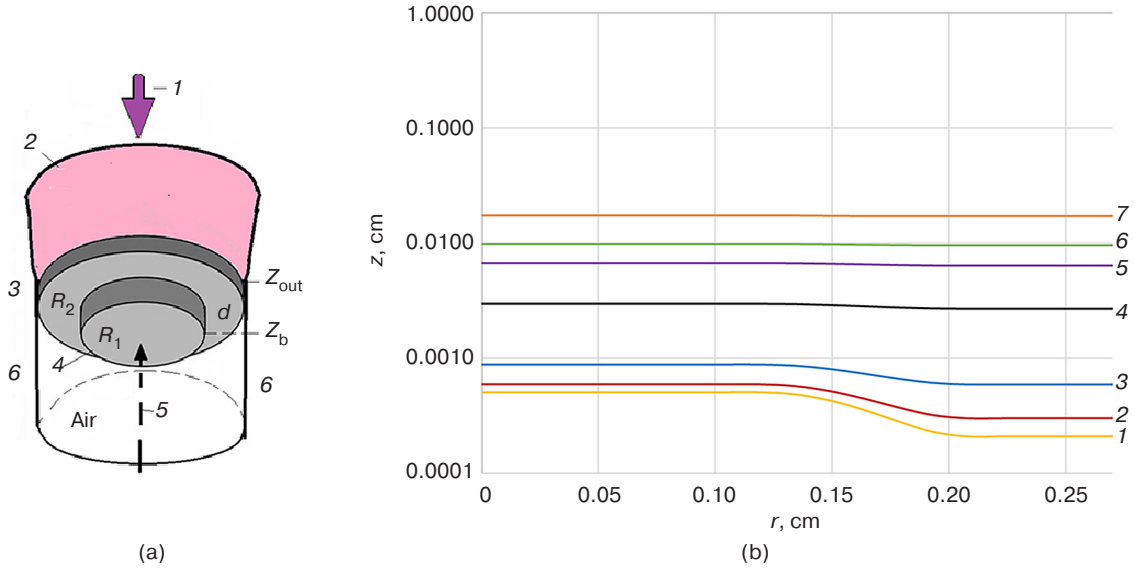

Fig. 1. (a) Setup of the computational experiment: (*1*) laser beam; (*2*) plasma corona; (*3*) polymer sole of the profiled target with a thickness of d_2 and radius R_2; (*4*) step with a thickness of d and radius R_1; (*5*) direction of the 0z axis. (*6*) walls of the LST cell. (b) Evolution of the layer thickness $d_0(r) = Z_{out}(r) - Z_b(r)$ at times t, ns: (*1*) 0, (*2*) 1, (*3*) 2, (*4*) 5, (*5*) 8, (*6*) 10, (*7*) 14; $Z_{out}(r)$ and $Z_b(r)$ are contact boundaries 'vacuum–film' and 'film–internal gas (air)'

[3] https://lebedev.ru/. Accessed September 12, 2025. (In Russ.).

propagate along the CH layer, tending to equalize the pressure and boundaries of the layer (Fig. 1b). The laser pulse ends at the moment t = 100 ns. While at the initial stage the thickness of the piston is greater at the axis, by the moment t = 14 ns the dense layer has equalized its internal $Z_b(r)$ and external $Z_{out}(r)$ boundaries; the thickness of the CH layer does not significantly depend on the radius (Fig. 1b and Table).

The fourth column of the table shows the dependence of the relative deviation of the layer thickness from the average value $\beta = \frac{(d_0(R_{max}) - d_0(0)) \cdot 100\%}{d_0(R_{max}) + d_0(0)}$.

Table. Values of piston thickness on the axis, $d_0(0)$ near the channel wall $d_0(R_{max})$ and β at different points in time t

t, ns	$d_0(0)$, cm	$d_0(R_{max})$, cm	β, %
0	$5.04 \cdot 10^{-4}$	$2.11 \cdot 10^{-4}$	41.0
1	$5.92 \cdot 10^{-4}$	$2.99 \cdot 10^{-4}$	32.8
2	$8.83 \cdot 10^{-4}$	$5.92 \cdot 10^{-4}$	19.8
5	$2.69 \cdot 10^{-3}$	$2.97 \cdot 10^{-3}$	5.1
8	$6.67 \cdot 10^{-3}$	$6.40 \cdot 10^{-3}$	2.1
10	$9.83 \cdot 10^{-3}$	$9.57 \cdot 10^{-3}$	1.34
14	$1.74 \cdot 10^{-2}$	$1.73 \cdot 10^{-2}$	0.32

A dense layer of unevaporated film (piston) with variable density ρ ≈ 0.05–1 g/cm^3 moves inside the LST at supersonic speed to form an SW in the air with a practically flat front, although small-scale density and pressure disturbances inside this layer, as well as fragments of film particles, may persist for a long time. Moreover, due to the development of Richtmyer–Meshkov instability [17, 18] near the contact boundary Z, these small-scale disturbances can develop to form a turbulent layer [19]. Modeling these processes requires different approaches and is not considered in this work.

By the end of the laser pulse t = 100 ns, the contact boundary velocity has reached $V_b \approx 4$ km/s. Figure 2 shows the propagation of the SW front $Z_{sw}(t)$ at different points in time.

The next series of calculations modeled the heterogeneous irradiation of a flat target from CH (piston) and the formation of SW in LST. The intensity of the laser flux had the following form: $q(t, r) = I_{t1}(t)I_{r1}(r) + I_{t2}(t)I_{r2}(r)$.

Here, the functions $I_{t1}(t)$, $I_{t2}(t)$ are trapezoidal, while $I_{r1}(r)$ and $I_{r2}(r)$ are normalized to 1: $\int_0^{t4} I_{t1}(t)dt = E_{las1}$, $\int_0^{R_0} I_{r1}(r)rdr = 1$, $\int_0^{t4} I_{t2}(t)dt = E_{las2}$, $\int_0^{R_0} I_{r2}(r)rdr = 1$, while R_0 is the transverse boundary of the counting region.

If the front of the first pulse is flat, then the second pulse has a Gaussian shape: $I_{r2}(r) = \frac{C_2}{e^{r/R_f}}$, C_2 is the normalization constant, R_f is the radius of the focal spot. In this way, the effect of the superposition of a homogeneous pulse and a speckle with an effective radius $R_f < R_0$ was modeled.

A series of five calculations was performed to simulate the heterogeneity of irradiation of a flat target (Zvor9 variants): in all variants $I_{r1}(r)$ = const at values $0 \le r \le R_0$, while the time form in four variants is a trapezoid with values t_1 = 0, t_2 = 30 ns, t_3 = 60 ns, t_4 = 100 ns at the vertices of the trapezoid. E_{las1}, E_{las2} varied as follows: (1) $E_{las1} = 9.9$ J, $E_{las2} = 0.1$ J; (2) $E_{las1} = 9.7$ J, $E_{las2} = 0.3$ J; (3) $E_{las1} = 9.5$ J, $E_{las2} = 0.5$ J; (4) E_{las1} = 9.0 J, E_{las2} = 1.0 J. In variant 5, the values E_{las1} = 9.0 J and E_{las2} = 1.0 J, but the time shape of the pulse was changed: the duration of the second pulse was reduced by a factor of 2: t_2 = 15 ns, t_3 = 30 ns, t_4 = 50 ns, which led to a twofold increase in the peak intensity of the speckle. The total absorbed laser energy

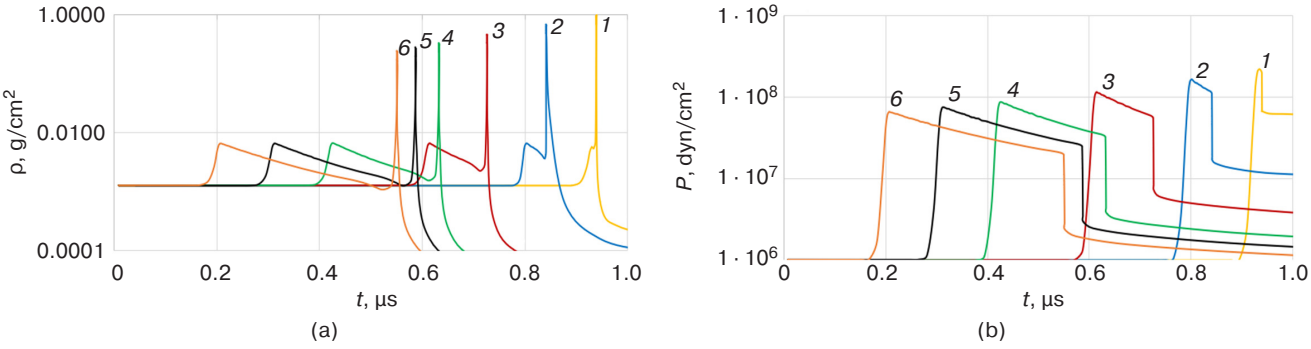

Fig. 2. Distributions: (a) density ρ(z), (b) pressure $P(z)$ at r = 0 and times t, μs: (*1*) 0.2, (*2*) 0.5, (*3*) 1.0, (*4*) 1.6, (*5*) 2.0, (*6*) 2.4

in all five variants was 10 J at $R_0 = R_{max} = 0.282$ cm and $R_f = 0.0705$ cm. The calculations were made on differential grids (22 × 212), where 22 nodes are located along the 0r axis and 212 nodes are located along the 0z axis.

Along with the general acceleration of the film, its deformation is observed due to the heterogeneity of irradiation. Since there was increased radiation intensity near the axis, the target's flight speed in this subarea is higher. As in the first series of calculations, the transverse SW partially aligns the boundary of the $Z_b(r)$ layer. Therefore, the SW front in the gas has a more gradual shape than the piston. In the case where the energy of the second pulse was 10% of the total (i.e., variants 4 and 5), the Lagrangian grid broke by the end of the laser pulse ($t \geq 90$ ns) and the count was stopped. This fact can be interpreted as a piston rupture. Figures 3 and 4 show two-dimensional distributions of density (ρ) and pressure (P) at the moments of time $t = 100$ ns (end of the laser pulse) and $t = 1500$ ns for variant 3. By the moment $t = 1500$ ns, the piston is severely deformed. A jet forms near the axis ($r < 0.02$ cm) to create a second SW diverging from the axis. Towards the periphery of the calculation area, the overall SW front partially flattens out, and most of the surface, except for the vicinity of the 0z axis, acquires an almost flat shape.

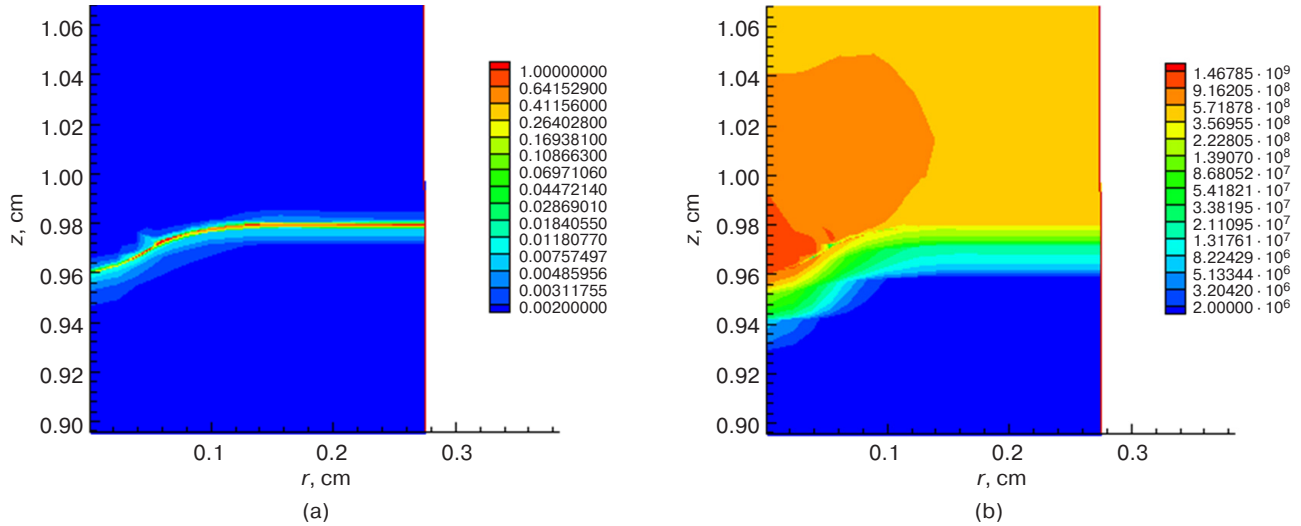

Fig. 3. Density (a) and pressure (b) fields at $t = 100$ ns

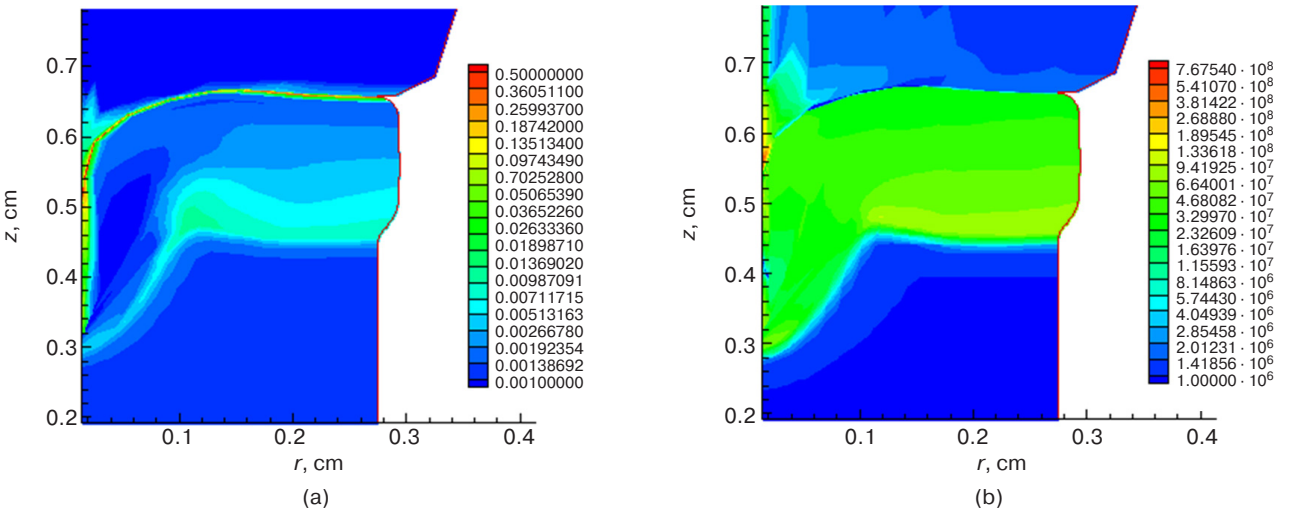

Fig. 4. Density (a) and pressure (b) fields at $t = 1500$ ns

3. DYNAMICS OF SW AT DIFFERENT MODES OF FORMATION OF THE PLASMA CORONA AND ENERGY VALUES IN A LASER PULSE

A series of quasi-one-dimensional calculations was performed for films with constant thickness and uniform laser flux intensity. In this case, finite difference grids with a significantly smaller number of nodes in the transverse direction (only 5–7 nodes) were used. This made it possible to significantly reduce the processing time for calculations. Two types of tasks were considered:

1. In the Zvor1 variants, the dispersion of the evaporated polymer film substance was not limited (open corona). At the vacuum–piston boundary, there is a condition $P_{out} = P_0$, where P_0 is the initial pressure in the piston and gas inside the LST. In this case, when the laser flux is absorbed, the pressure increases sharply to sublimate the outer layers of the piston and scatter them at supersonic speed. The calculations took into account the reflection of laser beams from the critical surface. Thus, each laser beam propagating strictly along the $0z$ axis passed through the plasma corona twice.
2. In the Zvor7 variants, the spread of the substance was limited by a transparent plate located on the upper side of the LST where the laser beam falls. The laser ray passes through the transparent layer and is absorbed in the outer layers of the polymer film. In this case, the pulse transmitted to the unevaporated layers of the target is greater than in the first case. We will refer to this irradiation mode as a closed corona.

Figure 5a shows the propagation of the SW front $Z_{sw}(t)$ for a film d_0 = 5 μm and three values of absorbed laser energy E_{las} = 5 J (Zvor1a), 10 J (Zvor1b) and 17.5 (Zvor1c) J. Figure 5b shows the movement of the air–CH contact boundary $Z_b(t)$ for the same conditions. If the curve $Z_{sw}(t)$ at the time interval $0.2 < t < 0.2$ reaches a practically constant slope (i.e., the velocity $V_{sw}(t)$ = const), then the curve $Z_b(t)$ asymptotically tends to a constant value, i.e., the velocity $V_b(t) \to 0$. The values of the SW traveled from $Z_{sw}(t)$, which were obtained in experiments on the LST, are marked with crosses.

Remark 1. Figure 5 shows the values of $Z_{sw}(t)$, obtained in calculations and experiments at the LST at LPI RAS (marked with crosses on the graph, see [20] for details). In the experiments, the energy of the laser beam entering the target chamber was measured. The fraction of energy reflected and scattered in the plasma was not measured. The calculations assumed that the energy of the laser pulse propagated in the plasma and was reflected strictly backward from the critical surface (refraction of the rays was not taken into account). The fraction of reflected laser energy that exited the plasma (in percent) $\varepsilon = (E_{ref}/E_{las}) \cdot 100\%$, was 50.7% (for variant Zvor1a), ε = 43.8 (for variant Zvor1b), ε = 33% (for variant Zvor1c).

With a laser radiation energy density of ~10^9 W/cm^2 and a focus area of ~0.5 cm^2, a relatively short plasma jet is formed (i.e., its length is less than the transverse size of the focal spot). The less energy absorbed, the shorter the length of the plasma corona and the greater the proportion of reflected laser energy.

Remark 2. The physical and mathematical model of the *Atlant_C* program does not take into account molecular diffusion and turbulent mixing. Physical and mathematical models of turbulent mixing and numerical codes are described in [2]. Taking these processes into account could lead to a blurring of the contact boundary and an increase in the proportion of scattered laser flux.

Figure 6 shows the results of comparisons of calculations of the path traveled by SW $Z_{sw}(t)$ (Fig. 6a) along with the film-air contact boundary $Z_b(t)$ (Fig. 6b) in the case of a closed corona for films (piston) with an initial thickness of d_0 = 5 μm. The data from experiments in [20] are marked with crosses. In this series of calculations (closed corona), all the laser energy that

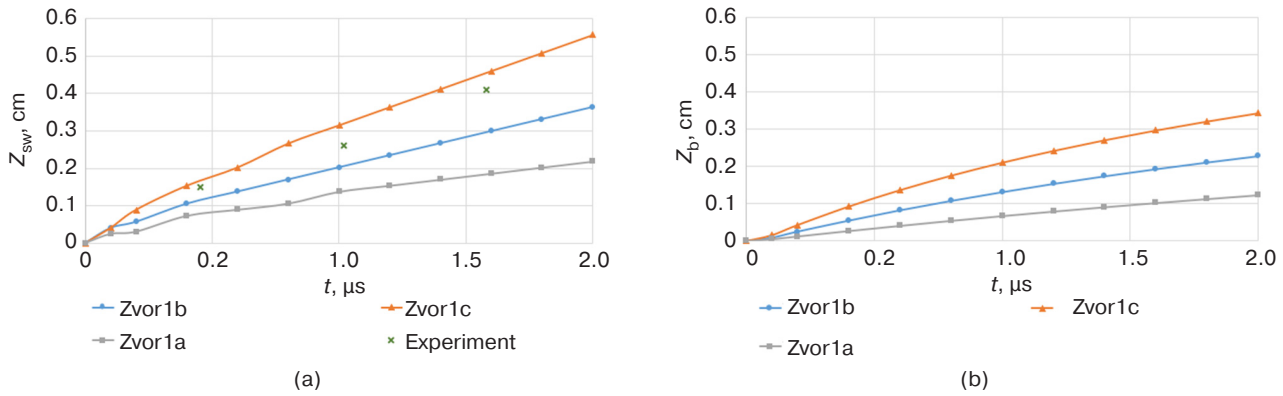

Fig. 5. Dependence of the path traveled by the SW on time $Z_{sw}(t)$:
(a) dependence of the path traveled by the contact boundary on time $Z_b(t)$;
(b) variant Zvor1a: E_{las} = 5 J, variant Zvor1b: E_{las} = 10 J, variant Zvor1c: E_{las} = 17.5 J

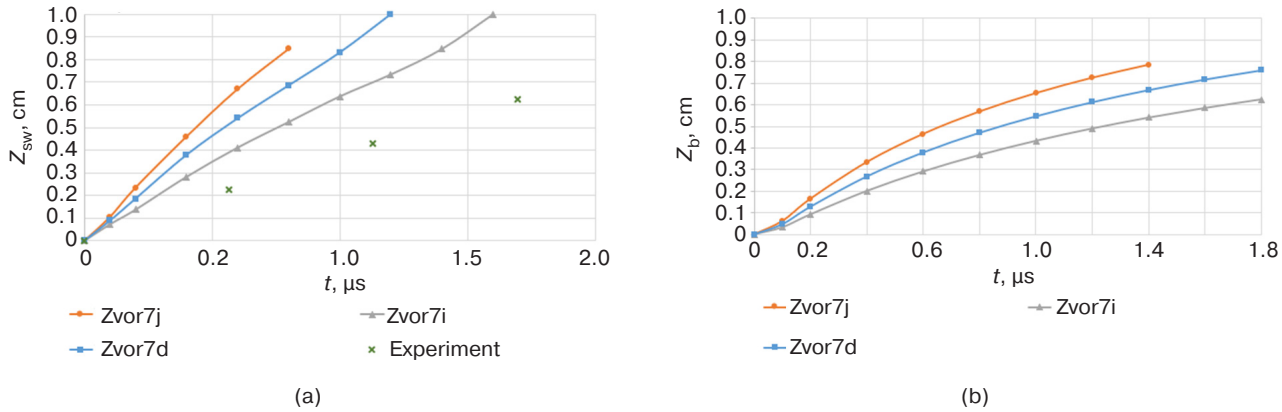

Fig. 6. Comparisons of distances passed by SW, $Z_{sw}(t)$ (a) and contact boundary $Z_b(t)$ (b) in the case of a closed corona for different values of absorbed laser energy: variant Zvor7i: E_{las} = 5 J, variant Zvor7d: E_{las} = 10 J, variant Zvor7j: E_{las} = 17.5 J

passed through the transparent plate was assumed to have been absorbed near the boundary between the outer transparent layer and the CH film (piston).

Remark 3. In the fourth series of calculations, the physical and mathematical formulations of the problem do not take into account the reflection of laser radiation from plasma since the mass and thickness of the transparent layer are large compared to these parameters in the film. For this reason, a new physical and mathematical model should be developed that takes into account the passage of a powerful laser beam, the dissociation and ionization of atoms, as well as the scattering of radiation on defects and cracks that could have arisen during the passage of the SW through the plexiglass. In fact, the calculations used a delta-shaped absorption mechanism near the film-plexiglass contact surface. Therefore, the experimental points lie below the calculated ones.

The size of the calculation area is $0 < z < 1$ cm. In the time interval $0 < t < 0.2$ μs, an SW is formed in the gas near the contact boundary ($z \approx 1$ cm), while in the case of a closed corona, the acceleration and velocity of the piston after the end of the laser pulse are significantly greater than in the case of an open corona. When the SW reaches the lower end of the calculation area ($z = 0$), it is reflected. The air flow behind the SW front is slowed down at the lower end. The calculations were made up to this point; thus, in the case of a closed corona, the time interval $t \in [0, 2.0]$ μs.

4. DISCUSSION ON THE COMPUTATION RESULTS

The article presents the results of four series of calculations modeling the propagation of SW radiation in LST, where the driver is a powerful KrF laser with an energy of up to 100 J and a pulse duration of 100 ns.

In the first series of calculations, the SW propagation in a profiled (step-shaped) target was modeled. It was shown that SW propagating in a dense layer during the laser pulse leads to the flattening of the contact boundary of the piston and the formation of a flat SW front in the gas.

The second series of calculations examined the effect of target irradiation heterogeneity on SW formation. In the presence of a laser pulse having an intensity several times higher than the average radiation density incident on the target and an energy of ~5–10% of the main pulse, a jet forms with the capability of overtaking the average SW front in the gas across the focal spot and form transverse SWs.

The third and fourth series of calculations studied the dynamics of SW radiation in gas under open and closed corona conditions (Figs. 5 and 6). The obtained results were compared with data from experiments on the LST. Calculations were performed for the propagation of SW radiation in the LUT at absorbed laser pulse energies of 5, 10, and 17.5 J and piston thicknesses of 5 μm. The UV velocity in gas is consistent with the data from full-scale experiments on LST [18] in the open plasma corona mode. In order to compare the data with that obtained from experiments with a closed corona, further development of the physical and mathematical model is required.

Based on the results presented, the following conclusions can be drawn:

1. The propagation of hypersonic SW with Mach numbers ≥10 and gas flow velocities of the order of the first (and, in the future, possibly the second and third) cosmic velocities can be studied under laboratory conditions using LST.
2. According to the results of computational experiments, the contact surface between the piston and gas becomes flattened when using a step-shaped piston target, while the SW propagates with an almost flat front. This situation occurs when the

first longitudinal wave passes through the target in a time much shorter than the duration of the laser pulse.

3. In the case of nonuniform heating of the target by a laser pulse, the CH film accelerates as a whole to form an almost flat SW front in the gas when the energy of the speckles is small compared to the energy of the main pulse (~1%).
4. When the energy of the speckle is ≥5–10% of the energy of the laser pulse and its intensity significantly exceeds the average value of the flux density in the spot, destruction of the layer and the formation of jets may occur.
5. When the target is heated by laser in the closed corona mode, the propagation speed of the SW front increases by approximately 40–50% (in the case under consideration).
6. When the film breaks down and fragments, a turbulent layer forms (with a density 1–2 orders of magnitude greater than the density of the gas in the LST). This piston forms the SW in the gas. Modeling the absorption of laser radiation and the development of a turbulent layer during acceleration requires the development of new physical and mathematical models and programs.

CONCLUSIONS

Studying the characteristics of hydrodynamic instabilities is an important and relevant task in fundamental physics, as well as in research on laser thermonuclear fusion and astrophysics. Along with costly measurements that are unique in their accuracy, this research requires the development of complex physical and mathematical models and programs in order to compare data from field and computational experiments. For the purposes of such research, the described LST tool is a promising resource. The results of computational experiments carried out on the LST along are presented along with a comparison of published experimental data and prospects for further research.

ACKNOWLEDGMENTS

The work was conducted as part of the National Center for Physics and Mathematics (NCPM) program “Gas Dynamics and Explosion Physics,” topic “Investigation of Physical Processes at Fusion Power and in the Star Systems.”

Authors’ contributions

I.G. Lebo—design of the physicomathematical model and numerical code, problem statement and calculations.

V.A. Komarova, M.A. Ryzhkov—plotting, analyzing calculation results, and preparing the article for publication.

REFERENCES

1. Basov N.G., Lebo I.G., Rozanov V.B. *Fizika lazernogo termoyadernogo sinteza* (*Physics of Laser Thermonuclear Fusion*). Moscow: Znanie; 1988, 172 p. (In Russ.).
2. Nevmerzhitskii N.V., Razin A.N., Kozlov V.I. *Gidrodinamicheskie neustoichivosti v mishenyakh inertsial’nogo termoyadernogo sinteza* (*Hydrodynamic Instabilities in Inertial Thermonuclear Fusion Targets*): Monograph. Sarov; 2024, 416 p. (In Russ.). ISBN 978-5-9515-0558-3
3. Zel’dovich Ya.B., Raizer Yu.P. *Fizika udarnykh voln i vysokotemperaturnykh gidrodinamicheskikh yavlenii* (*Physics of Shock Waves and High-Temperature Hydrodynamic Effects*). Moscow: Fizmatlit; 2008, 652 p. (In Russ.). ISBN 978-5-9291-0938-3
4. Landau L.D., Lifshits E. *Gidrodinamika* (*Hydrodynamics*). Moscow: Nauka; 1986, 736 p. (In Russ.).
5. Lebo I.G., Tishkin V.F. *Issledovanie gidrodinamicheskoi neustoichivosti v zadachakh lazernogo termoyadernogo sinteza* (*Study of Hydrodynamic Instability in Laser Thermonuclear Fusion Problems*). Moscow: Fizmatlit; 2006, 304 p. (In Russ.). ISBN 5-9221-0683-X
6. Bragin M.D., Gus’kov S.Y., Zmitrenko N.V., et al. Experimental and Numerical Investigation of the Dynamics of Development of Rayleigh–Taylor Instability at Atwood Numbers Close to Unity. *Math. Models Comput. Simul.* 2023;15(4):660–676. https://doi.org/10.1134/S2070048223040038
   [Original Russian Text: Bragin M.D., Gus’kov S.Yu., Zmitrenko N.V., Kuchugov P.A., Lebo I.G., Levkina E.V., Nevmerzhitskii N.V., Sin’kova O.G., Statsenko V.P., Tishkin V.F., Farin I.R., Yanilkin Yu.V., Yakhin R.A. Experimental and Numerical Investigation of the Dynamics of Development of Rayleigh–Taylor Instability at Atwood Numbers Close to Unity. *Matematicheskoe modelirovanie*. 2023;35(1):59–82 (in Russ.). https://doi.org/10.20948/mm-2023-01-05, https://elibrary.ru/qfskuw
7. Craxton R.S., Anderson K.S, Boehly T.R., et al. Direct drive inertial confinement fusion: A review. *Phys. Plasmas*. 2015;22(1):110501. https://doi.org/10.1063/1.4934714
8. Lebo I.G. Mathematical modeling of experiments on the interaction of a high-power ultraviolet laser pulse with condensed targets. *Russian Technological Journal.* 2023;11(3):86–103. https://doi.org/10.32362/2500-316X-2023-11-3-86-103
9. Samarskii A.A., Popov Yu.P. *Raznostnye metody resheniya zadach gazovoi dinamiki* (*Difference Methods for Solving Problems of Gas Dynamics*). Moscow: Nauka; 1992, 422 p. (In Russ.). ISBN 5-02-014577-7
10. Belotserkovskii O.M., Davydov Yu.M. *Metod krupnykh chastits v gazovoi dinamike* (*Large Particle Method in Gas Dynamics*). Moscow: Nauka; 1982, 391 p. (In Russ.). https://elibrary.ru/xqocjj

11. Godunov S.K., Zabrodin A.V., Ivanov M.Ya., Kraiko A.N., Prokopov G.P. *Chislennoe reshenie mnogomernykh zadach gazovoi dinamiki* (*Numerical Solution of Multidimensional Gas Dynamics Problems*). Moscow: Nauka; 1976, 400 p. (In Russ.).
12. Samarskii A.A. *Teoriya raznostnykh skhem* (*Theory of Difference Schemes*). Moscow: Nauka; 1990, 616 p. (In Russ.). ISBN 5-02-014576-9
13. Lebo I.G., Obruchev I.V. The modeling of two-dimensional vortex flows in a cylindrical channel using parallel calculations on a supercomputer. *Russian Technological Journal.* 2022;10(1):60–67. https://doi.org/10.32362/2500-316X-2022-10-1-60-67
14. Zvorykin V.D., Lebo I.G. Application of a high power KrF laser for the study of supersonic gas flows and the development of hydrodynamic instability in layered media. *Quantum Electron.* 2000;30(6):540–544. https://doi.org/10.1070/QE2000v030n06ABEH001761
[Original Russian Text: Zvorykin V.D., Lebo I.G. Application of a high power KrF laser for the study of supersonic gas flows and the development of hydrodynamic instability in layered media. *Kvantovaya Elektronika*. 2000;30(6):540–544 (in Russ.).]
15. Samarskii A.A., Mikhailov A.P. *Matematicheskoe modelirovanie: Idei. Metody. Primery* (*Mathematical Modeling*: *Ideas. Methods. Examples*). Moscow: Fizmatlit; 2005, 316 p. (In Russ.). ISBN 5-9221-0120-X
16. Zvorykin V.D., Lebo I.G. Laser and Target Experiments on KrF GARPUN laser installation at FIAN. *Laser Part. Beams*. 1999;17(1):69-88. https://doi.org/10.1017/S0263034699171064
17. Richtmyer R.D. Taylor instability in shock acceleration of compressible fluids. *Commun. Pure Appl. Math.* 1960;13(2): 297–319. https://doi.org/10.1002/cpa.3160130207
18. Meshkov E.E. Instability of the interface of two gases accelerated by a shock wave. *Fluid Dyn.* 1969;4(5):101–104. https://doi.org/10.1007/BF01015969
[Original Russian Text: Meshkov E.E. Instability of the interface of two gases accelerated by a shock wave. *Izvestiya AN SSSR. Seriya Mekhanika zhidkosti i gaza*. 1969;5:151–158 (in Russ.). Available from URL: https://mzg.ipmnet.ru/ru/get/1969/5/151-158. Accessed September 12, 2025]
19. Aleshin A.N., Zaitsev C.G., Lazareva E.V., Gamalii E.G., Lebo I.G., Rozanov V.B. A study of linear, non-linear and transition stages of Richtmyer–Meshkov instability. *Dokl. Math*. 1990;35(2):177–180.
[Original Russian Text: Aleshin A.N., Zaitsev S.G., Lazareva E.V., Gamalii E.G., Lebo I.G., Rozanov V.B. A study of linear, non-linear and transition stages of Richtmyer–Meshkov instability. *Doklady Akademii Nauk SSSR*. 1990;310(5):1105–1108 (in Russ.).]
20. Zvorykin V.D. Dynamics of Hypersonic Shock Waves Generated by Laser Acceleration of Thin-Film Targets in a Laser-Driven Shock Tube and Free Space. *JETP Lett.* 2025;122(6):354–360. https://doi.org/10.1134/S002136402560805X
[Original Russian Text: Zvorykin V.D. Dynamics of Hypersonic Shock Waves Generated by Laser Acceleration of Thin-Film Targets in a Laser-Driven Shock Tube and Free Space. *Pis'ma v Zhurnal Eksperimental'noi i Teoreticheskoi Fiziki*. 2025;122(5-6):344–350 (in Russ.). https://www.elibrary.ru/xuqtzo]

СПИСОК ЛИТЕРАТУРЫ

1. Басов Н.Г., Лебо И.Г., Розанов В.Б. *Физика лазерного термоядерного синтеза*. М.: Знание; 1988, 176 с.
2. Невмержицкий Н.В., Разин А.Н., Козлов В.И. *Гидродинамические неустойчивости в мишенях инерциального термоядерного синтеза*: монография. Саров: РФЯЦ ВНИИЭФ; 2024, 416 с. ISBN 978-5-9515-0558-3
3. Зельдович Я.Б., Райзер Ю.П. *Физика ударных волн и высокотемпературных гидродинамических явлений*. М.: Физматлит; 2008, 652 с. ISBN 978-5-9291-0938-3
4. Ландау Л.Д., Лифшиц Е. *Гидродинамика*. М.: Наука. Гл. ред. физ.-мат. лит.; 1986, 736 с.
5. Лебо И.Г., Тишкин В.Ф. *Исследование гидродинамической неустойчивости в задачах лазерного термоядерного синтеза*. М.: Физматлит; 2006, 304 с. ISBN 5-9221-0683-X
6. Брагин М.Д., Гуськов С.Ю., Змитренко Н.В., Кучугов П.А., Лебо И.Г., Левкина Е.В., Невмержицкий Н.В., Синькова О.Г., Стаценко В.П., Тишкин В.Ф., Фарин И.Р., Янилкин Ю.В., Яхин Р.А. Экспериментальное и численное исследование динамики развития неустойчивости Рэлея – Тейлора при числах Атвуда близких к единице. *Математическое моделирование.* 2023;35(1):59–82. https://doi.org/10.20948/mm-2023-01-05, https://elibrary.ru/qfskuw
7. Craxton R.S., Anderson K.S, Boehly T.R., et al. Direct drive inertial confinement fusion: A review. *Phys. Plasmas*. 2015;22(1):110501. https://doi.org/10.1063/1.4934714
8. Лебо И.Г. Численное моделирование экспериментов по взаимодействию мощных ультрафиолетовых импульсов с конденсированными мишенями. *Russian Technological Journal.* 2023;11(3):86–103. https://doi.org/10.32362/2500-316X-2023-11-3-86-103
9. Самарский А.А., Попов Ю.П. *Разностные методы решения задач газовой динамики.* М.: Наука; 1992, 422 с. ISBN 5-02-014577-7
10. Белоцерковский О.М., Давыдов Ю.М. *Метод крупных частиц в газовой динамике*. М.: Наука; 1982, 391 с. https://elibrary.ru/xqocjj
11. Годунов С.К., Забродин А.В., Иванов М.Я., Крайко А.Н., Прокопов Г.П. *Численное решение многомерных задач газовой динамики*. М.: Наука; 1976, 400 с.
12. Самарский А.А. *Теория разностных схем*. М.: Наука; 1990, 616 с. ISBN 5-02-014576-9

13. Лебо И.Г., Обручев И.В. Моделирование двумерных вихревых течений в цилиндрическом канале с помощью параллельных вычислений на суперкомпьютере. *Russian Technological Journal*. 2022;10(1):60–67. https://doi.org/10.32362/2500-316X-2022-10-1-60-67
14. Зворыкин В.Д., Лебо И.Г. Применение мощного KrF-лазера для исследования сверхзвуковых течений газа и развития гидродинамических неустойчивостей в слоистых средах. *Квантовая электроника*. 2000;30(6):540–544.
15. Самарский А.А., Михайлов А.П. *Математическое моделирование*: *Идеи. Методы. Примеры*. М: Физматлит; 2005, 316 с. ISBN 5-9221-0120-X
16. Zvorykin V.D., Lebo I.G. Laser and Target Experiments on KrF GARPUN laser installation at FIAN. *Laser Part. Beams*. 1999;17(1):69-88. https://doi.org/10.1017/S0263034699171064
17. Richtmyer R.D. Taylor instability in shock acceleration of compressible fluids. *Commun. Pure Appl. Math.* 1960;13(2): 297–319. https://doi.org/10.1002/cpa.3160130207
18. Мешков Е.Е. Неустойчивость границы раздела двух газов, ускоряемой ударной волной. *Известия АН СССР. Сер. Механика жидкости и газа.* 1969;5:151–158. URL: https://mzg.ipmnet.ru/ru/get/1969/5/151-158. Дата обращения 12.09.2025.
19. Алешин А.Н., Зайцев С.Г., Лазарева Е.В., Гамалий Е.Г., Лебо И.Г., Розанов В.Б. Исследование линейной, нелинейной и переходной стадий развития неустойчивости Рихтмайера – Мешкова. *Докл. АН СССР*. 1990;310(5):1105–1108.
20. Зворыкин В.Д. Динамика гиперзвуковых ударных волн, генерируемых при лазерном ускорении тонкопленочных мишеней в лазерной ударной трубе и в свободном пространстве. *Письма в ЖЭТФ*. 2025;122(5-6):344–350. https://www.elibrary.ru/xuqtzo

About the Authors

Ivan G. Lebo, Dr. Sci. (Phys.-Math.), Professor, Department of Higher Mathematics, Institute of Artificial Intelligence, MIREA – Russian Technological University (78, Vernadskogo pr., Moscow, 119454 Russia). E-mail: lebo@mirea.ru. Scopus Author ID 7003412908, RSCI SPIN-code 9416-5542, https://orcid.org/0000-0001-8341-9453

Victoria A. Komarova, Student, MIREA – Russian Technological University (78, Vernadskogo pr., Moscow, 119454 Russia). E-mail: viki.kom@mail.ru. https://orcid.org/0009-0001-3342-6636

Maxim A. Ryzhkov, Postgraduate Student, Department of Radio Electronic Systems and Complexes, Institute of Radio Electronics and Informatics, MIREA – Russian Technological University (78, Vernadskogo pr., Moscow, 119454 Russia). E-mail: ryzhkov@mirea.ru. RSCI SPIN-code 5476-3273, https://orcid.org/0009-0000-4475-0039

Об авторах

Лебо Иван Германович, д.ф.-м.н., профессор, кафедра высшей математики, Институт искусственного интеллекта, ФГБОУ ВО «МИРЭА – Российский технологический университет» (119454, Россия, Москва, пр-т Вернадского, д. 78). E-mail: lebo@mirea.ru. Scopus Author ID 7003412908, SPIN-код РИНЦ 9416-5542, https://orcid.org/0000-0001-8341-9453

Комарова Виктория Александровна, студент, ФГБОУ ВО «МИРЭА – Российский технологический университет» (119454, Россия, Москва, пр-т Вернадского, д. 78). E-mail: viki.kom@mail.ru. https://orcid.org/0009-0001-3342-6636

Рыжков Максим Анатольевич, аспирант, кафедра радиоэлектронных систем и комплексов, Институт радиоэлектроники и информатики, ФГБОУ ВО «МИРЭА – Российский технологический университет» (119454, Россия, Москва, пр-т Вернадского, д. 78). E-mail: ryzhkov@mirea.ru. SPIN-код РИНЦ 5476-3273, https://orcid.org/0009-0000-4475-0039

Translated from Russian into English by Lyudmila O. Bychkova
Edited for English language and spelling by Thomas A. Beavitt

Mathematical modeling

Математическое моделирование

UDC 519.95:621.3
https://doi.org/10.32362/2500-316X-2026-14-2-124-133
EDN DPUAHF

RESEARCH ARTICLE

Performance analysis and timing characteristics in industrial networks with random and deterministic node distributions

Alexander S. Leontyev, Dmitry V. Zhmatov @

MIREA – Russian Technological University, Moscow, 119454 Russia
@ *Corresponding author, e-mail: zhmatov@mirea.ru*

• **Submitted:** 21.10.2025 • **Revised:** 20.11.2025 • **Accepted:** 05.02.2026

Abstract

Objectives. The aim of the study was to develop mathematical tools to assess the performance and probabilistic-temporal characteristics of packet transmission processes in industrial networks employing random multiple access. Our study specifically examined strict packet delivery time constraints and the impact of collisions.

Methods. The research applies methods from the theory of random processes. We used the Laplace–Stieltjes transform to derive key relationships analytically and prove the main theorem.

Results. We formulated and proved a theorem which defines the Laplace–Stieltjes transform for the packet transmission time distribution function. The result incorporates packet retransmissions caused by conflicts in the multiple access environment. We analyzed information transmission processes in industrial networks with random multiple access, considering variations in the number of workstations and packet flow intensities at network nodes. Our evaluation included throughput, node and transmission medium utilization, and packet transmission times under collision conditions. The results reveal significant differences in the temporal characteristics of packet transmission between central and edge nodes. We developed and implemented a software package, in order to automate the study and evaluate various network operating modes during scaling and under increased nodal load.

Conclusions. The study of industrial networks with random multiple access established that while network throughput increases with the number of nodes during scaling, it degrades under significantly high node and transmission medium utilization. The utilization of edge nodes and their packet delivery times increase markedly faster than those of central nodes. This is due to a higher collision rate. As the network size increases, the performance and temporal characteristics exhibit only marginal dependence on the node distribution type: random or deterministic equidistant. In order to ensure balanced operation in an industrial network with random multiple access, we propose reducing the load on edge nodes by 10–15%. This strategy can maintain approximately uniform utilization of both the transmission medium and the nodes as their number increases.

Keywords: industrial network, performance, temporal characteristics, Laplace–Stieltjes transform, multiple access, scalability

For citation: Leontyev A.S., Zhmatov D.V. Performance analysis and timing characteristics in industrial networks with random and deterministic node distributions. *Russian Technological Journal.* 2026;14(2):124–133. https://doi.org/10.32362/2500-316X-2026-14-2-124-133, https://www.elibrary.ru/DPUAHF

Financial disclosure: The authors have no financial or proprietary interest in any material or method mentioned.

The authors declare no conflicts of interest.

НАУЧНАЯ СТАТЬЯ

Анализ производительности и временных характеристик промышленных сетей со случайным и детерминированным эквидистантным распределением узлов

А.С. Леонтьев, Д.В. Жматов @

МИРЭА – Российский технологический университет, Москва, 119454 Россия
@ *Автор для переписки, e-mail: zhmatov@mirea.ru*

• **Поступила:** 21.10.2025 • **Доработана:** 20.11.2025 • **Принята к опубликованию:** 05.02.2026

Резюме

Цели. Цель работы – разработка математического аппарата для оценки производительности и вероятностно-временных характеристик процессов передачи пакетов в промышленных сетях, использующих метод случайного множественного доступа. Особенностью исследования является учет строгих ограничений на время доставки пакетов и влияние коллизий.

Методы. В основе исследования лежат методы теории случайных процессов. Для аналитического вывода ключевых соотношений и доказательства основной теоремы применяется аппарат преобразования Лапласа – Стилтьеса.

Результаты. Сформулирована и доказана теорема, определяющая форму преобразования Лапласа – Стилтьеса для функции распределения времени передачи пакета. Этот результат учитывает повторные передачи пакетов, вызванные конфликтами в среде с множественным доступом. Проведен анализ процессов передачи информации в промышленных сетях со случайным множественным доступом, включая изменение количества рабочих станций и интенсивности потоков пакетов. Анализировались пакеты, поступающие в узлы сети, оценивались производительность системы, степень загрузки узлов и канала передачи, а также время доставки пакетов с учетом возникающих конфликтов. Выявлено значительное различие во временных характеристиках передачи между центральными и периферийными узлами сети. Для автоматизации исследований и оценки различных режимов работы сети при ее масштабировании и увеличении нагрузки на узлы разработан и реализован программный комплекс.

Выводы. При проведении исследования промышленных сетей со случайным множественным доступом выявлено, что при масштабировании сети с увеличением количества узлов возрастает производительность сети, однако при значительном увеличении загрузки узлов и передающей среды производительность падает. Загрузка крайних узлов и время передачи пакетов из-за повышенного возрастания конфликтов возрастают значительно быстрее по сравнению с центральными узлами. Производительность и временные характеристики при увеличении количества узлов несущественно зависят от типа распределения узлов – случайного или детерминированного эквидистантного. Для обеспечения сбалансированности режимов работы промышленной сети со случайным множественным доступом предлагается на 10–15% уменьшить нагрузку на крайние узлы. При этом можно обеспечить примерно одинаковую загрузку передающей среды и узлов при увеличении их количества.

Ключевые слова: промышленная сеть, производительность, временные характеристики, преобразование Лапласа – Стилтьеса, множественный доступ, масштабирование

Для цитирования: Леонтьев А.С., Жматов Д.В. Анализ производительности и временных характеристик промышленных сетей со случайным и детерминированным эквидистантным распределением узлов. *Russian Technological Journal*. 2026;14(2):124–133. https://doi.org/10.32362/2500-316X-2026-14-2-124-133, https://www.elibrary.ru/DPUAHF

Прозрачность финансовой деятельности: Авторы не имеют финансовой заинтересованности в представленных материалах или методах.

Авторы заявляют об отсутствии конфликта интересов.

INTRODUCTION

When analyzing the effectiveness of industrial communication networks, the characteristics of data transmission processes occurring at the first three levels of the open systems interconnection (OSI) reference model need to be taken into account. These levels determine the correctness of frame formation, addressing, error control, and physical channel security.

One of the key requirements for industrial networks integrated into automated control systems for various purposes is the limitation on data delivery time. Compliance with this parameter is crucial for maintaining the required time indicators of technological processes and ensuring the stable operation of distributed control systems.

In order to evaluate the performance and probabilistic-temporal characteristics of data transmission processes, an industrial network was studied in which the Carrier Sense Multiple Access with Collision Detection (CSMA/CD) method was implemented. This method provides shared access for multiple nodes to a common transmission medium by preemptively monitoring the channel status and stopping transmission when a signal conflict is detected. The data transmission channel bandwidth in the simulation was assumed to be equal to $C = 1$ Gbit/s, which corresponds to the characteristics of typical wired industrial Ethernet networks.

During the analysis, the dependencies of the study parameters on the number of network nodes were examined for both peripheral and central elements. The differences between random distribution of nodes along the communication line and their uniform (equidistant) placement were also considered.

1. LAPLACE-STIELTJES TRANSFORMATION THEOREM FOR PACKET TRANSMISSION TIME

As an integral indicator of industrial network efficiency, similar to the approach proposed in [1], the total intensity of data flow processed in a timely manner by all system nodes was used:

$$\lambda_{\text{tot}} = \sum_{i=1}^{N} \lambda_i Q_i, \qquad (1)$$

wherein Q_i is the probability of timely delivery of packets arriving from the ith node; λ_i is the intensity of packets arriving at the ith node.

As shown in [1], the probability that no conflicts will arise when servicing a packet which has arrived at the kth node, no conflicts will arise, is estimated using the following formula:

$$q_k = \prod_{\substack{n=1 \\ n \neq k}}^{N} \mathrm{e}^{-\lambda_n 2\frac{L_{nk}}{V_{\text{med}}}}, \; k = \overline{1, N}, \qquad (2)$$

wherein N is the number of nodes in the network, L_{nk} is the distance between the kth and nth nodes in the network, and, V_{med} is the signal propagation speed in the transmission medium.

The probability P_n that a packet arriving at the kth node will be transmitted after exactly n attempts (i.e., $n - 1$ collisions will occur during transmission) is equal to:

$$P_n = (1 - q_k)^{n-1} q_k. \qquad (3)$$

Based on the original results obtained earlier by A.S. Leontiev and published for the first time in 2001 on the development of mathematical methods for studying local networks [1], the following theorem can be formulated:

Theorem. The Laplace–Stieltjes transform $Z_k^*(s)$ of the distribution function of the packet transmission time from the kth node is estimated using the formula:

$$Z_k^*(s) = q_k T^*(s) \frac{1}{1 - (1 - q_k) X^*(s) V_k^*(s)}, \qquad (4)$$

where $V_k^*(s) = \int_0^\infty \mathrm{e}^{-st} dV_k(t)$ is the distribution function of the packet resolution time coming from the kth node; $X^*(s) = \int_0^\infty \mathrm{e}^{-st} dX(t)$; $X(t)$ is the distribution function of the delay time before packet retransmission in case of a conflict; $T^*(s) = \int_0^\infty \mathrm{e}^{-st} dT(t)$; $T(t)$ is the distribution function of the packet transmission time without conflict.

Proof. Derivation of the Laplace–Stieltjes transform formula for the packet transmission time distribution function, taking into account possible conflicts.

The Laplace–Stieltjes transform for a function $F(t)$ which derivative is equal to $F'(t) = f(t)$ is defined as follows:

$$F^*(s) = \int_0^\infty e^{-st} f(t)dt.$$

The Laplace–Stieltjes transform is characterized by the multiplicative property [2–6]:

if random variables $\xi_\Sigma = \xi_1 + \xi_2 + \ldots + \xi_N$ are independent and have distribution functions $F_i(t)$, then the Laplace–Stieltjes transform for the cumulative distribution function is defined as the product of the transforms of the individual functions:

$$F_\Sigma^*(s) = F_1^*(s) \cdot F_2^*(s) \cdot \ldots \cdot F_N^*(s).$$

Let us apply this data to derive functional relationships for packet transmission times in industrial networks. Let P_n denote the probability that a packet will be successfully transmitted exactly on the nth attempt. In this case, the packet transmission time for n attempts can be expressed as follows:

$$\xi_{\text{trans}(n)} = \xi_1 + \xi_2 + \ldots + \xi_{n-1} + \eta_1 + \eta_2 + \ldots + \eta_{n-1} + T_{\text{trans}} = \sum_{i=1}^{n-1} \xi_i + \sum_{i=1}^{n-1} \eta_i + T_{\text{trans}},$$

wherein ξ_i is the resolution time of the ith conflict; $\sum_{i=1}^{n-1} \xi_i$ is the total resolution time of $n - 1$ conflicts; η_i is the delay time before retransmitting the packet when the ith conflict occurs; $\sum_{i=1}^{n-1} \eta_i$ is the total delay time when $n - 1$ conflicts occur; T_{trans} is the packet transmission time (nth attempt).

If all ξ have the same distribution function $V(t)$, and all η have the same distribution function $X(t)$, then the Laplace–Stieltjes transform of the distribution function of the packet transmission time exactly after n attempts will take the form:

$$B_n^*(s) = (V_k^*(s))^{n-1} (X^*(s))^{n-1} T^*(s).$$

The Laplace–Stieltjes transform of the packet transmission time distribution function from the kth node, taking into account the conflicts that arise, will be determined by the expression:

$$Z_k^*(s) = \sum_{n=1}^\infty P_n B_n^*(s) = \sum_{n=1}^\infty \left[P_n (X^*(s))^{n-1} (V_k^*(s))^{n-1} T^*(s) \right], \quad (5)$$

$$Z_k^*(s) = \sum_{n=1}^\infty (1-q_k)^{n-1} q_k (X^*(s))^{n-1} (V_k^*(s))^{n-1} T^*(s) = q_k T^*(s) \frac{1}{1-(1-q_k)X^*(s)V_k^*(s)}, \quad (6)$$

wherein $q_k T^*(S)$ is the first term, and $(1-q_k)X^*(s)V_k^*(s)$ is the denominator of an infinitely decreasing geometric progression. Expression (6) coincides with formula (4), which proves the theorem.

Differentiating the resulting expression with respect to s, we obtain expressions for $Z_k^{(1)}$ and $Z_k^{(2)}$ of the distribution function, $Z_k(t)$, $B_k^{(1)}$, $B_k^{(2)}$. They can be used to derive functional relationships for the packet transmission times in networks [1, 2, 7].

During modeling, the network length was assumed to be 500 and 1000 m, respectively. The distribution of nodes in the network can be deterministic with equal intervals or random. In the case of random distribution, the positions of the nodes were set arbitrarily [8–16].

2. RESULTS OF THE ANALYSIS OF INDUSTRIAL NETWORK CHARACTERISTICS

The communication channel bandwidth was assumed to be C = 1 Gbit/s during modeling, and the speed of electromagnetic signal propagation along the line was $V_c = 2.9 \cdot 10^8$ m/s. The maximum retransmission delay upon collision detection (overlap of packets transmitted simultaneously) was τ = 0.0005 s. A packet with a length of L_{int} = 36 bits was used, in order to simulate interference. The directive transmission time of one packet was taken to be equal to $T_{\text{dir}}^{(1)} = 0.001$s, and the length of the transmitted packet is L_{pack} = 4096 bits. The intensity of data arrival at the nodes of the simulated network (λ_n) varied from 1200 to 1800 pack/s with an interframe interval of Δt = 0.0005 s.

The results of the numerical experiment are shown in Figs. 1–7. Analysis of the dependencies (Fig. 1) shows that with an increase in the number of network nodes and their random placement along the length of the communication line L_{network} = 500 m, as well as with a traffic intensity of λ_n = 1800 pack/s, $N = \overline{1,110}$, a uniform load ρ is achieved in the central sections of the network and the transmission channel. At the same time, the border nodes demonstrate a higher load level,

exceeding the average value by approximately 10–15%. This is due to an increase in the probability of packet conflicts at the network boundaries where mutual interference is more frequently observed. The results confirm the influence of the geometric location of nodes and the topological features of the network on the efficiency of the data transmission channel. This leads to a significant increase in the transmission time of packets from edge nodes when scaling the network due to the high load on edge nodes. The load remains virtually the same even with a deterministic equidistant distribution of nodes along the network length.

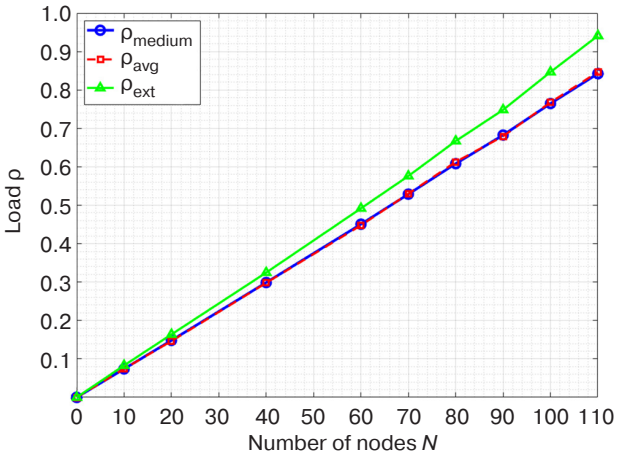

Fig. 1. Loads of the transmission medium (ρ_{medium}), extreme (ρ_{ext}), and average (ρ_{avg}) nodes with random distribution of nodes in the network

Figure 2 shows the dependence of packet transmission time on the number of network nodes N at a packet arrival rate λ_n = 1800 pack/s, where the delivery time from the average and extreme nodes is compared for two node distribution schemes: random and deterministic equidistant. The influence of network topology and node location on delivery characteristics is also shown.

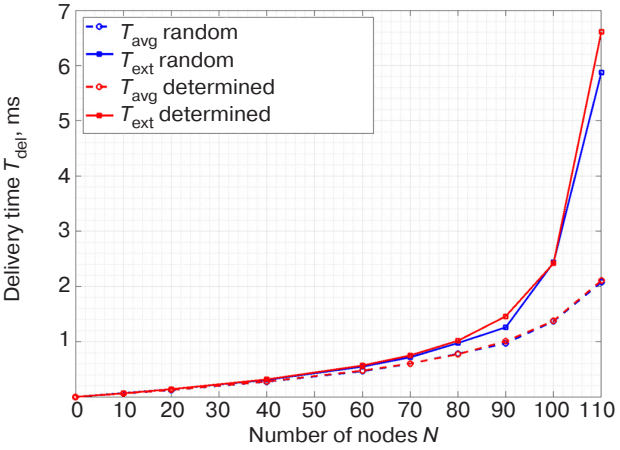

Fig. 2. Delivery time for packets arriving from the average (T_{avg}) and extreme (T_{ext}) nodes with random and deterministic equidistant distribution

The average delivery time for packets coming from extreme nodes given a large number of nodes (and accordingly when heavily loaded), can exceed the average delivery time for packets coming from middle nodes by several times. This was observed both in the case of random and deterministic equidistant node distribution. The time characteristics of packet transmission with random and deterministic equidistant placement differ insignificantly when scaling the network.

Figure 3 shows how the probability of timely delivery of Q packets depends on the total number of nodes N in the network. The analysis was performed separately for packets arriving from average and extreme nodes with a traffic generation intensity of λ_n = 1800 pack/s at each node. The graph allows us to compare how different node distribution schemes—random and deterministic equidistant—affect the guarantee of timely delivery for different categories of nodes when scaling the network. When scaling the network (increasing the number of nodes), the probability of timely packet delivery drops sharply. This drop is more pronounced for the edge nodes of the network. The nature of the network node distribution (random or deterministic equidistant) has less of an impact on the probability of timely packet delivery.

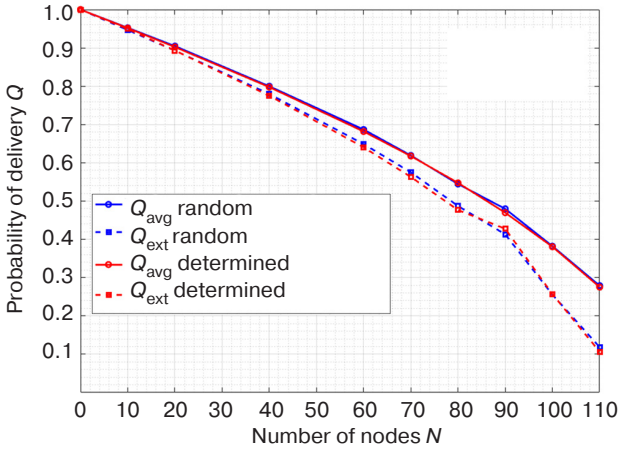

Fig. 3. Probability of timely delivery of packets coming from the middle (Q_{avg}) and extreme (Q_{ext}) nodes with random and deterministic equidistant distribution of nodes

Figure 4 shows the dependence of network performance λ_{tot} on the total number of nodes N. The study was conducted for a constant packet generation rate by each node, equal to λ_n = 1800 pack/s, $N = 1{,}110$. The graph allows us to compare the effect of network topology (random and deterministic equidistant distribution of nodes) on throughput. Analysis of the curves shows how network scaling affects its overall performance under different organizational principles.

As can be seen in Fig. 4, the type of node distribution (random or deterministic) has no significant

effect on performance. When scaling the network by increasing the number of nodes, performance first increases, then reaches a maximum and drops sharply. This is due to the fact that as the number of nodes increases, the load on the nodes and the transmission medium increases, the packet transmission time increases sharply, and, accordingly, the probability of processing packets within a time not exceeding the directive decreases. This leads to a decrease in performance.

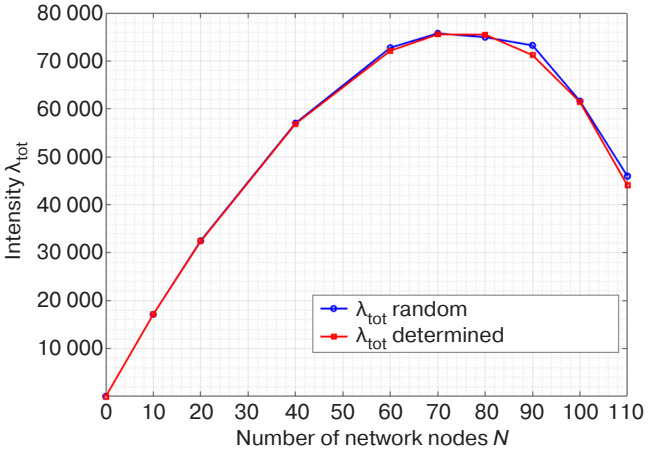

Fig. 4. Network performance with random and deterministic equidistant distribution of network nodes

Figures 5–7 demonstrate how the main characteristics of an industrial network with random multiple access change when scaled down when the intensity of packets arriving at network nodes decreases to λ_n = 1200 pack/s, $N = 1,110$.

Figure 5 shows how the number of nodes N in a network affects the load on its key elements: the transmission medium, as well as the edge and middle nodes. The data was obtained for two topology scenarios: with deterministic and random node placement at an incoming traffic intensity of λ_n = 1200 pack/s at each node. The graphs show that the load on the nodes and the transmission medium does not significantly depend on the type of node distribution, but depends significantly on the length of the network. As can be seen from the graphs, the load on the transmission medium increases much faster than the load on the nodes. At the same time, with a reduced intensity of the incoming packet flow, the growth in the load on both the nodes and the transmission medium occurs much more slowly as the network scales up. This indicates more stable system operation under moderate loads. The maximum values of the transmission channel and network node load, taking into account the influence of collisions, are achieved only with a larger total number of active network elements. This confirms the dependence of the system's efficiency on the density of its topological structure and traffic intensity. In this case in particular, the critical number of nodes N is equal to 190, while at λ_n = 1800 pack/s the critical value is N = 110 (Fig. 1).

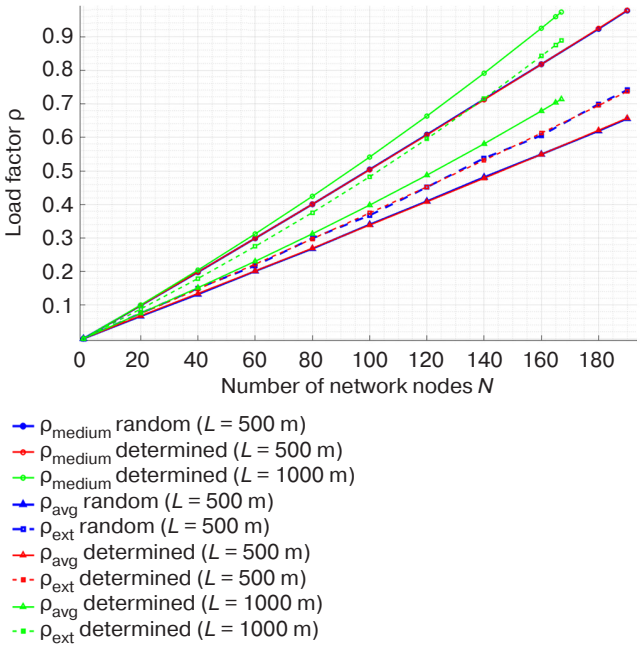

Fig. 5. Dependence of the transmission medium load (ρ_{medium}), extreme (ρ_{ext}), and average (ρ_{avg}) network nodes under deterministic and random node distribution with different network lengths

Figure 6 shows the effect of the total number of network nodes N on the packet delivery time T_{del}. The dependence was analyzed separately for packets generated by nodes located at the network boundary and nodes located at its center. In all experiments, the load intensity generated by each node was fixed and equal to λ_i = 1200 pack/s. The graph allows us to estimate how the choice of network topology—deterministic or random node distribution—affects data transmission delays when the system scale changes.

As can be seen from the graphs, the type of node distribution (random or deterministic) does not significantly affect the temporal characteristics when scaling the network. In the critical operating area (N = 190) the packet transmission time is significantly less than in the critical operating area at a packet arrival rate of λ_n = 1800 pack/s, $n = 1, N$. It was established that the critical value of the number of network nodes is N = 110. When this threshold is reached, the system transitions to saturation mode, as characterized by a change in the ratio between the load on the nodes and the data transmission channel. Analysis of the dependencies obtained (Figs. 2 and 6) showed that when the transmission medium is overloaded, the difference in the time characteristics of packet transmission between peripheral and central nodes is significantly less than in the case of overload of the

extreme nodes of the network. This indicates that under high loads, the data transmission channel becomes the determining factor in equalizing delays across the entire length of the network. Hence, it follows that when scaling an industrial network, the principle of balance should be observed, i.e., the load on the transmission medium and the load on the nodes should change approximately equally, taking into account the conflicts which may arise. To achieve this, not only must the intensity of the flows entering the nodes be selected in such a way that the load on the central nodes corresponds to the load on the transmission medium, but also the intensity of the packet flows coming for processing from the extreme nodes be reduced by 10–15% compared to the central nodes.

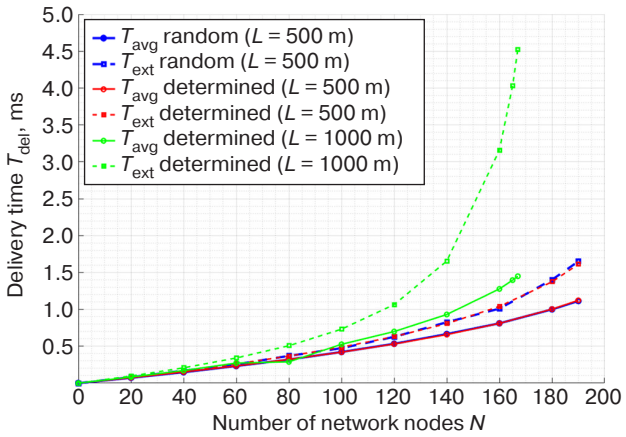

Fig. 6. Delivery time of packets arriving from the average (T_{avg}) and extreme (T_{ext}) nodes with random and deterministic node distribution for different network lengths

According to the data in Fig. 7, the performance λ_{tot} of an industrial network demonstrates the expected dependence on scale: it decreases with an increase in the number of the nodes N. However, the key result is that the type of topology (both random and deterministic equidistant distribution of nodes) does not have a significant effect on performance. This conclusion is confirmed by the graphs constructed for incoming traffic intensity λ_n = 1200 pack/s. They also indicate the dominant role of the total number of nodes, rather than their spatial distribution, in determining network throughput.

The drop in performance in the critical area of operation caused by heavy transmission medium load at N = 160–190 (Fig. 7) is significantly weaker than in the critical area caused by heavy load on the extreme nodes at N = 90–110 (Fig. 4). This is caused by the fact that the time characteristics of packet transmission increase more sharply with a high load on the extreme nodes, taking into account potential conflicts, (Fig. 2) when compared to a high load on the transmission medium (Fig. 6).

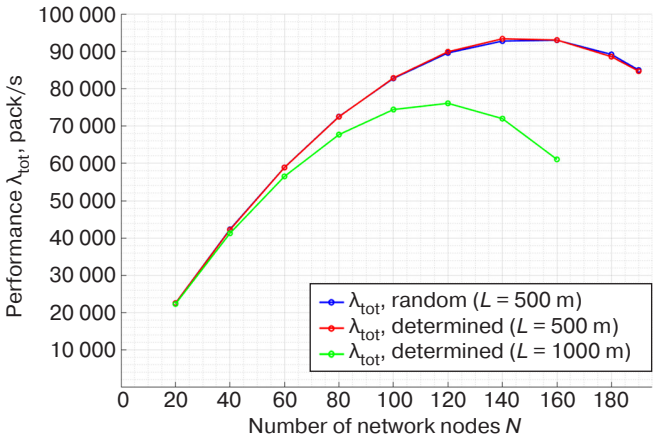

Fig. 7. Network performance λ_{tot} with a random and deterministic equidistant distribution of network nodes at different network lengths and packet arrival rates at network nodes λ_i = 1200 pack/s, $i = \overline{1,N}$

CONCLUSIONS

The performance and probabilistic-temporal characteristics of industrial networks with random multiple access were evaluated, taking into account restrictions on packet transmission time. The study formulated and then proved a theorem on the Laplace–Stieltjes transform of the packet transmission time distribution function, taking into account emerging conflicts.

The study also conducted an analysis of information transfer processes in industrial networks with random multiple access. It included changes in the number of workstations and the intensity of packet flows arriving at network nodes. A set of programs was developed and implemented, in order to automate research and evaluate various network operating modes during scaling and increased load on nodes.

The simulation showed that in the initial stages of network scaling, accompanied by an increase in the number of active nodes, there is an increase in its overall performance due to the more efficient use of available channel bandwidth. However, with a further increase in traffic intensity and load on both nodes and the transmission medium, the system's performance begins to decline. At the same time, there is a sharp increase in packet transmission delays, indicating a decrease in the efficiency of data exchange at high network traffic density. In addition, the study established that nodes located at the periphery of the network are characterized by a faster increase in packet transmission time and load level when compared to the central elements of the topology. This is due to the increased likelihood of collisions and signal interference arising from simultaneous attempts to transmit data at the edge of the network.

Taking into account potential conflicts when the number of nodes increases, studies have shown that performance and timing characteristics do not significantly depend on the type of node distribution: random or deterministic equidistant. However, they do depend significantly on the length of the network. The study also showed that the timing characteristics of packet transmission, taking into account emerging conflicts, increase more sharply with high load on the extreme nodes when compared to high load on the transmission medium.

It can be thus concluded that when scaling an industrial network, the principle of balance should be observed. The load on the transmission medium and the load on the nodes should change approximately equally, taking into account emerging conflicts. In order to achieve this, not only must the intensity of the flows entering the nodes be selected in such a way that the load on the central nodes corresponds to the load on the transmission medium, but also the intensity of the packet flows coming for processing from the extreme nodes be reduced by 10–15% when compared to the central nodes.

Authors' contribution. All authors contributed equally to the research work.

REFERENCES

1. Zhmatov D.V., Leontyev A.S. Analysis of information transmission processes in multimode fiber-optic networks with a token-based access method. *Russian Technological Journal.* 2025;13(5):41–50. https://doi.org/10.32362/2500-316X-2025-13-5-41-50
2. Leontyev A.S. Development of Analytical Methods, Models, and Techniques for Local Area Networks Analysis. In: *Theoretical Issues of Software Engineering: Interuniversity Collection of Scientific Papers*. Moscow: MIREA; 2001. P. 70–94 (in Russ.).
3. Leontyev A.S., Zhmatov D.V. Study of the probabilistic and temporal characteristics of wireless networks using the CSMA/CA access method. *Russian Technological Journal.* 2024;12(2):67–76. https://doi.org/10.32362/2500-316X-2024-12-2-67-76
4. Ferguson C., Kleinrock L. Optimal Update Times for Stale Information Metrics Including the Age of Information. *IEEE Journal on Selected Areas in Information Theory*. 2023;4:734–746. https://doi.org/10.1109/JSAIT.2023.3344760
5. He Z., Kleinrock L. Optimization of Assisted Search Over Server-Mediated Peer-to-peer Networks. In: *GLOBECOM 2022 – 2022 IEEE Global Communications Conference*. Rio de Janeiro, Brazil. 2022. P. 4928–4934. https://doi.org/10.1109/GLOBECOM48099.2022.10000846
6. Sapna, Sharma M. Performance evaluation of a wired network with & without Load Balancer and Firewall. In: *2010 International Conference on Electronics and Information Engineering*. Kyoto, Japan. 2010. P. V2-515–V2-519. https://doi.org/10.1109/ICEIE.2010.5559755
7. Smirnova E.V. *Tekhnologii sovremennykh setei Ethernet. Metody kommutatsii i upravleniya potokami dannykh* (*Technologies of Modern Ethernet Networks. Methods of Switching and Data Flow Control*). Moscow: BHV-Peterburg; 2017, 480 p. (in Russ.).
8. Ivanichkina L.V., Neporada A.L. The reliability model of a distributed data storage in case of explicit and latent disk faults. *Trudy Instituta sistemnogo programmirovaniya RAN = Proceedings of the Institute for System Programming of the RAS*. 2015;27(6):253–274 (in Russ.). https://doi.org/10.15514/ISPRAS-2015-27(6)-16
9. Wei M., Chen Z. Study of LANs access technologies in wind power system. In: *IEEE PES General Meeting*. Minneapolis, MN, USA. 2010. https://doi.org/10.1109/PES.2010.5590088
10. Alshaev I.A., Lavrukhin V.A. Wi-Fi networks designand optimization. *Informatsionnye tekhnologii i telekommunikatsii = Telecom IT.* 2016;4(1):87–95 (in Russ.). https://www.elibrary.ru/wbdxbt
11. Zvonareva G.A., Buzunov D.S. Using Simulation Modeling to Estimate Time Characteristics of a Distributed Computing System. *Otkrytoe obrazovanie = Open Education.* 2022;26(5):32–39 (in Russ.). https://doi.org/10.21686/1818-4243-2022-5-32-39
12. Talalaev A.A., Frolenko V.P. Fault-tolerant system for organizing high-performance computing for solving data stream processing problems. *Programmnye sistemy: Teoriya i prilozheniya = Program Systems: Theory and Applications*. 2018;9(1-36): 85–108 (in Russ.). https://doi.org/10.25209/2079-3316-2018-9-1-85-108
13. Pavsky V.A., Pavsky K.V. Mathematical Model for Calculating Reliability Indicators of Scalable Computer Systems Considering Switching Time. *Izvestiya YuFU. Tekhnicheskie nauki = Izvestiya SFedU. Engineering Sciences*. 2020;2(212):134–145 (in Russ.). https://doi.org/10.18522/2311-3103-2020-2-134-145
14. Ahmed W., Wu Y.W. A survey on reliability in distributed systems. *J. Comput. System Sci*. 2013;79(8):1243–1255. https://doi.org/10.1016/j.jcss.2013.02.006
15. Bakhareva N.F. Performance analysis of network structures by methods of queuing theory. *Informatika, telekommunikatsii i upravlenie = Computing, Telecommunication and Control.* 2009;3(80):25–34 (in Russ.). https://www.elibrary.ru/kxxbqv
16. Sharafullina A.Yu., Galyamov R.R., Zaripova R.S. Technical principles for creating a wireless local network Wi-Fi. *T-Comm: Telekommunikatsiya i transport = T-Comm.* 2021;15(7):28–33 (in Russ.). https://doi.org/10.36724/2072-8735-2021-15-7-28-33

СПИСОК ЛИТЕРАТУРЫ

1. Жматов Д.В., Леонтьев А.С. Анализ процессов передачи информации в многомодовых оптоволоконных сетях с маркерным методом доступа. *Russian Technological Journal*. 2025;13(5):41–50. https://doi.org/10.32362/2500-316X-2025-13-5-41-50
2. Леонтьев А.С. Разработка аналитических методов, моделей и методик анализа локальных вычислительных сетей. *Теоретические вопросы программного обеспечения: Межвузовский сборник научных трудов*. М.: МИРЭА; 2001. С. 70–94.
3. Леонтьев А.С., Жматов Д.В. Исследование вероятностно-временных характеристик беспроводных сетей с методом доступа CSMA/CA. *Russian Technological Journal.* 2024;12(2):67–76. https://doi.org/10.32362/2500-316X-2024-12-2-67-76
4. Ferguson C., Kleinrock L. Optimal Update Times for Stale Information Metrics Including the Age of Information. *IEEE Journal on Selected Areas in Information Theory*. 2023;4:734–746. https://doi.org/10.1109/JSAIT.2023.3344760
5. He Z., Kleinrock L. Optimization of Assisted Search Over Server-Mediated Peer-to-peer Networks. In: *GLOBECOM 2022 – 2022 IEEE Global Communications Conference*. Rio de Janeiro, Brazil. 2022. P. 4928–4934. https://doi.org/10.1109/GLOBECOM48099.2022.10000846
6. Sapna, Sharma M. Performance evaluation of a wired network with & without Load Balancer and Firewall. In: *2010 International Conference on Electronics and Information Engineering*. Kyoto, Japan. 2010. P. V2-515–V2-519. https://doi.org/10.1109/ICEIE.2010.5559755
7. Смирнова Е.В. *Технологии современных сетей Ethernet. Методы коммутации и управления потоками данных*. М.: БХВ-Петербург; 2017, 480 с.
8. Иваничкина Л.В., Непорада А.Л. Модель надежности распределенной системы хранения данных в условиях явных и скрытых дисковых сбоев. *Труды Института системного программирования РАН*. 2015;27(6):253–274. https://doi.org/10.15514/ISPRAS-2015-27(6)-16
9. Wei M., Chen Z. Study of LANs access technologies in wind power system. In: *IEEE PES General Meeting*. Minneapolis, MN, USA. 2010. https://doi.org/10.1109/PES.2010.5590088
10. Альшаев И.А., Лаврухин В.А. О проектировании и оптимизации сетей Wi-Fi. *Информационные технологии и телекоммуникации*. 2016;4(1):87–95. https://www.elibrary.ru/wbdxbt
11. Звонарева Г.А., Бузунов Д.С. Использование имитационного моделирования для оценки временных характеристик распределенной вычислительной системы. *Открытое образование*. 2022;26(5):32–39. https://doi.org/10.21686/1818-4243-2022-5-32-39
12. Талалаев А.А., Фроленко В.П. Отказоустойчивая система организации высокопроизводительных вычислений для решения задач обработки потоков данных. *Программные системы: Теория и приложения*. 2018;9(1-36):85–108. https://doi.org/10.25209/2079-3316-2018-9-1-85-108
13. Павский В.А., Павский К.В. Математическая модель для расчета показателей надежности масштабируемых вычислительных систем с учетом времени переключения. *Известия ЮФУ. Технические науки*. 2020;2(212):134–145. https://doi.org/10.18522/2311-3103-2020-2-134-145
14. Ahmed W., Wu Y.W. A survey on reliability in distributed systems. *J. Comput. System Sci*. 2013;79(8):1243–1255. https://doi.org/10.1016/j.jcss.2013.02.006
15. Бахарева Н.Ф. Анализ производительности сетевых структур методами теории массового обслуживания. *Информатика, телекоммуникации и управление*. 2009;3(80):25–34. https://www.elibrary.ru/kxxbqv
16. Шарафуллина А.Ю., Галямов Р.Р., Зарипова Р.С. Технические принципы создания беспроводной локальной сети Wi-Fi. *T-Comm: Телекоммуникация и транспорт*. 2021;15(7):28–33. https://doi.org/10.36724/2072-8735-2021-15-7-28-33

About the Authors

Alexander S. Leontyev, Cand. Sci. (Eng.), Senior Researcher, Associate Professor, Department of Mathematical Support and Standardization, Institute of Information Technologies MIREA – Russian Technological University (78, Vernadskogo pr., Moscow, 119454 Russia). E-mail: leontev@mirea.ru. RSCI SPIN-code 5798-9721, https://orcid.org/0000-0003-3673-2468

Dmitry V. Zhmatov, Cand. Sci. (Eng.), Associate Professor, Department of Mathematical Support and Standardization, Institute of Information Technologies MIREA – Russian Technological University (78, Vernadskogo pr., Moscow, 119454 Russia). E-mail: zhmatov@mirea.ru. Scopus Author ID 56825948100, RSCI SPIN-code 2641-6783, https://orcid.org/0000-0002-7192-2446

Об авторах

Леонтьев Александр Савельевич, к.т.н., старший научный сотрудник, доцент, кафедра математического обеспечения и стандартизации информационных технологий, Институт информационных технологий, ФГБОУ ВО «МИРЭА – Российский технологический университет» (119454, Россия, Москва, пр-т Вернадского, д. 78). E-mail: leontev@mirea.ru. SPIN-код РИНЦ 5798-9721, https://orcid.org/0000-0003-3673-2468

Жматов Дмитрий Владимирович, к.т.н., доцент, кафедра математического обеспечения и стандартизации информационных технологий, Институт информационных технологий, ФГБОУ ВО «МИРЭА – Российский технологический университет» (119454, Россия, Москва, пр-т Вернадского, д. 78). E-mail: zhmatov@mirea.ru. Scopus Author ID 56825948100, SPIN-код РИНЦ 2641-6783, https://orcid.org/0000-0002-7192-2446

Translated from Russian into English by Lyudmila O. Bychkova
Edited for English language and spelling by Dr. David Mossop

UDC 378.1
https://doi.org/10.32362/2500-316X-2026-14-2-134-145
EDN BYDBUX

RESEARCH ARTICLE

Formation of a comprehensive approach to developing the scientific and educational infrastructure of a modern engineering university

Stanislav A. Kudzh, Natalia B. Golovanova @, Yuri G. Grafov

MIREA – Russian Technological University, Moscow, 119454 Russia
@ Corresponding author, e-mail: golovanova@mirea.ru

• **Submitted:** 05.12.2025 • **Revised:** 15.12.2025 • **Accepted:** 18.02.2026

Abstract

Objectives. The work sets out to develop a comprehensive approach to grounding decisions aimed at advancing the scientific and educational infrastructure of an engineering university. This includes selecting modernization policies for the scientific and educational infrastructure, substantiating the format of scientific and educational infrastructure objects in light of the diversity of current tasks, involving industry partners in implementing infrastructure policies, as well as addressing resource support issues using mathematical formalization and analytical evaluation tools.

Methods. Methods of systems and strategic analysis, comparison and formalization, modeling and statistical indicators, as well as change management, risk assessment, and strategy actualization approaches, were used.

Results. Ensuring the contribution of modern engineering universities to technological leadership is an ambitious task that requires a focused approach to the development of scientific and educational infrastructure. One effective solution consists in the creation of specialized laboratories, or mega-laboratories, which are considered as an optimal format for the scientific and educational infrastructure. Such laboratories combine educational, research, and communication zones, along with their respective advantages and typologies. The importance of collaboration with industry partners in driving innovation, helping to ensure that educational programs, research, and development align with market needs, is demonstrated. A mathematical model is developed for evaluating projects associated with the establishment of a mega-laboratory based on a comprehensive system of indicators. This model was used to formalize the procedure for selecting and financing of newly created scientific and educational infrastructure.

Conclusions. Infrastructure constraints defined at the state level in the context of technological development and the need to ensure technological independence are becoming a key challenge for engineering universities. This necessitates the development of tools for seeking, justifying, and making managerial decisions. The described comprehensive approach takes into account current requirements for scientific and educational infrastructure facilities, including a high degree of integration between education and science, and the involvement of industry partners in the development process in order to bridge the gap between education, science, and the demands of the real economy. The formulated recommendations and proposed solutions effectively address the issues faced by modern engineering universities within development programs.

Keywords: engineering university, scientific and educational infrastructure, mega-laboratories, industrial partnership, infrastructure project assessment, strategic planning, interdisciplinary research, technological development, mathematical model, performance indicator system

For citation: Kudzh S.A., Golovanova N.B., Grafov Yu.G. Formation of a comprehensive approach to developing the scientific and educational infrastructure of a modern engineering university. *Russian Technological Journal.* 2026;14(2): 134–145. https://doi.org/10.32362/2500-316X-2026-14-2-134-145, https://www.elibrary.ru/BYDBUX

Financial disclosure: The authors have no financial or proprietary interest in any material or method mentioned.

The authors declare no conflicts of interest.

НАУЧНАЯ СТАТЬЯ

Формирование комплексного подхода к развитию научно-образовательной инфраструктуры современного инженерного университета

С.А. Кудж, Н.Б. Голованова [@], Ю.Г. Графов

МИРЭА – Российский технологический университет, Москва, 119454 Россия
[@] Автор для переписки, e-mail: golovanova@mirea.ru

• **Поступила:** 05.12.2025 • **Доработана:** 15.12.2025 • **Принята к опубликованию:** 18.02.2026

Резюме

Цели. Целью статьи является разработка комплексного подхода к обоснованию решений, направленных на развитие научно-образовательной инфраструктуры инженерного университета, включающего выбор политики модернизации научно-образовательной инфраструктуры, обоснование формата объектов научно-образовательной инфраструктуры с учетом многообразия актуальных задач, вовлечение индустриальных партнеров в реализацию инфраструктурной политики, а также вопросы ресурсного обеспечения, реализуемого с применением инструментов математической формализации и аналитической оценки.

Методы. В исследовании использованы методы системного и стратегического анализа, методы сравнения и формализации, методы моделирования и статистических показателей, методы управления изменениями и рисками, а также метод актуализации стратегии.

Результаты. Масштабные задачи по обеспечению вклада современных инженерных университетов в достижение технологического лидерства требуют особого внимания к вопросам развития научно-образовательной инфраструктуры. Эффективным решением является создание лабораторий особого типа – мегалабораторий, которые рассматриваются как оптимальный формат объекта научно-образовательной инфраструктуры, сочетающий учебные, исследовательские и коммуникационные зоны с их преимуществами и типологией. Обоснована значимость партнерства с индустриальными партнерами как ключевого драйвера развития, обеспечивающего соответствие образовательных программ, исследований и разработок потребностям рынка. Разработана математическая модель оценки проекта создания мегалаборатории, основанная на комплексной системе показателей, позволяющая формализовать процедуру выбора и принятия решения о финансировании вновь создаваемых объектов научно-образовательной инфраструктуры.

Выводы. Определенные на государственном уровне инфраструктурные ограничения в условиях технологического развития и необходимости достижения технологического лидерства становятся для инженерных университетов ключевым вызовом, требующим формирования инструментария поиска, обоснования и принятия управленческих решений по развитию объектов научно-образовательной инфраструктуры. Использование комплексного подхода позволяет максимально учесть актуальные требования к объектам

научно-образовательной инфраструктуры, включая высокий уровень интеграции образования и науки, необходимость учета и включения в процесс развития индустриальных партнеров как залог сближения образования, науки и потребностей реальной экономики. Сформулированные рекомендации и предложенные решения позволяют эффективно решать задачи, стоящие перед современными инженерными университетами в рамках программ развития.

Ключевые слова: инженерный университет, научно-образовательная инфраструктура, мегалаборатории, индустриальное партнерство, оценка инфраструктурных проектов, стратегическое планирование, междисциплинарные исследования, технологическое развитие, математическая модель, система показателей эффективности

Для цитирования: Кудж С.А., Голованова Н.Б., Графов Ю.Г. Формирование комплексного подхода к развитию научно-образовательной инфраструктуры современного инженерного университета. *Russian Technological Journal*. 2026;14(2):134–145. https://doi.org/10.32362/2500-316X-2026-14-2-134-145, https://www.elibrary.ru/BYDBUX

Прозрачность финансовой деятельности: Авторы не имеют финансовой заинтересованности в представленных материалах или методах.

Авторы заявляют об отсутствии конфликта интересов.

INTRODUCTION

During a strategic session on education development in autumn 2024, which was chaired by the Prime Minister of the Russian Federation, M.V. Mishustin[1], and also attended by the Minister of Science and Higher Education of the Russian Federation, V.N. Falkov, infrastructure limitations were highlighted as one of the current challenges faced by the higher education system and engineering universities[2]. Therefore, university management focuses on developing the required material and technical basis, which largely determines the ability to train qualified engineering personnel for the Russian high-tech economy, conducting scientific research and development (R&D) to achieve technological leadership, and thus ensuring technological independence.

In today's socioeconomic climate, the development of the material and technical infrastructure of an engineering university presents a complex challenge. While the search for funding is undoubtedly an important aspect, universities also need to adapt to the rapidly evolving technological landscape and respond to ongoing changes. The "Concept of Technological Development of the Russian Federation until 2030," approved by Directive No. 1315-r of the Government of the Russian Federation on May 20, 2023[3], identifies the rapid acceleration in the creation and diffusion of novel technologies, including digital technologies that are radically changing markets and production systems, as one of the main threats to technological advancement. If an engineering university fails to address this issue effectively, it may be forced to adopt a "catch-up" development model, resulting in a lag in training engineering personnel and a decline in innovative R&D efforts.

The main task of any university administration is to create favorable conditions for learning. This includes maintaining buildings, structures, and land plots in a state that is conducive to education and scientific research, e.g., carrying out preventive maintenance on air conditioning and ventilation systems, etc. It is also necessary to provide constant support for developing the interest of students in mastering modern, innovative solutions, software and hardware complexes, conducting advanced scientific research, as well as organizing closer cooperation with leading companies in the Russian Federation, including in the production of goods and the introduction of new product quality control methods. The key to effective learning consists in motivating the desire of students for continuous improvement and the acquisition of new knowledge. In this regard, the students' conviction that their practical skills are being developed using the latest equipment and modern instruments becomes a crucial element.

STRATEGIC DEVELOPMENT DIRECTION OF SCIENTIFIC AND EDUCATIONAL INFRASTRUCTURE

One of the key areas of development for a modern engineering university, since underpinning its educational and scientific activities, is widely considered to lie in the modernization of material and technical resources, primarily laboratories. However, despite the importance of considering approaches to infrastructure policy implementation, issues related to laboratory facility development strategy and proposed project evaluation have not received adequate attention.

[1] http://government.ru/news/53144/. Accessed February 04, 2026. (In Russ.).

[2] https://www.minobrnauki.gov.ru/press-center/news/novosti-ministerstva/90823/. Accessed February 04, 2026. (In Russ.).

[3] The Concept of Technological Development of the Russian Federation until 2030. Directive of the Government of the Russian Federation of May 20, 2023 г. No. 1315-r. http://government.ru/docs/48570/. Accessed February 04, 2026. (In Russ.).

Research into engineering university development, particularly in terms of the training of engineering personnel, is attracting increased interest[4] [1–4]. With regard to scientific and educational infrastructure, only isolated statements acknowledge the role and importance of laboratories without revealing the full depth and complexity of the issue of creating and developing such infrastructure. For example, it is stated in the study by L.B. Sobolev that "only strong (and wealthy) scientific laboratories at universities are capable of creating a basis for the transition to a digital economy" [5]. According to F.F. Sharipov, educational and scientific laboratories at universities are one of the key elements in tackling the tasks set out in the Strategy for Scientific and Technological Development [6]. Nevertheless, the study fails to adequately address the question of how to create laboratories that will actively contribute to scientific and technological development or how to solve the problems that inevitably arise as part this process.

Clearly, infrastructure policy can be implemented in a variety of ways, with the specific approach taken depending on the particular strategy adopted for developing scientific and educational infrastructure. However, it is clear that the development of a university's material and technical base is will require active management. Otherwise, "the lack of proper attention to this issue... has a negative impact on the quality of the educational process as a whole" [7].

RTU MIREA's strategy involves the creation of mega-laboratories (mega-labs) as unique scientific and educational complexes. At present, mega-labs form the core of RTU MIREA's scientific and educational infrastructure. Boasting the most advanced technological solutions, these facilities offer a wide range of possibilities for use in both educational and research activities.

In addition to identifying a location for laboratory work or a researcher's workspace, the establishment of a mega-lab involves also entails organizing the procurement and installation of equipment, along with its appropriate placement in a designated space. A mega-lab is a specialized type of educational and research facility, encompassing a scientific and academic complex that includes classrooms, areas for collaborative research, offices, communications spaces, and informal areas. It is designed to be a comfortable working environment with various infrastructure components for all concerned parties.

Several compelling reasons can be adduced to justify the emphasis on establishing mega-labs.

Firstly, the mega-lab concept structures the development of large, well-equipped facilities focused on executing significant educational and research initiatives, which are capable of addressing their own resource requirements.

Secondly, it provides an opportunity for the implementation of interdisciplinary projects that are strategically significant for the overall development of the university, the realization of its development program, and the enhancement of the volume and quality of work and services provided for the benefit of all concerned parties.

Thirdly, mega-labs provide a convenient means of attracting industrial partners and leveraging co-financing mechanisms for projects that utilize the mega-lab concept for educational and research activities.

Fourthly, economies of scale are achieved through the introduction of the most advanced equipment, sophisticated systems, technologies, software, and hardware solutions, which are utilized by various departments of institutes for education and research. This serves to reduce unit costs and operating expenses.

Fifthly, there is an opportunity to apply for state support in relation to the implementation of regional and national projects, as well as securing co-funding for basic or applied scientific research in areas where RTU MIREA has achieved significant progress. This is of particular relevance when participating in competitions organized by the Russian Ministry of Education and Science (Minobrnauka)[5], Ministry of Industry and Trade (Minpromtorg)[6], etc., for the implementation of which projects the university is required to attract external funding.

Sixthly, the concept structures the upgrading of material and technical infrastructure of previously established mega-labs that have proven their efficacy in terms of providing an excellent basis for developing professional expertise.

Finally, the establishment of mega-labs develops model solutions for scientific and educational infrastructure that can be scaled and replicated to further enhance engineering education and improve the effectiveness of scientific R&D in line with the national scientific and technological development agenda. For this reason, all mega-lab projects are equipped with a comprehensive range

[4] Analytical report of the HSE Labor Market Research Laboratory: "Graduates of Engineering Specialties: Resistance of Materials in the Russian Labor Market." https://www.hse.ru/data/2025/04/15/1951597714/Report_20250415.pdf. Accessed February 04, 2026. (In Russ.).

[5] The Ministry of Science and Higher Education of the Russian Federation (Minobrnauka). https://minobrnauki.gov.ru/. Accessed February 04, 2026. (In Russ.).

[6] The Ministry of Industry and Trade of the Russian Federation (Minpromtorg). https://minpromtorg.gov.ru/. Accessed February 04, 2026. (In Russ.).

of methodological, educational aids, and materials, including video lectures for conducting classes at universities at which programs and projects are carried out in collaboration with strategic partners of RTU MIREA. This is certainly beneficial for partner organizations that need to select a site for testing technological and organizational solutions as model solutions for future implementation.

When developing the university's scientific and educational infrastructure through the establishment of mega-labs, the decision regarding the feasibility of a given project should be informed by its typological differentiation. This is important since each identified type of mega-lab is characterized not only by its specific functional purpose and objectives, but also by its financial model.

One typological approach includes projects for developing mega-labs focused on fundamental disciplines. While the primary purpose of such mega-labs consists in the provision of support for educational activities, they may also serve as platforms for conducting fundamental research. Funding for these projects is provided through the RTU MIREA centralized fund.

The second type of mega-lab is associated with projects that are developing future technologies. These are research and development platforms where work is carried out on tasks that may not have an identified end user at the current stage, but whose results are likely to be in high demand in the near future. These labs can be "seen as a testing ground for promising ideas and for identifying potential leaders who will organize new areas of research."[7] Financial support for these projects is provided through the RTU MIREA centralized fund, taking into account the obligations of the educational and research departments to explore new areas of activity.

The third—most prevalent—type of mega-lab focuses on addressing urgent practical issues, such as the training of engineering personnel, as well as the conduct of scientific research and development that is in high demand. These laboratories primarily concentrate on interdisciplinary and multidisciplinary projects within educational and research activities, as well as the creation of experimental production facilities. There is "increasing demand for technical universities to act as production laboratories for promising innovations."[8] The establishment of such mega-labs necessitates active collaboration with industrial partners.

PARTNERSHIP AS A DRIVER OF SUSTAINABLE DEVELOPMENT OF THE ENGINEERING UNIVERSITY

The interaction between universities, organizations, and businesses is a rapidly evolving trend in modern higher education [8]. Such interaction, which allows engineers to be trained to meet specific employer needs, involves research and development carried out on products and technological solutions that align with a company's current technical capabilities and future goals.

The issue of collaboration between universities and industry partners is not new [9]. However, as noted in one publication, "domestic universities often implement traditional and conventional technologies and methods for working with companies," and "the scope and effectiveness of such collaboration is often constrained by a lack of a systematic approach" [10].

Active collaboration can clearly emerge where the interests and expertise of universities and businesses intersect, creating a continuous scientific and industrial chain "from concept to implementation" for specific products. Therefore, partnerships between engineering institutions and business entities, which should be long-term rather than one-time events or initiatives, must be aimed at promoting university growth. However, such expansion and development will only occur if the collaboration satisfies the interests of both parties, with mutual benefit acting as a sort of "strategic screening mechanism" that allows for informed management decisions and guarantees advantages for each participant.

The interaction between universities and industry partners is developing especially dynamically among those participating in the Priority 2030 program. As noted by D.N. Chernyshenko, Deputy Prime Minister of the Russian Federation, universities are "building and strengthening partnerships with companies in the real economy. Over the past two and a half years, more than 420 consortia have been formed as part of the program, uniting universities, research organizations, and businesses. Over 6000 agreements have been concluded with industrial partners totaling more than RUR 62 bn."[9]

In light of the ongoing collaborative efforts between universities and industry partners, a strategic approach should set out to involve industry representatives in the development the university's academic and research infrastructure. Partner involvement is essential for several reasons. Firstly, it involves the formulation of a comprehensive schedule for establishing a new academic and research environment that addresses current challenges. Such an environment should provide physical and technical facilities that take into account the interests

[7] https://www.rbc.ru/society/14/11/2022/63720d159a794767085e7261. Accessed February 04, 2026. (In Russ.).

[8] https://rectorspeaking.ru/tekhnicheskie-vuzy-dolzhny-stat. Accessed February 04, 2026. (In Russ.).

[9] https://www.minobrnauki.gov.ru/press-center/news/novosti-ministerstva/90675/. Accessed February 04, 2026. (In Russ.).

of all concerned parties. Secondly, establishing each mega-lab at a major engineering institution like RTU MIREA is a costly undertaking that requires significant financial resources. Through partnership with industry, universities can share costs and leverage expertise and resources to ensure the success of the associated projects.

The financial strategy of a modern university necessarily involves the development of initiatives to diversify the sources of funding for its operations, including attracting investments from employers and other concerned parties [11]. This diversification process is based on the engagement of various parties in innovative activities such as the implementation of R&D results in the operations of existing enterprises and the establishment of new ones. Additionally, it involves collaboration with partners in research and design activities, which enhances the potential for scientific research and innovation.

In most cases, opportunities for collaboration and engagement with an industrial partner are realized in mega-lab projects of the third type, which are the most ambitious and focus on interdisciplinary and multidisciplinary development. The financial model for these projects involves co-funding from an industrial partner who acquires the status of strategic partner to the university. This includes the replication of proposed solutions across universities throughout the country, as well as the implementation of research and project activities through network interaction and networked educational projects and programs (including continuing education programs).

The development of these processes is facilitated by a number of developments in higher education. These include the transition of educational organizations to autonomous status, the establishment of a financing system that is aligned with modern economic conditions, and the development of an endowment fund system. Such developments should contribute to enhancing the independence of educational institutions. However, in order to attract such funding, a well-established system of collaboration, cooperation, and partnership with businesses and organizations becomes essential.

EVALUATION OF MEGA-LAB DEVELOPMENT PROJECTS FUNDED BY THE CENTRALIZED FUND

Although the mega-lab development projects at RTU MIREA receive funding from a centralized fund, a substantial portion of this funding comes from revenue-generating activities. This constitutes an important financial asset for the university today, enabling it to pursue its development objectives, including those pertaining to its scientific and educational infrastructure [12].

In light of the increasing need to modernize the material and technical infrastructure, as well as the development of new areas of scientific and academic activity, it is essential that the decision regarding funding be justified based on established criteria. Since the choice regarding which project to pursue for the development of the scientific and academic infrastructure is a managerial decision, the selected criteria must be clearly related to the institution's operations and aimed at achieving strategic goals [13]. Given limited resources, the primary criterion for making such a decision should be to maximize the project's benefit to the institution. Simultaneously, it is critical to ensure transparency in competitive processes, which enhances employee confidence in management decisions and, ultimately, improves the efficiency and efficacy of operations.

Given the limited financial resources available to educational institutions, a transparent process is necessary for the selection of laboratory development projects. This process serves as a reliable and efficient tool for university administration in the development of scientific and educational infrastructure [14].

The creation of a system to select mega-lab projects supported by the university has resulted in the following research goals being identified: the development of a set of indicators to provide a comprehensive evaluation of the proposed projects; the selection and validation of an approach for integrating project evaluation; and the creation of a rating system to inform decisions regarding project support.

The primary consideration for selecting a project is the expected value and potential benefits of the mega-lab in addressing challenges in critical areas of activity. Based on this criterion, a framework of indicators has been established to describe the key aspects of the proposed mega-lab. This framework consists of five groups of indicators, which are further divided into specific sub-indicators (Table 1):

These include:

- educational activities;
- research and development;
- collaboration with industry partners;
- relevance and significance of the project;
- uniqueness of the project.

The list of indicators above shows how each project is evaluated. The evaluation is based on two main types of activity: education and research. The involvement of industrial partners is also evaluated as an indicator of the project's value to the real economy. In addition to the aforementioned three components, the proposed system of indicators incorporates image characteristics that take improved perceptions of the project into account.

Except for those in the fifth group, each indicator's logical formula is based on the principle of relative value in the form of an index (Table 2). This ensures the comparability of all heterogeneous indicators and results, and enables them to be aggregated into a summary indicator despite the multidimensionality of the source information [15].

Table 1. Comprehensive system of indicators for evaluating the mega-lab project

No.	Group of Indicators	Sub-indicator
1	Educational activities	1.1. Expected workload of the mega-lab with training sessions 1.2. Expected coverage of students in classes at the mega-lab 1.3. Expected involvement of educational and research departments in using the mega-lab for educational purposes
2	Research and development (R&D)	2.1. Profitability of research projects conducted at the mega-lab 2.2. Publication activity aligned with the focus of the mega-lab 2.3. Contribution of R&D outcomes generated at the mega-lab to the university's overall research efforts 2.4. Efficiency in human resource utilization 2.5. Engagement of young researchers in R&D
3	Collaboration with industry partners	3.1. Participation of an industry partner in co-funding the establishment of a mega-lab 3.2. Use by the industry partner of a targeted training program for personnel development 3.3 Employment of university graduates in enterprises and organizations of an industrial partner
4	Relevance and significance of the project	4.1 Correspondence of the topics of scientific and educational projects and mega-lab activities with the national technological leadership project (NTLP) directions. 4.2 Integration of mega-lab's core activities into RTU MIREA strategic goals
5	Uniqueness of the project	5.1 Absence of analogues: A fundamentally new mega-lab 5.2 Uniqueness of individual mega-lab components 5.3 Modernization of existing mega-lab

Table 2. Index system for evaluating projects for the development of scientific and educational infrastructure

1	**Educational activities** $I_{EA} = \frac{I_l + I_{cov} + I_{con}}{3}$ is the index of the mega-lab workload in educational activities
1.1	I_l is the index of the mega-lab expected load. $I_l = \frac{TCH}{ML}$, where TCH is total volume of classroom hours scheduled (prescribed) for laboratory work and practical exercises in mega-lab for the academic year, in hours; ML is the maximum possible workload of mega-lab, in hours
1.2	I_{cov} is the index of the expected coverage of students. $I_{cov} = \frac{C_1 + C_2 + ... + C_i}{C_{total}}$, where C_i is the expected number of students (or individuals) from academic departments participating in the mega-lab activities, persons; C_{total} is the total number of students at the university at the time of applying, persons
1.3	I_{inv} is the index of expected involvement of academic and research departments. $I_{inv} = \frac{N}{M}$, where N is the number of academic and research departments whose students plan to participate in mega-lab activities; M is the total number of academic and research departments at the university
2	**Research and development** $I_R = \frac{I_{profit} + I_{hr} + I_{yr} + I_{inv} + I_{pa}}{5}$ is the index of mega-lab utilization for R&D
2.1	I_{profit} is the profitability index of research projects carried out at mega-lab. $I_{profit} = \frac{(P_{exp} + P_{spec} + P_{exist}) - (E_{exp} + E_{spec} + E_{exist})}{P_{exp} + P_{spec} + P_{exist}}$, where: P_{exp} is the expected profit for research projects scheduled to be carried out at the mega-lab, RUR mln; P_{spec} is the profit gained by the university from completed research projects under existing contracts (stages) in the relevant field of specialization over the past three years, RUR mln; P_{exist} is the expected profit from research projects under existing contracts (stages) within the relevant field of specialization, RUR mln;

Table 2. Continued

2.1	E_{exp} is estimated expenses (excluding contributions to the centralized fund of the university) for research projects scheduled to be conducted at the mega-lab, RUR mln; E_{spec} is expenses (excluding contributions to the centralized fund of the university) for completed contracts (stages) for research projects within the relevant field of specialization over the past 3 years, RUR mln; E_{exist} is expected expenses (excluding contributions to the centralized fund of the university) for research projects (stages) with the relevant field of specialization, RUR mln
2.2	I_{hr} is the human resource utilization index. $I_{hr} = \frac{C_{emp}}{C_{fte}}$, where C_{fte} is the number of full-time equivalents allocated for carrying out R&D projects; C_{emp} is the number of full-time employees in R&D projects, person
2.3	I_{yr} is the recruitment index for young researchers to carry out R&D. $I_{yr} = \frac{P_{yr}}{P_{emp}}$, where P_{yr} is the number of young researchers involved in the R&D implementation: up to 35 years old without an academic degree, up to 35 years old with the Candidate of Science degree or up to 40 years old with the Doctor of Sciences degree, persons; P_{emp} is the number of employees actually involved in the R&D implementation, persons
2.4	I_{con} is the contribution index of the R&D performed at the mega-lab to the results of the university's research activities. $I_{con} = \frac{C_{fsp}}{C_{total}}$, where C_{fsp} is the cost of field-specific projects performed over the past 3 years (certificates of acceptance of works), RUR mln; C_{total} is the total cost of completed R&D projects at the university over the past 3 years (certificates of acceptance of works), RUR mln
2.5	I_{pa} is the publication activity index related to the mega-lab specific field. $I_{pa} = \frac{PUB_{sf}}{PUB_{total}}$, where PUB_{sf} is the number of publications related to the specific field of the mega-lab in the year preceding the project application; PUB_{total} is the total number of university publications in the year preceding the project application
3	**Collaboration with industrial partners** $I_{eng} = \frac{I_{cof} + I_{tgt} + I_{empl}}{3}$ is the industrial partner engagement index into the mega-lab project
3.1	I_{cof} is the index of industrial partner's participation in co-funding the establishment of a mega-lab. $I_{cof} = \frac{F_{cof}}{F_{total}}$, where F_{cof} is the amount of funding that the industrial partner plans to allocate to the implementation of the project, RUR mln; F_{total} is the total project cost, in million rubles
3.2	I_{tgt} is the index of industrial partner's use of target training mechanisms for personnel training. $I_{tgt} = \frac{S_{tgt}}{S_{tgt\ total}}$, where S_{tgt} is the number of target students from an industrial partner, persons; $S_{tgt\ total}$ is total number of students enrolled in target training, persons
3.3	I_{empl} is the employment index for the university graduates in the entities affiliated with the industrial partners. $I_{empl} = \frac{G_{empl}}{G_{empl\ tgt}} = \frac{G_{empl}}{28}$, where G_{empl} is the number of university graduates employed in the industrial partner organization over the past 4 years, persons; $G_{empl\ tgt}$ is the number of graduates employed by an industrial partner's organization over the past 4 years, persons. This is based on an annual target of recruiting at least 70% of the current year's graduates, in the interests of the industrial partner
4	**Relevance and significance of the project in relation to the strategic objectives of university development** $I_{rel} = \frac{I_{NTLP} + I_{sg}}{2}$ is the index of the project's relevance and significance for the university development
4.1	I_{NTLP} is the correspondence index between the topics of educational projects along with mega-lab specialization and NTLP specialization. $I_{NTLP} = \frac{NTLP_{sched}}{NTLP}$, where $NTLP_{sched}$ is the number of NTLP whose tasks will involve work scheduled to be done at the mega-lab; and NTLP is the total number of ongoing NTLPs

Table 2. Continued

4.2	I_{sg} is the index of integration of the main fields of the mega-lab specialization in achieving the strategic goals of RTU MIREA, as set out in the Priority 2030 program. $I_{sg} = \frac{SI_{sched}}{SI}$, where SI_{sched} is the number of strategic initiatives under the Priority 2030 that will involve work at the mega-lab; SI is the total number of strategic initiatives specified in the Priority 2030
5	**Uniqueness of the mega-lab project** $I_{uniq} = \frac{A/C/U}{5}$ is the project uniqueness index
5.1	A is the absence of analogs in the Russian Federation, meaning the establishing of a fundamentally new laboratory (5 points)
5.2	C is the presence of separate laboratory components in other organizations (2 points)
5.3	U is the upgrade of existing mega-lab complexes (1 point)

As a result, the overall assessment index for the project to establish a mega-lab includes five sub-indices:

- I_{EA} is the index of the mega-lab utilization for educational activities;
- I_R is the index of the mega-lab utilization for R&D;
- I_{eng} is the engagement index of an industry partner into a mega-lab project;
- I_{rel} is the index of the project relevance and significance for the university advancement;
- I_{uniq} is the project uniqueness index.

Each I_i index can range from 0 to 1, with 1 representing the maximum possible score and therefore the highest potential value and usefulness of the mega-lab.

To ensure the ability to defend the submitted project and address any issues that may arise during the review process, a project presentation assessment (PP) is incorporated as a separate component of the overall estimation. In order to make it comparable with other estimations presented in a similar format, PP assessment is binary, meaning it can only take one of two possible values: 0 or 1.

Therefore, the integral estimation of the submitted project (IEP) is as follows:

$$\text{IEP} = F(I_{EA}, I_R, I_{eng}, I_{rel}, I_{uniq}, \text{PP}).$$

The following mathematical formulation is derived from the current practice of obtaining a comprehensive assessment in the form of a composite index:

$$\text{IEP} = K_1 \frac{I_{EA} + I_R + I_{eng}}{3} + K_2 \frac{I_{rel} + I_{uniq}}{2} + K_3 \text{PP},$$

where K_i represents the weighting coefficient of each IEP component.

Since K_1 is a weighting factor for indicators that are directly linked to and represent strategically significant areas of activity, the first three indicators are included in the comprehensive assessment with a relative importance of 3. The remaining two components of the comprehensive assessment are included with an equal weighting of 1. Accordingly, the following integrated estimation model is derived:

$$\text{IEP} = 3 \cdot \frac{I_{EA} + I_R + I_{eng}}{3} + \frac{I_{rel} + I_{uniq}}{2} + \text{PP}.$$

The maximum possible score for the integral estimation of the mega-lab project is 5 points. To assess the level of the project presented, the actual estimation value must be compared to the maximum possible value:

$$\gamma = \frac{\text{IEP}_{actual}}{5}.$$

This demonstrates how close the actual project estimation value is to the maximum possible value of 5. As a result, the decision is based on the following ratios:

- $0.7 \leq \gamma \leq 1.0$: the project is accepted for implementation;
- $0.4 \leq \gamma < 0.7$: "grey area," meaning that the project is proposed for revision, primarily by strengthening its integration into the solution of tasks that are strategically important for the university;
- $0 \leq \gamma < 0.4$: the project is rejected.

The primary benefit of the proposed methodology is its comprehensive and objective nature. This ensures that the resulting integrated estimation of the project provides a robust basis for appropriate decision-making.

CONCLUSIONS

The dynamic, sustainable, and socially-beneficial development of engineering universities greatly depends on the effective modernization of their material and technical infrastructure. Experience

shows that, in addition to financial investment, this process requires well-planned infrastructure policies and strategic planning for the development of scientific and educational facilities. These measures enable decisions that ensure the long-term sustainability and development of educational organizations, as well as the achievement of goals set out in their development programs.

The diverse range of activities currently undertaken by engineering universities, coupled with the significant cost of establishing and maintaining scientific and academic infrastructure, necessitates a structured and formal approach to the selection of projects aimed at enhancing the material and technological base of these institutions. Such an approach, as proposed by educational, research, and academic units, ensures maximum objectivity in the evaluation process. The implementation of the systematic and comprehensive project selection methodology proposed in this paper will facilitate the identification and development of effective solutions within the core areas of university operations, particularly in the context of interdisciplinary initiatives in innovation, education, and research.

Authors' contribution

All authors contributed equally to the research work.

REFERENCES

1. Opletina N.V. Engineering Education in the Context of a New Technological Paradigm of Social Development. *Naukovedcheskie issledovaniya = Science Studies.* 2022;2:55–70 (in Russ.). https://www.elibrary.ru/uizigx
2. Zhmud V.A. Modern Problems of Higher Technical Education. *Avtomatika i programmnaya inzheneriya = Automation and Software Engineering.* 2021;2(36):20–47 (in Russ.). https://www.elibrary.ru/cqymyg
3. Kiryushina N.A. Modern Engineering Education: Problems and Prospects. *Innovatsionnoe razvitie professional'nogo obrazovaniya = Innovative Development of Vocational Education*. 2024;3(43):70–77 (in Russ.). https://www.elibrary.ru/jeqcwg
4. Prokhorov V.A. Problems of lifelong learning in the field of engineering. *Nepreryvnoe obrazovanie*: *XXI vek = Lifelong Education*: *The 21st Century*. 2019;4(28) (in Russ.). http://doi.org/10.15393/j5.art.2019.5156
5. Sobolev L.B. Problems of engineering education in Russia. *Ekonomicheskii analiz: teoriya i praktika = Economic Analysis: Theory and Practice*. 2017;17(7):1252–1267 (in Russ.). https://doi.org/10.24891/ea.17.7.1252
6. Sharipov F.F. Management of educational and scientific laboratory: new requirements and competences. *E-Management*. 2020;3(1):36–42 (in Russ.). https://doi.org/10.26425/2658-3445-2020-1-36-42
7. Giryuk I.A., Varkulevich T.V. On the Issue of the Need to Improve the Sphere of Information and Logistics Support for the System of Higher Education in the Russian Federation. *Molodoi uchenyi = Young Scientist*. 2023;10(457):138–142 (in Russ.). https://elibrary.ru/adkoqo
8. *Vzaimodeistvie vuzov s industrial'nymi partnerami* (*Interaction between Higher Education Universities and their Partners*). V. 10. Moscow: Plekhanov Russian University of Economics; 2022, 132 p. (In Russ.).
9. Shtykhno D.A., Petrov A.M. Interaction between Higher Education Universities and their Partners. *Nauchnye trudy Vol'nogo ehkonomicheskogo obshchestva Rossii* (*Nauchnye trudy VEHO Rossii*) = *VEO of Russia Today*. 2023;243(5):85–97 (in Russ.). https://doi.org/10.38197/2072-2060-2023-243-5-85-97
10. Boyko E.A., Pikolova A.A. Strategic Interaction of University with Industrial Partners. *Professional'noe obrazovanie v Rossii i za rubezhom = Professional Education in Russia and Abroad*. 2022;4(48):51–58 (in Russ.). https://doi.org/10.54509/22203036_2022_4_51
11. Skvortsov N.I., Pavlov N.S., Ermilov V.G. Features of Implementation of Financial Policy in the Field of Higher Education. *Vestnik MGPU. Seriya Ehkonomika = MCU Journal of Economic Studies.* 2023;1(35):37–51 (in Russ.). https://doi.org/10.25688/2312-6647.2023.35.1.03
12. Meliksetyan S.N., Otrishko M.O. Development of Extra budgetary Sources for the Financing for Higher Education Institutions. *Finansovye issledovaniya = Financial Research*. 2020;3(68):92–97 (in Russ.). https://elibrary.ru/tszgmr
13. Kasharnaya G.B., Naidenova L.I. *Prinyatie upravlencheskikh reshenii* (*Management Decision-Making*). Penza: PSU Publ.; 2020, 68 p. (In Russ.).
14. Konova T.A., Nesterov V.L. Estimation of the efficiency of use of material-technical base of universities in the system of indicators of the quality of training. *Fundamental'nye issledovaniya = Fundamental Research*. 2015;3:187–191 (in Russ.). https://elibrary.ru/tniqxf
15. Shkuropat A.V. Composite Indices as a Tool for Regional Development Policy. *Rossiiskii vneshneekonomicheskii vestnik = Russian Foreign Economic Bulletin*. 2021;6:58–69 (in Russ.). https://elibrary.ru/rkrotb

СПИСОК ЛИТЕРАТУРЫ

1. Оплетина Н.В. Инженерное образование в контексте новой технологической парадигмы общественного развития. *Науковедческие исследования*. 2022;2:55–70. https://www.elibrary.ru/uizigx
2. Жмудь В.А. Современные проблемы высшего технического образования. *Автоматика и программная инженерия*. 2021;2(36):20–47. https://www.elibrary.ru/cqymyg
3. Кирюшина Н.А. Современное инженерное образование: проблемы и перспективы. *Инновационное развитие профессионального образования*. 2024;3(43):70–77. https://www.elibrary.ru/jeqcwg
4. Прохоров В.А. Проблемы системы непрерывного инженерного образования. *Непрерывное образование*: *XXI век.* 2019;4(28). http://dx.doi.org/10.15393/j5.art.2019.5156
5. Соболев Л.Б. Проблемы инженерного образования в современной России. *Экономический анализ: теория и практика*. 2017;17(7):1252–1267. https://doi.org/10.24891/ea.17.7.1252
6. Шарипов Ф.Ф. Управление учебно-научной лабораторией: новые требования и компетенции. *E-Management*. 2020;3(1):36–42. https://doi.org/10.26425/2658-3445-2020-1-36-42
7. Гирюк И.А., Варкулевич Т.В. К вопросу о необходимости совершенствования сферы информационного и материально-технического обеспечения системы высшего образования в Российской Федерации. *Молодой ученый*. 2023;10(457):138–142. https://elibrary.ru/adkoqo
8. *Взаимодействие вузов с индустриальными партнерами*. Выпуск 10. М.: РЭУ им. Г.В. Плеханова; 2022, 132 с.
9. Штыхно Д.А., Петров А.М. Взаимодействие вузов с индустриальными партнерами. *Научные труды Вольного экономического общества России* (*Научные труды ВЭО России*). 2023;243(5):85–97. https://doi.org/10.38197/2072-2060-2023-243-5-85-97
10. Бойко Е.А., Пиколова А.А. Стратегическое взаимодействие вуза с индустриальными партнерами. *Профессиональное образование в России и за рубежом*. 2022;4(48):51–58. https://doi.org/10.54509/22203036_2022_4_51
11. Скворцов Н.И., Павлов Н.С., Ермилов В.Г. Особенности реализации финансовой политики в сфере высшего образования. *Вестник МГПУ. Серия Экономика.* 2023;1(35):37–51. https://doi.org/10.25688/2312-6647.2023.35.1.03
12. Меликсетян С.Н., Отришко М.О. Развитие внебюджетных источников функционирования высших учебных заведений. *Финансовые исследования*. 2020;3(68):92–97. https://elibrary.ru/tszgmr
13. Кашарная Г.Б., Найденова Л.И. *Принятие управленческих решений*. Пенза: Изд-во ПГУ; 2020, 68 с.
14. Конова Т.А., Нестеров В.Л. Оценка эффективности использования материально-технической базы вузов в системе показателей качества подготовки специалистов. *Фундаментальные исследования*. 2015;3:187–191. https://elibrary.ru/tniqxf
15. Шкуропат А.В. Интегральные индексы как инструмент управления региональным развитием. *Российский внешнеэкономический вестник*. 2021;6:58–69. https://elibrary.ru/rkrotb

About the Authors

Stanislav A. Kudzh, Dr. Sci. (Eng.), Professor, Rector, Professor, Department of Instrumental and Applied Software, Institute of Information Technologies, MIREA – Russian Technological University (78, Vernadskogo pr., Moscow, 119454 Russia). E-mail: kudzh@mirea.ru. Scopus Author ID 56521711400, ResearcherID AAG-1319-2019, RSCI SPIN-code 8173-1572, https://orcid.org/0000-0003-1407-2788

Natalia B. Golovanova, Dr. Sci. (Econ.), Professor, Deputy First Vice-Rector, Professor, Department of Economics, Institute of Management Technologies, MIREA – Russian Technological University, (78, Vernadskogo pr., Moscow, 119454 Russia). E-mail: golovanova@mirea.ru. Scopus Author ID 57191447039, RSCI SPIN-code 7197–9948, https://orcid.org/0000-0002-9901-8897

Yuri G. Grafov, Cand. Sci. (Econ.), Vice Rector (Digital Transformation and Finance), MIREA – Russian Technological University, (78, Vernadskogo pr., Moscow, 119454 Russia). E-mail: grafov@mirea.ru. RSCI SPIN-code 5584-6010

Об авторах

Кудж Станислав Алексеевич, д.т.н., профессор, ректор, профессор кафедры инструментального и прикладного программного обеспечения, Институт информационных технологий, ФГБОУ ВО «МИРЭА – Российский технологический университет» (119454, Россия, Москва, пр-т Вернадского, д. 78). E-mail: kudzh@mirea.ru. Scopus Author ID 56521711400, ResearcherID AAG-1319-2019, SPIN-код РИНЦ 8173-1572, https://orcid.org/0000-0003-1407-2788

Голованова Наталия Борисовна, д.э.н., профессор, заместитель первого проректора, профессор кафедры экономики, Институт технологий управления, ФГБОУ ВО «МИРЭА – Российский технологический университет» (119454, Россия, Москва, пр-т Вернадского, д. 78). E-mail: golovanova@mirea.ru. Scopus Author ID 57191447039, SPIN-код РИНЦ 7197–9948, https://orcid.org/0000-0002-9901-8897

Графов Юрий Германович, к.э.н., проректор (цифровая трансформация, экономические и финансовые вопросы), ФГБОУ ВО «МИРЭА – Российский технологический университет» (119454, Россия, Москва, пр-т Вернадского, д. 78). E-mail: grafov@mirea.ru. SPIN-код РИНЦ 5584-601

Translated from Russian into English by K. Nazarov
Edited for English language and spelling by Thomas A. Beavitt

MIREA – Russian Technological University.
78, Vernadskogo pr., Moscow, 119454 Russian Federation.
Publication date March 31, 2026.
Not for sale.

МИРЭА – Российский технологический университет.
119454, РФ, г. Москва, пр-т Вернадского, д. 78.
Дата опубликования 31.03.2026 г.
Не для продажи.

https://www.rtj-mirea.ru